OCS Study
MMS 2002-053

Northeastern Gulf of Mexico Circulation Modeling Study

Final Report

Authors

Y. Hsueh
Florida State University

Robert Weisberg
University of South Florida

Prepared under MMS Cooperative Agreement
14-35-0001-30804
by
Department of Oceanography
Florida State University
Tallahassee, FL 32306-4320

Published by
U. S. Department of the Interior
Minerals Management Service
Gulf of Mexico OCS Region

Herndon, VA
September 2002

DISCLAIMER

REPORT AVAILABILITY

While supplies last, copies of the report may be obtained from:

U.S. Department of the Interior
Minerals Management Service
Environmental Division
381 Elden Street
Herndon, VA 20170
Telephone Number: (703) 787-1642

CITATION

Suggested Citation:

Hsueh, Y., and Robert H. Weisberg. Northeastern Gulf of Mexico Circulation Modeling Study: Final Report, MMS Cooperative Agreement 14-35-0001-30804. OCS Study MMS 2002-053, U.S. Dept of the Interior, Minerals Management Service, Herndon, VA. 187pp.

ACKNOWLEDGEMENTS

The Program Manager wishes to extend thanks to Prof. W. Sturges for numerous fruitful discussions, Prof. P. Niiler for providing surface drifter data, and Drs. P. Hamilton, and T. Berger for making available moored current meter data in DeSoto Canyon. Ms. Paula Tamaddoni Jahromi helped with preparing the pdf version and Dr. Reinard Harkema helped with the CD production. The continuing, enthusiastic and timely support of Dr. Walter Johnson, the MMS Contract Officer's Technical Representative, during all phases of this project is gratefully acknowledged.

Table of Contents

LIST OF FIGURES

Executive Summary

The project examines the flow on the continental shelf in the northeastern Gulf of Mexico (NEGOM) on the basis of two numerical models, each for a distinct portion of the shelf. The Princeton Ocean Model (POM) deals with the flow near the coast driven by local forcing and the Geophysical Fluid Dynamics Laboratory Model (GFDL) deals with that near the shelf-break driven by local and open-ocean forcing.

The spin-up on the inner shelf follows the fast Ekman-geostrophic track and the presence of the Big Bend and the Florida Keys accentuates the response of the central west Florida coast water to local wind forcing. Baroclinic effects as a result of surface heating are important for seasonal variations in inner shelf circulation.

The flow on the outer shelf is strongly influenced by the Loop Current. A southward shelf break jet is discovered, driven by pressure imposed by the Loop Current. The flow in DeSoto Canyon in winter is found to be an extension of the southward flow on the west Florida shelf set up by the passage of continental shelf waves. Monthly mean temperature variation in DeSoto Canyon features large cross-shelf gradients in May-June and November-December, following semi-annual peaking of strong anti-cyclonic wind-stress curl in NEGOM. Apparently, the wind-stress curl drives downward the isotherms in the deep water and the associated geostrophic currents to the east along the shelf-break give rise to bottom Ekman flow onshore, raising the isotherms in the shallow region. Thus, the large monthly mean temperature contrast in DeSoto Canyon.

1. Introduction

The purpose of the cooperative program is to enhance the present understanding of the circulation in the Northeastern Gulf of Mexico through the use of computer models. The focus is on the wind-driven flows near the coast and the influence on them by the Gulf of Mexico Loop Current. The program involves a group of investigators from the Florida State University and the University of South Florida and parallels the field program directed by W. Sturges, as well as that conducted by the Science Applications International Corporation (SAIC).

There is a strong tie-in of the numerical modeling effort with the observational program. The observations in various forms, including that from satellite-tracked surface drifters, from moored current meters, from remote sensing, and from hydrographic surveys, collectively provide a basis for calibrating the performance of the models. Conversely, a well-calibrated model provides outputs that form a basis for the interpretation of the observations in terms of the dynamics.

The program has been a success in that useful models are developed and model/observation comparisons are concluded with positive results.

2. 2. FSU Modeling Effort

Prof. Y. Hsueh
Department of Oceanography
with
Scientific Associates:
Drs. Dongliang Yuan and Yury Golubev

Graduate Students
Dr. Robert H. hetland and Howard Huang

2.a Model Configuration

The FSU model is based on the Bryan-Cox code with z-levels in the vertical. In order to represent properly the Loop Current and its rings, the model encompasses the whole Gulf of Mexico, from 18^{o} N to 31^{o} N from 100^{o}W to 80^{o}W. The horizontal grid size is one-sixth of a degree in both longitude and latitude. The vertical span is covered with a variable grid that is stretched in favor of a higher resolution in the surface layer than in the deep portion.

The geometry and topography are extracted from ETOPO5 and are shown in Figure 1.

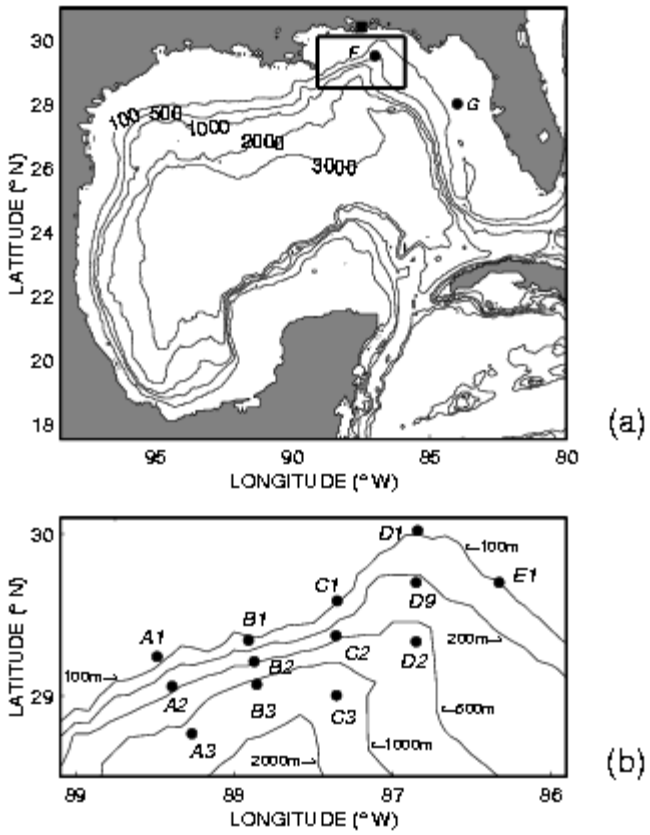

Figure 1. (a). Topography of the Gulf-of-Mexico model. Contours shown are 100, 500, 1000, 2000, 3000m. Solid circles, F and G, mark locations where inflow-outflow model experiment time series are extracted. The solid square at the top marks Pensacola. (b). SAIC moorings.

The circulation is initially driven with an inflow of 30 Sv across the southern open boundary in a 100 km wide boundary current next to the Yucatan Peninsula. An outflow of the same transport is implemented across the opening in the eastern boundary in the Florida Straits.

The model is initialized with the climatological temperature and salinity fields (Levitus et al., 1994). The initial velocity field is obtained from adding the thermal-wind velocity to the barotropic velocity forced by the imposed transports. Across the inflow and outflow ports, the tracer fields and the baroclinic velocity are relaxed to those from the Levitus climatology. At the sea surface, the first level temperature and salinity are relaxed to their climatological values.

Since the pioneering numerical work of Hurlburt and Thompson (1980) in which Loop Current ring shedding was reproduced for the first time, there have been several more models of the Gulf-of-Mexico basin-wide circulation (Dietrich et al., 1993, Oey, 1996; Welsh, 1996; Frantantoni, 1998). Except for the high resolution (7 km) model of Frantantoni (1998) used to study the Dry Tortugas eddies, these models, as well as that of Hurlburt and Thompson (1980), are designed to focus on the circulation in the western Gulf of Mexico and the evolution and role of the anti-cyclonic rings generated from the Loop Current. As

such, they lack the vertical resolution necessary to resolve the continental shelf topography west of Florida. Although Oey (1996) uses improved vertical resolution to include a continental shelf, the simulated Loop Current bends unrealistically far away from the west Florida shelf. The effect of this bending is to decouple the Loop-Current forced circulation from the topographic influence of the west Florida shelf, a key factor in the formation of the southward flow on the west Florida shelf (see later). The present model avoids this excessive bending with the use of a biharmonic horizontal mixing formulation, which helps preserve the inertial current characteristics of the Loop Current.

2b. Major Findings

A basic model run with no wind forcing is first made to establish the fundamentals of the Loop Current dominated circulation. The inflow-outflow condition produces the basic flow patterns with nearly periodic Loop Current ring separation at a period of around 13 months. Figure 2 shows, in eight panels, the evolution of surface temperature through a typical ring-shedding cycle of the 10-year long model integration. The 200 m and 1000 m isobaths are also drawn to delineate the shelf area. On Day 1230 of the run (Panel 1), ring shedding is imminent. This is the time when the Loop Current has nearly achieved its maximum penetration into the Gulf of Mexico and the Loop-Current front is near its closest to the northwest Florida shelf (the Big Bend). A noticeable cyclonic eddy (marked by the letter C in Panel 1) is gaining in strength at this time southwest of Key West. This cyclonic eddy grows and moves to the west and causes a "necking-down" of the Loop Current, leading to the eventual separation of an anti-cyclonic ring (Vukovich et al., 1979; Pratt and Stern, 1986; Vukovich, 1986). Panel 2 shows the temperature distribution two months later. A warm-core ring is clearly seen separated from the main stream of the Loop Current and the Loop Current has retreated to a minimum penetration state. In the meantime, the isolated ring moves to the west and southwest at a speed of about 4cm/s and is eventually dissipated off the Mexico coast (Panels 3-6) as is found elsewhere (Sturges et al., 1993). It takes about a year for the Loop Current to regain its full penetration and start another round of ring shedding (Panels 7-8). The ring shedding cycle repeats itself and constitutes the anticipated periodic solution for the Gulf of Mexico circulation (Pichevin and Nof, 1997).

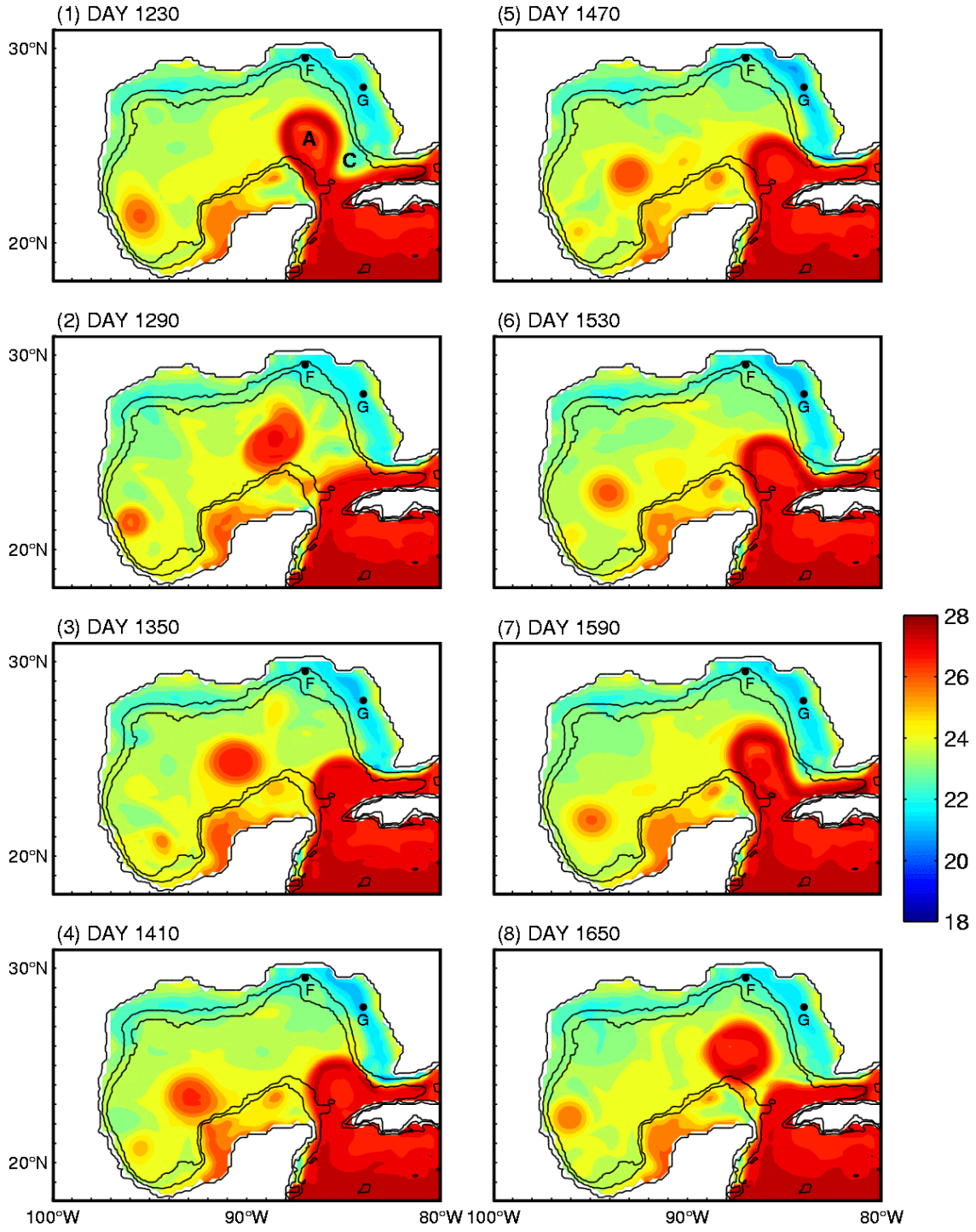

Figure 2 Evolution of temperature at the 5 m depth in the inflow-outflow experiment. The 200 m and 1000 m isobaths are plotted to identify the shelf area. The letters F and G mark the positions where velocity time series are extracted. In Panel 1, the anti-cyclonic and cyclonic eddies are marked by the letters A and C, respectively.

The influence of this Loop Current evolution on the west Florida shelf circulation is shown in Figure 3. The upper panel shows the evolution of the north-south velocity component for more than 5 years at 5 m depth in 40 m of water at the solid circle marked G in Figure 1 (84^o W, 28^o N) off Tampa (similarly marked in Figure 2). The velocity at this location is qualitatively representative of the velocity on the west Florida shelf. The mean current over the time span is southward, suggesting that, on the average, the Loop Current generates a shelf flow to the south. The oscillation on the ring-shedding period appears phase-locked to the ring-shedding cycle. The time span of each trough (large southward velocity) roughly begins with the time when a ring has just separated (Panels 2 and 3 in Fig. 2).

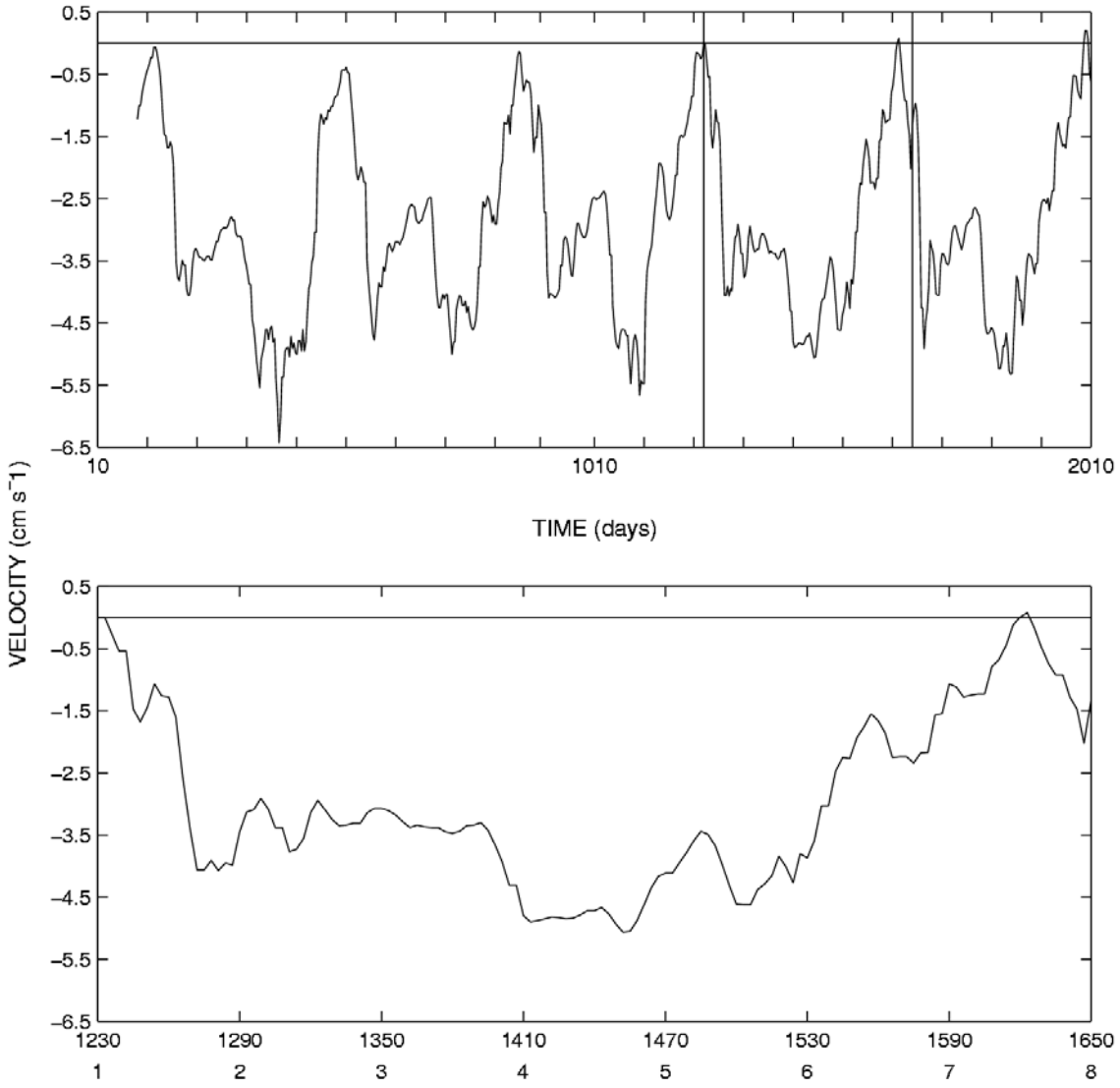

Figure 3. Time series of north-south velocity component at 5m depth at G (84° W, 28° N) on the west Florida shelf in the inflow-outflow experiment. The upper panel shows the time series during more than five years of integration. The lower panel shows the time series between the two vertical lines in the upper panel. The expanded portion covers the time window of Figure 2. Numbers in the lower panel mark the time of the panels in Figure 2. The horizontal lines are zero velocity lines.

The lower panel shows an expanded portion of the north-south velocity time series. The expanded portion corresponds to the time window spanned by Figure 2. Notice that, at the time (marked "1") when the Loop-Current front is the closest to the Big Bend shelf, the southward drift over the shelf is at its minimum. This suggests that the flow over the shelf is not simply frictionally dragged by the Loop Current. The forcing of the Loop Current on the shelf circulation must be through other mechanisms. It turns out that the drop in dynamic pressure brought about by the Bernoulli effect as the Loop Current careens along the continental slope/shelf edge effects just such a flow in accordance with the arrested topographic wave (ATW) theory (Csanady, 1978; Csanady and Shaw, 1983). The manner with which the pressure is imposed varies with the Loop Current position. The variation created in the shelf flow appears to explain the phase lead over the northward position of the Loop Current of southward flows inferred from the coastal sea-level fluctuations found in Sturges and Evans (1983). The detailed quasi-steady-state physics of this pressure forcing process forms the theme for a Ph. D. dissertation and is discussed in two publications (Hetland, 1999; Hetland et al., 1999; Hetland et al. 2001). Based on the results so far presented, it suffices to say that the Loop Current generally forces a southward flow over the west Florida shelf and the low-frequency variations of the flow occur primarily at the Loop Current ring-shedding frequency.

The influence of the Loop Current variation on the circulation inside DeSoto Canyon is shown in Figure 4, in which are plotted, over the same time period as in Figure 3, the velocity time series at 5 m depth in 324 m of water at the solid circle marked F in Figure 1 (87^o W, 29.5^o N) at the center of DeSoto Canyon (also marked similarly in Figure 2). The solid curve represents the east-west velocity component and the dashed curve represents the north-south velocity component. The east-west component is particularly comparable to that shown in Figure 3, both being roughly alongshore. The east-west component time series in Figure 4 shows more irregularities, but the phase-locking with the Loop Current variations emerges again. Again, the maximum occur at the time when the Loop Current is farthest away to the south. The alongshore flow in DeSoto Canyon appears simply to respond to the southward flow over the west Florida shelf. This is again consistent with the ATW theory and attributable to the insulating effect of the continental slope topography, isolating the shelf flow, which roughly follows the isobaths. The east-west velocity component at F thus varies similarly with the north-south velocity component at G, 180^o out of phase with the extent of the northward penetration of the Loop Current. A contour plot (not shown) of east-west velocity against time for the meridian through F from 26^o N to 30^o N shows that not until the latitude of 27^o N does the east-west velocity begin to vary in phase with the northward penetration of the Loop Current.

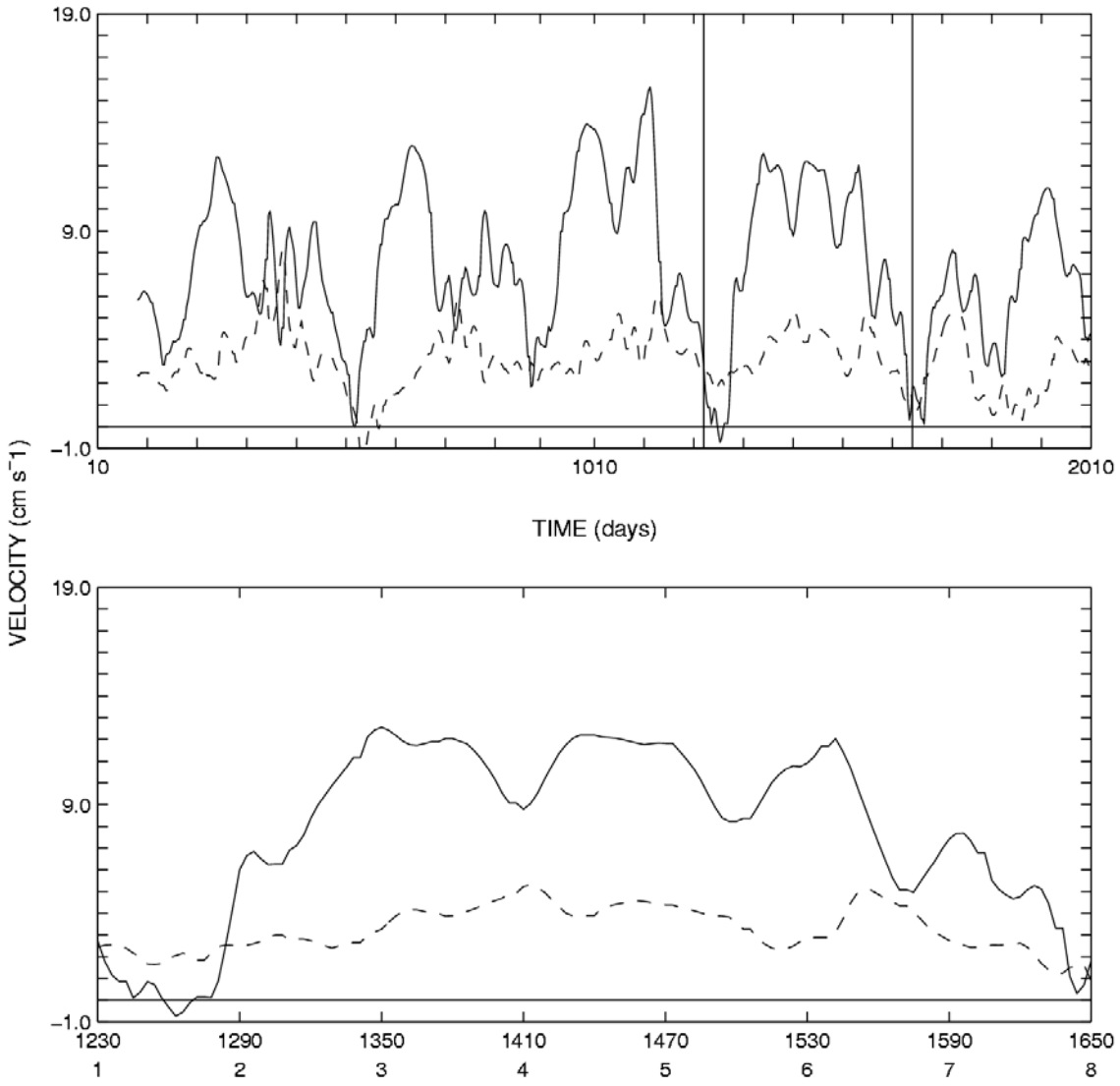

Figure 4. Time series plot same as in Figure 3, but at F (87^{o} W, 29.5^{o} N) inside DeSoto Canyon. Solid curve represents the east-west velocity component and dash curve represents the north-south component. The horizontal lines are zero velocity lines.

On the basis of the validity of the inflow-outflow experiment, a hindcast for the circulation is then conducted for the period of March 1997-April 1998 for which direct current measurements in DeSoto Canyon are available from a Science Applications International Corporation (SAIC) mooring experiment (SAIC, 1998). Use is made of six-hourly wind stresses derived from the NCEP/NCAR 40-year reanalysis winds (Kalnay et al., 1996). The hindcast results form the basis for two manuscripts. One manuscript, now in press, demonstrates that the flow in winter in DeSoto Canyon is but a part of the NEGOM continental shelf flow in response to the wind-driven southward current on the west Florida shelf (Hsueh and Golubev, 2001). The other, in review,

shows that the observed large DeSoto Canyon cross-shelf gradients in monthly mean temperature are the manifestation of shelf response to semi-annual peaking (in April and October) in the negative wind-stress curl field over NEGOM (Golubev and Hsueh, 2001). A third one has just been prepared and deals with the variability in surface currents surmised from the trajectory of the drifters. All three manuscript are attached in the Appendix.

In addition, for comparison purposes, the output is obtained for the Gulf of Mexico region from a similar model (Carton and Chao, 1999). An examination of the output has led to the discovery of a mechanism by which upwelled water from Campech Banks can propagate along the Loop Current to the west Florida shelf. The mechanism is one of frontal dynamics involving the Loop Current and imbedded eddies. The theoretical work form the basis of a Ph. D. dissertation research currently underway (Huang, 2001).

2c. Accomplishments

The following is a list of papers and dissertations published, submitted, or in preparation.

1). Hetland, Robert, Y. Hsueh, Bob Leben, and P. P. Niiler, 1999: A Loop Current-induced jet along the edge of the West Florida Shelf. *Geophys. Res. Letters*. 26, 2239-2242.

2). Robert D., Y. Hsueh, and Dongliang Yuan, 2001: On the decay of a baroclinic jet flowing along a continental slope. *J. Geophys. Res.* 106, 19,797-19807.

3). Hsueh, Y., and Yury Golubev, 2002: A numerical model calculation of the flow in DeSoto Canyon in response to northerly wind bursts in winter. *Gulf of Mexico Science*. 20 (1), 44-59.

4). Golubev, Yury, and Y. Hsueh, 2002: Temperature variability in the northeastern Gulf of Mexico in 1997-1998. Submitted to *Gulf of Mexico Science*.

6). Golubev, Yury, and Y. Hsueh, 2002: Low-frequency variability of surface currents on the NEGOM shelf. In preparation.

5). Hetland, Robert D., 1999: The dynamics of a Loop Current forced shelf break jet on the west Florida shelf. Dissertation. Department of Oceanography, Florida State University. 68 pp.

6). Huang, Haosheng, 2002: Embedded eddies in the Loop Current. Dissertation. Department of Oceanography, Florida State University. In progress.

3. USF Modeling Efforts

Robert H. Weisberg
Professor, Physical Oceanography

With

Scientific Associates: Drs. M. Luther, H. Yang, and Z. Li,
Graduate Student: R. He, and
Technical Staff: R. Cole, J. Donovan, C. Merz, and P. Smith.

College of Marine Science
University of South Florida
140 7th Ave. S.
St. Petersburg, FL. 33701

3a. Introduction

Continental shelves may be discussed in terms of three regions, each controlled by different physical processes. The inner-shelf is where divergent surface and bottom frictional boundary layers play a major role; the outer-shelf (shelf-break) is where strong interactions occur with the adjacent ocean; and the middle-shelf is a transition region. Of these regions, the inner-shelf is the least studied, either through *in-situ* observations, or through the application of analytical and numerical models. Yet, in many respects, depending upon the shelf width, this may be the scientifically most interesting region because of its physical, biological, chemical, and geological interactions in response to synoptic and seasonal forcing.

The WFS is broad enough so that its inner, middle, and outer-shelf regions are relatively distinct, allowing the dominant processes within each region to be viewed somewhat independently from one another. Important inner-shelf scientific questions can therefore be addressed through the combination of *in-situ* measurements and models. These questions include the nature of: (i) the coastal jet's three-dimensional structure, time dependence, and turbulence evolution; (ii) its rectification by stratified boundary layer effects and how this impacts along and across-shelf transports; and (iii) the seasonal modulation of these processes by local and offshore forcing. The gently sloping WFS therefore provides an excellent natural laboratory for studying the physical processes that set the stage for biological (blooms), chemical (nutrient concentrations), and geological (sediment resuspension) events.

At USF, we initiated a WFS circulation study in 1993 with USGS support that subsequently evolved with support from the MMS, the State of Florida, NOAA, and ONR. Presently ongoing is an Ecology of Harmful Algal Blooms (ECOHAB) regional field study to advance our understanding and forecasting ability for red-tides; a State of Florida supported Coastal Ocean Monitoring and Prediction System (COMPS) to provide real-time data for emergency management use; and ONR supported *in-situ* measurements and modeling. We adhere to the tenet that the *in-situ* measurements and modeling must be interactive. Measurements are sparse and require a multiple scale context. Models are critically dependent upon their parameterizations, initial state, and boundary conditions, so they must be pegged to measurements to be useful.

Our evolving program of study was aided substantially by a cooperative agreement with the Minerals Management Service coordinated through the Florida State University, MMS 14-35-0001-30804. Over the four-year period: 9/30/95-9/29/99, plus a one-year no cost extension, USF personnel, under the direction of R.H. Weisberg, engaged in numerical model experiments on the WFS circulation. We recognize that the shelf responds to both local and offshore forcing. Local forcing is by the combined effects of momentum and buoyancy inputs at the sea surface and buoyancy inputs at the coast. Offshore forcing is by momentum and buoyancy inputs from the deep ocean at the shelf-break. By virtue of its width, the WFS is an end member in the spectrum of continental shelves for which local forcing should be important. Thus our emphasis has been on local forcing and its effects on the inner-shelf.

Our model domains have been regional ones, and the model that we chose to use is the Princeton Ocean Model (POM). Two different versions were employed. The first includes the domain between the DeSoto Canyon in the northwest and the Florida Keys in the southeast. As shown in Figure 5 it has three open boundaries for which radiation conditions are applied. Horizontal resolution for this curvilinear coordinate system model over the inner-shelf averages at about 9 km, and the model employs 16 sigma layers. The second encompasses the region from west of the Mississippi River to the Florida Keys. As shown in Figure 6 it has one open boundary governed by a radiation condition. Horizontal resolution for this curvilinear coordinate system model over the inner-shelf averages at about 2 km, and the model employs 21 sigma layers. Both model configurations employ realistic topography (ETOPO5 with some smoothing in the southeast where a spurious shoal is encountered). As an evolving modeling project we employed different forcing functions and initializations depending on the scientific questioned asked. The simplest density fields and forcing functions consisted of constant density and switched-on, spatially uniform winds.

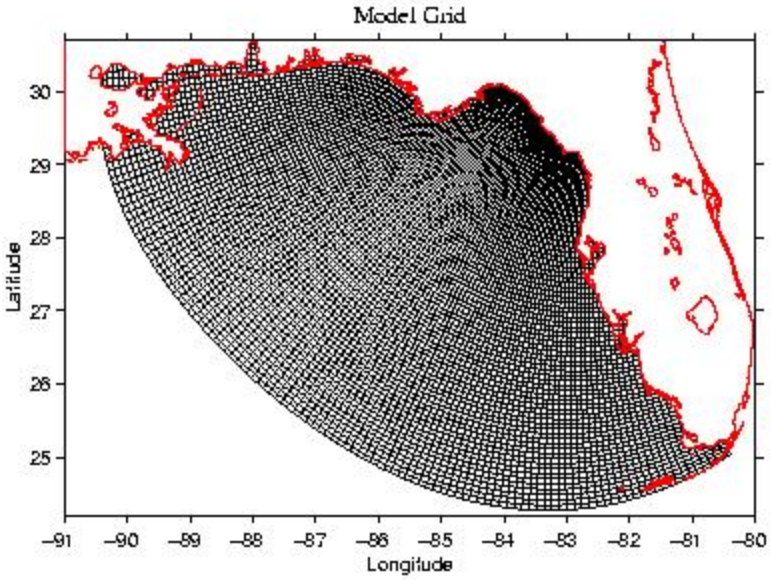

Figure 5. USF model domain of DeSoto Canyon to Florida Keys.

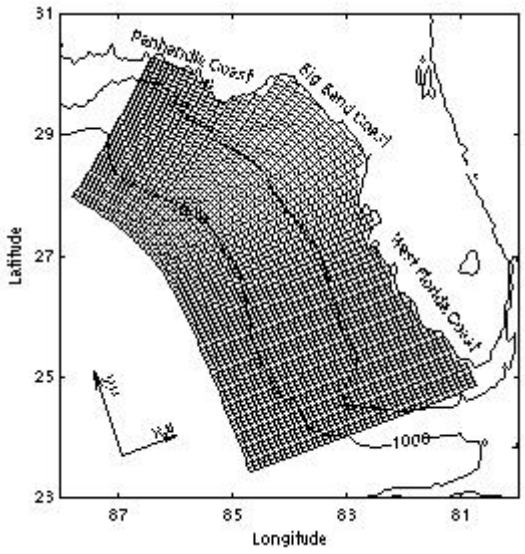

Figure 6. USF model domain of Mississippi River to Florida Keys.

The most elaborate experiments used fully baroclinic density fields driven by spatially and temporally varying winds, surface heat fluxes, and river inflows. We also have an automated experimental nowcast/forecast system (available at http://ocg6.marine.usf.edu) using NCEP Eta model winds.

3b. Major Findings

Our approach has been to apply various versions of these POM-based models in a stepwise manner to develop an understanding on how the WFS responds to tidal, synoptic, and seasonal scale forcing. The first and simplest sets of experiments were designed to determine how the WFS responds to upwelling favorable winds directed either along-shore or offshore (relative to the west Florida shoreline). The Figure 5 model grid was used where the outermost open boundary is sufficiently offshore so that it does not interfere with the model responses over the continental shelf. While constant density and barotropic, the model runs are fully three-dimensional and directed toward understanding the response to synoptic scale winds (previous model experiments were either two-dimensional or employed unrealistic geometries). Li and Weisberg (1999a) describes the model response kinematics and the companion paper, Li and Weisberg (1999b) describes the model response dynamics. Relevant findings are as follows. The model spin up follows an Ekman-geostrophic route resulting in a rapid adjustment over the course of a pendulum day. Surface Ekman layer divergence effects a sea surface slope that causes a geostrophic coastal jet that, in turn, causes a bottom Ekman layer response. While the WFS is gently sloping, subtle variations in coastline geometry have major effects on the fully three-dimensional circulation fields. In particular, partial closure in the south by the Florida Keys and the coastline curvatures of the Florida Big Bend conspire to yield strong responses to uniform winds directed either along-shore or offshore with respect to the central west Florida coastline. This may seem surprising based on two-dimensional arguments that offshore winds should not effect a coastal jet/upwelling response. Nevertheless, these findings are borne out by observations, and they are attributable to the coastline and isobath geometries. These geometry effects result in fully three-dimensional circulation patterns that are relevant to material property transports. The dynamics analyses define the inner-shelf as the region over which the sea surface slope sets up. We describe, in a vertically integrated sense, the interactions that occur between the along-shelf and across-shelf momentum balances in establishing the flow fields. The offshore scale of the inner-shelf is a frictional one associated with the divergence of the surface and bottom Ekman layers. This varies with bottom slope as shown for different regions along the coast. Offshore of the west Florida coastline, where we have corroborating data, the inner-shelf under a constant density setting extends out to about the 50-75m isobath. Fully three-dimensional momentum balance analyses provide further diagnoses of the model responses and how the Ekman and geostrophic regions interact.

Another preliminary examination was on the seasonal cycle. Yang and Weisberg (1999) asked the question of whether or not the seasonal variations in the circulation can be accounted for by seasonally varying winds alone. Climatological monthly mean winds were used to drive monthly model simulations. While interesting patterns are found suggesting that the WFS has

wind-driven seasons of predominantly upwelling and downwelling circulations, monthly mean winds alone can not account fully for the seasonal variations in the circulation. Baroclinic effects must also be important, along with the surface heat fluxes that facilitate these.

Given the simultaneous surface drifter program we examined whether or not the model could be used to simulate the drifter tracks. Yang et al. (1999) compares observed Lagrangian surface drifter tracks with numerical model simulations. We demonstrate that model drifters can mimic *in-situ* drifters over time scales of the synoptic weather events, at least on the shelf where the model responses to these synoptic weather events exceed the effects of the Loop Current or eddies positioned on or offshore of the shelf-break. We also attempt to explain the curious finding that no drifters deployed to the north of the west central Florida shelf tracked toward the shoreline – hence the title of the paper.

A specific case study of an upwelling event recorded both in satellite AVHRR imagery and *in-situ* data was examined by Weisberg et al. (2000). While upwelling (and downwelling) occur regularly on continental shelves with the passage of each synoptic weather front, rarely do all the necessary ingredients of nature coincide to make the upwelling response visible in satellite imagery. In this case, the winds were light for several days prior to a strong, upwelling favorable wind event, and we had *in-situ* velocity measurements for comparison. Through a combination of data and model analyses we clearly demonstrate the Ekman-geostrophic spin-up route described earlier. Using both constant density and stratified runs (stratification estimated from velocity shear by thermal wind) we describe the relative effects and explain the finding of maximum upwelling just offshore and to the south of Tampa Bay. We also explain other regions of local upwelling maxima south of Cape San Blas.

The circulation physics highly influences the biology of the WFS. Walsh et al. (2001) is our first attempt at combining the physical models developed under this project with the ecological models developed by Dr. J. Walsh. Here we attempt to simulate the evolution of the 1979 red tide, providing some insights into the joint workings of the biology and physics that culminate in near shore red tide effects. This work is continuing under separate NOAA ECOHAB funding, and we appreciate the influence played by the MMS in helping to facilitate this continuing research.

Spring and summer of 1998 exhibited large stratification over the inner-shelf, even right up to the shoreline. *In-situ* data shows that the circulation is very sensitive to stratification. By separating the surface and bottom Ekman layers, stratification in increases across-shelf transports. Weisberg et al. (2001) describes the *in-situ* data and the numerical model simulation for the month of April, 1998 and, buoyed by the fidelity between the two, uses the model to analyze the dynamics. A new finding is identified. The data show a rectification of the inner-shelf responses to synoptic wind forcing wherein upwelling favorable

winds produce disproportionately larger responses in both sea level and currents than downwelling favorable winds. Stratification accounts for the rectification, and this is most readily understood in terms of the streamwise component of vorticity. For downwelling favorable winds, the buoyancy torque due to isopycnals bending into the sloping bottom opposes the tendency by planetary vorticity tilting due to the vertically sheared coastal jet. This thermal wind effect negates the need for large relative vorticity dissipation by the across-shelf flow in the bottom Ekman layer. The opposite occurs for upwelling favorable winds. Buoyancy torque adds constructively with planetary vorticity tilting requiring larger dissipation of relative vorticity by the bottom Ekman layer. By enhancing (upwelling) or suppressing (downwelling) the bottom Ekman layer the entire response is reduced or increased, respectively. Such rectification is evident on the WFS because the WFS is wide enough to distinguish the frictional inner-shelf (which this paper also helps to better define) from the shelf break.

We are also applying the POM to three-dimensional analyses of hurricane storm surges along Florida's west coast. Yang and Weisberg (2000) reports on the effects of prototypical Saffir-Simpson Categories 2 and 4 hurricanes that approach Florida's west coast from several different directions and make landfall at several different locations. We show the space-time evolution of sea level along with sea level time series at specific points along the coast. Surge magnitude depends on local geometry and storm track, but for a given track it appears to scale approximately as the wind stress. Thus, for the recent "hurricane" Gordon we were able to surmise, from our real-time buoy winds (over which the storm closely passed) and model, that while the storm may have had hurricane winds aloft, it was not a hurricane on the ground. The ratio of the observed surge to that modeled (for a category 2 hurricane) scaled as the square of the observed and modeled wind speeds. Our results were disseminated to the NWS, emergency managers, and local weather reporters.

After laying the groundwork for interpreting our model results we are now using more realistic forcing functions to simulate longer-term WFS responses to local forcing. Our overall goal is to determine quantitatively the relative influences of local and deep ocean forcing on the west Florida shelf circulation on time scales from tidal to inter-annual and such forcing impacts material property distributions on the shelf. He and Weisberg (2001a) is a spring 1999 simulation in which the model, extending from west of the Mississippi River to the Florida Keys, is forced by NCEP reanalysis winds, surface heat fluxes (with flux correction), and river inflows (climatological). We show that local forcing, independent of the Loop Current, can account for the spring season transition and much of the synoptic scale variability. In preparation are similar manuscripts on other seasons (for which we have data) and on the inter-annual variations among these. This work will form the basis for a Ph.D. dissertation by R. He.

He and Weisberg (2001b) is an analysis of the four principal tidal constituents in the northeast Gulf of Mexico: M2, S2, O1, and K1. By forcing our

regional model at its open boundary by a global tidal model, we produce tidal current ellipses and sea level variations for comparison with *in-situ* observations. On the basis of these comparisons we describe the tides from the Mississippi River to the Florida Keys. We also analyze the tidal residual flows.

Finally, MMS support facilitated the Ph.D. dissertation of Dr. Zhenjiang Li.

Despite our inner-shelf emphasis we understand that offshore effects can permeate the inner-shelf in a variety of ways. We have not published specific results on this topic, but we did initiate collaborations with other groups that have larger scale models inclusive of the Gulf of Mexico Loop Current, and these collaborations are continuing. One way to approach this problem is to use the larger scale model fields to provide open boundary conditions for the regional scale model. Another way is to assimilate enough data directly into a regional model to maintain the baroclinic structure imposed by the deep ocean at the shelf break. We are exploring both approaches in our continuing research. Adequate initial fields and assimilative fields are required as are sufficient and accurate surface fluxes, by both *in-situ* measurements and atmosphere models, and we are progressing in each of these areas.

3c. Accomplishments
Refereed Publications

1) Li, Z. and R.H. Weisberg (1999a). West Florida Shelf response to upwelling favorable wind forcing, Part 1: Kinematics. *J. Geophys. Res*., 104, 13,507-13,527.

2) Li, Z. and R. H. Weisberg (1999b). West Florida Shelf response to upwelling favorable wind forcing, Part 2: Dynamics. *J. Geophys. Res*., 104, 23427-23442.

3) Yang, H. and R. H. Weisberg (1999). West Florida continental shelf circulation response to climatological wind forcing, *J. Geophys. Res*., 104, 5301-5320.

4) Yang, H., R.H. Weisberg, P.P. Niiler, W. Sturges, and W. Johnson (1999). Forbidden zone over the West Florida Shelf, *Cont. Shelf. Res*., 19, 1221-1245.

5) Weisberg, R.H., B. Black, Z. Li (2000). An upwelling case study on Florida's west coast, *J. Geophys. Res.*, 105, 11459-11469

6) Weisberg, R.H., Z. Li, and F.E. Muller-Karger (2001). West Florida shelf response to local wind forcing: April 1998. *J. Geophys. Res.,* 106, 31239-31262.

7) Walsh, J.J. K.D. Haddad, D.A. Dieterle, R.H. Weisberg, Z. Li, H. Yang, F.E. Muller-Karger, C.A. Heil, and W.P. Bissett (2002). A numerical analysis of the landfall of the 1979 red tide of *Karenia brevis* along the west coast of Florida - the fall/winter upwelling mode. *Cont. Shelf Res.,* 22, 15-38

8) He, R. and R.H. Weisberg (2002a). West Florida Shelf circulation and temperature budget for the 1999spring transition. *Cont. Shelf Res.,* in press.

9) He, R. and R.H. Weisberg (2002b). Tides on the West Florida shelf. *J. Phys. Oceanogr.*, submitted

10) He, R. and R.H. Weisberg (2002c). A Loop current intrusion case study on the West Florida Shelf. *J. Phys. Oceanogr.*, submitted.

11) Weisberg, R.H. and R. He (2002). Local and deep ocean forcing contributions to anomalous water properties on the West Florida Continental Shelf. *J. Geophys. Res.* Submitted.

12) Walsh, J.J., R.H. Weisberg, D.A. Dieterle, R. He, B.P. Darrow, J.K. Jolliff, K.M. Lester, G.A. Vargo, G.J. Kirkpatrick, K.A. Fanning, T.T. Sutton, A E. Jochens, D.C. Briggs, B. Nababan, C. Hu, and F. Muller-Karger (2002). The phytoplankton response to intrusions of slope water on the West Florida Shelf. *J. Geophys. Res.*, submitted.

Technical Reports and Dissertations

1) Li, Z. (1998). Upwelling circulation on the west Florida continental shelf. Ph.D. dissertation, Department of Marine Science, University of South Florida, St. Petersburg, FL., 33701.

2) Yang, H. and R.H. Weisberg (2000). A three dimensional numerical study of storm surges along the west Florida coast. COMPS Technical report, December 2000. USF College of Marine Science, St. Petersburg, FL. 33701, 54pp.

Representative Papers Appended

1) Weisberg, R.H., Z. Li, and F.E. Muller-Karger (2001). West Florida shelf response to local wind forcing: April 1998. *J. Geophys. Res.,* 106, 31239-31262.

2) He, R. and R.H. Weisberg (2002a). West Florida Shelf circulation and temperature budget for the 1999spring transition. *Cont. Shelf Res.,* in press.

In summary, we achieved our program objectives of developing a better understanding on how the WFS inner-shelf circulation responds to various forcing functions and the role of the seasonally varying stratification in modulating these responses. We published five papers in refereed scientific journals, three more are in press, and one is ready to be submitted. Additionally, we published a technical report on hurricane storm surge simulation and produced one Ph.D. The modeling work, greatly assisted by this MMS support, is presently continuing under NOAA/ECOHAB and ONR support. A preliminary version of a nowcast/forecast product is available at http://ocg6.marine.usf.edu.

The dissertation work of R. He (in progress) will further clarify the relative importance of local versus offshore forcing in determining the circulation of the NEGOM region. Our preliminary results show that much of the variability on both seasonal and inter-annual time scales can be accounted for by local forcing. We close this final report by noting that we will make additional important NEGOM contributions over the next year that had their beginnings with the funding herein.

4. References

Carton, James A., and Yi Chao, 1999: Caribbean Sea eddies inferred from TOPEX/ Poseidon altimetry and a 1/6^{o} Atlantic Ocean model simulation. *J. Geophys. Res.*, 104, 7743-7752.

Csanady, G. T., 1978: The arrested topographic wave*. J. Phys. Oceanogr*. 8,47-62.

Csanady, G. T., and Ping Tung Shaw, 1983: The “insulating” effect of a steep continental slope. *J. Geophys. Res.*, 88, 7519-7524.

Dietrich, D. E., D.-S. Ko, and L. A. Yeske, 1993: On the application and evaluation of the relocatable Diecast ocean circulation model in coastal and semi-enclosed seas. Technical Report 93-1, Mississippi State University, 71pp.

Frantantoni, Paula Sue, 1998: The formation and evolution of Tortugas Eddies in the southern Straits of Florida and Gulf of Mexico. Ph. D. Dissertation, University of Miami, Coral Gables, Florida.

Golubev, Yury, and Y. Hsueh, 2001: Temperature variability in the northeastern Gulf of Mexico in 1997-1998. Submitted to *Gulf of Mexico Science*.

He, R. and R.H. Weisberg, 2001a: The circulation and temperature budget on the west Florida continental shelf during the 1999spring transition. Cont. Shelf Res., in press.

He, R. and R.H. Weisberg, 2001b: Tides on the west Florida shelf observed and modeled. Draft complete for submittal to J. Phys. Oceanogr.

Hetland, R. D., 1999: The dynamics of a Loop Current forced shelf break jet on the west Florida shelf. Ph. D. dissertation, 69pp., Florida State University.

Hetland, Robert, Y. Hsueh, Bob Leben, and P. P. Niiler, 1999: A Loop Current-induced jet along the edge of the West Florida Shelf. *Geophys. Res. Letters*. 26, 2239-2242.

Hetland, Robert D., Ya Hsueh, and Dongliang Yuan, 2001: On the decay of a baroclinic jet flowing along a continental slope. *J. Geophys. Res.* 106, 19,797-19807.

Hsueh, Y., and Yury Golubev, 2001: A numerical model calculation of the flow in DeSoto Canyon in response to northerly wind bursts in winter. Gulf of Mexico Science., 20 (1), 44-59.

Huang, Haosheng, 2001: Embedded eddies in the Loop Current. Dissertation. Department of Oceanography, Forida State University. In preparation.

Hurlburt, H. E., and J. Dana Thompson, 1980: A numerical study of loop current intrusions and eddy-shedding. *J. Phys. Oceanogr.*, 10, 1611-1651.

Kalnay, E., M. Kanamitsu, R. Kistler, W. Collins, D. Deaven, L. Gandin, M. Iredell, S. Saha, G. White, J. Woollen, Y. Zhu, A. Leetmaa, R. Reynolds, M. Chelliah, W. Ebisuzaki, W.Higgins, J. Janowiak, K. C. Mo, C. Ropelewski, J. Wang, Roy Jenne, Dennis Joseph, 1996: The NCEP/NCAR 40-year reanalysis project. *Bulletin of the American Meteorological Society*, 77, 437-471.

Li, Z. and R.H. Weisberg, 1999a. West Florida Shelf response to upwelling favorable wind forcing, Part 1: Kinematics. *J. Geophys. Res*., 104, 13,507-13,527.

Li, Z. and R. H. Weisberg, 1999b. West Florida Shelf response to upwelling favorable wind forcing, Part 2: Dynamics. *J. Geophys. Res*., 104, 23427-23442.

Oey, L.-Y., 1996: Simulation of meso-scale variability in the Gulf of Mexico: sensitivity studies, comparison with observations, and trapped wave propagation. *J. Phys. Oceanogr*., 26, 145-175.

Pichevin, T., and D. Nof, 1997: The momentum imbalance paradox. *Tellus*, 49A, 298-319.

Pratt, L. J., and Melvin E. Stern, 1986: Dynamics of potential vorticity fronts and eddy detachment. *J. Phys. Oceanogr*., 16, 1101-1120.

Science Applications International Corporation, 1998: DeSoto Canyon eddy intrusion study. Data Products: Set 2 and Set 3. Science Applications International Corporation, Raleigh, North Carolina.

Sturges, W., and J. C. Evans, 1983: On the variability of the Loop Current in the Gulf of Mexico. *J. Mar. Res*., 41, 639-653.

Sturges, W., J. C. Evans, S. Welsh, and W. Holland, 1993: Separation of warm-core rings in the Gulf of Mexico. *J. Phys. Oceanogr*., 23, 250-268.

Sturges, W., 1994: The frequency of ring separation from the Loop Current. *J. Phys. Oceanogr.*., 24, 1648-1651.

Vukovich, F. M., B. W. Crissman, M. Bushnell, and W. J. King, 1979: Some aspects of the oceanography of the Gulf of Mexico via satellite and in situ data, *J. Geophys. Res*., 84,7749-7769.

Vukovich, F. M., 1986: Aspects of the behavior of cold perturbations in the Eastern Gulf of Mexico: a case study. *J. Phys. Oceanogr*., 16, 175-188.

Walsh, J.J. K.D. Haddad, D.A. Dieterle, R.H. Weisberg, Z. Li, H. Yang, F.E. Muller-Karger, C.A. Heil, and W.P. Bissett, 2001. A numerical analysis of the landfall of 1979 red tide of *Gymnodinium breve* along the west coast of Florida - the fall/winter upwelling mode. Cont. Shelf Res., in press.

Weisberg, R.H., B. Black, Z. Li, 2000. An upwelling case study on Florida's west coast, *J. Geophys. Res.*, 105, 11459-11469.

Weisberg, R.H., Z. Li, and F.E. Muller-Karger, 2001: West Florida shelf response to local wind forcing: April 1998. J. Geophys. Res., in press.

Welsh, S. E., 1996: Numerical simulation of Gulf of Mexico circulation under present and glacial climate conditions. Ph. D. dissertation, Louisiana State University, 146pp.

Yang, H., R.H. Weisberg, P.P. Niiler, W. Sturges, and W. Johnson, 1999. Forbidden zone over the West Florida Shelf, *Cont. Shelf. Res*., 19, 1221-1245.

Yang, H. and R.H. Weisberg, 2000: A three dimensional numerical study of storm surges along the west Florida coast. COMPS Technical report, December 2000. USF College of Marine Science, St. Petersburg, FL. 33701, 54pp..

5. Appendix

5a. A numerical model calculation of the flow in DeSoto Canyon in response to northerly wind bursts in winter

A Numerical Model Calculation of the Flow in DeSoto Canyon In Response to Northerly Wind Bursts in Winter

by

Y. Hsueh and Yury Golubev
Department of Oceanography
Florida State University
Tallahassee, FL 32306

Abstract

The continental shelf currents observed at the head of DeSoto Canyon offshore of Pensacola, Florida, during November 1997-February 1998 are studied with the aid of a Bryan-Cox model of the entire Gulf of Mexico. The basic model circulation with no winds features a Loop Current and a weak flow in DeSoto Canyon. In contrast, the model response to northerly wind bursts produces strong Canyon currents. Wind-driven southward currents on the West Florida Shelf (WFS) appear to pull a strong flow around DeSoto Canyon, giving rise to a strong up-canyon flow on the west flank. The wind-enhanced flow in DeSoto Canyon is reproduced with a model run that incorporates wind stresses derived from the NCEP/NCAR reanalysis winds for March 1997-April 1998. The model flow for the winter period (November 1997-February 1998) is compared to observed currents at three canyon-head locations in 100m of water available from a Science Applications International Corporation (SAIC) mooring experiment. Model and observed velocities in the general around-Canyon direction track each other reasonably well with peaks synchronized roughly with but lagging slightly northerly wind bursts. The lag time appears consistent with the generation at Key West of first-mode continental shelf waves responsible for wind-driven alongshore currents on the WFS. Pressure gradient slightly in excess of that necessary for a geostrophic balance with the (eastward) alongshore flow appears to generate onshore flows, giving rise to coastal upwelling following northerly wind bursts.

1. Introduction

The wintertime, wind-driven continental shelf currents in DeSoto Canyon are studied using a Bryan-Cox model of the entire Gulf of Mexico. DeSoto Canyon is a broad, northward tending submarine canyon south of the Florida Panhandle coast in the northeastern Gulf of Mexico (NEGOM) with the 200m isobath just 72km away from the coast (at approximately 30°24'N) (Figure 1a). The width of the canyon measured at the 100m isobath along 29° 30'N is about 120km, much greater than the 24km internal deformation radius based on climatology. It is known that warm Gulf-of-Mexico water can move shoreward along the western rim of the canyon to within 8 km of the shore during northerly wind bursts in winter (Huh et al., 1981). Additional current measurements have since become available that bear upon the intrusion issue. The additional data come from the Science Applications International Corporation (SAIC) mooring experiment of March 1997 - April 1998, which includes three head-of-the-canyon moorings along the 100m isobath, C1 (87°21.0'W, 29°35.15'N), D1 (86° 50.5'W, 30°04'N), and E1 (86°19.73'W, 29°42.0'N) (see Figure 1b). The purpose of the present paper is to present a comparison of the model current with these measurements for the wintertime intrusion flow in DeSoto Canyon and to suggest, on the basis of model dynamics, that the intrusion flow may be a wind-driven response of continental shelf water in NEGOM as a whole. This basic response seems to explain the long suspected episodic intrusion of deep Gulf water along the western rim of the Canyon (Schroeder et al., 1994).

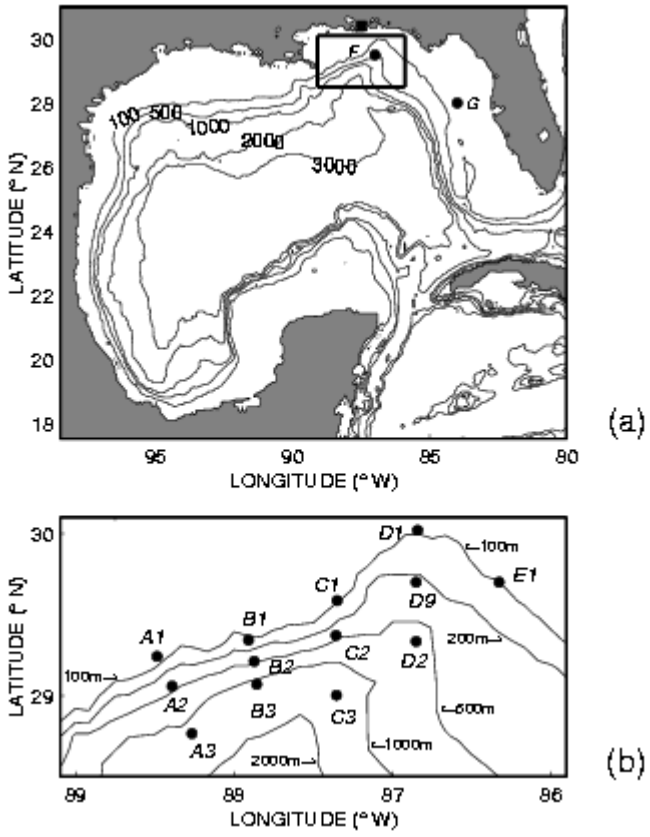

Figure 1. (a). Topography of the Gulf-of-Mexico model. Contours shown are 100, 500, 1000, 2000, 3000m. Solid circles, F and G, mark locations where inflow-outflow model experiment time series are extracted. The solid square at the top marks Pensacola where the model wind-stress time series are shown. (b). SAIC moorings. Data from C1, D1, and E1 form the basis for model verification.

Submarine canyon flows have been studied on both coasts of the United States mostly with canyon width less than or on the order of the internal deformation radius (Klink, 1996; Hickey, 1997; She and Klinck, 2000). The wind-driven continental shelf flow in the vicinity of such deep and narrow canyons exhibits characteristics consistent with intense generation of relative vorticity due to vortex stretching (Hickey, 1997). In the case of broad canyons, as is the case at hand where the deformation radius is much less than the radius of curvature of the isobaths, the dynamics are predominantly linear (Klinck, 1996). In this case, the flow is expected to go approximately along isobaths and to exhibit the familiar linear dynamics (Hsueh, 1980). In the concept of such a flow, DeSoto Canyon thus becomes an extension of the WFS. It has been shown that wind-driven sea-level heights over the WFS are reasonably explained by the linear long-wave theory (Mitchum and Clarke, 1986). It stands to reason that the flow in DeSoto Canyon is just a part of this wave response. In addition, on the long-term, Sturges and Evans (1983) find that the 8-month band sea-level fluctuations along the west Florida coast interpreted as southward currents are coherent with, but lead, the northward penetration positions of the Loop Current, indicating Loop Current influence.

To study the intrusion in DeSoto Canyon with both these forcing possibilities, a model of the entire Gulf of Mexico is constructed (see Figure 1a for the model domain). The model is of a Bryan-Cox type (Cox, 1984) with a rigid-lid with increased vertical resolution in the upper water column to resolve the topography of the continental shelf and slope west of the Florida peninsula. (For future reference, the rigid-lid assumption produces a slight error in the phase speed of the continental shelf wave. The error is on the order of the square of the ratio of shelf width to the barotropic deformation radius, thus quite negligible even for a shelf as wide as the WFS (Clarke, 1977).) The forcing in the model includes wind stress at the surface and open boundary conditions in the Caribbean Sea and in the Straits of Florida. The southern boundary of the model cuts through the Caribbean Sea so that the structure of the inflow through the Yucatan Straits is not specified as in Hurlburt and Thompson (1980). A volume transport of 30 Sv is imposed across the southern open boundary and through the Straits of Florida to represent the mean Loop Current transport. No attempt has been made to study the model sensitivity to the flow specification at these open boundaries. The purpose is to achieve a Gulf of Mexico model with a broad-scale representation of the circulation to serve as background for a few process studies in continental shelf waters.

Since the pioneering numerical work of Hurlburt and Thompson (1980) in which Loop Current ring shedding was reproduced for the first time, there have been several more models of the Gulf-of-Mexico basin-wide circulation (Dietrich et al., 1993, Oey, 1996; Welsh, 1996; Frantantoni, 1998). Except for the high resolution (7 km) model of Frantantoni (1998) used to study Dry Tortugas eddies, these models, as well as that of Hurlburt and Thompson (1980), are designed to

focus on the circulation in the western Gulf of Mexico and the evolution and role of the anti-cyclonic rings generated from the Loop-Current. As such, they lack the vertical resolution necessary to resolve the continental shelf topography west of Florida. Oey (1996) uses improved vertical resolution to include a continental shelf and successfully simulates the irregular shedding of Loop Current rings. The Loop Current and the migration path of its rings in Oey (1996), as in the present model, bend unrealistically to the west, hinting at an overly diffusive representation due perhaps in part to a lack of horizontal resolution. Even though the present model uses a biharmonic formulation, the flow is still too frictional so that there is a complete absence of filaments and parasite eddies often observed around the Loop Current (Perez et al., 1999) and the model Loop Current never reaches so high a latitude as the observed 28^{o}N (Sturges, 1992).

The outline of the paper is as follows. In the next section, a description is given of the model configuration and then in section 3 are reported model flows driven by the Loop Current. Section 4 considers the response of the WFS and the DeSoto Canyon waters to winds during November 1997- February 1998, the SAIC experiment winter period. The dynamics of the flow are discussed in section 5. A final section 6 contains the conclusions.

2. The Model

As mentioned above, the model used in this study is the z-level model of Bryan-Cox's (Cox, 1984). The model domain covers the entire Gulf of Mexico, from 18^o N to 31^{o}N and from 100^o W to 80^o W, with topography obtained from the 5-minute ETOPO global relief model (see Figure 1a). The horizontal grid resolution is 1/6^o by 1/6^o. The total number of levels in the vertical is 30, with larger vertical spacings in the deeper ocean. The smallest vertical spacing is 10 m at the sea surface, small enough only to give the Ekman veering and transport crucial for the Ekman-geostrophic response in coastal waters, which is more important here than the detailed Ekman layer structure not resolved. The number of levels above the 200 m depth is 8 and the number of levels above the 1000 m depth is 16. With this grid, both the continental shelf and the continental slope are reasonably resolved.

At the southern open boundary across the Caribbean Sea, a 30 Sv (1 Sv=$10^6 m^3 s^{-1}$) volume transport is specified across a 100 km section next to the Yucatan Peninsula to represent nominally the western boundary current of the Caribbean Sea. The same volume transport leaves the model domain through a 100 km section in the northern Straits of Florida at the eastern open boundary. A five-grid-interval buffer layer is used along the open boundaries to relax salinity and temperature fields to their climatological values (Levitus et. al., 1994; Levitus and Boyer, 1994) and the velocity to the geostrophic velocity. The geostrophic velocity at the open boundaries is obtained by combining the barotropic velocity based on the specified transport with the thermal-wind velocity calculated from the climatological tracers fields. The relaxation coefficients at the open boundaries correspond to time scales of a few hours. Weak relaxation with a

time scale of 50 days is used at the sea surface for temperature and salinity. Radiation boundary conditions for temperature, salinity, and velocity similar to that of Carmelengo and O'Brien (1980) are used on the eastern open boundary. The strategy of the open-boundary condition specification has been explained in detail in Schultz (1994) and in Hsueh et al. (1997). It must be noted that the inflow and outflow conditions are probably far too simple to represent the full reality. Again, the aim here is to achieve in a broad sense an inflow-outflow configuration for the Gulf of Mexico for process studies. The effect of open boundary conditions on the flow is obviously a worthy study subject on its own right but is outside the present scope.

At closed boundaries, the no-slip velocity and no-normal-flux temperature and salinity conditions are employed. A biharmonic horizontal mixing formula is used in the momentum and tracer equations with a biharmonic coefficient of $-4x10^{18}cm^4s^{-1}$. The use of a biharmonic formulation is intended to reduce damping and preserves the nonlinear characteristics of inertial currents (Holland, 1978). (The model, however, still proves too diffusive (see later).) Vertical mixing and diffusion are embodied in a Laplacian with a coefficient of $1cm^2s^{-1}$. The quadratic-law bottom friction is used in the momentum equations with a friction coefficient of 10^{-3}. The model is initialized with climatological temperature and salinity fields and with a geostrophic velocity field obtained from adding the climatological thermal-wind velocity to the barotropic velocity forced by the imposed transports (Hsueh et al., 1997).

3. An Inflow-Outflow Experiment

In order to assess the influence of the Loop Current on the circulation over the WFS and inside DeSoto Canyon, a run (referred to as GOM-01) is first made of the model without the wind stress. Under the forcing of the open-boundary conditions, the inflow-outflow combination gives rise to a Loop Current in the Gulf of Mexico, which sheds anti-cyclonic rings of 300-400 km radius at a period of around 13 months. The lack of a spread in separation periods points to the fact that the model leaves out important factors which contribute to the Loop Current behavior and ring separation (Sturges, 1994; Sturges and Leben, 2000). It does however conform to what is anticipated in an analytical theory (Pichevin and Nof, 1997).

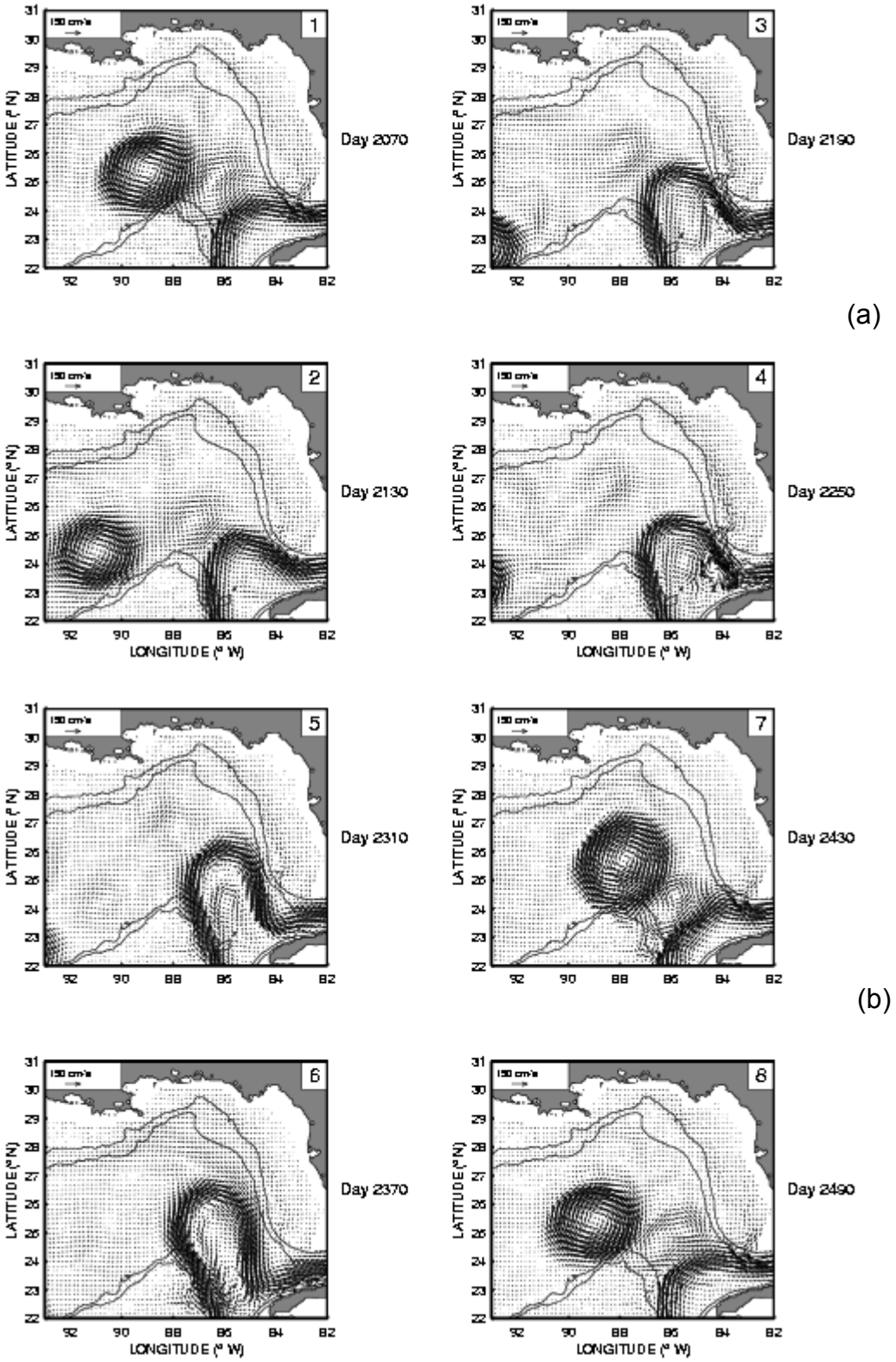

Figure 2 Evolution of velocity at the 5 m depth in the inflow-outflow experiment in eight panels (panels 1-4 in Figure 2a and panels 5-8 in Figure 2b) dated in integration days and numbered in the upper right corner. The 200 m and 1000 m isobaths are plotted to identify the shelf area.

Figures 2a and 2b show, in eight panels, the evolution of the 5m velocity over NEGOM through a typical ring-shedding cycle of the model integration. On Day 2070 of the run (Panel 1), an anti-cyclonic ring is clearly seen separated from the main stream of the Loop Current and the Loop Current has retreated to near its southernmost position. The isolated current ring proceeds to move to the west and southwest at a speed of about 4cms^{-1} as is found elsewhere (Sturges et al., 1993). In the meantime, the Loop Current begins to grow northward. In early stages in this growth (Panels 3-4), a shelf-break jet is seen formed, apparently from the impingement of the Loop Current on the WFS (see later). As the Loop Current reaches nearly its maximum northward penetration with its axis at its closest to the WFS (Panels 5-6), a weak cyclonic eddy is gaining in strength southwest of Key West. This cyclonic eddy grows and moves to the west and causes a "necking-down" of the Loop Current, leading to the eventual separation of an anti-cyclonic current ring (Panels 7-8) (Vukovich et al., 1979; Pratt and Stern, 1985; Vukovich, 1986). The spawning of this cyclonic circulation cell and its possible triggering effect for ring separation have been widely acknowledged (Hurlburt and Thompson, 1982; Dietrich and Lin, 1994; Frantantoni, 1998). It takes about a year for the model Loop Current to regain its full penetration and start another round of ring shedding. The model ring shedding cycle repeats itself and constitutes the anticipated simplified periodic solution found in theoretical studies (Pichevin and Nof, 1997). In reality, the ring shedding is quite aperiodic and the appearance of the Loop Current is irregular with filaments and parasite eddies, exposing the overly diffusive nature of the present model run (see Oey, 1995 for a successful model in this regard).

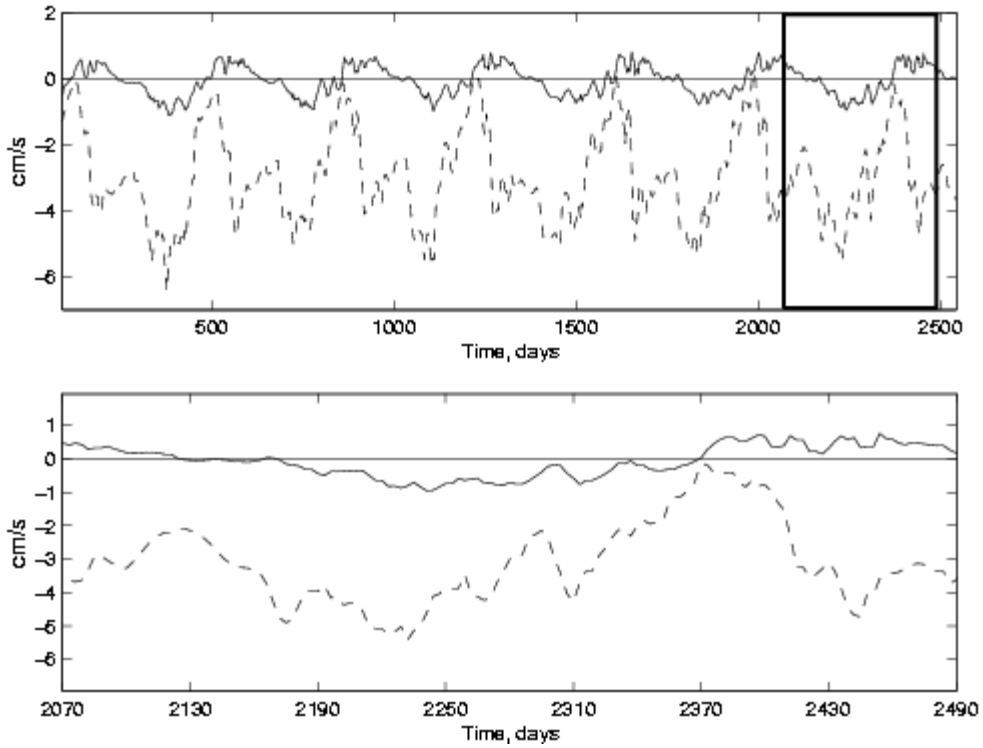

Figure 3 Time series of north-south velocity component (dashed) at 5 m depth at 84° W, 28° N (G in Figure 1a) on the WFS in the inflow-outflow experiment. The upper panel shows the time series during more than five years of integration. The lower panel shows the boxed portion of time series in the upper panel. The expanded portion covers the time window of Figure 2. The horizontal lines are zero velocity lines.

The influence of this simple model Loop Current evolution on the WFS circulation is shown in Figure 3. The upper panel shows the evolution of the north-south velocity component (dashed) (the solid curve is for the east-west velocity which is much weaker) for more than 5 years at the 5 m depth in 40 m of water at the solid circle marked G in Figure 1a (84° W, 28° N) off Tampa. The velocity at this location is qualitatively representative of the velocity on the WFS. The mean current over the time span is southward, suggesting that, on the average, the Loop Current generates a shelf flow to the south. The oscillation on the ring-shedding period appears phase-locked to the ring-shedding cycle. The time span of each trough (large southward velocity) roughly begins with the time when a ring has just separated (Panels 2 and 3 in Fig. 2).

The lower panel shows an expanded portion of the north-south velocity time series. The expanded portion corresponds to the time window spanned by Figure 2. Notice that, at the time (marked 2370) when the Loop-Current front is closer to the WFS, the southward drift over the shelf is weaker than, say, that on Day 2250 when the front is farther away. This suggests that the flow over the

shelf is not simply generated frictionally by the Loop Current. The forcing of the Loop Current on the shelf circulation must be through other mechanisms. It turns out that the drop in dynamic pressure brought about by the Bernoulli effect as the Loop Current careens along the continental slope/shelf edge after it collides with the continental mass effects just such a flow in accordance with the arrested topographic wave (ATW) theory (Csanady, 1978; Csanady and Shaw, 1983). The manner with which this along-shelf-edge pressure change is imposed varies with the Loop Current position. This change in shelf-edge pressure as a function of the Loop Current position induces a corresponding change in shelf flow making the southward flow to appear to lead the northward position of the Loop Current (Sturges and Evans,1983). The detailed steady-state physics of this pressure forcing process is discussed elsewhere (Hetland et al., 1999). Based on the evidence so far presented, it suffices to say that the model Loop Current generally forces a southward flow over the WFS and the low-frequency variations of the flow occur primarily at the Loop Current ring-shedding frequency.

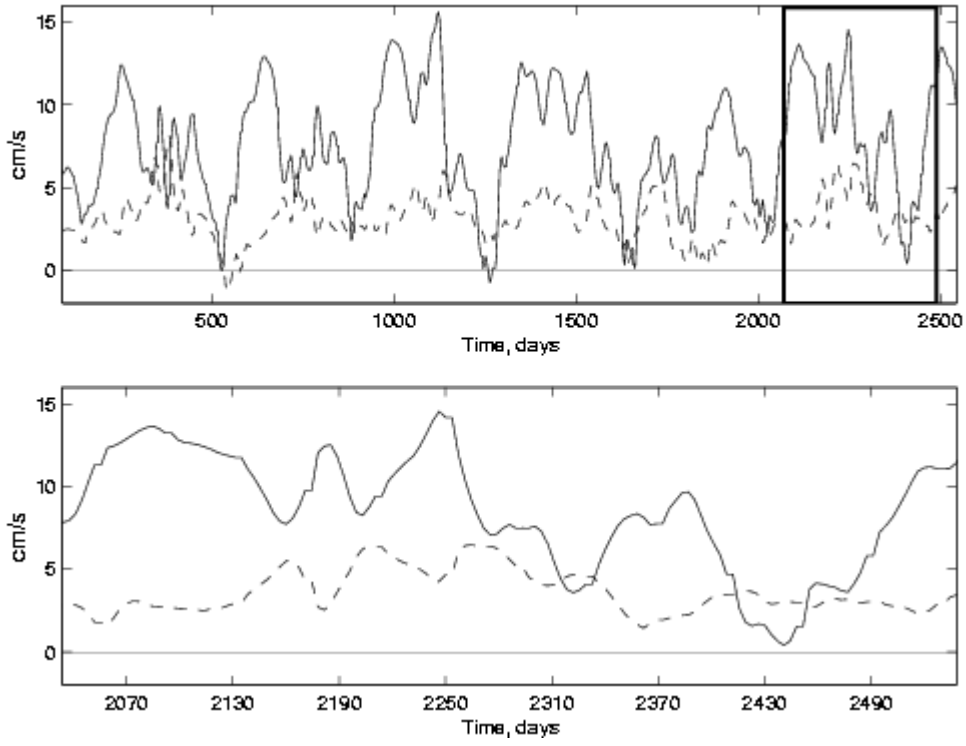

Figure 4 Time series plot same as in Figure 3, but at 87^{o}W, 29.5^{o}N (F in Figure 1a) inside DeSoto Canyon. Solid curve represents the east-west velocity component and dash curve represents the north-south component. The horizontal lines are zero velocity lines.

The influence of the model Loop Current variation on the circulation inside DeSoto Canyon is shown in Figure 4, in which are plotted, over the same time period as in Figure 3, the velocity time series at 5 m depth in 324 m of water at the solid circle marked F in Figure 1a (87^o W, 29.5^o N) at the center of DeSoto Canyon. The solid curve represents the east-west velocity component and the dashed curve represents the north-south velocity component. The east-west component is particularly comparable to the north-south component shown in Figure 3, both being roughly alongshore. The east-west component time series in Figure 4 shows more irregularities, but the phase-lock with the Loop Current variation emerges again. Again, larger velocity tends to occur at a time when the Loop Current is farther away to the south (Day 2250 vs. Day 2310). The alongshore flow in DeSoto Canyon appears simply to respond to the southward flow over the WFS. This is again consistent with the ATW theory and attributable to the insulating effect of the continental slope topography, confining the shelf flow to follow roughly the isobaths. The east-west velocity component at the solid circle F thus varies similarly with the north-south velocity component at G, 180^o out of phase with the extent of the northward penetration of the Loop Current. A time-distance contour plot (not shown but see www.ocean.fsu.edu/oce/gom) of east-west velocity at 5m along the meridian through F from 26^o N to 30^o N shows that not until the latitude of 27^o N is reached does the east-west velocity begin to vary in phase with the northward penetration of the Loop Current.

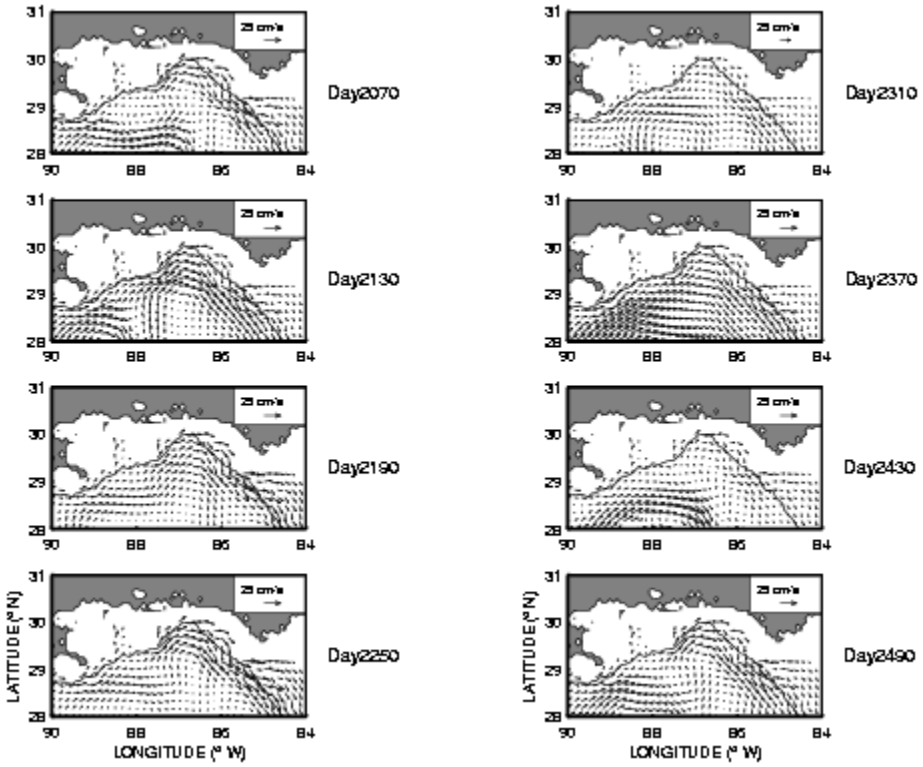

Figure 5 Horizontal velocity charts at 16.4m in the DeSoto Canyon area in the inflow-outflow experiment. The times of the panels correspond to those in Figure 2. The 100 m isobath is drawn to identify DeSoto Canyon.

Figure 5 shows the velocity vector plots at 16.4m in the DeSoto Canyon area at the time of the eight panels in Figure 2. The Loop Current-driven flow inside DeSoto Canyon remains weak and basically follows the isobaths. Since the observed intrusion in DeSoto Canyon suggests strong currents, causes in addition to the low-frequency influence of the Loop-Current must be found to explain the intrusion. It must be stressed that the results of weak direct Loop Current influence in both the WFS and DeSoto Canyon are probably a model artifact due to the inability of the model in resolving Loop Current filaments and parasite eddies. Model runs with better resolution and mixing representation than used in the present run are needed to address the influence of these small-scale Loop Current structures. With their influence suppressed, the model presents an opportunity for studying, in almost a default isolation, other factors influencing continental shelf flows in NEGOM, such as the wind.

4. A Hindcast for November 1997 – February 1998

Direct current measurements made by Science Applications International Corporation (SAIC) in NEGOM, particularly at the head of DeSoto Canyon for March 1997 - April 1998 become recently available. To take advantage of the opportunity thus provided, a hindcast (GOM-09) for currents is conducted with the imposition at the model sea surface of 6-hourly wind stresses converted from the 10 m surface winds from the NCEP/NCAR 40-year reanalysis data (Kalnay et al., 1996), using a drag coefficient of 1.3×10^{-3}. (Time series plots (not shown but see www.ocean.fsu.edu.edu/oce/gom) of NCEP/NCAR winds together with those observed at Pensacola and at a number of buoys in the northeastern Gulf of Mexico show that the two track each other closely most of the time.) The initial condition is the GOM-01 output at Day 2070 (Panel 1 in Figure 2). A TOPEX/Poseidon sea-surface height anomaly map for March 1, 1997 (not shown but see www.ocean.fsu.edu.edu/oce/gom) shows approximately the same Loop Current position as in the chosen frame of the GOM-01 output.

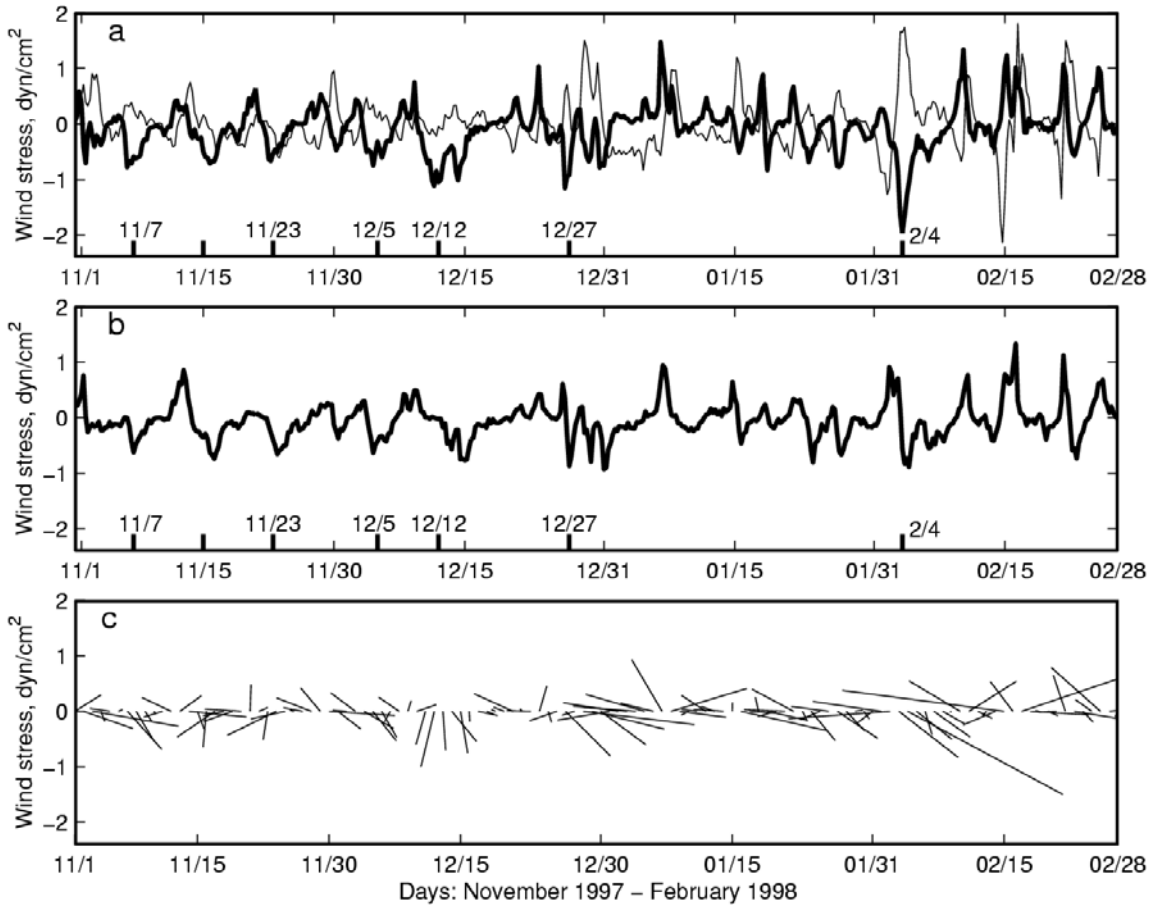

Figure 6 Plot of the model-used 6-hourly wind stress at Pensacola in November 1997 – February 1998. The upper panel shows the time series of the east-west (thin) and north-south (heavy) components of the wind stress. The lower panel shows the stick plot of the daily averaged Pensacola wind stress. Times of northerly wind bursts discussed are marked with heavy tick marks. In the middle panel, the model north-south wind stress component time series at a point (84.45°W, 27.07°N) on the WFS south of G is shown.

Figure 6 shows the model wind-stress time series at Pensacola for the selected hindcast period. The middle panel shows the model north-south wind stress at a point south of G at (84.45°W, 27.07°N). A number of northerly wind bursts are clearly identifiable (November 7, 15, 23, December 5,12-15, 27, and February 4, for example). Each burst lasts for several days and then collapses.

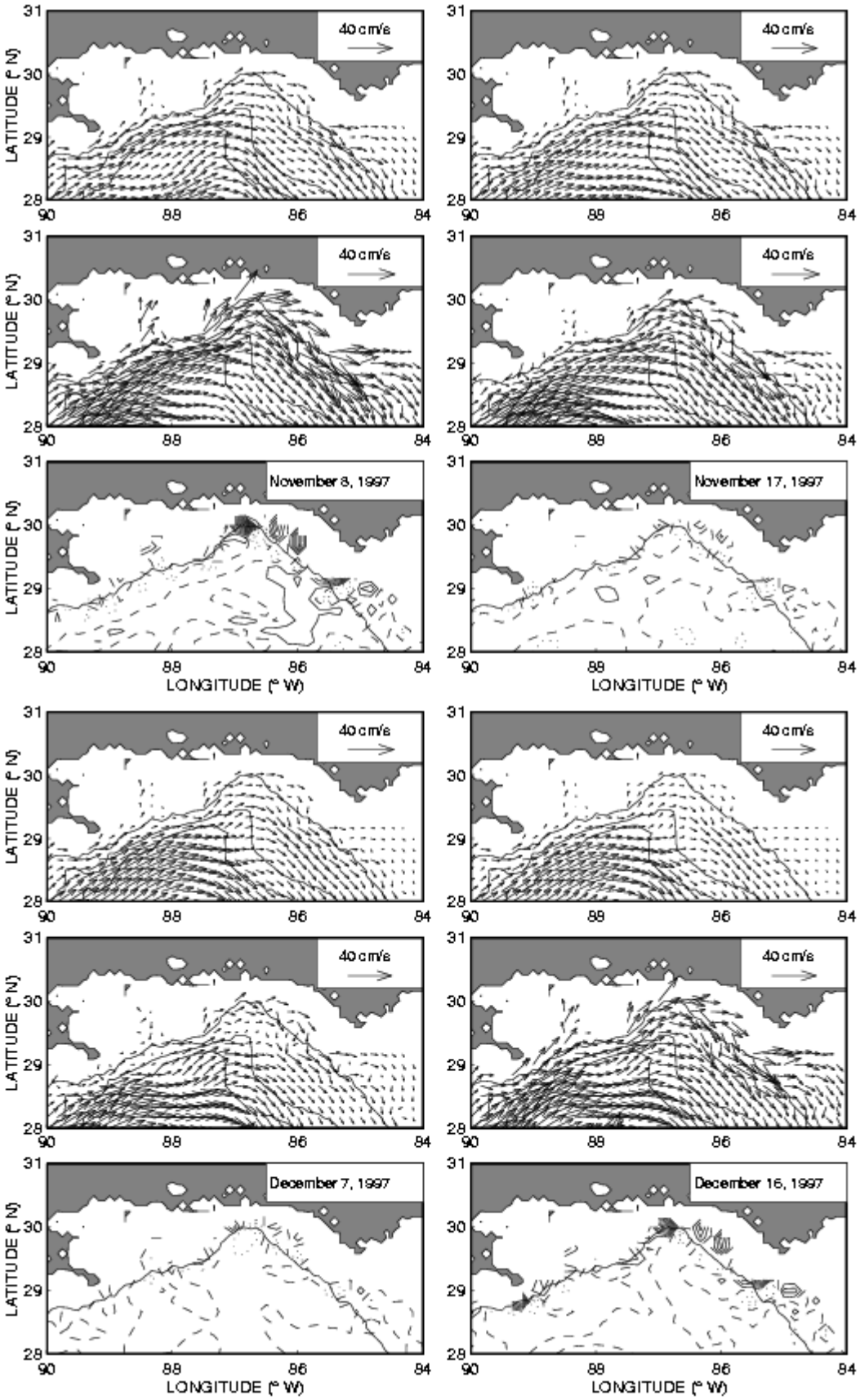
40 cm/s
LATITUDE (° N)
LONGITUDE (° W)
31
30
29
28
90
88
86
84
November 8, 1997
November 17, 1997
December 7, 1997
December 16, 1997

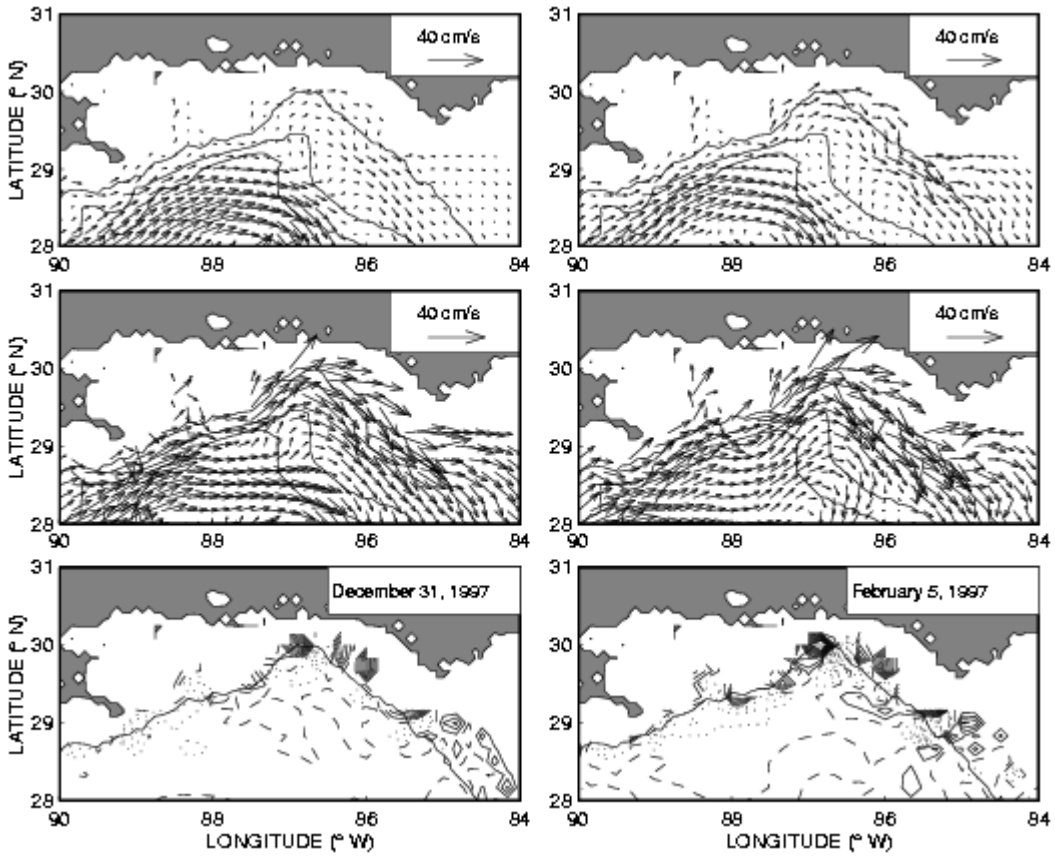

Figure 7 Model velocity vector plots at 16m in the DeSoto Canyon area during northerly wind bursts. Plots are for November 8, 17 (Figure 7a), December 7, 16 (Figure 7b), December 31 and February 5 (Figure 7c). For each case, the corresponding plot from the inflow-outflow experiment is shown in the top panel. The plot from the hindcast is in the middle. The plot of the vertical velocity in contours of $2x10^{-3}cms^{-1}$ appears in the bottom panel, where the zero contour is dashed and negative values are contoured in dashed curves. The 100m isobath is drawn to identify DeSoto Canyon.

Figure 7 presents comparison between the hindcast and the inflow-outflow experiment (GOM-01) in terms of DeSoto Canyon area velocity vector plots at the time about one to two days later of several of these wind burst events (with Day 2070 in GOM-01 as March 1, 1997). The hindcast clearly produces strong onshore flows on the west flank of DeSoto Canyon not otherwise present. To verify this hindcast model response, use is made of SAIC direct current velocity measurements during November 1997 – February 1998 at C1 ($87^{o}21.0'W$, $29^{o}35.15'N$), D1 (86^{o} 50.5'W, 30^{o} 04'N), and E1 ($86^{o}19.73'W$, $29^{o}42.0'N$) (see Figure 1b).

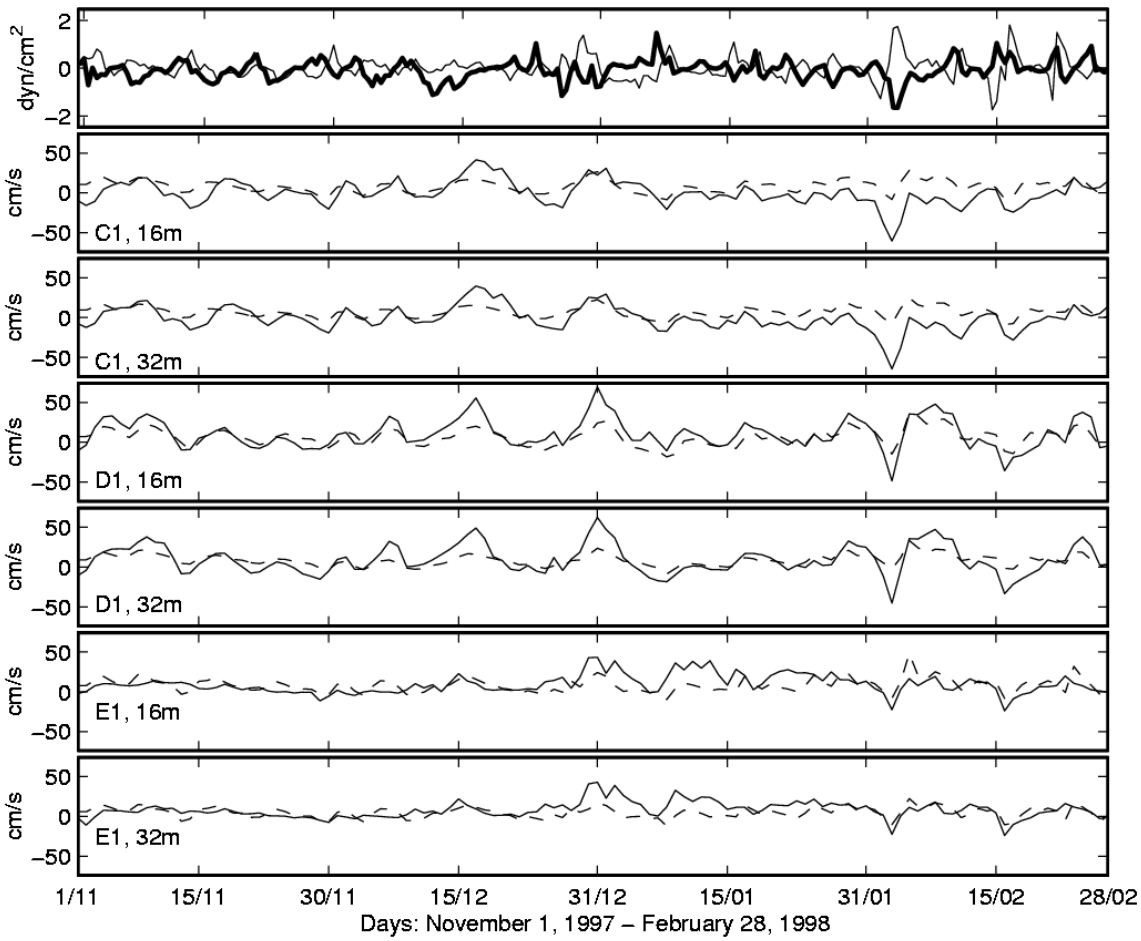
dyn/cm2
2
0
−2
cm/s
50
0
−50
C1, 16m
C1, 32m
D1, 16m
D1, 32m
E1, 16m
E1, 32m
1/11
15/11
30/11
15/12
31/12
15/01
31/01
15/02
28/02
Days: November 1, 1997 – February 28, 1998

(a)

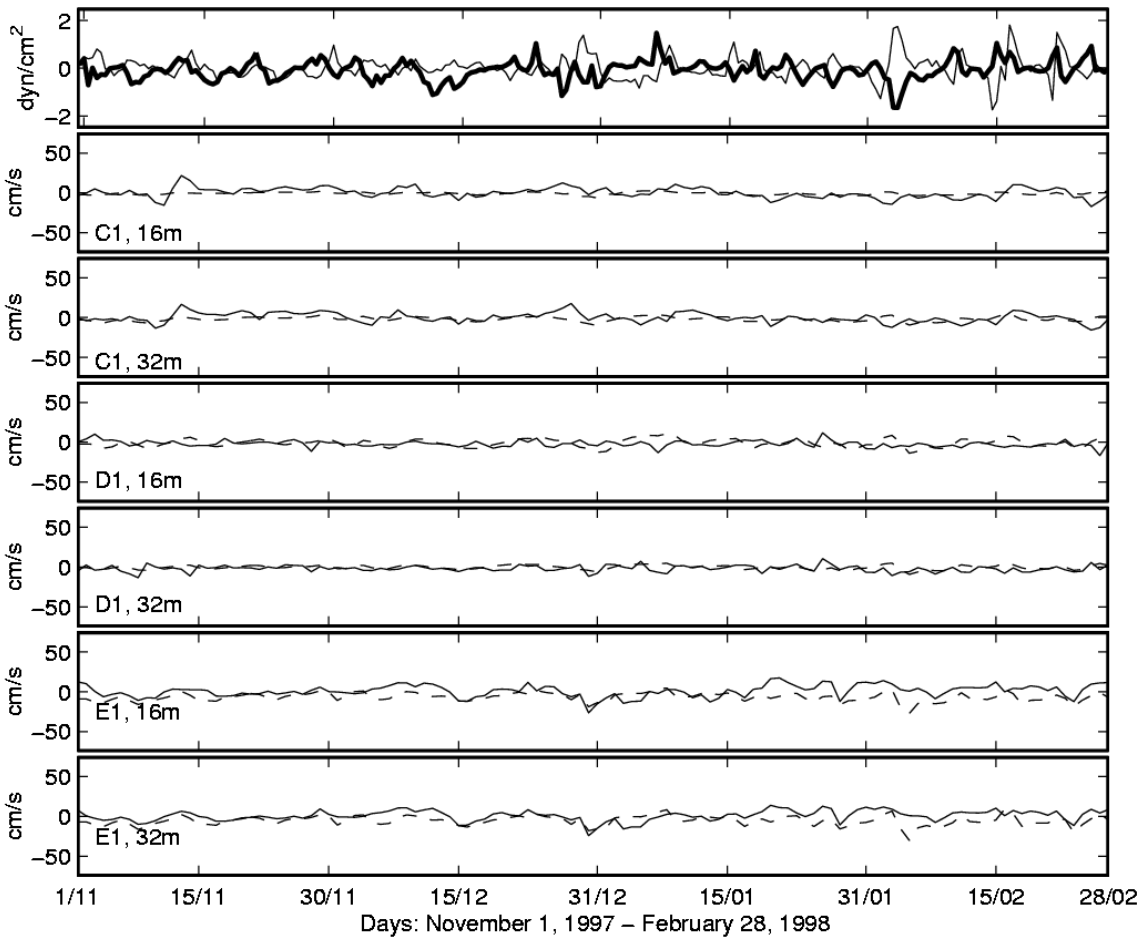

(b)

Figure 8 Time series plots of (a) around-canyon and (b) crosswise velocity components at 16m and 32m at C1, D1, and E1 for November 1997 – February 1998. The model results are dashed and observations are solid. The wind stress component time series shown in Figure 6 is reproduced in the upper panel for easy comparison.

Figure 8 shows time series comparisons, at two interior depths 16 and 32m, of the around-canyon and crosswise velocity components from data with the corresponding calculation from the model. (Because of the bottom slope, the depth of 48m represents the last depth for which model velocities are calculated at D1.) The local around-canyon directions (positive y-axis) are 45^{o}, 75^{o}, and 170^{o} clockwise from north for C1, D1, and E1, respectively. The crosswise direction (positive x-axis) is generally offshore. At all locations, there is a measure of similarity in the around-canyon component between the observation and the hindcast. In particular, the strong model flow as indicated by the around-canyon velocity peaks shortly after northerly wind bursts of November 7, 15, 23, December 5, 12-15, 27, and February 4 seems well substantiated by the direct

measurements. In all events, the current lags slightly the wind. This is consistent with the notion that the DeSoto Canyon flow simply responds to the southward flow on the WFS which is established by the passage of continental shelf waves originated at the end of the WFS following the onset of each wind burst (Mitchum and Clarke, 1986).

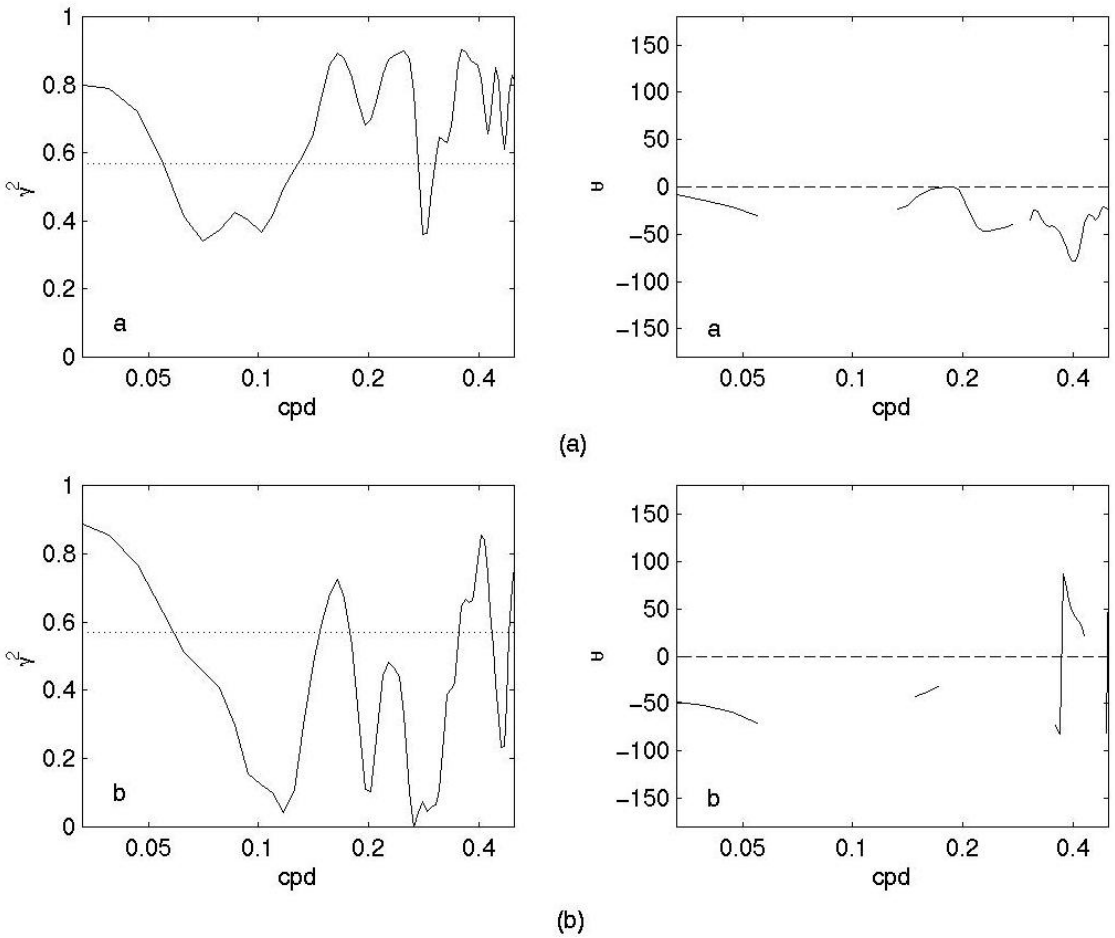

Figure 9. Coherence squared (γ^2) and phase (θ) with cycles per day (cpd) between the 6-hourly north-south wind component and 6-hourly around-canyon velocity at station D1 at the depth of 16m for (a) modeled currents and (b) observed currents. The dashed line in the coherence squared plots indicates the 95% confidence level. Negative phase indicates the wind leads. Phase is calculated only for the frequency band in which the coherence squared is above the 95% confidence level.

Figure 9 shows the coherence squared and phase between the north-south wind component and the around-canyon current at station D1 at the depth of 16m. In the three to ten-day band, a lag of a couple of days is detected for the around-canyon currents, both observed and modeled, consistent with the first mode continental shelf wave phase speed for the WFS (Mitchum and Clarke, 1986)). There is little similarity in the crosswise component, which is much weaker. The difficulty is typical of that encountered in modeling cross-shore flows on the continental shelf (Hsueh, 1989).

There remains the question of the degree to which the around-canyon flow is locally driven by the east-west wind bursts of which there are several at the time of north-south wind bursts (for example, December 31 and February 4). In order to address this issue, three model runs with a constant wind stress to the southeast (at 1 dyne/cm^2 for the components) are conducted from a common initial condition: one with the wind over the entire Gulf of Mexico, one with the wind covering only the domain east of 87^{o}W, and one with the wind covering the domain east of 88^{o}W with the wind stress ramping from zero at 88^{o}W to the constant value of 1dyne/cm^2 at 87^{o}W for both components. Against these runs, a control run is made with no wind forcing. In each case the model is run for 15 days. (The continental shelf flow pattern becomes steady at about the 10-day mark.) The around-canyon velocity at station D1 at 32m from the run with no wind is then subtracted from that from the three experimental runs. The wind-driven around-canyon velocity thus obtained differs very little (3 cm/s in 40 cm/s), with the one from the experiment with the forcing ramp the greatest. This result indicates empirically that the local wind-driven around-canyon velocity is small. Theoretically, one could estimate the amplitude of the first-mode continental shelf wave at D1 by integrating along the characteristics (in this case, the 100m isobath) the along-characteristics wind-stress from Key West to D1 (see, for example, Mitchum and Clarke, 1986). Since the east-west running portion of the isobath is relatively short compared with the north-south running portion on the WFS, it stands for reason that the amplitude contribution from east-west wind forcing in the neighborhood of D1 will be small. A few words for the event around February 4 are in order. Although, the winds at Pensacola are northerly, those on WFS are actually southerly a couple of days earlier (see Figure 6, middle panel). This southerly wind drives a northward coastal flow, leading to a negative around-canyon velocity on February 4 (Figure 8a).

The idea that the DeSoto Canyon flow is but a part of the continental shelf flow over the NEGOM is demonstrable with the hindcast model output. Figure 10 shows a time-distance plot of the north-south velocity at 48m for the hindcast period along the parallel at 29^{o}40'N for the segment spanned by C1, D9, and E1 (see Figure 1b). (No data return at shallower depth than 48m at D9.) During this winter period, it is clear that the flow is predominantly northward (red) on the west half and southward (blue) on the east. The contrast is particularly strong for the times of northerly wind bursts. The plot from interpolation from observed currents at C1, D9, and E1 shows a similar tendency. Thus the flow around

DeSoto Canyon is clockwise under these northerly wind bursts, connecting the flow off the Florida Panhandle with that of the WFS.

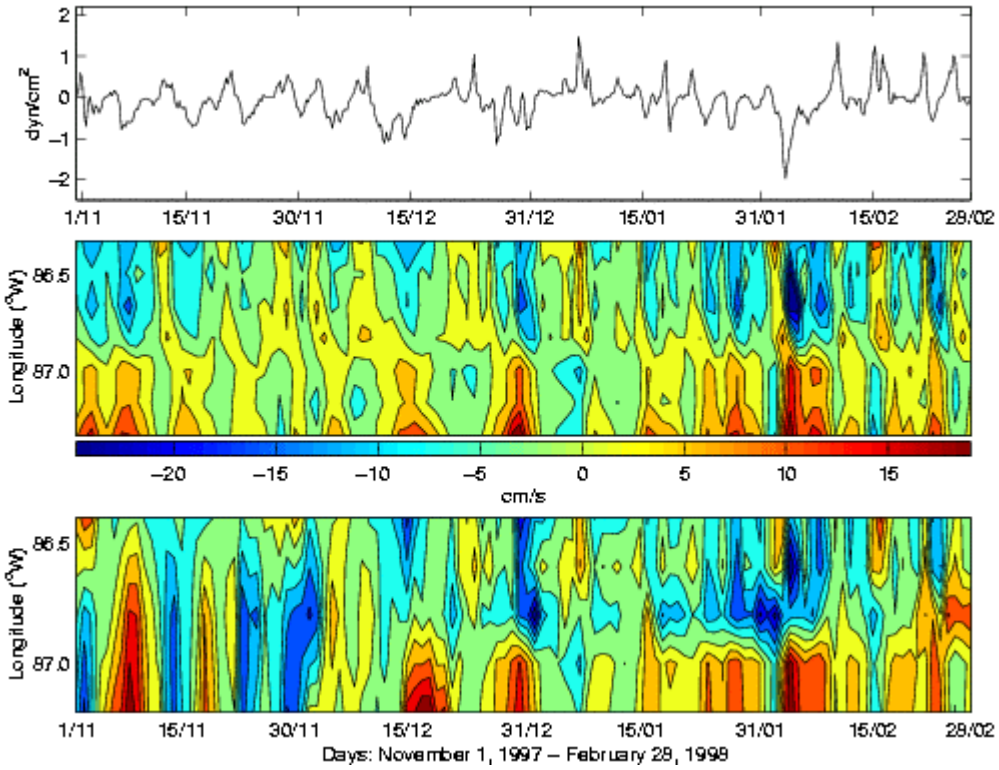

Figure 10. Time-distance plot of 16m north-south velocity components along the segment of the parallel at 29°40'N spanned by C1, D9, and E1. Model results are in the middle panel and observations are in the lower panel. The wind stress component time series shown in Figure 6 is reproduced in the top are contoured dashed. The contour interval is 4.5cms^{-1}.

An important consequence of strong currents in DeSoto Canyon following northerly wind bursts is that it leads to coastal upwelling. In the bottom panels of Figure 7 are found model vertical velocity contour plots in the DeSoto Canyon area during the six intrusion events in response to the northerly-wind bursts. Clearly, there is a strong upwelling center at the head of DeSoto Canyon due to onshore flows associated with strong around-canyon currents. It has been suggested that upwelling here could be due to the bottom Ekman flow under a strong clockwise current around DeSoto Canyon. Unfortunately, Ekman layer over a sloping terrain in a z-level model is decimated and not well resolved (Winton et al., 1998). As a consequence, north-south velocity at a near-boundary grid-point like the one at D1 is set to zero at the next level (72m) below 49m to satisfy the no-normal flow condition, leading to an exaggerated frictional effect at mid-column depth. An effect that is represented reasonably correctly in the model that also leads to upwelling is the production of onshore flow due to a

slight excess in pressure gradient in the geostrophic balance associated with a clockwise around-canyon currents (see later in Discussion). The onshore flow over the shoaling topography then leads to upwelling. Because of this upwelling associated with strong around-canyon currents and flow to the southwest on the east flank, it is perhaps not surprising that peak monthly mean pigment concentration along the 40m isobath over the WFS should be found consistently for November through April (Gilbe et al., 1996).

5. Discussion

It is argued here that strong currents in the DeSoto Canyon region result from the establishment of coastal currents over the WFS by the passage of continental shelf waves originating from the end of the WFS following each northerly wind burst.

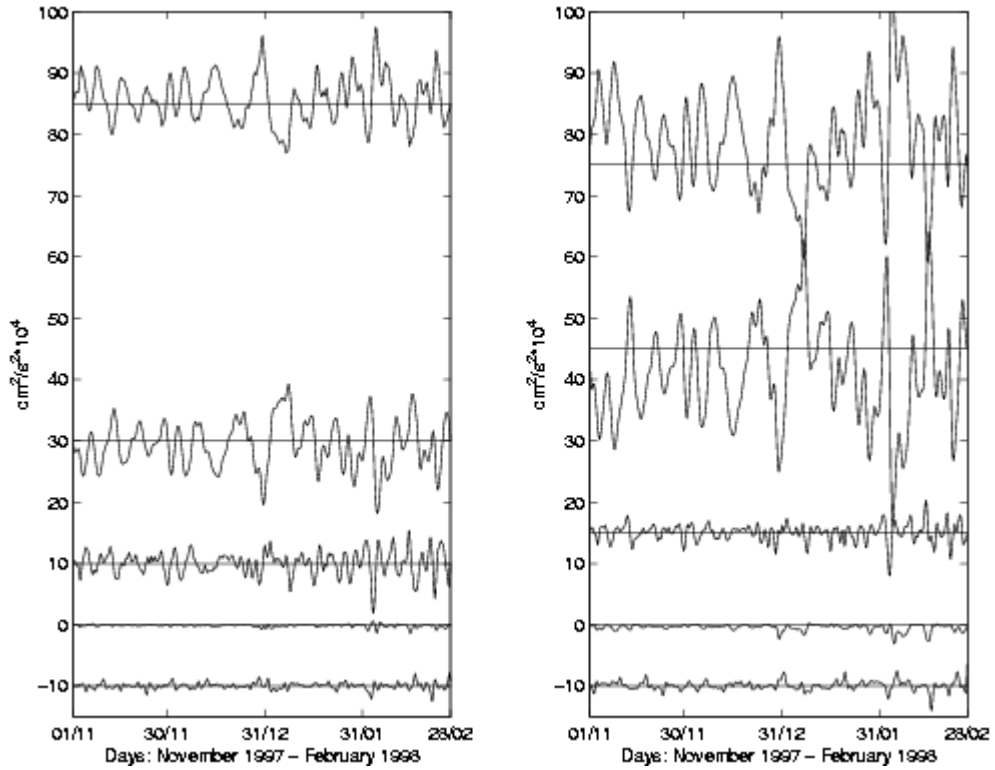

Figure 11. Around-canyon (left panel) and crosswise (right panel) momentum balance are shown at the 16.4 m depth at D1 at the head of DeSoto Canyon. Here, positive y direction is eastward and positive x direction is offshore. From top to bottom in the left panel, the curves represent, $-fv$, $-\partial p/\partial y$, $-\partial v/\partial t$, nonlinear term, and $A_v\partial^2 v/\partial z^2$. From top to bottom in the right panel, the curves represent, fv, $-\partial p/\partial x$, $-\partial u/\partial t$, nonlinear term, and $A_v\partial^2 u/\partial z^2$. The unit is 10^{-4}cms^{-2}.

To substantiate this argument the model term balance (with all terms moved to the right side of the equation) at 16m in both the around-canyon and crosswise momentum equations at D1 in Figure 1b during the hindcast period of

November 1997 – February 1998 is shown in Figure 11 (nonlinear terms are negligibly small and not shown). The crosswise momentum is nearly in geostrophic balance, with the crosswise pressure gradient nearly balancing the Coriolis term arising from the around-canyon flow. In the around-canyon direction, the balance must include the local time derivative of the around-canyon velocity, suggesting a continental shelf wave-like dynamics (Mitchum and Clarke, 1986).

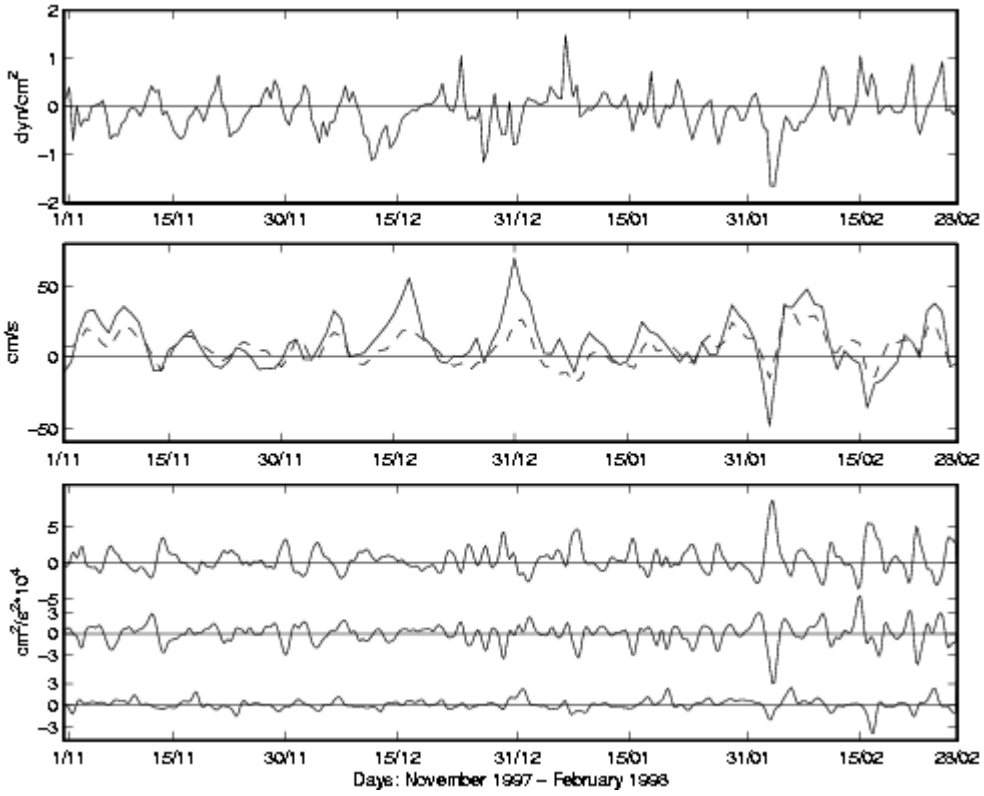

Figure 12. Bottom Panel. Crosswise pressure gradient excess (sum of top curves in right panel of Figure 11, $fv - \partial p / \partial x$) at 16m at D1 for the hindcast period. The lower two curves in Figure 11, $-\partial u / \partial t$ and $A_v \partial^2 u / \partial z^2$, are reproduced in the same order here as the lower curves. Upper Panel. North-south wind stress component at Pensacola. Middle Panel. Around-canyon velocity component at16m at D1 reproduced from Figure 8.

Figure 12 shows at 16m at D1 (in the lower panel) the time series of the excess crosswise pressure gradient (sum of the first two curves in the crosswise momentum balance in Figure 11), negative of local derivative, and the (exaggerated) vertical friction. The north-south component of wind-stress at

Pensacola (upper panel) and the model around-canyon velocity at 16m at D1 from Figure 8 (middle panel) are reproduced here for easy reference. It is interesting to note that after northerly wind bursts when the around-canyon velocity is generally eastward, the excess pressure gradient force is onshore, balancing a crosswise local onshore acceleration. This is particularly clear around December 7,31, and February 4. The excess is perhaps due to the pile-up of surface water under the northerly wind. (Plots (not shown) in the DeSoto Canyon area of model surface pressure gradient diagnosed for the November 7 northerly wind event seems to confirm this in that the greatest offshore gradient (high pressure offshore) is found just after the passage of strong northerly winds.) It is the crosswise acceleration due to this pressure gradient that gives rise to a flow across the shoaling topography, leading to coastal upwelling in Figure 7. The contribution from vertical friction is small but not always negligible. A model with terrain-following coordinates is needed to properly assess the effect of the bottom Ekman flow, which can also produce upwelling under an eastward around-canyon current.

6. Conclusions

A numerical study is conducted of both the Loop Current-driven and wind-driven circulation in the northeastern Gulf of Mexico. The Loop Current of the Gulf of Mexico generally imposes an eastward drift in DeSoto Canyon and a southward drift over the WFS. The Loop Current-driven drift inside DeSoto Canyon produces only a weak flow. But, this picture of a suppressed role of the Loop Current could be due to the fact that the model is deficient in representing filaments and parasite eddies of the Loop Current that could extend the Loop Current influence to the continental shelf. Given this model deficiency, northerly winds are found to generate large around-canyon water movements in DeSoto Canyon. The dynamics of the wind-driven flow appears primarily to be that of the setup of coastal currents by continental shelf waves all along the NEGOM shelf.

An important aside is the discovery that strong coastal upwelling is found in the model at the head of DeSoto Canyon during the northerly wind bursts. This is apparently, in part, the result of excess in pressure gradient in the crosswise momentum balance brought by the northerly wind pile-up. The pressure gradient excess accelerates flow onshore across the shoaling topography, leading to coastal upwelling. Upwelling could also be due to bottom Ekman flow under the strong clockwise circulation around DeSoto Canyon following northerly wind bursts. Unfortunately the present model does not resolve the Ekman layer structure over the sloping shelf. Further clarification of the contribution of bottom friction to upwelling in DeSoto Canyon must await future studies using a model with terrain-following coordinates.

ACKNOWLEDGEMENTS

This research is supported by the Minerals Management Service Cooperative Agreement 14-35-0001-30804 and Contract 1435-01-99-CT-31027. We thank Thomas Berger and Peter Hamilton of Science Applications International Corporation who kindly supplied the current meter data. Dr. Dongliang Yuan helped with model development.

REFERENCES

Carmelengo, A. L., and J. J. O'Brien, 1980: Open-boundary condition in rotating fluid. *J. Comp. Phys*., 35, 12-35.

Clarke, Allan J., 1977: Observational and numerical evidence for wind-forced coastal trapped long waves. *J. Phys. Oceanogr*, 7, 231-247.

Cox, M. D., 1984: A primitive equation three-dimensional model of the ocean. *GFDL Ocean Group Tech. Rep.* No. 1. GFDL/NOAA, Princeton University, Princeton, NJ, 144 pp.

Csanady, G. T., 1978: The arrested topographic wave. *J. Phys. Oceanogr*., 8,47-62.

Csanady, G. T., and Ping Tung Shaw, 1983: The “insulating” effect of a steep continental slope. *J. Geophys. Res.*, 88, 7519-7524.

Dietrich, D. E., D.-S. Ko, and L. A. Yeske, 1993: On the application and evaluation of the relocatable Diecast ocean circulation model in coastal and semi-enclosed seas. Technical Report 93-1, Mississippi State University, 71pp.

Dietrich, Dave E., and Charles A. Lin, 1994: Numerical studies of eddy shedding in the Gulf of Mexico. *J. Geophys. Res*., 99, 7599-7615.

Frantantoni, Paula Sue, 1998: The formation and evolution of Tortugas Eddies in the southern Straits of Florida and Gulf of Mexico. Ph. D. Dissertation, University of Miami, Coral Gables, Florida.

Hetland, Robert, Y. Hsueh, Bob Leben, and P. P. Niiler, 1999: A Loop Current-induced jet along the edge of the West Florida Shelf. *Geophys. Res. Letters*. 26, 2239-2242.

Hickey, Barbara M., 1997: The response of a steep-sided, narrow canyon on time-variable wind forcing. *J. Phys. Oceanogr*. 27, 697-726.

Holland, William R., 1978: The role of mesoscale eddies in the general circulation of the ocean - Numerical experiments using a wind-driven quasi-geostrphic model. *J. Phys. Oceanogr*., 8, 363-392.

Hsueh, Y., 1980: On the theory of deep flow in the Hudson Shelf Valley. *J. Geophys. Res.*, 85, 4913-4918.

Hsueh, Y., 1989: Coastal trapped long waves in the Yellow Sea. *J. Phys. Oceanogr*., 19, 612-625.

Hsueh, Y., J. Schultz, and W. Holland, 1997: The Kuroshio flow-through in the East China Sea: A Numerical Model. *Prog. Oceanogr*., 39,79-108.

Huh, O. K., W. J. Wiseman, Jr., and L. J. Rouse, Jr., 1981: Intrusion of Loop Current Waters Onto the West Florida Continental Shelf. *J. Geophys. Res*., 86, 4186-4192.

Hurlburt, H. E., and J. Dana Thompson, 1980: A numerical study of loop current intrusions and eddy-shedding. *J. Phys. Oceanogr.*, 10, 1611-1651.

Hurlburt, H. E., and J. D. Thompson, 1982: The dynamics of Loop Current and shed eddies in a numerical model of the Gulf of Mexico. Hydrodynamics of semi-enclosed seas by J. C. J. Nihoul (editor), 243-297.

Kalnay, E., M. Kanamitsu, R. Kistler, W. Collins, D. Deaven, L. Gandin, M. Iredell, S. Saha, G. White, J. Woollen, Y. Zhu, A. Leetmaa, R. Reynolds, M. Chelliah, W. Ebisuzaki, W.Higgins, J. Janowiak, K. C. Mo, C. Ropelewski, J. Wang, Roy Jenne, Dennis Joseph, 1996: The NCEP/NCAR 40-year reanalysis project. *Bulletin of the American Meteorological Society*, 77, 437-471.

Klinck, John M., 1996: Circulation near submarine canyons: A modeling study. *J. Geophys. Res*., 101, 1211-1223.

Levitus, S., R. Burgett, and T. P. Boyer, 1994B: World Ocean Atlas 1994 Volume 3:Salinity. NOAA Atlas NESDIS 3. 99pp.

Levitus, S., and T. P. Boyer, 1994C: World Ocean Atlas 1994 Volume 4:Temperature. NOAA Atlas NESDIS 4. 117 pp.

Mitchum, G., and A. J. Clarke, 1986: Evaluation of frictional, wind-forced long-wave theory on the west Florida shelf. *J. Phys. Oceanogr*., 16, 1029-1037.

Oey, Lie-Yuaw, 1995: Eddy- and wind-forced shelf circulation. *J. Geophys. Res*., 100, 8621-8637.

Oey, L.-Y., 1996: Simulation of meso-scale variability in the Gulf of Mexico: sensitivity studies, comparison with observations, and trapped wave propagation. *J. Phys. Oceanogr.*, 26, 145-175.

Perez, Roberto, Frank E. Muller-Karger, Ivan Victoria, Nelson Melo, and Sergio Cerdeira, 1999: Cuban, Mexico, U. S. Researchers probing mysteries of Yucatan Current. *EOS, Transaction, American Geophysical Union*, 80 (14), pages 153, 158.

Pichevin, T., and D. Nof, 1997: The momentum imbalance paradox. *Tellus*, 49A, 298-319.

Pratt, L. J., and Melvin E. Stern, 1986: Dynamics of potential vorticity fronts and eddy detachment. *J. Phys. Oceanogr.*, 16, 1101-1120.

Schroeder, William W., Scott P. Dinnel, Frank J. Kelly, and Wm. J. Wiseman, 1994: Overview of the physical oceanography of the Louisiana-Mississippi-Alabama continental shelf. In *Northeastern Gulf of Mexico physical oceanograpy workshop*; proceedings of a workshop held in Tallahassee, Florida, April 5-7, 1994. Ed. by Allan I. Clarke. Prepared by Florida State University. OCS Study MMS 94-0044. U.S. Department of the Interior, Minerals Management Service, Gulf of Mexico OCS Region, New Orleans, La. 257pp.

Schultz, J., 1994: A numerical model of the Kuroshio in the East China Sea. Ph. D. dissertation, Florida State University, 144pp.

Science Applications International Corporation, 1998: DeSoto Canyon eddy intrusion dtudy. Data Products: Set 2 and Set 3. Science Applications International Corporation, Raleigh, North Carolina.

She, Jun, and John M. Klinck, 2000: Flow near submarine canyons driven by constant winds. *J. Geophys. Res.*, 105, 28,671-28,694.

Sturges, Wilton, 1992: The spectrum of Loop Current variability from gappy data. *J. Phys. Oceanogr.*, 22, 1215-1256.

Sturges, W., and J. C. Evans, 1983: On the variability of the Loop Current in the Gulf of Mexico. *J. Mar. Res.*, 41, 639-653.

Sturges, W., J. C. Evans, S. Welsh, and W. Holland, 1993: Separation of warm-core rings in the Gulf of Mexico. *J. Phys. Oceanogr.*, 23, 250-268.

Sturges, W., 1994: The frequency of ring separation from the Loop Current. *J. Phys. Oceanogr.*., 24, 1648-1651.

Sturges, W., and R. Leben, 2000: Frequency of ring separations from the Loop Current in the Gulf of Mexico: A revised estimate. *J. Phys. Oceanogr*, 30, 1814-1819.

Vukovich, F. M., B. W. Crissman, M. Bushnell, and W. J. King, 1979: Some aspects of the oceanography of the Gulf of Mexico via satellite and in situ data, *J. Geophys. Res*., 84,7749-7769.

Vukovich, F. M., and G. A. Maul, 1985: Cyclonic eddies in the eastern Gulf of Mexico. *J. Phys. Oceanogr*., 15, 105-117.

Vukovich, F. M., 1986: Aspects of the behavior of cold perturbations in the Eastern Gulf of Mexico: a case study. *J. Phys. Oceanogr*., 16, 175-188.

Welsh, S. E., 1996: Numerical simulation of Gulf of Mexico circulation under present and glacial climate conditions. Ph. D. dissertation, Louisiana State University, 146pp.

Winton, M., R. Hallberg, and A. Gnanadesikan, 1998: Simulation of density-driven frictional downslope flow in z-coordinate ocean models. *J. Phys. Oceanogr*., 28, 2163-2174.

5b. Temperature variability in the northeastern Gulf of Mexico in 1997-1998

Temperature variability in the northeastern Gulf of Mexico in 1997-1998

by

Yury Golubev and Y. Hsueh
Department of Oceanography
Florida State University
Tallahassee, FL 32306-4320

Abstract

Observations made during 1997-1998 in the northeastern Gulf of Mexico (NEGOM) show that the monthly mean temperature at stations located near the shelf break behaves differently from that at stations in deep water 30-70 km away. Semi-annual variability is found in monthly mean temperatures at stations in both groups. But, there is a phase difference of about 180 degrees between the two groups. This phase difference makes for large monthly mean temperature contrasts at neighboring stations across the shelf break from each other and, accordingly, large cross-shelf temperature gradients in NEGOM. A basin-wide circulation model of the Gulf of Mexico run for the time period of the observation produces variability of monthly mean temperature along sections across the shelf break qualitatively similar to that observed. The cause is traced to the wind stress curl (mostly negative) in NEGOM, which has a strong semi-annual variability. Following periods of particularly intense negative wind-stress curl in April and October, currents directed eastward along the shelf break in NEGOM associated with the wind-stress curl-driven anti-cyclonic deep water circulation intensify and generate onshore flow due to bottom friction, causing the isotherms near the shelf break to rise. At the same time, isotherms at deep-water stations are depressed on account of the vorticity balance forced by the negative wind-stress curl. Model balances lend support to this scenario. Thus, the observed phase difference in the monthly mean temperature at the semi-annual frequency. Two individual events of anomalously intense cooling observed in NEGOM are addressed separately. It is shown that the dynamics leading to these events is probably associated with short-term responses to northerly wind bursts which produce strong eastward alongshore currents and super-geostrophic pressure gradients. Both are capable of uplifting isotherms over shoaling topography.

1. Introduction

It is recognized that the circulation in the northeastern Gulf of Mexico (NEGOM) is dominated in the deep basin by the Loop Current (LC) and, on the continental shelf, by local winds (Hsueh and Golubev, 2001). Irregular northward penetration of the LC into NEGOM and shedding of anti-cyclonic rings from the LC occur at periods that fall into two ranges, 8-9 and 11-14 months (Sturges, 1992,1994; Vukovich, 1995). The penetration of the LC itself in NEGOM apparently does not reach much beyond 27^{o}N (Hsueh and Golubev, 2001). Thus, it is not expected that the LC heat and momentum have much of a direct effect in determining long-term variability (on the order of season) in the northern part of the NEGOM deep region. There is ample evidence of wind-driven currents on the continental shelf around NEGOM on the seasonal time scale (Blaha and Sturges, 1981; Mitchem and Sturges, 1982; Weisberg et al, 1996). Hsueh and Golubev (2001) show that on short time scales (3-10 days) the southward wind-driven current over the West Florida Shelf (WFS) pulls a strong flow along the continental shelf in NEGOM, leading to open ocean water intrusion and coastal upwelling in DeSoto Canyon. A still unanswered question remains, however, about the extent and manner in which the temperature field in the intervening region between the LC dominated deep Gulf and the wind-driven continental shelf is affected by wind-induced circulation on the seasonal time scale. The availability of current and temperature data from a recent mooring experiment carried out by Science Applications International Cooperation (SAIC) (SAIC, 1998) in the DeSoto Canyon area in NEGOM provides an opportunity for an examination of this question.

The goal of this paper is thus primarily to study processes governing the low-frequency temperature variability in the vicinity of the continental shelf break in NEGOM. Special attention will also be given to two individual events when the observed temperature at about the 100 m depth contour is anomalously low. Temperatures and currents from the SAIC observations and from a Bryan-Cox model will be compared to show and explain the dominant features in the shelf break area around DeSoto Canyon.

The paper is organized as follows. In the next section, a description is given of the data used and a presentation of the data is given. The configuration of the Bryan-Cox model of the basin-wide Gulf of Mexico circulation and results of the simulation are presented in Section 3. The nature of the two individual cooling events in December 1997 and January 1998 is discussed in Section 4. Concluding remarks are found in Section 5.

2. Data

a. Data description

There are thirteen current-meter moorings with various types of instruments in the year long (March, 1997 - April, 1998) SAIC measurement program that covers the Desoto Canyon area shown in Figure 1.

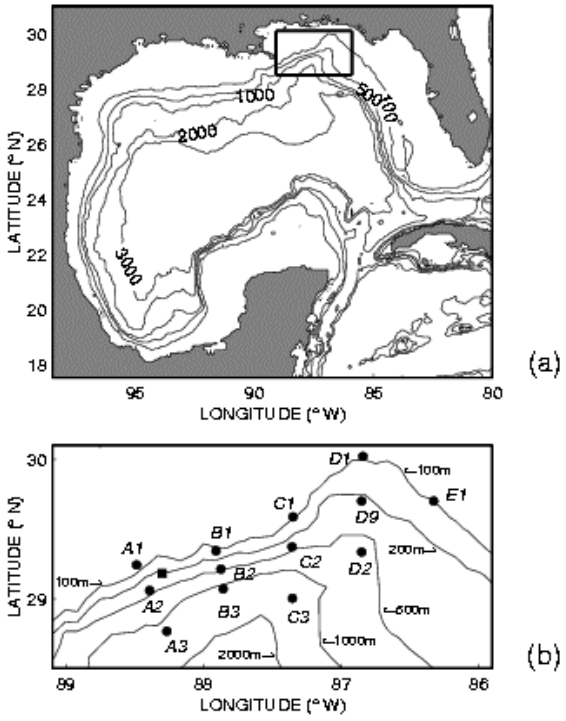

Figure 1. (a) The Gulf of Mexico model domain with the DeSoto Canyon study area in a rectangle. (b) SAIC mooring locations (solid circles) for the April 1997-March 1998 experiment with the solid square indicating the location of NDBC buoy 42040.

The array is bracketed by two approximately along-shore lines. The line strung with moorings indicated with the index "1" in Figure 1(b), where velocity and near bottom temperature are measured, runs in about 100m of water. The deep water line (strung with moorings with index "3") are located at depths greater than 1000m. Between these two lines the depth changes sharply, especially between stations B1 and B3 where depth goes approximately from 100m to 1100m in a distance of about 20 km. A catalogue of current and temperature data is given in Table 1.

Table 1. SAIC Station number, Lat. and Long., Depth and Period of Temperature and Current Measurements NEGOM March 1997-April 1998.

Station	Lat	Long, W	Depth, m	Period
A1	88.485	29.241	80	97/03/21 - 98/04/01*
A2	88.390	29.059	90	97/03/21 - 98/04/01
A3	88.265	28.766	80	97/03/20 - 98/04/01
B1	87.908	29.342	80	97/03/28 - 98/04/08
B2	87.872	29.212	90	97/03/28 - 98/04/03
B3	87.856	29.070	80	97/03/22 - 98/04/03
C1	87.349	29.586	82	97/03/23 - 98/04/08
C2	87.356	29.371	90	97/03/24 - 98/04/08
C3	87.353	29.003	80	97/03/24 - 98/04/04
D1	86.841	30.068	95	97/03/26 - 98/03/28
D9	86.852	29.334		No Temperature Obs.
D2	86.852	29.700	90	97/03/25 - 98/04/06
E1	86.328	29.700	80	97/03/27 - 98/04/07

* No observations from 11/13/97 to 11/21/97.

Hourly mean temperature at 80-90 m for all but two moorings (D9 with no temperature observations and E1 with monthly mean values very close to that at D1) are used to calculate daily and monthly mean values. Velocity data at the 16m and 72m depths are also used. The location and measurement duration of each mooring are presented in Table 1. The level of 80-90m corresponds approximately to the lower boundary of the upper mixed layer. Hourly values of temperature and velocity components are arithmetically averaged for each of the month from April 1997 through March 1998. It will be convenient for subsequent presentation to divide the moorings from which data are used into four sets: set "A" (moorings A1, A2, and A3), set "B" (moorings B1, B2, and B3), set "C" (moorings C1, C2, and C3), and set "D" (moorings D1 and D2).

Three sets of wind data are used. The first one consists of winds observed at the meteorological buoy 42040 (29.2^{o}N, 88.25^{o}W) located in the northern Gulf of Mexico (marked by the solid square in Figure 1(b)), from which data are available at the National Data Buoy Center. The second is the Hellerman and Rosenstein (1983) winds. The third is the 6-hourly, 10m surface winds from the NCEP/NCAR 40-year reanalysis data set (Kalnay et al., 1996).

Similar to the Hellerman and Rosenstein winds, the NCEP winds are arranged in a grid with a 2-degree resolution. The NCEP winds are converted into wind stresses for the period from April 1997 through March 1998 using bulk formula and a drag coefficient of 1.3×10^{-3}.

b. Climatic features of temperature in NEGOM.

It would be useful to first give a brief description of the annual variability of temperature in NEGOM from climatic data. Monthly mean temperatures at 50, 75, and 100m from Levitus (1982) are shown at two points in NEGOM (Figure 2(a)).

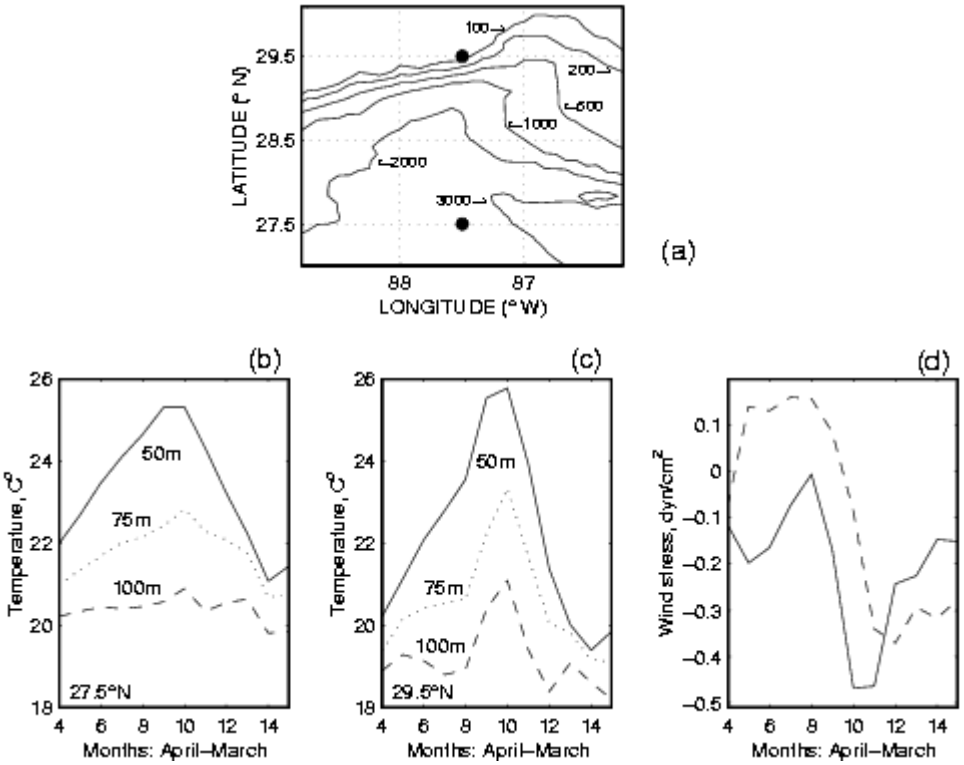

Figure 2. (a) Solid circles mark the locations in NEGOM where the climatological monthly mean temperatures from Levitus (1982) at 50, 75, and 100m are shown in (b) (the southern location at 27.5°N) and (c) (the northern location at 29.5°N). (d) Climatological monthly mean meridional (dashed) and zonal (solid) component of windstress for the region in (a) from Hellerman and Rosenstein (1983).

The northern point (solid circle near top) is located at the shelf break in 100m of water and the southern one (solid circle near bottom) is located in water 2800m deep. The temperature variability during the year differs from one point to the other. The difference in the shape of the curve becomes particularly noticeable at the point with large depth (Figures 2(b)). For both locations, the temperature at 100m shows a maximum in October of 21°C. Most likely, this maximum represents what remains of the downward propagating temperature

signal arising from intense heating at the sea surface in July-August. In months other than September-October temperatures at 75 and 100m are much lower at the northern (shelf break) point than at the southern (deep water) point. Because of the location, it seems that the lower temperature at the northern point might indicate coastal upwelling. The lack of a favorable zonal wind stress (solid curve in Figure 2(d)) from the Hellerman and Rosenstein (1983) data set discounts this. The zonal wind-stress component is mostly directed toward the west during the entire year, favoring down-welling instead. This wind generates shoreward Ekman transport in the upper layer, opposite to what is necessary for the appearance of cold water near the shelf break in July and December (Figure 2(c), 100m). So, the reason for the appearance of low monthly-mean temperature near the shelf break has to be other than a direct result of the local along-shelf wind-stress and its associated Ekman transport. Strong currents of short duration in DeSoto Canyon can, however, arise from the establishment of southward wind-driven currents on the WFS, giving rise to an around-canyon flow conducive to an onshore bottom Ekman transport (Hsueh and Golubev, 2001). The onshore transport across the shoaling coastal topography then leads to upwelling. The efficacy of this dynamics on the monthly mean time scale is, however, doubtful. (The monthly mean wind stress is generally an order of magnitude smaller and the north-south component (not shown but see www.ocean.fsu.edu/oce/gom) over the WFS is northward for July, leading to a counterclockwise around-canyon flow.)

c. Variability of monthly mean temperature and velocity during 1997-1998.

Figure 3 presents monthly mean temperature at 80-90m at the shelf-break and deep water stations in each of the four mooring sets obtained from observations made during 1997-1998. The common features of temperature variation for all four mooring sets are:

I. Temperature at the shelf-break stations (lower curves) is generally lower and has two maxima in May and October of 1997 and two minima in July 1997 and January 1998. The second minimum is lower than the first one at stations A1, B1, and C1. At station D1 both minima have nearly equal values. These variations at the shelf-break moorings are qualitatively similar to those found in the climatic distribution at 100m at the northern point in Figure 2(c).

2. Temperature at the deep-water stations (upper curves) also has two highs and two lows but time-shifted so that the highs line up with the lows and the lows line up with the highs at the shelf-break. Furthermore, no clear resemblance is found in the variation at stations A3, B3, C3, and D2 with the climatic distribution at 100m (Figure 2(b)).

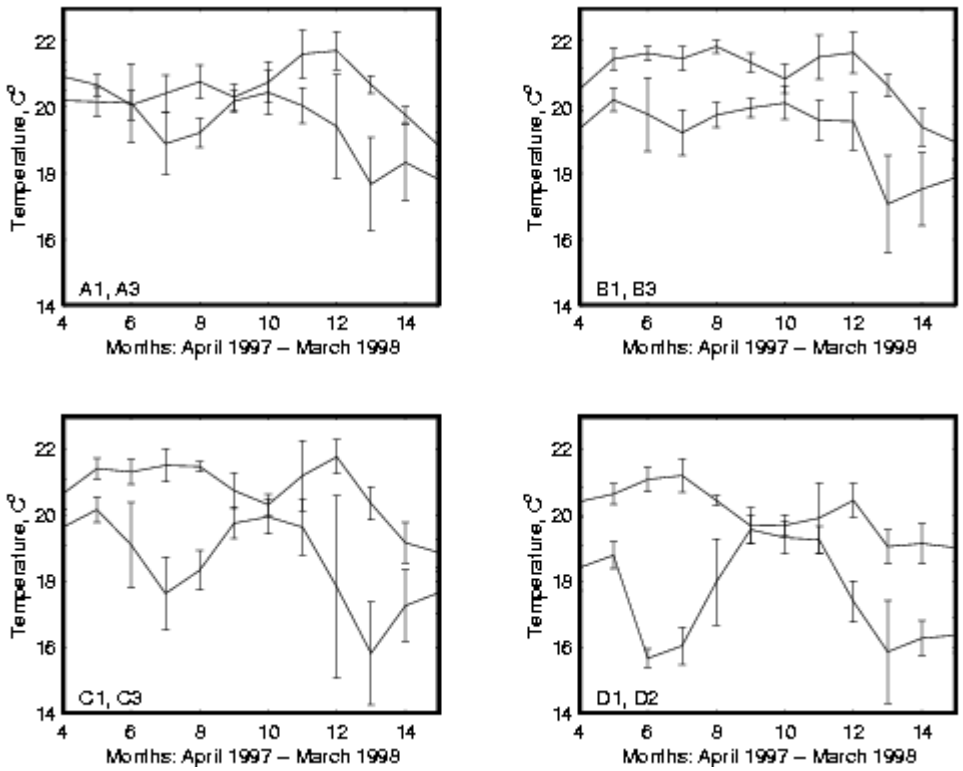

Figure 3. Monthly mean temperatures obtained from observations during March 1997-April 1998 at four pairs of mooring stations across the continental margin shown in Figure 1(b). The mooring pair is shown in the lower left-hand corner of each of the four panels. In each panel, the top curve is from the deep mooring and the lower curve from the shelf-break mooring. The vertical bars indicate the root-mean-square values for each month.

3. Temperature variations at A2, B2, and C2 between the shelf break and the deep water feature what is the average for the shelf-break and deep-water stations and the temperature curves (not shown) generally lie in between the two curves presented in Figure 3.

The vertical bars in Figure 3 represent the root-mean-square (rms) of temperature fluctuations for each month of the year. These values can be treated as a measure of temperature variability during each individual month. There are instances of particularly large rms' in December 1997 and January 1998. These reflect the presence of anomalous short-term cases, which will be discussed in Section 4.

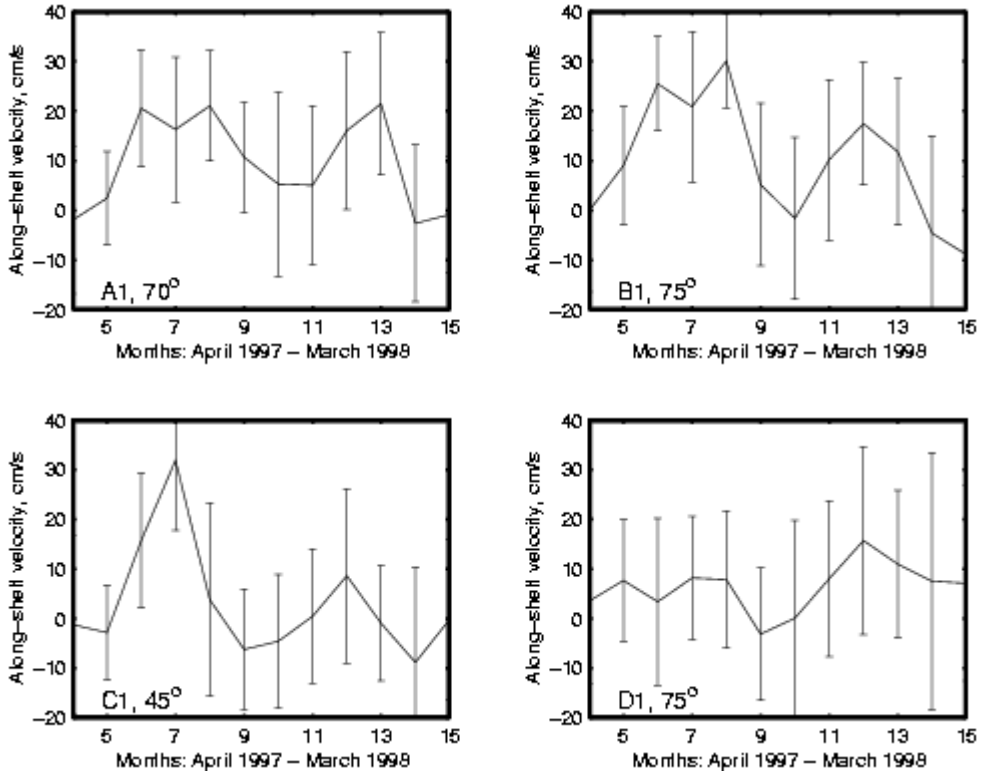

Figure 4. Monthly mean along-shelf component of velocity at 16m at the shelf-break moorings of the mooring pairs shown in Figure 3. The direction in angle of rotation clockwise from the north is given in each of the four panels. The vertical bars represent the root-mean-square values for each month.

Monthly mean values of the along-shelf component of observed currents at 16m at the four shelf-break moorings are presented in four panels in Figure 4. (The directions in angles of rotation clockwise from the north are indicated in each panel.) Curves (not shown but see www.ocean.fsu.edu/oce/gom) for 72m are qualitatively similar. There are two-peaks with the largest velocities in June-July and December-January. The velocity reaches a minimum in September-October. The peaks in velocity occur roughly at the time of temperature minima in Figure 3. This is particularly clear for the June-July peak.

It is particularly interesting to underline the large temperature contrasts found between shelf-break and deep-water moorings (temperature being higher at deep-water moorings). Monthly mean temperature at D2 exceeds that at D1 in July 1997 by more than 5^{o}C. It is 4^{o}C between C3 and C1, and almost 5^{o}C in December 1997-January 1998. Table 2 lists temperature contrasts and horizontal temperature gradients between pairs of moorings with indices 1 and 2 in each mooring set. Horizontal temperature gradients of 0.15^{o}C/km are large for the seasonal time scale and may have important impact, in particular, on the biology in NEGOM.

Table 2. Temperature Difference (Δ^{o}C) and Gradients (°C/km) for Stations with Indices 1 and 2 (Figure 1(b)).

	July, 1997		January, 1998	
	Δ	Gradient	Δ	Gradient
A2 – A1	1.46	0.072	2.63	0.131
B2 – B1	1.38	0.095	2.24	0.154
C2 – C1	3.39	0.141	2.45	0.102
D2 – D1	5.15	0.127	3.18	0.078

3. Model

a. Model design and configuration.

A numerical model for the Gulf of Mexico basin-wide circulation driven by both the Loop Current through the Yucatan Strait and the wind-stress field must be developed that is able to resolve dynamic processes on the continental shelf and over the sharply changing upper continental slope topography in NEGOM. The eddy-resolved circulation model employed to meet this requirement is the rigid-lid, primitive-equation model of Bryan and Cox (Bryan, 1969; Cox, 1984). A detailed description of the model in a hindcast for the observation period can be found elsewhere (Hsueh and Golubev, 2001). It suffices to say that the model reproduces the Loop Current, but is deficient in resolving small-scale flow structures such as Loop Current filaments and parasite eddies which may extend into the continental shelf region. The model thus accentuates the wind influence. Care has been taken to make sure that the initial condition for the integration features a Loop Current with a configuration similar to that found for March 1, 1997 from the TOPEX/Poseidon altimeter measurement (Hsueh and Golubev, 2001).

b. Temperature variability.

Monthly mean model temperature and velocity are examined for a number of north-south (nearly cross-shelf) sections over the shelf break in the area of the mooring experiment. Monthly mean temperature at each grid-point along one of these sections (Figure 5(a)) is shown in Figure 5(b).

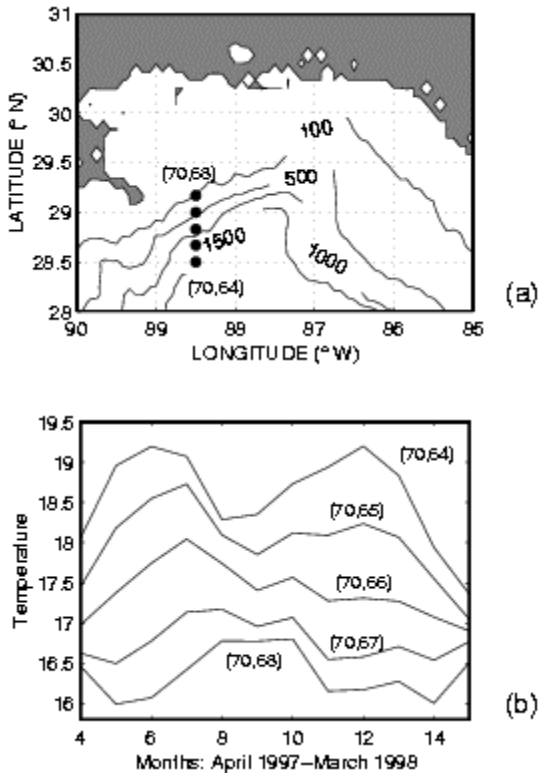

Figure 5. (a) A north-south section of model grid-points across the continental margin in the DeSoto Canyon area of the SAIC mooring experiment. (b) Monthly mean model temperature at 115m during April 1997-March 1998 at each of the grid-points in (a). The curves sort themselves out with decreasing depth from the top one to the one at the bottom.

The section is located near mooring set "A" (see Figure 1(b)). The northernmost grid-point (70, 68) is located on the 100m isobath. The southernmost point (70, 64) is in 1500m of water. So the section spans sharp changes in topography (with distance between (70, 64) and (70, 68) equal to 72 km). The monthly mean temperature at 115m at each grid-point is shown in Figure 5(b).

Two impressions immediately present themselves. First, the shape of the curves at both shallow and deep-water points is qualitatively similar to that of the observed (Figure 3). Quantitatively, the model cross-shelf gradients are much weaker than those found in observation. Be it as may, it is still remarkable that the gradient in May or June is almost twice as large as that in April or August and four time as large as that in March 1998. Second, in the model, the northernmost location of the northern boundary of the model LC during the year is around 27.5^{o}N (Hsueh and Golubev, 2001). So it must not be the model LC that is directly responsible for this variation in temperature. This leaves the wind as the only factor in this part of the Gulf that lies north of 28^{o}N. Since, as is allude to earlier, climatically, alongshore winds are mostly easterly, local winds are not able to lower temperatures in shallow water areas. Might it not be that it is actually the wind-stress curl field that is known to have semi-annual variability in NEGOM that is responsible for this large temperature contrasts from the shelf break to the deep?

c. Winds and currents in NEGOM and their influence on the temperature field.

Monthly mean values (averaged for the two marked locations in Figure 2(a)) of zonal component of model wind-stress for the period March 1997-April 1998 for the area in Figure 2(a) are presented in Figure 6(a).

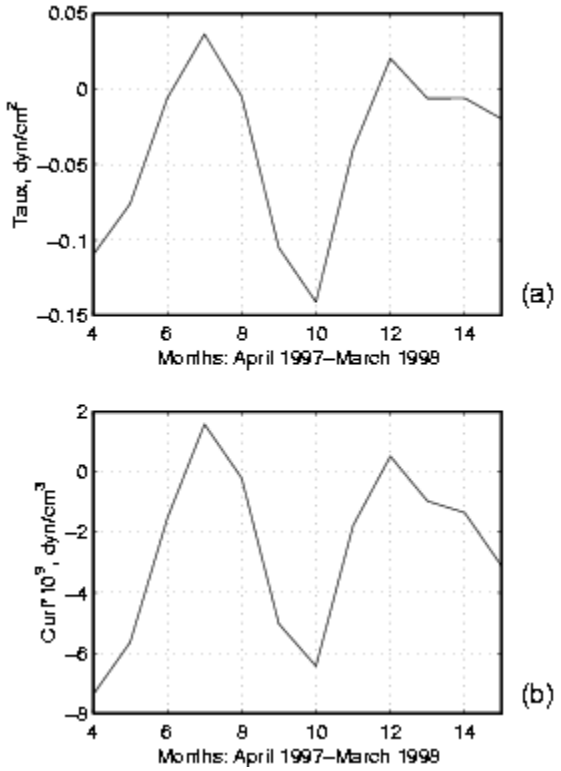

Figure 6. (a) Monthly mean zonal wind-stress component obtained from averaging the values used in the model at the two locations in Figure 2(a) and (b) monthly mean model wind-stress curl in the area in Figure 2(a) during April 1997-March 1998 calculated using NCEP/NCAR reanalysis data.

To the surprise of no one, the variation has many features common with that from Hellerman and Rosenstein (1983) presented in Figure 2(d). Most importantly, as in the case of the Hellerman and Rosenstein wind-stress, the wind-stress during 1997-1998 is predominant directed to the west (negative values) and so is the annual mean. This means, for April 1997-March 1998, with local winds alone the water temperature at the shelf-break stations would be higher than that at the deep water stations, not the other way around. It is thus safe to discard the possibility that local wind-stress-produced coastal upwelling would lead to the observed cross slope temperature difference. The appearance of cold water near the shelf break and warm water at the deep water stations must be rooted in the wind-driven circulation in other ways.

In the northern part of Gulf of Mexico (north of 24^{o}N), the wind field shows an anti-cyclonic rotation (Elliott, 1979; Krishnamurti and Krishnamurti, 1975) with a curl maximum in the western part of the Gulf (Blaha and Sturges, 1978, 1981). Monthly mean values of wind-stress curl for 1997-1998 derived from NCEP winds averaged for the area in Figure 2(a) is shown as Figure 6(b). The wind-

stress curl has two peaks in the anti-cyclonic sense, one in April and the other in October associated with the weakening of easterly and northeasterly winds in the northern part of the Gulf during mid-spring and mid-fall. Model results (see later Figure 8) show that this wind-stress curl produces anti-cyclonic circulations in NEGOM. Along-shelf component (directed in a direction obtained by rotating clockwise 70^o from north) of currents averaged for the five grid-points of the section in Figure 6(a) is shown in Figure 7.

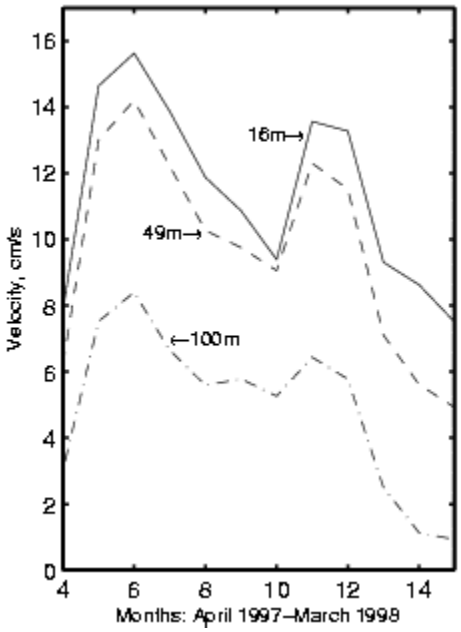

Figure 7. Monthly mean model velocities in the along-shelf direction (70^o clockwise from north) at three depths averaged over the five grid points in Figure 5(a).

Similar to the shape of the wind-stress curl, currents have two peaks during the year: May-June and November-December. These months all follow periods with strongest anti-cyclonic wind-stress curl in April and October (with a 1-1.5 months delay) (see Figure 6(b)). The time delay amounts to a phase shift of about one-quarter of a period for the semi-annual variability, reasonable for an inviscid forcing-response relationship (see later (1)).

Pictures of monthly mean horizontal model circulation averaged for the upper 100m in NEGOM is presented in Figure 8 for April and June (two upper panels).

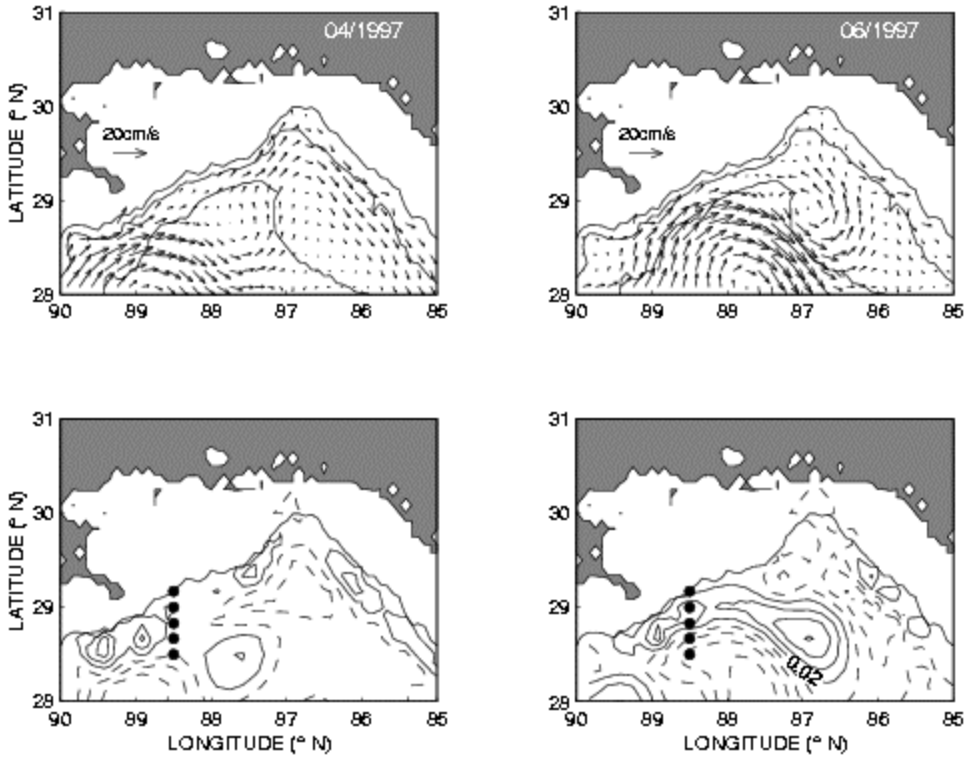

Figure 8. Vector plots of the average model currents in the upper 100m in April (upper left panel) and June (upper right panel). The corresponding average relative vorticity distributions for the same layer are shown in the lower panels, left for April and right for June. Contours of relative vorticity, at interval of $2x10^{-9}s^{-1}$, are dashed for negative values and solid for positive values. The depth contours are 100, 200, and 1000m in the upper panels and 100m in the lower panels.

There is a clear distinction between the two in terms of weak currents in April and strong circulation in June. (A similar contrast is also found for October and December, another month-pair when the currents change form being weak to strong.) All monthly mean pictures of such horizontal circulation share one common feature. The along-shelf currents have cyclonic vorticity to their northeastern side that is bounded by the shelf and anti-cyclonic vorticity on the seaward side (Figure 8 lower panels). In months when the circulation is strong (June and December) relative vorticity is also strong: negative relative vorticity is strong offshore because the anti-cyclonic circulation is more intense; positive relative vorticity is strong because the velocity at the shelf break is increased due to the intensification of anti-cyclonic circulation. The process is similar to the case with the Gulf Stream. In the coastal side of the Gulf Stream, large cyclonic vorticity values exceed the local parameter of Coriolis due to the intensification of the currents when the Gulf Stream axis shifts shoreward (Richardson et al., 1969; Gill, 1982).

The strong eastward currents along the shelf break associated with the anti-cyclonic circulation then drive an onshore Ekman transport over the shoaling topography, leading to cooling and raised isotherms at the shelf break. Figure 9 presents monthly mean along and cross-shelf model velocities at 49m at the grid-points that make up the section in Figure 5(a).

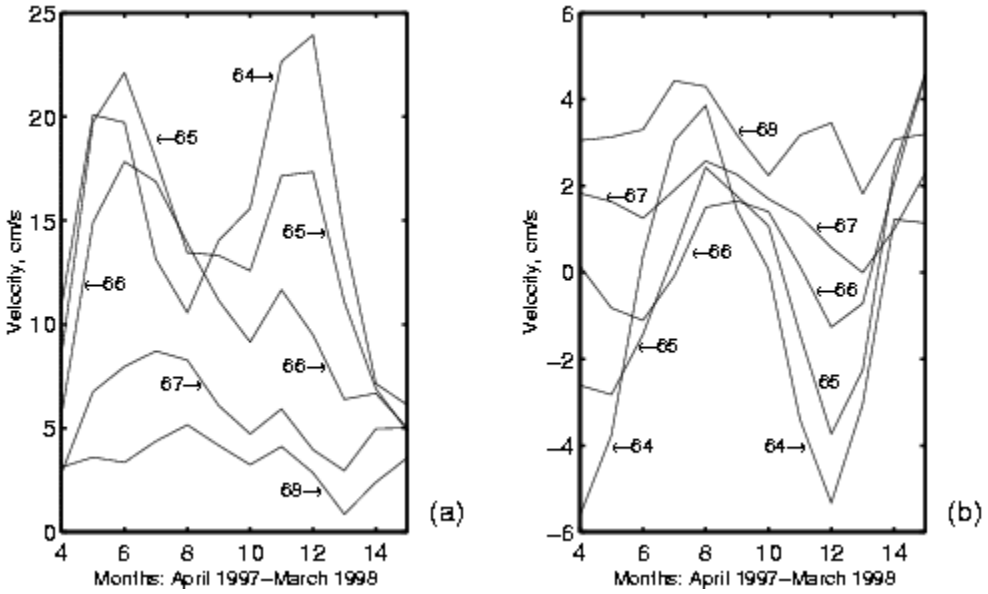

Figure 9. Model velocity components at 49m at the grid points in Figure 5(a) in a coordinate frame in which the positive along-shelf direction is 70^{o} clockwise from north. (a) Along-shelf components (positive to the east). (b) Cross-shelf components (positive onshore). The numbers on the curves give the north-south grid-points.

The cross-shelf velocities at (70, 68), where 49m being the deepest level of non-zero velocity, and (70, 67) are onshore (positive) when the along-shelf current is to the east (positive), indicating an Ekman flow. The reason that horizontal velocity is set to zero at a level (72m) below 49m is because the step representation of the slope bottom imposes a solid northern boundary at this depth for (70, 68). As a consequence, bottom friction is present at 49m, a mid-column depth. This is an aberration attributable to the nature of z-level models in dealing with a sloping bottom (Hsueh and Golubev, 2001). But, the qualitative effect of bottom friction in generating an onshore flow is probably still valid (see later Figure 12). In deep water off the shelf break, but still beyond the reach of the model LC, at grid-points (70, 64) and (70, 65), deep isotherms is depressed due to the presence of the anti-cyclonic wind-stress curl. So, the monthly mean temperature at the deep-water end of the section will show warming. Figure 10 summarizes the cooling and warming combination with a plot of the monthly mean depth of the 17.5^{o} C isotherm along the cross-shelf section in Figure 5(a) as a function of time and cross-shelf distance.

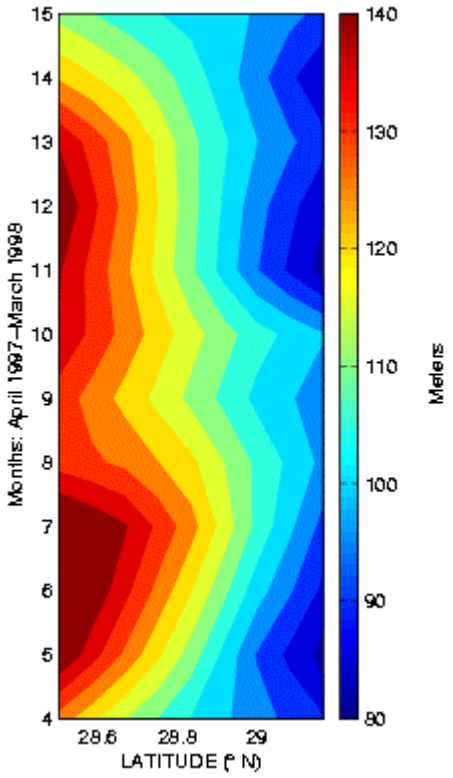

Figure 10. The depth of the 17.5° C isotherm in the model along the cross-shelf section in Figure 5(a) is contoured in a time-latitude plot.

In June, a month or so after the occurrence of a strong negative wind-stress curl (see Figure 6(b)) the isotherm deepens at the deep end. At almost the same time, the same isotherm at the shallow end moves up. The same out-of-phase oscillation shows up in November, again about one month after the occurrence of a strong negative wind-stress curl in Figure 6(b). The linear vorticity equation that might help to explain this is

$$\frac{\partial h}{\partial t} + \frac{1}{f \rho_0} curl\tau = 0 \qquad (1)$$

Here, h is the monthly mean thickness of the layer between the sea surface and the 17.5° C isotherm, f is the Coriolis parameter, and τ is the monthly mean wind-stress vector. Figure 11 presents the balance in (1) from the model output at grid-point (70, 64).

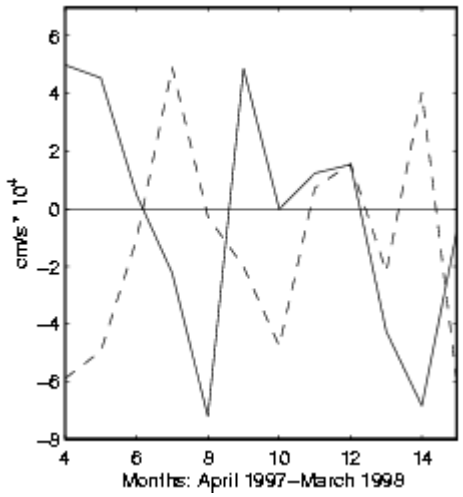

Figure 11. Plot of the monthly mean balance in (1) at model grid-point (70, 64), the southernmost point of the cross-shelf section in Figure 5(a). The solid curve represents the model calculation of $\frac{\partial h}{\partial t}$. The dashed curve represents the model wind-stress curl divided by the product of density (1.023g/cm^3) and the Coriolis parameter at (70, 64). Here, the Coriolis parameter is taken as a constant of 10^{-5} s^{-1}.

Other than the last four months or so where wind-stress curl becomes more variable, the qualitative impression is that, to the first order, the two terms tend to cancel each other.

So, the negative wind-stress curl generates an anti-cyclonic circulation in the deep part of NEGOM in a month or so and gives rise to a strong shelf-break current at 100m to the east on the west flank of DeSoto Canyon. The strong current to the east along the shelf break creates an Ekman onshore flow due to bottom friction that, when coupled with the shoaling topography, lifts the isotherms upward, causing cooling. Figure 12 presents the monthly mean balance of the cross-shelf momentum at 49m at grid-point (70,68).

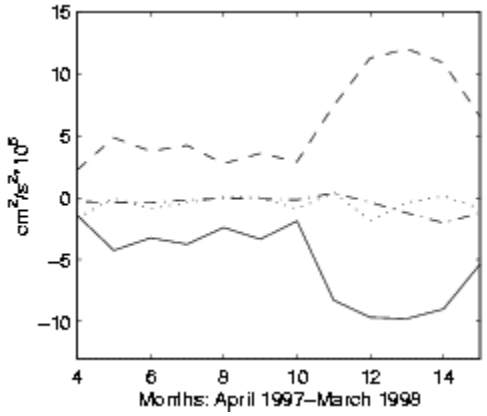

Figure 12. The monthly mean cross-shelf momentum balance is plotted at 49m at (70, 68), the northernmost grid-point on the cross-shelf section in Figure 5(a), in a coordinate frame in which the positive along-shelf (x-) direction is 70^o clockwise from north and the positive cross-shelf (y-) direction is onshore. All the terms in the cross-shelf momentum equation are moved to the right-hand side. The local derivative, $-\frac{\partial v}{\partial t}$, is dotted, advection dot-dashed, and ageostrophic term, $-fu-\frac{\partial p}{\partial y}$, dashed, and vertical friction solid.

The cross-shelf pressure gradient and the Coriolis term arising from the strong along-shelf current is combined to give the ageostrophic term so that it may be compared with friction to show the Ekman balance. The plot shows clearly that the (vertical) friction term nearly balances the ageostrophic term, giving support to the contention that on the monthly mean the cross-shelf flow is Ekman. (The onshore flow at the deep-water points (Figure 9(b)) is just a part of the geostrophic flow around the anti-cyclonic gyre.)

In the deep water, the deepening of the isotherms is argued to be due to the forcing of the anti-cyclonic wind-stress curl. The linear vorticity equation (1) shows a rough balance between the variation of the 17.5^{o}C isotherm depth and wind-stress curl. The deepening of isotherms in the deep water region due to the anti-cyclonic wind-stress curl and the raising of isotherms at the shelf break due to Ekman flow under eastward currents over the shelf break associated with the anti-cyclonic circulation in the deep water region thus combine to create the out of phase variation in monthly mean temperatures presented in Figure 3.

4. COOLING EVENTS IN NEGOM.

The main goal of this section is to examine the role of wind-driven currents in strong short-term cooling events in the northeastern Gulf of Mexico. First, temperature and current data in DeSoto Canyon will be examined to show two strong cooling events observed in December 1997-January 1998. Second, the Bryan-Cox model output will be analyzed to explain the dominant mechanisms that lead to these events.

Two strong cooling events are found in daily mean temperature time series at 85-90m at stations C1 and D1 (Figure 13). The first event is observed on December 17-18, 1997. During the 3-5 days temperature drops from 20^{o}C on December 13-14 to 12^{o}C at station C1. The drop is to 11.5^{o}C at station D1. The temperature does not recover fully after the event. The second event is found on January 1-2, 1998. The temperature drop from December 26 to January 1-2 is 7-8^{o}C and again the temperature does not recover completely after the event. It can also be noted that, in general, the temperature drops precipitously and recovers relatively gradually. Second, as Figure 13 shows, there are only two stations among the twelve-station set where these features in temperature are observed. There is no evidence that these cooling events occur at off-shelf stations.

The cooling events are detected in the observation at 85-90m below the sea surface. But, both leave a mark, especially the second one, in sea surface temperatures. Figure 14 shows two aerial AVHRR sea-surface temperature images at about the time of these events.

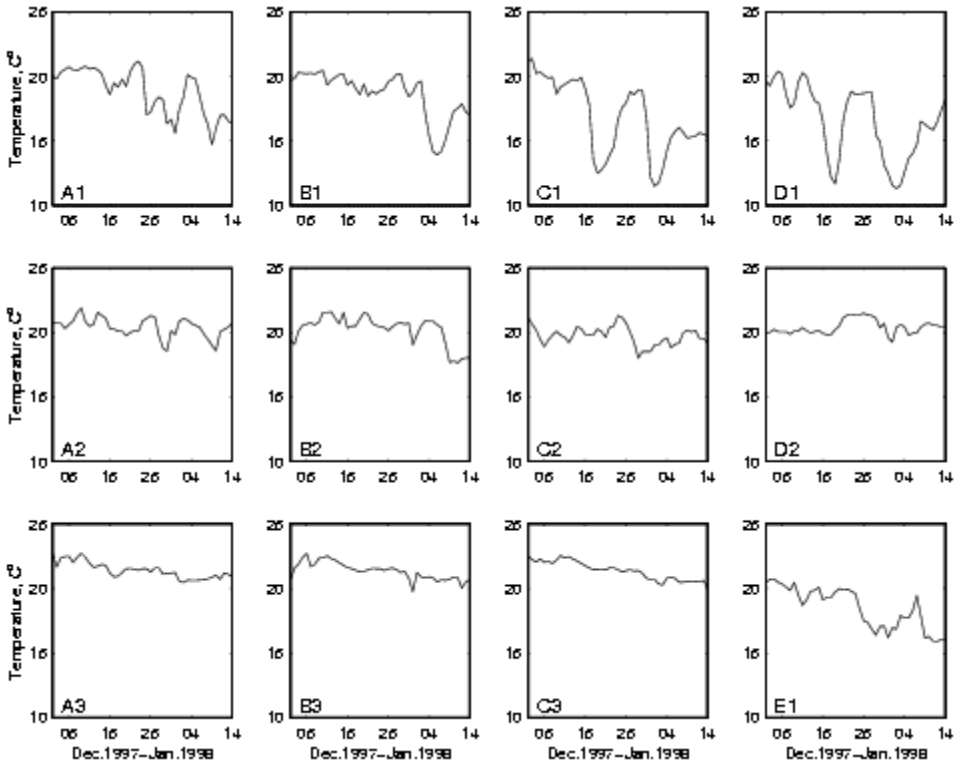

Figure 13. Daily mean temperature at the 85-90m depth at all mooring stations in Figure 1(b) except D9 during December 1, 1997 - January 14, 1998. Station designation is given in the lower left corner of each panel.

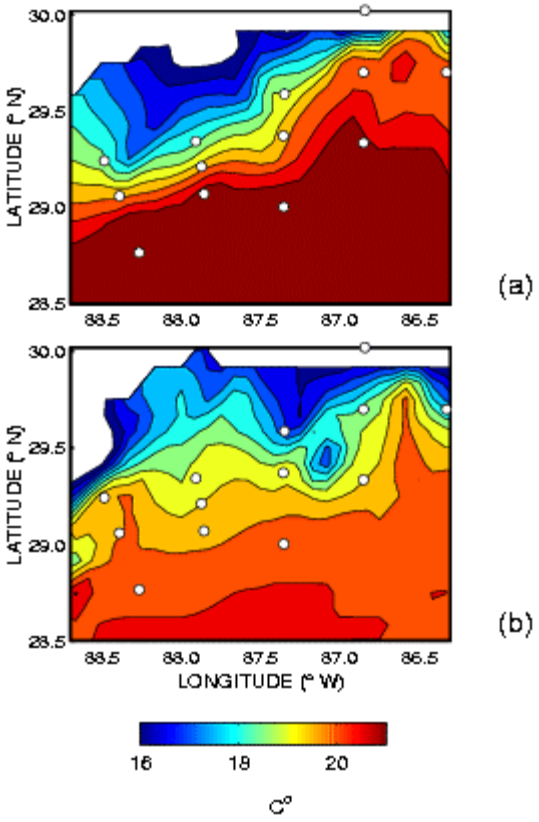

Figure 14. AVHRR sea surface temperature images for the region of observation from the Pathfinder 9km SST Climatology (http://podaac.jpl.nasa.gov). (a) December 17-23, 1997. (b) January 1-6, 1998. White dots on both plates show the mooring locations (Figure .1(b)).

As can be seen, stations C1 and D1 are indeed located in the area of low water temperatures. Strong temperature contrasts, particularly in the January case, are found across the shelf. To the east of 87.5°W, the isotherms basically follow the shelf break.

An examination of wind data at NDBC buoy 42040 during December 1997 - January 1998 uncovers two cases of strong winds in NEGOM during this period. The first case occurs on December 12, 1997 when the wind is northerly with a daily mean velocity of about 10 m/s, translating into a wind-stress of more than 1 dyne/cm^2 (Figure 15(a)).

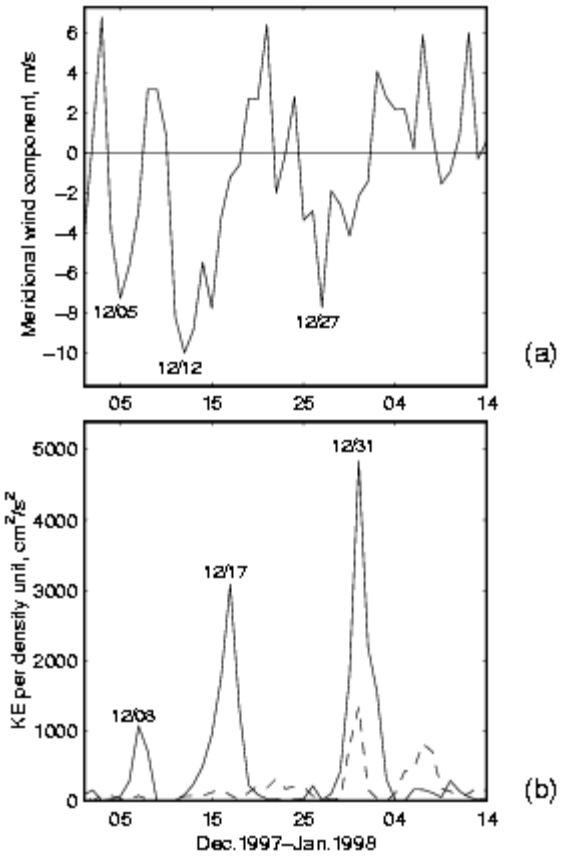

Figure 15. (a) Daily mean meridional wind velocity at NDBC buoy 42040 during December 1, 1997 - January 14, 1998. The two days with the strongest northerly winds are indicated. (b) Model current kinetic energy at D1 for the considered period of time. Solid curve represents the kinetic energy at 16m and the dashed curve for 72m. Days with maximum of current intensity are indicated.

The second strong wind event with west-northwesterly winds occurs on December 29, 1997. As can be seen from Figure 15(b)), after each wind event, the kinetic energy of model horizontal circulation peaks on December 17 and December 31, 1997, just before the occurrence of the cooling events.

There are interesting differences in pictures of currents before and after wind action (Figure 16).

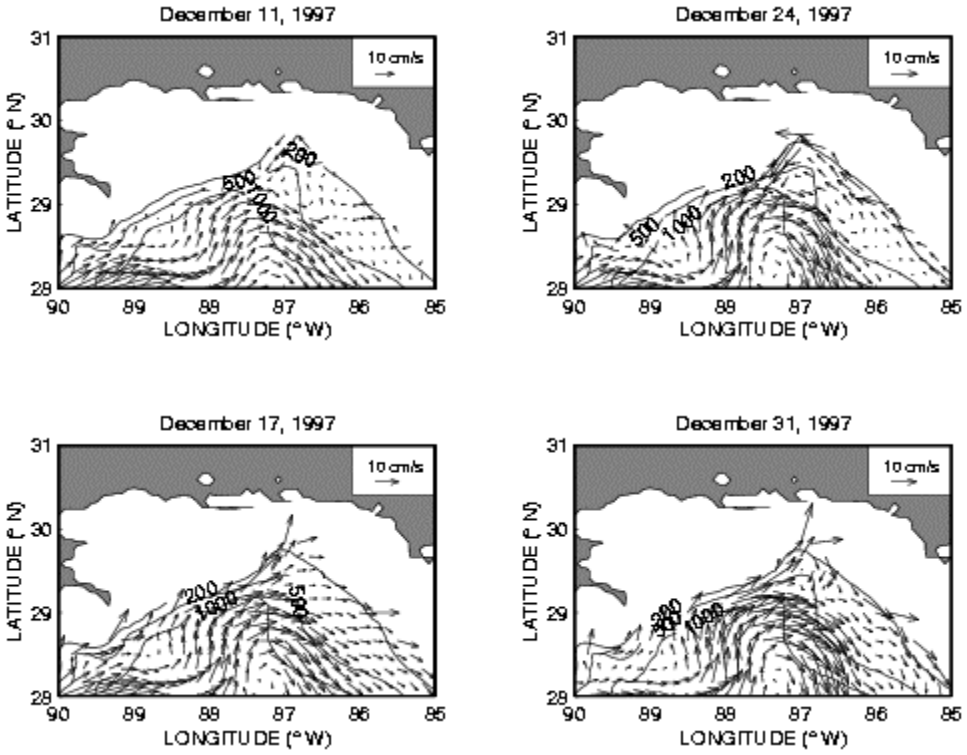

Figure 16. Vector plots of model currents at 72m in NEGOM. Two upper panels represent currents on December 10 and 24 before strong winds. Two lower panels show currents after strong of winds of the two days indicated in Figure 15.

The pattern features meandering along-shelf currents with approximately equal intensity for all cases. In days with relatively weak winds (December 10 and 24 - two upper panels) the current near the shelf break is either weak or cyclonic. After the wind action (two lower panels), strong and narrow along-shelf currents emerge particularly along the west side of DeSoto Canyon with maximum onshore velocities at the head of the canyon (Figure 17a).

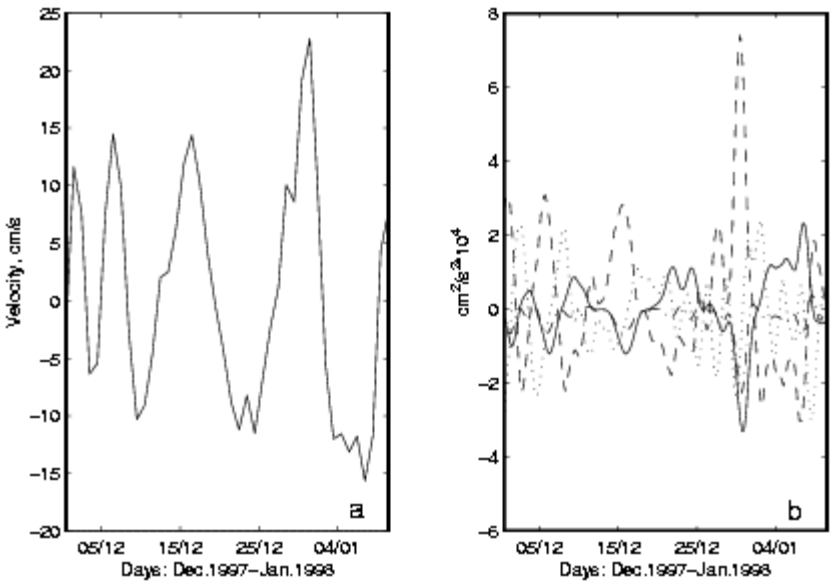

Figure 17. (a) Daily mean model cross-shelf velocity at 72m at (79, 72), a grid-point just south of D1. (b) Plot of the daily mean cross-shelf momentum balance at 72m at the same grid-point. All the terms in the momentum equation are moved to the right-hand side. Local acceleration is dotted, advection is dot-dashed, ageostrophic term is dased, and vertical friction term is solid.

Apparently, the strong along-shelf current to the east is able to produce, near the bottom, an Ekman veering to transport cold water from the deep to the shelf. As mentioned early on, because of the step-wise representation of the sloping bottom in a z-level model, the bottom friction effect appears at shallower depth than in reality (Hsueh and Golubev, 2001). In fact, in both these cases, a viable mechanism may be that of excess onshore pressure gradient forcing an onshore flow, leading to upwelling at the canyon head. The case on December 17 is indeed one of the cases discussed in such light in Hsueh and Golubev (2001). Even with exaggerated bottom friction effect, the term balance for cross-shelf (north-south) momentum at 72m (Figure 17b) shows the Ekman dynamics compensates only 35-40% of ageostrophic term. The rest is balanced by the local acceleration (the one term stressed in the super-geostrophic pressure gradient argument (Hsueh and Golubev (2001)) and advection terms. In addition, unlike the case with monthly mean balance (Figure 12), sometimes (December 31) a significant part of the ageostrophic term is balanced by advection. Thus, some of the cross-shelf flow may be a result of flow over-shooting along the west flank of DeSoto Canyon, an aspect not discussed in Hsueh and Golubev (2001). Further work is clearly necessary to address the inertial nature of the along-shelf currents in NEGOM following strong northerly wind bursts.

5. Conclusions.

It is argued that the out-of-phase oscillation in the monthly mean temperature at 100m across the continental margin from the deep NEGOM to the shelf break observed in March 1997-April 1998 stems from the difference in the dynamics that operate in the deep Gulf of Mexico and over the shelf break, although all due to the prevalent anti-cyclonic wind-stress curl in NEGOM. The negative wind-stress curl generates an anti-cyclonic circulation in the deep part of NEGOM and gives rise to a strong shelf-break current at 100m to the east on the west flank of DeSoto Canyon. The strong current to the east along the shelf break creates an onshore flow from Ekman veering that, when coupled with the shoaling topography, lifts the isotherms upward, causing cooling.

During the occurrences of intense anti-cyclonic wind-stress curl, the deep isotherms at the deep-water moorings are lowered according to the linear vorticity balance on the month mean and the strong along-shelf current near the shelf break associated with the anti-cyclonic circulation in the deep Gulf generates a cross-shelf flow in the bottom Ekman layer, leading to elevated isotherms found at moorings over the shelf break. Both the bottom Ekman layer balance at the shelf-break stations and the vorticity balance at the deep-water stations are demonstrated using the numerical model as a proxy. The two mechanisms are consistent with each other and combine to produce the observed large temperature contrast across the continental margin in the DeSoto Canyon.

Two strong short-term cooling events are found in temperature series from stations C1 and D1 on December 17-18, 1997 and January 1-2, 1998 when temperatures at 85-90m drop by 7-8^{o}C during 3-5 days. An examination of model output shows the presence of strong eastward narrow along-shelf current during the days of the temperature drop, indicating perhaps a measure of Ekman veering in velocity in the lower water column. The term-balance for cross-shelf momentum shows the term responsible for the Ekman transport compensates only 35-40% of the ageostrophic term. The rest is balanced by the local acceleration and advection terms. The local derivative appears to come from an excess onshore pressure gradient found elsewhere (Hsueh and Golubev, 2001). The substantial amount of advection required for the second event indicates that the inertia of the along-shelf flowing current may sometimes lead to over-shooting that can produce additional cross-isobath flow, leading to upwelling and the appearance of cooling inshore.

Acknowledgements

Appreciation is noted of helpful discussions with W. Sturges and G. Weatherly. Thomas Berger and Peter Hamilton of Science Application International Corporation kindly supplied the data. Assistance rendered by Dr. Dongliang Yuan is also acknowledged. This research is supported by the U.S Minerals Management Service Cooperative Agreement 14-35-0001-30804 and Contract 1435-01-99-CT-31027.

REFERENCES

Blaha J., and W. Sturges, 1978: Evidence for wind forced circulation in the Gulf of Mexico, Technical Report, Department of Oceanography, Florida State University, 134pp.

Blaha J., and W. Sturges, 1981: Evidence for wind-forced circulation in the Gulf of Mexico, J.Mar.Res., 39(4),711-734.

Blanton,J., L.Atkinson, L.,Pietrafesa and T.Lee, 1981: The intrusion of Gulf Stream water arross the continental shelf due to topographically induced upwelling. Deep-Sea Res., 28A, 393-405.

Bryan, Kirk, 1969: A numerical method for the study of the circulation of the world ocean. *Journal of Computational Physics*, 4, 347-376.

Elliott, B.A., 1982: Anticyclonic rings in the Gulf of Mexico, J. Phys. Oceanogr., 12(11), 1292-1309.

Garrett, C., 1979: Topographic Rossby waves off East Australia: Identification and Role in Shelf Circulation, J. Phys. Oceanogr., 9, 244-253.

Gill A., 1982: Atmosphere-Ocean Dynamics, Academic Press, 876p.

Hellerman S, and M. Rosenstein, 1983: Normal monthly wind stress over the world ocean with error estimates, J. Phys. Oceanogr., 13, 1093-1104.

Hsueh, Y., and Yury Golubev, 2001: A numerical model calculation of the flow in DeSoto Canyon in response to northerly wind bursts in winter. Submitted to Gulf of Mexico Science.

Kalnay, E., M. Kanamitsu, R. Kistler, W. Collins, D. Deaven, L. Gandin, M. Iredell, S. Saha, G. White, J. Woollen, Y. Zhu, A. Leetmaa, R. Reynolds M. Chelliah, W. Ebisuzaki, W.Higgins, J. Janowiak, K. C. Mo, C. Ropelewski, J. Wang, Roy Jenne, Dennis Joseph, 1996: The NCEP/NCAR 40-year reanalysis project. *Bulletin of the American Meteorological Society*, 77, 437-471.

Krishnamurti, T.N. and R. Krishnamurti, 1979: Surface meteorology of the A-scale during one-hundred days of GATE. Deep-Sea Res., GATE Suppl. 26, 29-26.

Levitus, S., 1982: Climatological atlas of the world ocean. NOAA Prof. Pap.,13, US Government Printing Office, Washington DC, 172.

Mitchum, G., and W. Sturges, 1982: Wind-driven currents on the west Florida shelf. J. Phys. Oceanogr., 12, 1310-1317.

Science Application International Corporation: DeSoto Canyon Eddy Entrusion Study. MMS Contract 1435-01-96-CT-30825. Data Products: Set 1-5, SAIC, Raleigh, North Carolina, 1998.

Richardson W.S., Schmitz W.S., and Niiler P. 1969: The velocity structure of the Florida Currents from the Florida Strate to Cape Fear. Deep-Sea Res. 16, Suppl., 225-331.

Sturges, W., 1992: The spectrum of Loop Current variability from gappy data. J. Phys. Oceanogr., 22, 1245-1256.

Sturges, W., 1994: The frequency of ring separation from the Loop Current. J. Phys. Oceanogr., 24, 1647-1651.

Vukovich, Fred M., 1995: An updated evaluation of the Loop Current's eddy-shedding frequency. J. Geophys. Res.,100, 8655-8659.

Weisberg, R., B. D. Black, and H. Yang, 1996: Seasonal modulation of the west Florida continental shelf circulation. Geophys. Res. Lett., 23, 2247-2250.

5c. Low-frequency variability of surface currents on the northeastern Gulf of Mexico (NEGOM) shelf

LOW-FREQUENCY VARIABILITY OF SURFACE CURRENTS ON THE NORTHEASTERN GULF OF MEXICO (NEGOM) SHELF

by

Yury Golubev* and Ya Hsueh
Department of Oceanography
Florida State University
Tallahassee, FL 32306

Abstract

An examination of the paths of satellite-tracked drifters uncovers differences in the temporal variability of low-frequency surface currents on NEGOM shelf areas east and west of 85W. The monthly mean currents obtained from drifter paths east of this longitude are well correlated with sea surface heights (SSH) in the Straits of Florida, reflecting the offshore pressure forcing that drives a barotropic flow on the west Florida shelf (WFS) on a nearly annual frequency. In contrast, monthly mean surface currents on the shelf west of 85W are found to correlate highly with the zonal wind component, indicating the efficacy of alongshore winds in driving the alongshore shelf currents.

1. Introduction.

The study area of the northeastern shelf of the Gulf of Mexico (Figure 1) comprises of the area between the Mississippi River mouth and Cape San Blas in the Florida Panhandle and the northernmost part of the broad west Florida shelf (WFS) with a width on the order of 200km.

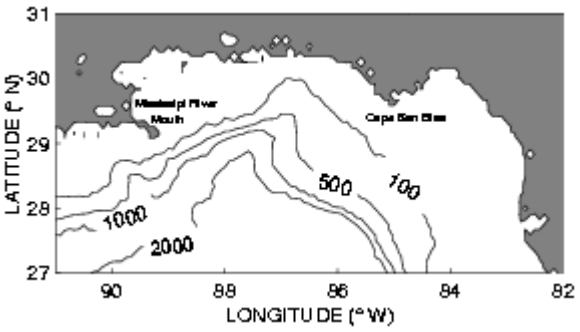

Figure 1. The map depicts the continental shelf in the northeastern Gulf of Mexico.

There have been a number of studies of the continental shelf circulation and its variability in the northeastern and eastern Gulf of Mexico. The general hydrography and current regime in this region are summarized in early literature (Ichiye et al., 1973; Jones, 1973). Direct current measurements are discussed in several more recent articles (Mitchum and Sturges, 1982; Marmorino, 1982; Weisberg et al., 1996; Yang and Weisberg, 1999). Drift bottle studies (Tolbert and Salsman, 1964) show a measure of seasonality in the surface circulation. Released in summer, drift bottles tend to return to the north and those released in winter tend to return to the south. Seasonal surface-current variability on the WFS has also been reported on the basis of data from satellite-tracked drifters (P.P. Niiler at al., personal communication, 1996).

As is well known, the Loop Current (LC) dominates the circulation in the deep part of the eastern Gulf of Mexico. Irregular northward penetrations of the LC into the eastern Gulf occur with periods between 8-9 and 13-14 months (Sturges, 1992,1994; Vukovich, 1995). The northward penetration usually culminates with the separation of an anti-cyclonic ring, followed by the collapse of the loop to its starting position around Cuba. Vukovich (1995) finds a predominant period of the LC northward penetration of 11.1 months. Sturges and Leben (2000) give two main frequencies of ring detachment, one at 9 and the other at 11.6 months. So, the northward penetration of the LC occurs at a nearly annual frequency. This wax and wane of the LC imparts variability on the WFS. An oddity actually is noted in the influence on the shelf flow of the LC and its variability. Sturges and Evans (1983) finds that on the low frequency, the southward flow inferred from coastal sea-surface elevations over the WFS does not reach its maximum strength at the time when the LC is fully extended into the Gulf, with the LC front in close proximity of the WFS. This phase miss-match indicates the LC influence on the WFS comes about not through lateral friction, but through pressure imposed by the LC along the shelf break (Hsueh and Golubev, 2001).

On the other hand, there is ample evidence of direct wind influence on a seasonal time scale in shelf currents in the Gulf of Mexico (Jones, 1973; Blaha and Sturges, 1981; Mitchum and Sturges, 1982; Weisberg et al, 1996). Thus, the above-mentioned seasonality in surface velocity data from the drifters in the study area can be either (locally) wind-driven or remotely induced by the LC careening around the south end of the WFS with a variability approximately at the annual period. The purpose of the present paper is to discuss, on the basis of a variety of available data, the role of these two factors, the wind and LC-related pressure, in the seasonal variability of drifter-based surface currents on the continental shelf in NEGOM. Section 2 describes the data source and data statistics. Data analysis is reported in section 3. A final section 4 contains the summary and conclusions.

2. Data description.

Three sets of data are used in the analysis. The first one is a surface velocity data set based on satellite-tracked drifters deployed from February 1996 through April 1997 in the eastern Gulf of Mexico (P. P. Niiler at al., personal communication, 1996) as a part of Mineral Management Service NEGOM Project. The second set of data comprises the sea surface height measurements obtained by the TOPEX/Poseidon satellite altimeter for the same time period. The third set of data used is wind velocity data from three NOAA stationary buoys in the northeastern Gulf of Mexico (see later Figure 3).

The following steps are taken to treat the velocity data for the study. First of all, drifter velocity components are binned into daily mean series with a 0.25 (longitude) by 0.17 (latitude) degree bin size in the area 27N-30.5N and 83W-89W from February 7,1996 through April 30, 1997. If there is only one drifter velocity in a particular bin square, it is accepted as the daily mean for that particular day. If there are several drifter velocities during a day in the square, the velocity components are averaged to give the daily mean. The number of days with non-zero daily mean velocity over the study area in the time period between February 7, 1996 and April 30, 1997 is shown at Fig. 2a.

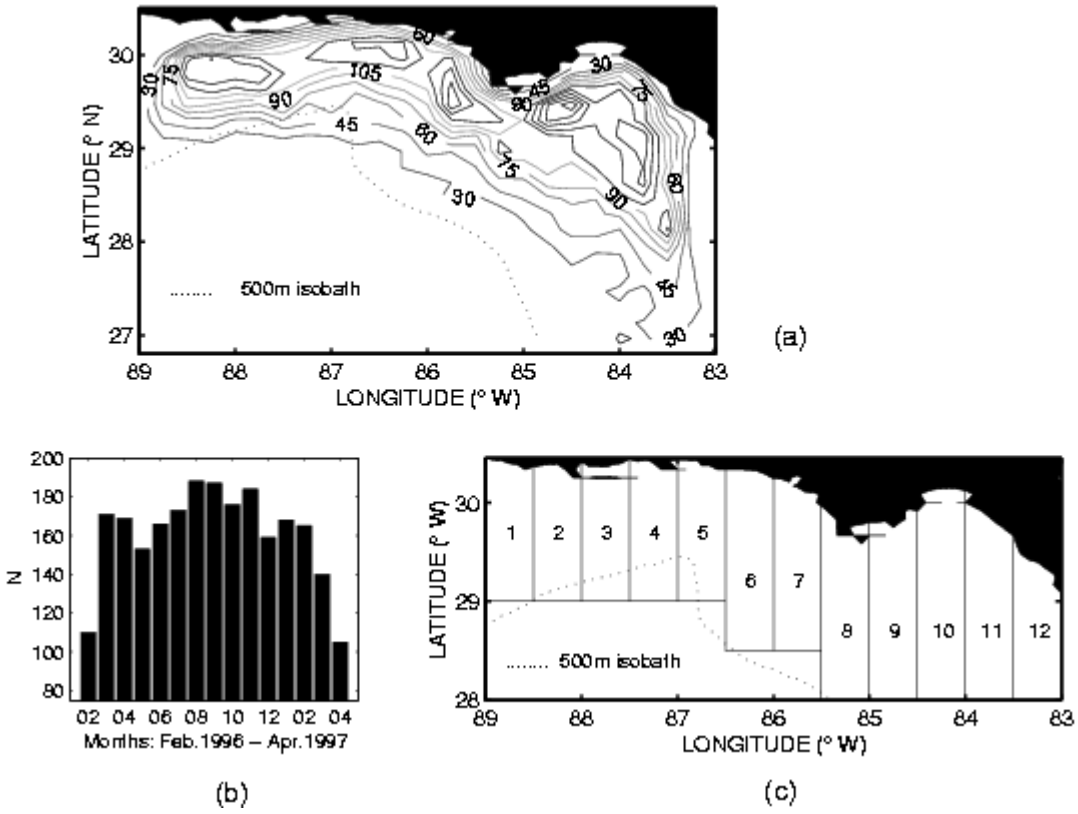

Figure 2. (a) The field of number-of-day with non-zero daily mean velocity from the drifter trajectories between February 7, 1996 and April 30, 1997 is contoured at an interval of 15. The total number of days with non-zero values for the entire study area is 448. (b) Bar-charted is the number-of-square with a non-zero monthly mean drifter velocity between February 1996 and April 1997. Each square measures 0.25 by 0.17 degrees. (c) The twelve meridional strips of NEGOM shelf area in which daily mean and 10-day mean drifter velocities are calculated.

As can be seen, the shelf area between 29N and 30.5N has the highest density of observations. To the south and southeast, the study area is bounded by the 500m isobath.

The next step is to obtain monthly mean drifter velocities at the center of the square. There are 15 months from February 1996 till April 1997. To obtain a monthly mean in a given square, the rule is that there must be at least two daily mean values in that square for that particular month. So, the smallest number of daily mean values is 30 for any area to be considered during the entire observational period. Thus the study area is further restricted to the area enclosed by the 30-day contour in Figure 2(a). Of course, obtaining a monthly mean by averaging two daily values is a very crude procedure and the calculated monthly means are subject to large errors near the boundary of the study area. One has also to be very careful with the interpretation of the monthly mean values. Figure 2(b) gives the number of squares with non-zero monthly mean for each of the month from February 1996 till April 1997. From Figure 2(b), the area covered by monthly mean data in a particular month can be estimated. Such area is the smallest in February 1996 and April 1997 when the area is 40% of the area enclosed by the 30-day contour in Figure 2(a). The area for the two months of August and September is about 70% of the full area, which contains 375 squares.

Finally, to compare drifter velocity with altimeter data and surface winds a daily mean and a 10-day mean of velocity components are calculated for the 12 meridional strips shown in Figure 2 (c). Each strip spans 0.5 degree in longitude. The area covered is bounded by 89W to the west, 83W to the east, the coastline to the north, and the 500m isobath and 28N to the south.

The next set of data used is the TOPEX/Poseidon altimeter measurements available every 10 days at points shown in Figure 3 (numbered north to south).

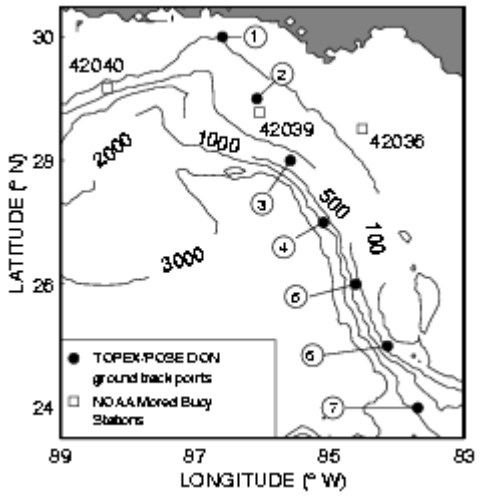

Figure 3. Seven points (black dots) on the TOPEX/Poseidon ground track where altimeter measurements are available every 10 days on the WFS. Open squares mark the location of NOAA buoys (42040, 42039, and 42036) where winds at 10m above the sea surface are measured.

In addition, monthly mean two-dimensional fields of sea level reconstructed for the entire Gulf of Mexico from the TOPEX/Poseidon altimeter data are used (Leben R., 1998; personal communication). The third set of data used contains the two components of wind velocity measured at three NOAA stationary buoys in NEGOM (Figure 3). Daily mean wind data are available from February 1, 1996 through April 30, 1997.

3. Data Analysis.

Monthly mean fields of surface velocity obtained from positioning satellite-tracked drifters are presented in Figures 4(a)-4(c).

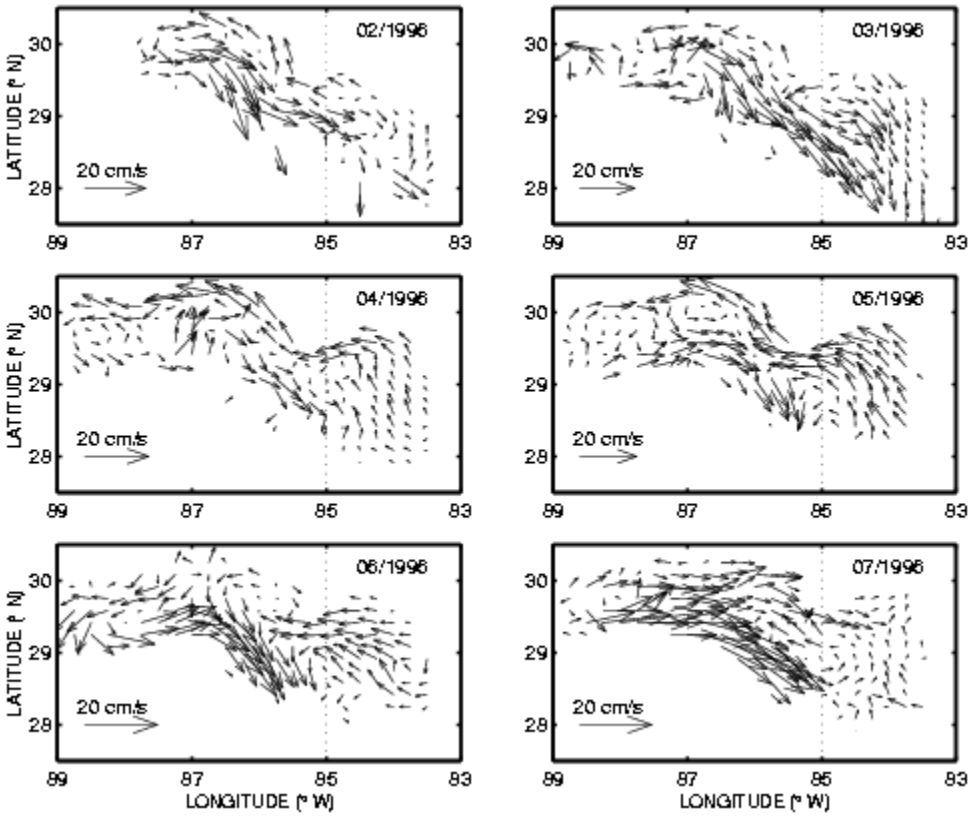

Figure 4. Monthly mean surface currents vectors from satellite-tracked drifters are shown for the study area during February 1996 – April 1997

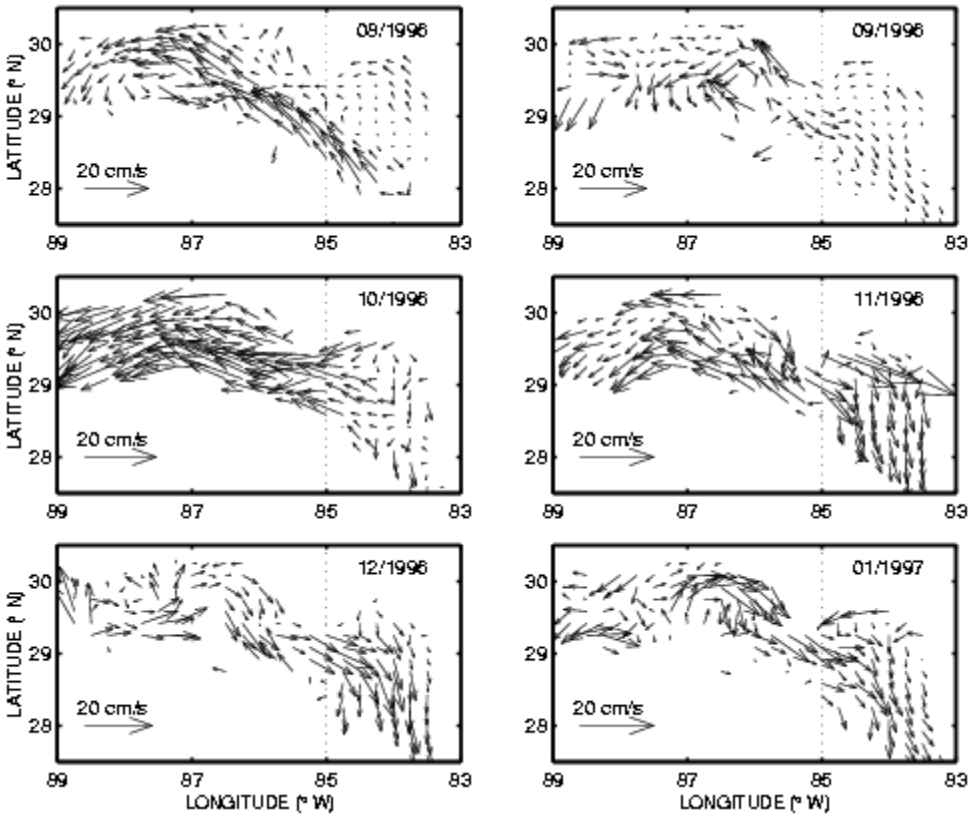

Figure 4. Continued.

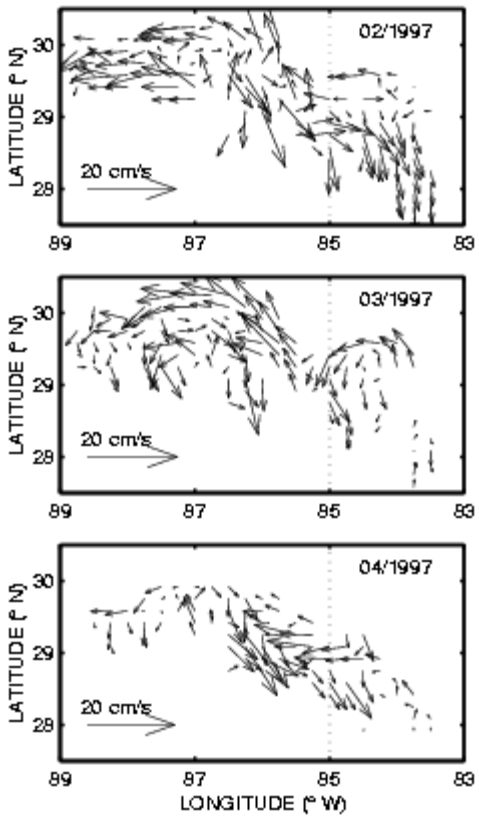

Figure 4. Continued.

The currents vary significantly during the year. They are the strongest in October 1996 when westward flow with speed up to 25 cm/s are obtained and they are the weak in September 1996 and in March-April 1997 when the speed does not exceed 10 cm/s. The meridional structure of currents also varies from month to month. In May 1996, currents in the northern portion of the area are westward, while those in the south are eastward or southeastward. In October, the strong westward flow is found nearly everywhere west of 85W. The motion appears disorganized in September 1996 and April 1997. A close look reveals that the monthly mean currents behave differently east and west of 85W (dashed line in Figure 4). The difference is particularly noticeable in June-July 1996 and in October and November 1996. Shown in Figure 5 are the kinetic energy of mean currents averaged over the squares for the area to the west of 85W (first eight strips in Figure 2(c)) and for the area to the east of 85W (strips 9 to 12 in Figure 2 (c)). To produce the curves in Figure 5, kinetic energy values are obtained for each 10-day period between February 9, 1996 and April 30, 1997 and then smoothed with a sliding mean.

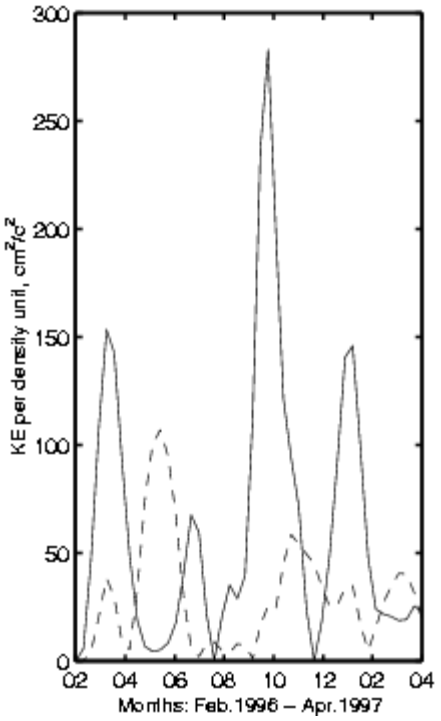

Figure 5. Kinetic energy of mean currents averaged over the squares to the west of 85W (solid) and to the east of 85W (dashed).

Figure 5 shows that the currents to the west of 85W are generally more intense and particularly so in October and also in March 1996 and January 1997. Currents to the east of 85W are generally less energetic and show peaks in May 1996 and November 1996. It appears that the currents on the shelf to the west of 85W and to the east of 85W have different origins. To expose the difference, two sets of correlation functions are calculated. The first comprises of correlation functions between wind and current velocity components (daily mean data are used). The second set comprises those between the sea level heights (SSH) at the seven points shown in Figure 3 and current velocity components (10-days mean data are used). Calculations are done for each of the twelve strips in Figure 2(c). It should be mentioned that in the case of wind and current velocity, the lag is 1-2 days (current velocity lagging the wind). In the case of SSH and current velocity, the lag is 40-50 days (current lagging behind SSH).

Distributions of maximum of correlation function (MCF) with longitude for both sets are shown in Figure 6.

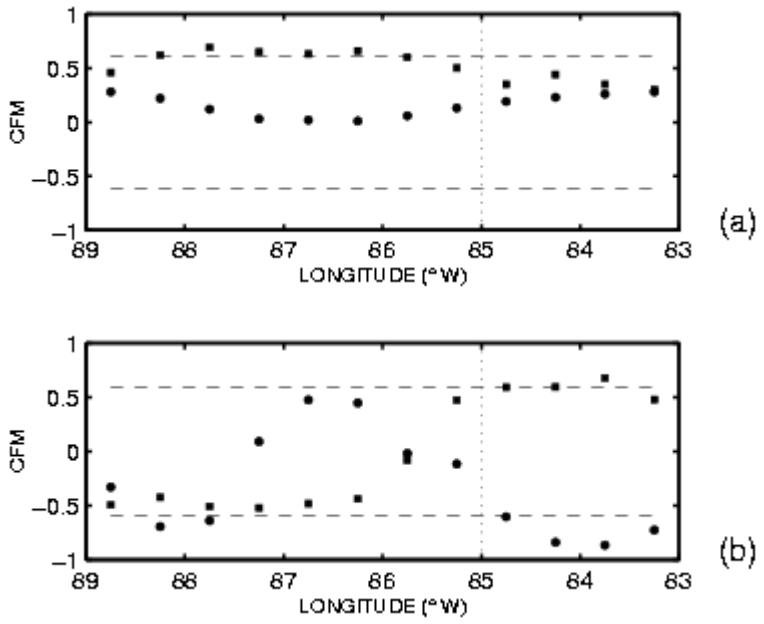

Figure 6. (a) Correlation function maximum (CFM) between wind stress and surface currents for the zonal (squares) and meridional (circles) components. (b) CFM between sea-level-height (SSH) at point 7 in Figure 3 and zonal (squares) and meridional (dots) surface current velocity component. The correlation functions are calculated for each of the twelve strips in Figure 2(c). Only the maxima are shown.

The upper panel links the wind and current velocity. For the zonal components, high values of MCF are found between 85.5W and 88.5W and the MCF values are lower outside this range of longitudes. The MCF values are generally small for the meridional component, particularly to the west. In the case of SSH and zonal component of current velocity, high values of MCF are found to the east of 85W and negative values between 85W and 88W. There is no marked difference in magnitude between the MCF's for the two components. Both components of current velocity are correlated with SSH, but the MCF variation in longitude shows a 180-degree phase shift. It should be noted that the results in the lower panel is for point 7 in Figure 3, in the Straits of Florida.

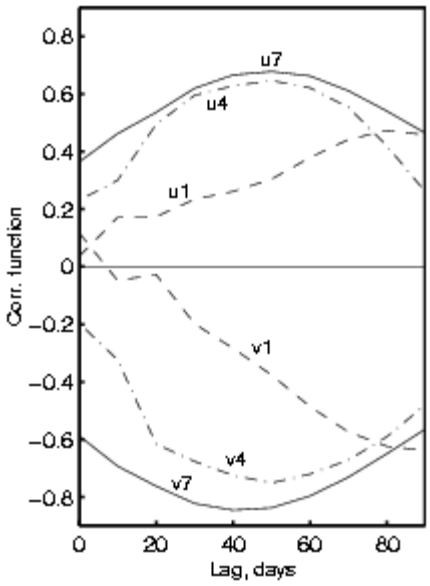

Figure 7. Correlation function between SSH at points 1, 4, and 7 in Figure 3 and zonal (u) and meridional (v) surface current velocity components in strip 11 in Figure 2(c).

At other TOPEX/Poseidon track points in Figure 3, the correlation is not as good. Figure 7 (a) shows correlation functions between SSH at points 1, 4, and 7 in Figure 3 and velocity components. As can be seen, the best result is found at point 7 despite the fact that this point is the farthest away from the study area. It should be noted that the variation of SSH at this point is the largest (see later Figure 9(b)). The origin of the oscillation seems obviously related to the Loop Current variability, leading to similar variability on the shelf the north.

The linkage between surface currents on the shelf to the west of 85W and local winds on a lag of 1-2 days seems obvious too: the currents here basically are wind-driven.

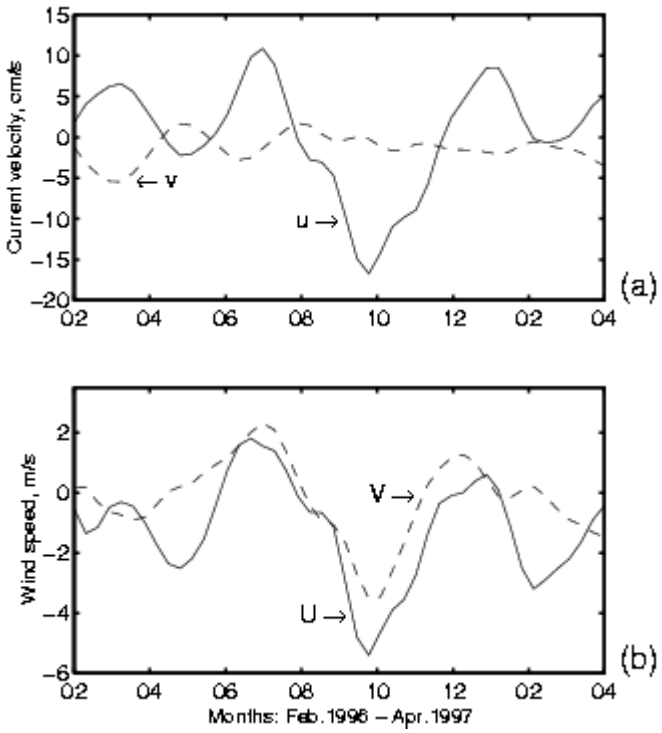

Figure 8. (a) Monthly mean surface velocity components from drifters averaged over the shelf area between 88W and 86W (strip 3 through 6 in Figure 2 (c)). (b) Monthly mean wind components averaged for the three NOAA buoys in Figure 3.

Figure 8 shows the variability of monthly mean values of zonal and meridional component of surface current velocity averaged for the area in Figure 2 (c) between 86W and 88W and the variability of the wind components there. It is clear that the zonal components of the current and wind are highly coherent.

The remaining questions are: What is responsible for the observed surface current variability in area to the east of 85W; how SSH oscillations in the Straits of Florida could affect surface currents on the northeastern shelf and what produces the SSH oscillations at the Straits of Florida?

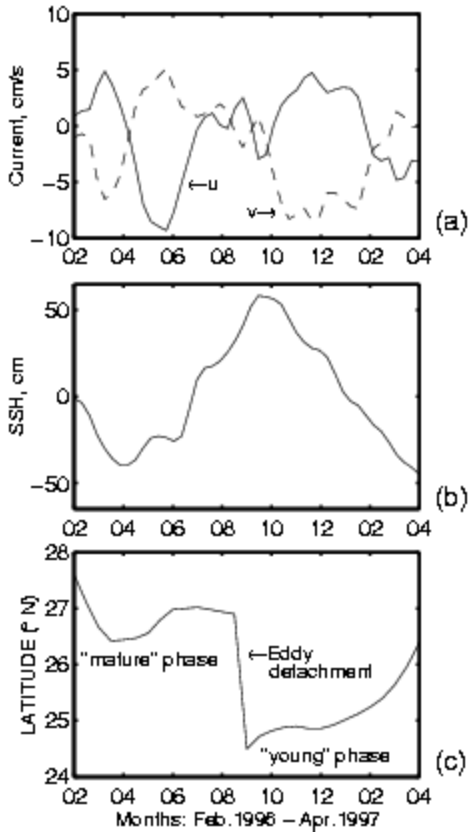

Figure 9. (a) Monthly mean surface current velocity components averaged over the area between 85W and 83W (strips 8 through 13 in Figure 2 (c). (b) Monthly mean SSH at point 7 in Figure 3. (c) Latitudinal location of the northern edge of the Loop Current during 1996-97.

Drifter-based monthly mean surface current velocity components averaged in the area between 85W and 83W are presented at Figure 9 (a). Compared to similar plots in Figure 8 (a) for the western portion of the study area, it is clear that the surface current here is no longer simply in a east-west orientation. The north-south component appears equally important. The monthly mean SSH at point 7 in the Straits of Florida is shown in Figure 9 (b). It appears that with a shift of 40-50 days the SSH curve is quite similar to the zonal component of the surface current velocity. Also, the meridional component seems 180-degree phase-shifted from the SSH. The flow is strongly southward when the SSH is high around November and December of 1996. Point 7 possesses the largest amplitude of SSH oscillation among all the points in Figure 3. The difference in SSH between April and September-October 1996 and between September-October 1996 and April 1997 is almost 1m. Figure 9(c) shows the approximate location of the LC northern boundary in latitude. This picture is obtained using the two-dimensional SSH fields from the Historical Altimeter Data Viewer web site (Colorado Center for Astrodynamics Research). The northernmost location of zero value isoline contouring anti-cyclonic eddy formed by the Loop Current is fixed. Period of February-August represents a phase of the mature LC with a well-developed anti-cyclonic ring which is about to separate from the LC. According to the two-dimensional SSH distribution there

are two imminent occurrence of ring separattion during this phase: in the mid of February and in the end of July - August 1996. Final detachment occurs in September; after that the LC collapse to the south and began to grow (a young phase). The SSH variability is consistent with the procession of the LC phases. The SSH is low during mature phase, when the LC follows the shelf break. The high values occur soon after the ring separation, when the LC runs into the shelf break near the location of point 7, giving rise to a high SSH. The step function structure of the imposed pressure along shelf-break leads to a flow to the south (Hetland et al., 1999).

4. Summary and conclusions.

Numerical simulation of the Gulf of Mexico with circulation driven solely by the LC inflow (Hetland et al., 1999) shows that the southward flow on the WFS varies out of phase with the northward penetration of the LC. The southward current on the WFS is caused by the north-to-south drop in dynamic pressure imposed on the shelf by the LC. When the LC is in its young phase with small northward penetration, it collides with the shelf break, creating a pressure drop to the east as the LC speeds up due to the constriction of the Straits of Florida. This pressure structure forces a southward flow that extends to the northern reaches of the WFS. When the LC is in its mature phase and its penetration to the north is at the fullest extent, pressure drop is much weaker, leading to a southward flow that may not extend too far to the north (Hetland, 1999; Hetland et al., 1999). The results presented here appear consistent with this, providing a link between surface current variability on the northeastern WFS and SSH variation in the Straits of Florida - the place where the SSH responds to the LC development. It is in some sense a surprise to find low correlation between currents and the wind to the east of 85.5W (Figure 6(a)). This result appears in contradiction with findings elsewhere (Yang et al., 1999), where the conclusion the seasonal winds may play a dominant role in the seasonal variations of surface currents at the WFs is made. Another important thing is the following. The wind in the northern and northeastern part of the Gulf of Mexico has predominant semiannual variability (Blaha and Sturges, 1978; Golubev and Hsueh, 2000; see also Fig.8) which can even be easily seen in the climatology wind data (Hellerman and Rosenstein, 1983). Different predominant harmonics in the wind-driven circulation (semi-annual) and the LC induced currents (almost annual) may be a point for separation of currents on the shelf forced by these two mechanisms simultaneously.

Acknowledgement

Dr. P. P. Niiler provides the drifters data. Mrs. Debria Hayes and other people from NODC (NOAA) have been very generous in sharing TOPEX/Poseidon altimetry data. The National Data Buoy Center staff helps with providing the wind data. The help is also acknowledged of the people at Colorado Center for Astrodynamics Research (CCAR) for the use the Gulf of Mexico Historical Altimeter Data Viewer at CCAR web site.

REFERENCES

Blaha, J., and W. Sturges. 1981. Evidence for wind-forced circulation in the Gulf of Mexico. J. Mar. Res., 39(4), 711-734.

Golubev, Y., and Y. Hsueh. 2001. Temperature variability in the northeastern Gulf of Mexico in 1997-1998. Submitted to Gulf of Mexico Science.

Hellerman, S,, and M. Rosenstein. 1983. Normal monthly wind stress over the world ocean with error estimates. J. Phys. Oceanogr., 13, 1093-1104.

Hetland, R. D., Y. Hsueh, R .R. Leben, and P. P. Niiler. 1999. A Loop Current-Induced Jet Along the Edge of the West Florida Shelf. Geophys. Res. Lett., 26, 2239-2242.

Hsueh, Y., and Yury Golubev. 2001. A numerical model calculation of the flow in DeSoto Canyon in response to northerly wind bursts in winter. Submitted to Gulf of Mexico Science.

Jones,J. I. 1973. Physical oceanography of the northeast Gulf of Mexico and Florida continental shelf area. A Summary of Knowledge of the Eastern Gulf of Mexico, J.I. Jones, R.E.Ring, M.O.Rinkel and R.E.Smith, Eds., Florida Institute of Oceanography, St. Petersburg, 28-96.

Ichiye, T., H.-H. Kuo, and M. R.Carnes. 1973. Assessment of currents and hydrography of the eastern Gulf of Mexico. Tech. Rep., Dept Oceanogr., Texas A&M University, College Station.

Marmorino, G. O.. 1983. Summertime coastal currents in the Northeastern Gulf of Mexico. J. Phys. Oceanogr., 13, 65-77, 1983.

Mitchum, G. T., and W. Sturges. 1982. Wind-driven currents on the West Florida Shelf. J. Phys. Oceanogr. 12, 1310-1317.

Sturges, W. 1992. The spectrum of Loop Current variability from gappy data. J. Phys. Oceanogr., 22, 1245-1256.

Sturges W. 1994. The frequency of ring separations from the Loop Current. J. Phys. Oceanogr., 24, 1647-1651.

Sturges, W., and J. C. Evans. 1983. On the variability of the Loop Current in the Gulf of Mexico. J. Mar. Res. 41, 639-653.

Sturges, W., and R. Leben. 2000. Frequency of ring separation from the Loop Current in the Gulf of Mexico: A revised estimate. J. Phys. Oceanogr., 30, 1814-1819.

Tolbert, W. H., and G. G. Salsman. 1964. Surface circulation of the eastern Gulf of Mexico as determined by drift-bottled studies. J. Geophys. Res., 69, 223-230.

Vukovich, F. M. 1988. Loop Current boundary variations. J. Geophys. Res., 93, 15,585-15,591.

Vukovich, F. M. 1995. An updated evaluation of the Loop Currents eddy-shedding frequency. J. Geophys. Res., 100, 8655-8659.

Weisberg, R. H., B. D., Black, and H. J., Yang. 1996. Seasonal modulation of the west Florida continental shelf circulation. Geophys. Res. Lett., 23, 2247 - 2250, 1996.

Yang, H. J., and R. H., Weisberg. 1999. Response of the West Florida Shelf circulation to climatological wind stress forcing. J. Geophys. Res., 104, 5301-5320, 1999.

Yang, H. J., R. H. Weisberg, and P. P., Niiler. 1999. Lagrangian circulation and forbidden zone on the West Florida Shelf Cont. Shelf Res. 19, 1221-1245.

5d. West Florida shelf response to local wind forcing April 1998

West Florida shelf response to local wind forcing: April 1998

Robert H. Weisberg*

Zhenjiang Li

And

Frank Muller-Karger

College of Marine Science
University of South Florida
St. Petersburg, Florida 33701

Final, April 2001

* *Corresponding author address*: Dr. Robert H. Weisberg, College of Marine Science, University of South Florida, 140 Seventh Avenue South, St. Petersburg, Florida 33701. Email: weisberg@marine.usf.edu

Abstract

We compare *in-situ* velocity and sea level data with a model simulation for the west Florida continental shelf during April 1998. Responses for three periods of downwelling and upwelling favorable winds are documented. Velocity profiles show coastal jets in the along-shelf direction that are accompanied by oppositely directed upper and lower layer flows in the across-shelf direction. These along- and across-shelf currents and their associated vertical velocity comprise the fully three-dimensional inner-shelf responses to local wind forcing. The responses are sensitive to stratification. Large velocity vector turning occurs under stratified conditions, whereas less turning occurs under well-mixed conditions. With an initial density field representative of April 1998 the model simulates velocity and sea level variations that agree with the observations. Without stratification substantial mismatches occur, both for currents and sea level. Local momentum input is a primary forcing agent for the inner-shelf circulation when the shelf is wide enough to distinguish the inner-shelf from the shelf-break. Inner-shelf responses, however, depend on the density field, which depends on local and offshore buoyancy fluxes. Modeling the inner-shelf responses to wind forcing requires maintenance of the density field through data assimilation and adequate surface, offshore, and land-derived buoyancy inputs.

Dynamical analyses define the inner-shelf as the region where the surface and bottom boundary layers are important in the momentum balance. Kinematically, this is where the surface Ekman layer divergence, fed by the bottom Ekman layer convergence, or conversely, sets up the across-shelf pressure gradient. With respect to vertically integrated vorticity, the inner-shelf is where bottom stress torque tends to balance bottom pressure torque, as contrasted with the shelf-break where the primary balance is between bottom pressure torque and the rate of change of relative vorticity.

Under stratified conditions the inner-shelf responds asymmetrically to upwelling and downwelling favorable winds, with the offshore scale and magnitude of the responses for upwelling favorable winds both being larger than for downwelling favorable winds. This asymmetry is a consequence of the bottom Ekman layer. With respect to the streamwise vorticity component, buoyancy torque by isopycnals bending into the bottom adds constructively (destructively) with planetary vorticity tilting by the sheared coastal jet under upwelling (downwelling) favorable winds causing the asymmetry. Such asymmetry may have important ramifications for material property distributions on the shelf.

1. Introduction

Continental shelf circulation results from both local and offshore forcing. Local forcing is by momentum and buoyancy input at the sea surface and buoyancy input at the land boundary. Offshore forcing is by momentum and buoyancy input at the shelf-break. The partition of influence between these contributing factors varies with shelf location and geometry, and nowhere is this partition quantitatively accounted for. How continental shelves are forced thus remains a fundamental question for both the circulation and for the biological, chemical, and geological consequences of the circulation.

The west Florida shelf (WFS) is an end member in the ensemble of continental shelves for which local forcing may be presumed to be of primary importance. This is because the WFS is wide enough for its inner-shelf to be distinguished from the shelf-break. Given the complex nature of continental shelves and the limitations of both *in-situ* data and models, it is useful to simplify the circulation problem by isolating factors and questioning how well a given data set can be explained by these factors. Along this vein, we ask how well coastal sea level and inner-shelf currents can be explained by the influence of local wind forcing alone. We compare *in-situ* data from April 1998 with a numerical model driven by observed time varying, but spatially uniform, winds. Our results suggest that inner-shelf currents may be accounted for by local wind forcing, given an appropriately specified initial density field. The density field, however, is shown to play an important role, and since the density field is determined by a combination of offshore and local buoyancy forcing, all such factors must be treated in order to produce useful model products.

The paper is organized as follows. Section 2 reviews background materials on the response of a continental shelf to synoptic wind forcing. Section 3 introduces the *in-situ* data and the model used to simulate these data. Comparisons between model results and data are given in section 4. Motivated by these comparisons, albeit at limited observational locations, we expand upon the model flow field kinematics in section 5, where fully three-dimensional structures are shown. For brevity, we emphasize one complete cycle of responses to successive downwelling and upwelling favorable winds, and an asymmetry between upwelling and downwelling responses is noted. Section 6 then exploits the model fields to develop the momentum and vorticity balances that help to define the inner-shelf separate from the shelf break. The results are summarized in section 7, where, along with discussing the asymmetry, it is recognized that the synoptic and seasonal scale variability can not be fully separated since responses of one depends upon the density field provided by the other. This is true for sea level, and more so for currents.

2. Background

Continental shelves are dynamically complex. In relatively deep water the surface and bottom boundary layers are separated by a bottom slope constrained geostrophic flow. As the water depth decreases towards the coast the surface and bottom boundary layers tend to merge across the geostrophic interior. Here, we define the inner-shelf as the near-coastal region where the

surface and bottom boundary layers are dynamically important. Our definition is somewhat different from that given by Lentz (1994), and this difference will be clarified in section 6. These boundary layer influences, coupled with the coastline constraint, result in kinematical and dynamical characteristics of the inner-shelf that may differ markedly from those occurring farther offshore. Generally, for synoptic scale variability where wind stress is the principal motive agent, the inner-shelf reacts to the presence of the coast through the establishment of a surface pressure gradient. This occurs through divergence brought about by surface and bottom Ekman layer transports (e.g., Gill, 1982, p394), and recent evidence for such adjustment on the WFS is given by the upwelling case study of Weisberg et al. (2000). Regularly occurring sub-tidal sea level variations show this adjustment to be a common feature of all shelves.

Descriptions of inner-shelf variability have emerged largely from observations on the continental shelves and Great Lakes of North America. Csanady (1982), Walsh (1988), and Brink et al. (1998) provide overviews, and recent representative works from different regions include those of Lentz (1994), Smith (1995), Weisberg et al. (1996), Weatherly and Thistle, (1997), Yankovsky and Garvine (1998), Lentz et al. (1999), and Munchow and Chant (2000). Insights on the dynamics of the inner-shelf are found in the analytical treatment of Mitchum and Clarke (1986). The complex nature of turbulent boundary layers, however, limits the use of analytical techniques, and this has led to numerical model studies of inner-shelf turbulence in simulations of one or two dimensions (e.g., Weatherly and Martin, 1978; Allen et al., 1995; Lentz, 1995). Two dimensions, however, exclude the interactions that may occur between local and large-scale processes and the possibility that the dynamical interactions controlling divergence and vertical motion may vary in the along-shelf direction. For example, in contrast with the two-dimensional circulation pattern of equal and opposite upper and lower layer flows reported by Lentz (1994) for the northern California coast, Munchow and Chant (2000) report a fully three-dimensional flow with a net across-shelf transport for the New Jersey coast. Three-dimensionality there is attributed to an along-shelf pressure gradient force due to coastal geometry and baroclinicity. Long-wave models that assume a boundary condition of no net across-shelf flow at some distance from the coast (e.g., Clarke and Van Gorder, 1986; Lopez and Clarke, 1989) are to some extent contrary to these findings, and additional sensitivity studies such as Samelson (1997) are warranted. While the general physical concepts espoused in all of these studies apply, it is becoming increasingly clear that each individual continental shelf environment is somewhat unique, and that the region of the inner-shelf, where important across-shelf transports occur, requires better understanding.

3. The Observations and the Model

3.1 Observations

Exploratory measurements of inner-shelf velocity profiles on the WFS were initiated in November 1996 with the deployment on the 20 m isobath offshore of Sarasota, FL of a bottom-mounted 300 kHz acoustic Doppler current

profiler (ADCP) manufactured by RD Instruments, Inc. Using 0.5 m bin spacing, and after editing surface effects, the data set yielded horizontal velocity profiles between depths of 2.5 m to 16 m. Ancillary data sets include sea level from the NOAA tide gauge at St. Petersburg, FL, surface winds from the NOAA buoy number 42036 located at mid-shelf, and velocity profile data from a buoy located at the 50 m isobath. These measurement locations are shown in Figure 1. The data collection effort was initially unsupported by hydrographic data. Through efforts by the Mote Marine Laboratory (G. Kirkpatrick, personal communication, 1998) and the University of South Florida, monthly hydrographic sections were initiated in March 1998.

Co-variations in winds, sea level, and currents occur throughout the record, as expected from previous WFS shelf observations (e.g., Mitchum and Sturges, 1982). A new finding is the variability in the relative turning of the velocity vectors with depth for each synoptic weather event. Responses to upwelling favorable winds generally show onshore flow near the bottom and offshore flow near the surface, and conversely for responses to downwelling favorable winds. These responses are oftentimes accompanied by bottom temperature changes. Once the supportive hydrographic sections commenced it became clear that the velocity vector turning is related to the density stratification. April 1998 is a particularly interesting month with a succession of synoptic weather events and large velocity vector turning. We focus our attention on this month for a comparison between the *in-situ* data and a numerical model simulation.

The April 1998 data are shown in Figure 2. With emphasis on the time scales of the synoptic weather variations, all of the data are low-pass filtered to remove oscillations at time scales shorter than 36 hours (subsequent model results are also low-pass filtered). Provided are velocity component isotachs for the along-shelf and across-shelf directions, coastal sea level, wind velocity vectors, and wind stress vectors. Along-shelf is defined as 333^0 relative to the true north. Clear contours are in this up-coast direction and shaded contours are in the reciprocal down-coast direction. For the across-shelf component clear (shaded) contours are directed onshore (offshore). The wind velocity (stress) variations for April 1998 are primarily in the along-shelf direction. Upwelling and downwelling favorable winds are observed over three distinctive periods, and sea level responds to each of these. In the along-shelf direction, each wind change gives rise to a coastal jet of varying vertical structure, i.e., some show subsurface maxima while others show surface maxima. Accompanying the coastal jets are opposing onshore and offshore flows over the upper and lower portions of the water column. The most pronounced response occurs on April 12 when the upwelling favorable winds are largest causing a coastal jet of magnitude 0.6 ms^{-1} with onshore (offshore) flow in the bottom (surface) Ekman layer exceeding 0.2 ms^{-1}. Although the wind stress magnitudes do not differ much from downwelling to upwelling events (April 12 being an exception), the responses in the currents to the upwelling winds are larger in all three cases than the responses to the downwelling winds. A response asymmetry on the WFS is thus observed. Asymmetric behavior in bottom boundary layer thickness has been reported

elsewhere (e.g., Trowbridge and Lentz, 1991 and Lentz and Trowbridge, 1991 for the northern California coast), and the destabilizing or stabilizing influences of either down or up slope density transports, respectively, has been offered in explanation. As we will discuss, however, these boundary layer turbulence arguments do not explain the response asymmetry reported here.

3.2 Model

We employ the Princeton Ocean Model (Blumberg and Mellor, 1987) based on the following attributes. As a primitive equation model, it allows us to diagnose dynamical balances. Its vertical sigma coordinate helps to resolve the flow structures on a gently sloping shelf, and its horizontal orthogonal curvilinear coordinates allows the model grid to conform to topography. By parameterizing friction with an embedded turbulence closure sub-model (Mellor and Yamada, 1982) the frictional forces evolve with the flow and density fields.

The model domain (Figure 1) extends about 750 km along-shelf from the Florida Panhandle to the Florida Keys and about 400 km offshore from the coast. It covers the entire WFS and part of the eastern Gulf of Mexico so that the shelf-break region is resolved. Realistic shelf bathymetry from the National Center for Atmospheric Research is used with 1500 m being the maximum depth beyond the shelf-break and 5 m being the minimum depth at the coastline. The horizontal grids range in size from 6.5 km to 15 km, with an average of 9 km. 16 sigma levels are used in the vertical, distributed logarithmically about the middle to achieve finer resolution of the surface and bottom boundary layers relative to the interior. Other WFS applications of this model grid, along with discussions of the open boundary conditions, are given by Li (1998) and Li and Weisberg (1999a,b).

The model is forced from mid-March through April 1998 by a spatially uniform, time-dependent wind stress. The wind stress components are computed from the *in-situ* wind velocity vectors observed at the NOAA buoy using a wind speed dependent drag coefficient (Wu, 1980). Forcings by surface heat and coastal buoyancy fluxes are excluded due to a lack of data.

To initialize the density field we use hydrographic sections from March and May 1998; April 1998 hydrography is not available. Each section shows a well-defined pycnocline. On this basis we initialize the model density field with a 4 sigma-t density change that spans 20 m in the vertical, centered on 20 m depth. To avoid specious baroclinic adjustments, this initial density field is input without horizontal gradient. Subsequent density field evolution occurs in dynamical balance with the applied forcing. A twin experiment with density set constant at 1023 kgm^{-3} is also performed to compare the responses under stratified and unstratified conditions. Clarke and Brink (1985), through scale analysis of the shallow water equations, show that the response of a wide shelf [with small Burger number, $(L_R/L)^2$, where L_R is the Rossby radius of deformation at the shelf-break and L is the shelf width] to synoptic wind fluctuations should be barotropic. Mitchum and Clarke (1986) suggest that $(L_R/L)^2 < 10^{-2}$ for the WFS, and this magnitude is consistent with the stratification used here. The stratified and constant density experiments provide an opportunity to examine this

barotropic response concept with a primitive equation model. 15 days of model start up is performed using observed winds prior to sampling the model results for April 1998. Since we find the pressure field response to be largely barotropic, consistent with the Burger number argument, the spin up time is on the order of a pendulum day and much less than the 15 days that we used.

4. Comparison Between the *in-situ* Data and the Model Results

4.1 Sea level

Comparisons between sea level observed and modeled at St. Petersburg, FL for the month of April 1998 are shown in Figure 3. The upper and middle panels are for the constant density and stratified cases, respectively, and the lower panel shows the wind stress vector time series used to force the model. Agreement is very good for the stratified case; it is not as good for the constant density case. While the general patterns of sea level responses to upwelling and downwelling favorable winds are replicated in both cases, considerable quantitative mismatch exists between in the model responses and the observations for the constant density case. In particular, the overestimate for the upwelling response around day 23 implies an excessive across-shelf volume transport over the inner-shelf region during this event. Since a vertically integrated across-shelf volume transport in excess of the volumetric rate of sea level change can only occur in a three-dimensional flow, such disparity on agreements with *in-situ* data between the stratified and constant density model simulations implies that stratification significantly affects the three-dimensional flow field.

4.2 Currents

Modeled along-shelf and across-shelf components of velocity from the 20 m isobath off Sarasota, FL are shown in Figure 4a. As is the case for sea level under stratified conditions, the model reproduces the general pattern evolution of the observed velocity component variations (Figure 2). All three upwelling favorable wind events drive down-coast jets with vertical structures similar to those observed, some with subsurface and others with near surface maxima. These down-coast jets are accompanied by onshore (offshore) flow over the lower (upper) portion of the water column. Similar statements apply for the responses to the downwelling favorable wind events, i.e., up-coast jets and across-shelf flow reversals with depth. While the pattern evolutions for the modeled and observed currents are generally similar, differences in details exist for several reasons. First, the model simulations are highly dependent upon stratification, and our initial stratification is merely a guess based upon limited measurements. Second, no provision is made for (unknown) surface heat fluxes or for correcting inevitable departures of the model stratification from nature over the course of the 45-day integration. Third, we use spatially uniform winds when the spatial structure of each synoptic weather system may be different. Despite these shortcomings, the quantitative agreements are surprisingly good, with the best agreements occurring during the downwelling/upwelling sequence of April 7-13. Here the model underestimates the magnitude of the along- and across-shelf

components by about 20%. For other sequences this magnitude mismatch is either larger or smaller, and for the reasons stated above there is little gained by more detailed comparisons. One clear deficiency comparing the model with the data lies within the upper 3 m of the water column where there is no data. The model purports large vertical shear over the upper few meters because its turbulence closure routine yields small eddy viscosity (turbulence length scale is zero at the surface). Whether or not such near surface shear is realistic remains to be determined.

Also depicted in Figure 4a are the modeled isopycnal variations. Relative maxima in isopcynal displacements occur when the across-shelf component is zero suggesting that advective changes through horizontal divergence and vertical velocity are the primary contributors. Across-shelf advection over the lower portion of the water column occurs as a boundary layer response to the coastal jet. Since the coastal jet tends to be maximum when the sea level response is maximum, across-shelf and vertical advection are also maxima at that time. Thus, upwelling and downwelling isopycnal displacement maxima occur at the transitions between upwelling and downwelling favorable winds, accounting for the lag between the isopycnal displacements and sea level. This phase relationship constrasts that of an inviscid, standing baroclinic mode for which the isopycnal and sea level responses occur in an anti-phase relationship, demonstrating the importance of the frictional boundary layers. By not imposing a surface heat flux the isopycnals also tend to slope up with time reducing the stratification.

As with sea level, the twin experiment without stratification yields results for the currents (Figure 4b) that are both qualitatively and quantitatively different from the observations. For the along-shelf component the vertical shear is much more uniform with depth, but the more interesting contrast is in the across-shelf component. Without stratification there is very little turning in the surface and bottom boundary layers, and hence there is very little across-shelf circulation relative to the results with stratification. This behavior for the across-shelf component mimics the longer term observational record that shows pronounced velocity vector turning during times of anticipated stratification versus little turning during times when the water column is expected to be well mixed.

Based on the general agreements between the *in-situ* data and the stratified model results we now use the model to discuss the flow field kinematics and dynamics with emphasis on the downwelling/upwelling response sequence from April 7-14.

5. Model Flow Field Kinematics

The order of presentation includes planar views of sea level, cross-sections of velocity and density at the Sarasota transect, and planar views of currents. We begin with daily snapshots of sea level from day 7 through day 14 (Figure 5a) for the stratified experiment. Peak downwelling and upwelling responses in the sea level fields (as with all other fields) appear on days 9 and 12, respectively. During these peaks the set-down at the coast for the upwelling

response in general is more than a factor of two larger than the set up at the coast for the downwelling response. Moreover, the offshore scale for the upwelling response largely exceeds that for the downwelling response. The transitions to these peak responses show along- and across-shelf surface height gradients of comparable magnitude. While no clear sense of propagation emerges, it does appear that the along-shelf variations in geometry, particularly the relatively narrow shelf in the north and the partial closure by the Florida Keys in the south, play roles in determining the sea level adjustments. The end results are monotonic sea level slopes with coastal maxima, but the transitions to these end states are more convoluted, suggestive of complicated flow patterns.

Similar plots for the constant density experiment are given in Figure 5b. Contrasted with the asymmetric responses of Figure5a (in both magnitude and offshore scale), the constant density experiment yields sea level displacement magnitudes that are nearly proportionate with the wind stress and that have comparable offshore scales for either upwelling or downwelling.

Cross-sections for the along-shelf, across-shelf, and vertical velocity components, and density offshore of Sarasota, FL. are shown in Figure 6a. Our focus is again on the day 9 and day 12 peak responses. On day 9 we see an up-coast jet in the along-shelf component, with onshore flow over the upper half and offshore flow over the lower half of the water column in the across-shelf component, and with downwelling occurring synchronously with the offshore flow. In a parallel, but opposite sense, on day 12 we see a down-coast jet in the along-shelf component, with offshore flow over the upper half and onshore flow over the lower half of the water column in the across-shelf component, and with upwelling occurring synchronously with the onshore flow. Due to the frictional effects of the boundary layers the coastal jet has a vertical shear structure with isotachs bending offshore with depth. This accounts for the subsurface maxima that occur in both the *in-situ* data and the model simulation. In summing the geostrophic interior with the frictional boundary layer flows the velocity vector turns counterclockwise over most of the water column. This is shown for the WFS by Weisberg et al. (2000) and for the New Jersey shelf by Munchow and Chant (2000). As is the case for sea level, the magnitudes and offshore scale for the peak upwelling response are substantially larger than for the peak of the downwelling response. Since the bottom Ekman layer is a response to the coastal jet, across-shelf transports over the lower portion of water occur over the entire offshore extent of the coastal jet for either upwelling or downwelling situations. Since the upwelling response exists over a larger offshore scale than the downwelling response, the across-shelf transports of water for upwelling occur over larger distances than for downwelling.

Similar plots for the constant density experiment are given in Figure 6b. As found for sea level, the asymmetry in the currents under stratified conditions is replaced by a more proportionate response under constant density. With the offshore scales of the coastal jet the surface displacement being equal, the difference in scales for the upwelling and downwelling responses under stratified and constant density conditions parallels that in Figures 5a,b.

Evidence for this model-based assertion of asymmetry exists in simultaneous *in-situ* data that were collected on the 50 m isobath (Figure 7). The same coastal jets as seen in shallower water (Figure 2) appear here, but with less vertical structure, as in the model. For each wind-driven flow reversal we see that the near surface Ekman layer response (extending down to about 20 m depth) is larger than the near bottom Ekman layer response, also consistent with the model. Moreover, for the peak downwelling response around day 9 we see nearly zero across-shelf flow in the bottom Ekman layer versus about 0.05 $msec^{-1}$ onshore flow in the bottom Ekman layer for the peak upwelling response around day 12. These observations are consistent with larger offshore extents for the surface height field and the coastal jet under upwelling favorable winds.

The horizontal structure of the velocity field is complex. Horizontal velocity vector maps for the depth average, near surface, mid-depth, and near bottom fields are shown in the Figure 8 panels a-d, respectively, for the day 9 peak downwelling response. The depth average flow is the simplest of the fields. An up-coast directed jet, confined to the proximity of the shore, is seen with maximum speeds occurring where the sea surface height gradient is maximum. The jet is fed by surface Ekman layer transports that are only partially offset by bottom Ekman layer transports since the bottom Ekman layer is effected only where the surface height gradient and coastal jet are established. Thus the coastal jet accelerates downstream. The character of the near bottom flow also changes from the inner-shelf region, where it is related to the coastal jet, to the shelf break region where it arises by topographic wave variability. The origin of these near bottom flow variations will be evident in the section 6 dynamical analyses. The mid-depth vectors look very similar to the depth average vectors since there the across-shelf flows due to the opposing surface and bottom Ekman layer flows are minimal.

A parallel set of velocity maps are given in Figure 9 for the day 12 peak upwelling response. Similarities exist with Figure 8 (albeit with opposite sign). Contrasting these two figures, however, is the larger offshore scale for the upwelling fields. Strong onshore flows in the bottom Ekman layer exist out to about the 100 m isobath, particularly in the northern part of the domain where the magnitude of the coastal jet is largest. Bottom Ekman layer flows in the southern portion of the domain are reduced by the adverse pressure gradient due to the partial closure by the Florida Keys. Stratification also tends to promote regions of flow field confluence as seen at mid-depth.

A result of the flow field kinematics in switching from downwelling to upwelling favorable winds is manifest in sea surface temperature (SST). Figures 10a,b show satellite AVHRR SST images on April 10 and 13 when the downwelling and upwelling circulations, respectively, culminate in isopycnal displacement maxima. The month of April, in general, shows a cold tongue that extends down-coast at mid-shelf from a region of seasonally coldest SST in the northeastern Gulf of Mexico. Associated with this boreal spring cold tongue is a chlorophyll plume, referred to as the "green river" by Gilbes et al. (1995). This cold tongue is evident on April 10 with warmer waters both inshore and offshore. Transitioning from downwelling to upwelling winds, the cold tongue on April 13 is

greatly amplified and the inshore waters are several degrees colder than on April 10. A region of locally coldest SST is also seen south of Tampa Bay on about the 25 m isobath consistent both with the region of maximum vertical velocity in Figure 6a and with the upwelling case study results of Weisberg et al. (2000). Farther south is a diminution of cold SST consistent with the bottom Ekman layer inhibition by adverse pressure gradient shown in Figure 9. Right at the shoreline in the Florida Big Bend region and along the Florida Panhandle west of Apalachicola Bay we also see eruptions of cold water to the surface. While we do not imply that surface heat flux is not a contributing factor, these SST changes are consistent with the kinematical features of the numerical model simulation described in this section.

6. Model Flow Field Dynamics

6.1 Momentum Balances

We begin with vertically integrated momentum and mass balances (Figure 11) calculated at the 20 m isobath offshore from Sarasota, FL. The wind stress is the lead term in the along-shelf direction (panel a). This causes a local acceleration as the currents tend to adjust to the time varying winds, followed by an along-shelf pressure gradient, a bottom stress, and a Coriolis acceleration, with all of these response terms being of comparable magnitude (although the along-shelf pressure gradient is generally the largest of these). In a purely two dimensional flow the bottom stress would be comparable to the surface stress, whereas in this three-dimensional result the bottom stress is no larger than the other secondary terms. The vertically integrated across-shelf momentum balance (panel b) is much simpler (note the scale change between panels a and b). Here the vertically integrated flow is essentially geostrophic since the ageostrophic contributions from the surface and bottom Ekman layers tend to cancel. The magnitudes of the terms in the across-shelf momentum balance are about a factor of four larger than those in the along-shelf momentum balance.

The three-dimensionality of the flow field is also evident in the vertically integrated across-shelf mass transport (panel c). The four time series are: 1) the Ekman transport associated with the wind stress, 2) the vertically integrated upper and 3) lower layer transports directed either onshore or offshore depending on wind stress, and 4) the total vertically integrated transport. The Ekman transport is computed as $U_e = \tau^w / (\rho_0 f)$, where τ^w is the along-shelf component of the wind stress. The upper and lower layer transports are defined as $U^{upper} = \int_{d_r}^{\eta} u^{upper} dz$, $U^{lower} = \int_{-H}^{d_r} u^{lower} dz$, where u is the velocity component in the across-shelf direction, d_r is the depth at which the across-shelf flow reverses direction, η is the free surface elevation, and H is the mean water depth. The net across-shelf transport is $U^{net} = \int_{-H}^{\eta} u dz$. The upper layer transport is always less than the Ekman transport because the 20 m isobath is within the inner-shelf where there occurs an upper layer across-shelf transport divergence along with

the surface slope set-up. Seaward of the inner-shelf the upper layer transport is comparable to the Ekman transport. The upper layer transport at this particular location is generally over compensated for by the lower layer transport. A contributing factor is the along-shelf pressure gradient that supports an across-shelf geostrophic transport. The along-shelf pressure gradient appears to be larger for upwelling favorable winds than for downwelling favorable winds (panel a). With mass convergence/divergence inferred in the across-shelf direction there must be a mass divergence/convergence in the along-shelf direction to maintain continuity. The coastal jets offshore of Sarasota, FL are therefore spatially accelerating jets, and a consequence of this for upwelling favorable winds is an increase in the intensity of upwelling over what would occur without the spatial acceleration. This is consistent with the region of maximum surface cooling shown in Figure 10b.

An asymmetry in across-shelf transport between upwelling and downwelling is also evident in panel c. This asymmetry arises from the bottom Ekman layer as demonstrated by the ageostrophic portion of the across-shelf momentum balance (panel d). The ageostrophic part is defined as the residual after adding the Coriolis and pressure gradient terms. Both the magnitude and vertical extent of the ageostrophic residual that comprises the bottom Ekman layer at this location are larger for the three upwelling events than for the downwelling events (in particular, compare the April 9 and 12 patterns). This finding is opposite to what is expected from stability arguments for up and down slope flows in a stratified fluid (Trowbridge and Lentz, 1991). Here the bottom boundary layer is consistently larger for upwelling than for downwelling conditions!

To further explore these issues we analyze the across-shelf momentum balance over the Sarasota, FL. transect. Figure 12 shows the results for the peak downwelling event of April 9. Eight panels provide the sequential order of terms that comprise the momentum balance in this coordinate direction. Panels a and b are the Coriolis and pressure gradient terms. Their sum (the ageostrophic residual) is given in panel c for comparison with the frictional terms of panel d (where friction is almost entirely of vertical origin). The sum of panels c and d, in panel e, is for comparison with the advective acceleration terms in panel f. Finally, the sum of panels e and f, in panel g, is for comparison with the only remaining term, the local acceleration, in panel h. Closure is observed showing that the calculation is performed correctly. The lead terms are the Coriolis and pressure gradient terms. The ageostrophic residual is accounted for primarily by the surface and bottom Ekman layers, and the only other term of substance is the local acceleration. The pressure gradient is maximum near the coast and it decreases to zero by about the 50 m isobath. Modified by surface and bottom friction, the coastal jet seen in the Coriolis term follows the pressure gradient. The pressure gradient is relatively depth independent, i.e., it is primarily barotropic consistent with the Burger number arguments of Clarke and Brink (1985). The pressure gradient, however, does decrease across the bottom Ekman layer due to the sloping isopycnals there.

The comparable analysis for the peak upwelling event of day 12 is shown in Figure 13. The ordering of terms is the same as in Figure 12. The difference is in the magnitude and the offshore scale of the Coriolis and pressure gradient terms. Here the pressure gradient nodal line extends out to the 100 m isobath, the coastal jet is much stronger, and hence the bottom Ekman layer is much more developed. Opposite to the downwelling case, the pressure gradient increases across the bottom Ekman layer due to the slope of the isopycnals there. We will return to this point in section 7.

6.2 Vorticity Balance

Our analysis of the vertically integrated, vertical component of vorticity is similar to that of Ezer and Mellor (1994). Taking the curl of the vertically integrated momentum equations, we discuss the vorticity balance with respect to four terms: 1) stress torque, 2) bottom pressure torque, 3) stretching of planetary vorticity by free surface deformation (plus the planetary beta effect), and 4) the material rate of change of relative vorticity (plus the stretching and tilting of relative vorticity by the flow field). Since we employed a spatially uniform wind stress, the stress torque is entirely due to bottom stress. The bottom pressure torque, through the bottom kinematic boundary condition, is the stretching of planetary vorticity by geostrophic flow across the sloping bottom. This is generally much larger than the stretching by free surface deformation (or by the planetary beta effect that we lumped together with free surface term). The residual of these tendencies is the variation in relative vorticity (that we lumped together with the kinematical terms associated with the flow field deformations of relative vorticity and with the relatively insignificant horizontal diffusion terms).

These four terms calculated at the 20 m isobath offshore of Sarasota, FL. for April 1998 are given in Figure 14. The bottom stress and bottom pressure torques are the lead terms, although the other two terms may be of comparable magnitude during the transitions when the sea surface slope is rapidly changing and the coastal jets are weak. Since these time series are spatially dependent their horizontal fields help to define the inner-shelf.

Figure 15 shows the four fields for the day 9 peak downwelling response. Once the pressure field and coastal jets are established, the inner-shelf is the region where the primary vorticity balance is between the bottom stress and bottom pressure torques. At this time the stretching of planetary vorticity by free surface deformation is small everywhere except for regions of strong eddies that form along the shelf break. The bottom pressure torque is large everywhere, but this tendency to induce relative vorticity can only be offset where large near bottom currents are capable of producing large bottom stresses, i.e., only in the inner-shelf region for this local wind forced experiment. Elsewhere the imbalance in these vorticity tendency terms leads to a large material rate of change of relative vorticity. Thus, the primary balance for the inner-shelf is between the bottom stress and bottom pressure torques, whereas the primary balance for the shelf-break is between bottom pressure torque and material rate of change of relative vorticity. Similar field representations for the day 12 peak upwelling response are shown in Figure 16. The conclusions are

the same as with Figure15 with the added point of asymmetry. The offshore scale of the inner-shelf is larger for the day 12 upwelling response than it is for the day 9 downwelling response.

7. Summary and Discussion

How water move across the shelf is the underlying physical oceanographic question pertinent to multidisciplinary continental shelf studies. Boundary layer and eddy transport processes are involved because of the vorticity constraint by the sloping bottom. Understanding these processes presupposes an understanding of the shelf responses to its various forcing agents: momentum input at the sea surface and shelf break and buoyancy input at the sea surface, shelf break, and land. Since each continental shelf is different, and since so many processes are involved, it is useful to isolate regions and forcing conditions to answer smaller subsets of questions. Along this vein we focus on the WFS, which is wide enough for its inner-shelf to be distinguished from the shelf-break. Using *in-situ* data and a numerical model simulation we ask how well the currents over the inner-shelf are accounted for by local wind forcing alone. In doing this we describe the boundary layer effects that account for the transports across the inner-shelf, provide a dynamical definition of the inner-shelf, and describe an asymmetry in the inner-shelf responses to upwelling versus downwelling favorable winds.

The model and *in-situ* data comparison shows that a primitive equation model (in this case the sigma coordinate POM with Mellor/Yamada turbulence closure) is effective at describing the sea level and circulation of the inner-shelf when forced by local winds only. We conclude that local winds are a major driver of the inner-shelf circulation. However, stratification impacts the nature of the circulation and the across-shelf transports, and it does this by affecting turbulence and hence the vertical scales of the surface and bottom Ekman layers. When these layers are vertically constrained, through the suppression of turbulence by stratification, the velocity vector turning within the boundary layers increases over that for constant density. Stratification, in this way, largely increases across-shelf mass transport in response to local wind forcing.

Flow field kinematics and dynamics analyses show the WFS circulation to be fully three-dimensional (along-shore variations are significant). These analyses define the inner-shelf as the region where the surface and bottom Ekman layers play an important role in the momentum balance. Kinematically the inner-shelf is where the Ekman layers induce a sea surface slope through divergence. With respect to vertically integrated vorticity the inner-shelf is the region where the primary balance is between bottom stress and bottom pressure torques, as contrasted with the shelf break where the primary balance is between the bottom pressure torque and the material rate of change of relative vorticity.

An asymmetry is found in the WFS response to upwelling and downwelling favorable winds, wherein the magnitude and offshore extent of the responses to upwelling favorable winds exceed those for downwelling favorable winds under stratified conditions. While this asymmetry appears in all of the dynamical analyses, these analyses alone do not provide an explanation. The

asymmetry is due to stratification as demonstrated by comparing model twin experiments, one with and the other without stratification. Asymmetry only occurs in the stratified experiment.

While we are not aware of such downwelling/upwelling asymmetry being reported elsewhere, MacCready and Rhines (1991) and Garrett et al. (1993) provide a conceptual and analytical basis for it. Their argument is that stratification impedes across-shelf transport in the bottom Ekman layer on a slope when the buoyancy force tends to balance the Coriolis force of the along-shelf velocity component. We diagnose this concept from both momentum and vorticity perspectives. With respect to momentum, the sea level response to downwelling winds results in an offshore directed pressure gradient force that drives the offshore directed flow in the bottom Ekman layer. Isopycnals bending into the bottom result in a buoyancy force that opposes this (Figure 12). In contrast to downwelling, the sea level response to upwelling winds results in an onshore directed pressure gradient force that drives an onshore directed flow in the bottom Ekman layer. Isopycnals bending into the bottom now result in a buoyancy force that enhances this (Figure 13). Granted, fewer isopycnals bend into the bottom; nevertheless the ones that do act constructively rather than destructively.

The simplest explanation for the asymmetry derives from the streamwise component of vorticity. For a stratified Ekman layer we consider the balance between the tendencies to induce relative vorticity by: 1) the tilting of planetary vorticity by the vertically sheared along-shelf jet, 2) the buoyancy torque by the sloping isopycnals, and 3) the dissipation of relative vorticity by the vertically sheared across-shelf flow. Equation (1) expresses this balance, with terms 1-3 on the left hand side and the local rate of change of relative vorticity, plus the omitted residual terms on the right hand side:

$$f\frac{\partial v}{\partial z}+\frac{g}{\rho_0}\frac{\partial \rho}{\partial x}+\frac{\partial^2}{\partial z^2}(K\frac{\partial u}{\partial z})=\frac{\partial}{\partial t}(\frac{\partial u}{\partial z})+R \qquad (1)$$

where u, v are the across-shelf and along-shelf velocity components, respectively, ρ is density, K is the vertical eddy coefficient, and R is the residual. For downwelling, planetary vorticity tilting tends to be balanced by buoyancy torque, requiring less relative vorticity dissipation. For upwelling, the buoyancy torque, while reduced in magnitude from the downwelling case, adds to the planetary vorticity tilting, requiring increased relative vorticity dissipation. We demonstrate these effects in Figure 17 by comparing the peak downwelling and upwelling responses on days 9 and 12, respectively. Destructive interference between planetary vorticity tilting and buoyancy torque is observed for downwelling, versus constructive interference for upwelling. Similar results (not shown) are found for the other two downwelling and upwelling pairs. The buoyancy torque (by isopycnals bending into the sloping bottom) has the same sign for downwelling and upwelling, whereas the tilting term reverses sign.

A corollary affect, expanded on by Garrett et al. (1993) in relationship to the Lentz and Trowbridge (1991) and Trowbridge and Lentz (1991) findings, is an asymmetry in the bottom boundary layer vertical scale due to the stabilizing/destabilizing influences of up and down slope flows. While related, this is a different phenomenon that appears to be contrary to our finding (in Figure 11) that the bottom boundary layer scale is actually larger for upwelling. We reconcile this discrepancy by noting that our larger boundary layer scale for upwelling follows from the larger upwelling response. Had the upwelling and downwelling responses on the WFS been of equal magnitude with regard to the interior along-shelf flows, as in the numerical experiments reported by Garrett et al. (1993), then we would have expected results similar to theirs. Asymmetry in the bottom boundary layer is important in nature for the reasons espoused in these earlier papers, including Weatherly and Martin (1978).

The inner-shelf provides added importance to these stratified boundary layer concepts on a slope. For the inner-shelf, the surface pressure gradient set up by surface Ekman layer divergence, the geostrophic interior flow adjustment to the pressure gradient, and the bottom Ekman layer reaction to the interior flow all occur nearly in unison. Anything that impedes one of these three steps will impede all of them. Thus, by inhibiting (or promoting) the bottom Ekman layer, thereby reducing (or increasing) the near bottom divergence that is necessary to feed the near surface divergence, stratification produces the asymmetry in the magnitude and offshore extent of the responses to downwelling and upwelling favorable winds.

A physical consequence of asymmetry is the rectification of the shelf response to oscillatory winds. This provides a possible explanation of why the region south of Tampa Bay was found by Yang et al. (1999) to be devoid of surface drifter tracks during a year-long set of deployments. Stratification-induced asymmetry may also have important biological, chemical, and geological consequences. In analogy to a flapper valve, with upwelling responses favored over downwelling responses, near bottom material properties are more readily transferred into, than away from, the near-shore zone. Support for this comes from unpublished hydrographic data (G. Vargo, personal communication) that shows large chlorophyll fluorescence extending across the shelf in the bottom Ekman layer. In the along-shelf direction the rectification of material property transports by the coastal jets may also be important; impacting, for instance, long-term sediment transport. Further theoretical and observational studies are needed to explore the ramifications of stratification induced asymmetry on the continental shelf.

A related conclusion is that the seasonal and synoptic scales can not be fully separated. With synoptic scale wind forced responses dependent on stratification, it is necessary to either assimilate density data into a model, or simulate density changes through a combination of surface buoyancy fluxes and active offshore boundary conditions. In our case, a 45 day (15 days of start-up and 30 days of analysis) simulation worked well, whereas attempts to carry the model integration longer met with increasing deviations from the *in-situ* data due to density field changes. Nowcasting and forecasting of the inner-shelf must be

supported by sufficient *in-situ* data for density field assimilation and boundary conditions.

Acknowledgements. Support for this work derived from the Office of Naval Research, grant N00014-98-1-0158; the National Oceanic and Atmospheric Administration, grant NA76RG0463; and the Minerals Management Service, contract MMS 14-35-0001-30804. G. Mitchum offered helpful discussions; R. Cole, J. Donovan, R. He, and W Hemme assisted with the data collection and analyses.

References

Allen, J.S., P.A. Newberger, and J. Federiuk, Upwelling circulation on the Oregon continental shelf. Part I: response to idealized forcing, *J. Phys. Oceanogr.*, 25, 1843-1866, 1995.

Blumberg, A.F. and G.L. Mellor, A description of a three-dimensional coastal ocean circulation model, in *Three-dimensional Coastal Ocean Models*, Vol. 4, N. Heaps (ed.), 208-233, AGU, Washington, D. C., 1987.

Brink, K.H., Wind-driven currents over the continental shelf, in *The Sea* Vol. 10, K.H. Brink and A. Robinson, (eds.), Wiley, New York, 1998.

Clarke, A.J., and K.H. Brink, The response of stratified, frictional flow of shelf and slope waters to fluctuating large-scale, low-frequency wind forcing, *J. Phys. Oceanogr.*, 15, 439-453, 1985.

Clarke, A. J., and S. Van Gorder, A method for estimating wind-driven frictional, time-dependent, stratified shelf and slope water flow, *J. Phys. Oceanogr.*, 16, 1013-1027, 1986.

Csanady, *Circulation in the Coastal Ocean*, Reidel, Dordrecht, Netherlands, pp., 1982.

Ezer, T. and G.L. Mellor, Diagnostic and prognostic calculations of the North Atlantic circulation and sea level using a sigma coordinate ocean model, *J. Geophys. Res.*, 99, 14159-14171, 1994.

Garrett, C., P. MacCready, and P. Rhines, Boundary mixing and arrested Ekman layers: Rotating stratified flow near a sloping boundary, Annu. Rev. Fluid Mech., 25, 291-323, 1993.

Gilbes, F., C. Tomas, J.J. Walsh, and F. Muller-Karger, An episodic chlorophyll plume on the west Florida shelf, *Cont. Shelf Res.*, 16, 1201-1224, 1996.

Gill, A.E., *Atmosphere-Ocean Dynamics*, Academic Press, New York, 662pp., 1982

Lentz, S.J., The surface boundary layer in coastal upwelling region, *J. Phys. Oceanogr.*, 22, 517-1539, 1992.

Lentz, S.J., Current dynamics over the northern California inner shelf, *J. Phys. Oceanogr*, 24, 2461-2478, 1994.

Lentz, S.J., Sensitivity of the inner shelf circulation to the form of the eddy viscosity profile, *J. Phys. Oceanogr*, 25, 19-28, 1995.

Lentz, S.J., and J.H. Trowbridge, The bottom boundary layer over the northern California shelf, *J. Phys. Oceanogr*., 21, 1186-1202, 1991.

Lentz, S.J., R.T. Guza, S. Elgar, F. Feddersen, and T.H.C. Herbers, Momentum balances on the North Carolina inner shelf., *J. Geophys. Res*., 104, 18205-18226, 1999.

Li, Z., Upwelling circulation on the west Florida continental shelf, Ph.D. thesis, University of South Florida, St. Petersburg, Florida, 309 PP, 1998.

Li, Z, and R. H. Weisberg, WFS response to upwelling favorable wind forcing: Kinematics, *J. Geophys. Res*., 104, 13507-13527, 1999.

Li, Z, and R. H. Weisberg, WFS response to upwelling favorable wind forcing: Dynamics, *J. Geophys. Res*., 104, 23427-23442, 1999.

Lopez, M. and Clarke, A.J., The wind-driven shelf and slope water flow in terms of a local and a remote response, *J. Phys. Oceanogr*., 19, 1091-1101, 1989.

MacCready, P. and P.B. Rhines, Buoyant inhibition of Ekman transport on a slope and its effect on stratified spin-up, *J. Fluid Mech*., 223, 1991

Mellor, G.L. and T. Yamada, Development of a turbulence closure model for geophysical fluid problems, *Rev. Geophys*., 20, 851-875.

Mitchum, G.T., and W. Sturges, Wind-driven currents on the west Florida shelf, *J. Phys. Oceanogr*., 12, 1310-1317, 1982.

Mitchum, G.T., and A.J. Clarke, The frictional, near shore response to forcing by synoptic scale winds , *J. Phys. Oceanogr*., 16, 1029-1037, 1986.

Mitchum, G.T., and A.J. Clarke, Evaluation of frictional, wind forced long wave theory on the West Florida shelf, *J. Phys. Oceanogr*., 16, 934-946, 1986

Munchow, A., and R.J. Chant, Kinematics of inner shelf motions during the summer stratified seasons off New Jersey, *J. Phys. Oceanogr*., 30, 247-268, 2000.

Samelson, R.M., Coastal boundary conditions and the baroclinic structure of wind-driven continental shelf currents, *J. Phys. Oceanogr*., 27, 2645-2662, 1997.

Smith, R.L., The physical processes of coastal ocean upwelling systems, in *Upwelling in the Ocean: Modern Processes and Ancient Records*, Summerhayes et al. (eds.), 39-64, 1995.

Trowbridge, J.H., and S.J. Lentz, Asymmetric behavior of an oceanic boundary layer above a sloping bottom, *J. Phys. Oceanogr*., 21,1171-1185, 1991.

Walsh, J.J., On the Nature of Continental Shelves, Academic Press, San Diego, 520pp, 1988.

Weatherly, G.L., and P.J. Martin, On the structure and dynamics of the oceanic bottom boundary layer, *J. Phys. Oceanogr*., 8, 557-570, 1978.

Weatherly, G.L., and D. Thistle, On the wintertime currents in the Florida Big Bend region, c*ontinental Shelf Research*, 17, 1297-1319, 1997.

Weisberg, R.H., B.D. Black, and H. Yang, Seasonal modulation of the west Florida shelf circulation, *Geophys. Res. Lett*., 23, 2247-2250, 1996.

Weisberg, R.H., B.D. Black, and Z. Li, An upwelling case study on Florida's west coast, *J. Geophys. Res*., 105, 11459-11469, 2000.

Wu, J., Wind-stress coefficients over sea surface near neutral conditions—A revisit, *J. Phys. Oceanogr*., 10, 727-740, 1980.

Yang, H., R.H. Weisberg, P.P. Niiler, W. Sturges, and W. Johnson, Lagrangian circulation and forbidden zone on the west Florida shelf, Cont. Shelf Res., 19, 1221-1245, 1999.

Yankovsky, A.E., and R.W. Garvine, Subinertial dynamics on the inner New Jersey shelf during the upwelling season, *J. Phys. Oceanogr*., 28, 2444-2458, 1998.

List of Figures

Figure 1 West Florida shelf bathymetry and the measurement locations (upper panel) and numerical model domain with coordinate system description as applied herein (lower panel). The model seaward boundaries are open except for the southeast corner where the solid line represents closure by the Florida Keys. The solid line offshore from Sarasota denotes the section sampled for kinematical and dynamical analyses.

Figure 2 April 1998 measurements of: a) along-shelf and b) across-shelf velocity components sampled at the 20 m isobath offshore of Sarasota FL., c) sea level at St. Petersburg, d) wind velocity sampled at NOAA buoy 42036, and e) wind stress. The contour intervals are 0.05 ms^{-1} for the velocity components, north is up and east is to the right for the wind vectors, and all data are low pass filtered to exclude oscillations at time scales shorter than 36 hours.

Figure 3 Modeled (dashed-doted lines) and observed (solid lines) sea level variability for the constant density (panel a) and stratified (panel b) cases, along with the April 1998 wind vectors.

Figure 4a April 1998 stratified model simulations of: a) along-shelf and b) across-shelf velocity components, and c) isopycnal variations sampled at the 20 m isobath offshore of Sarasota FL, along with the wind vectors used to drive the model (with north up and east to the right). The contour intervals are 0.05 ms^{-1} for the velocity components and 0.5 sigma units for the density.

Figure 4b April 1998 constant density model simulations of: a) along-shelf and b) across-shelf velocity components sampled at the 20 m isobath offshore of Sarasota FL, along with the wind vectors used to drive the model (with north up and east to the right). The contour intervals are 0.05 ms^{-1} for the velocity components.

Figure 5a Daily snapshots of the stratified model simulated WFS sea surface topography spanning the period of downwelling and upwelling between days 7 to 14. The contour interval is 0.02 m, and the ranges for sea level are given in parentheses.

Figure 5b Daily snapshots of the constant density model simulated WFS sea surface topography spanning the period of downwelling and upwelling between days 7 to 14. The contour interval is 0.02 m, and the ranges for sea level are given in parentheses.

Figure 6a Daily snapshots of the along-shelf, across-shelf, and vertical velocity components and density sampled along a cross section offshore of Sarasota, FL. spanning the period of downwelling and upwelling between days 7 to 13. The contour intervals are 0.05 ms^{-1} for the horizontal velocity components, 10^{-5} $msec^{-1}$ for the vertical velocity component, and 0.5 sigma units for density.

Figure 6b Daily snapshots of the along-shelf, across-shelf, and vertical velocity components for the constant density case, sampled along a cross section offshore of Sarasota, FL. spanning the period of downwelling and upwelling between days 7 to 13. The contour intervals are 0.05 ms^{-1} for the horizontal velocity components and 10^{-5} $msec^{-1}$ for the vertical velocity component.

Figure 7 April 1998 measurements of: a) along-shelf and b) across-shelf velocity components sampled at the 50 m isobath offshore of Tampa Bay. The contour intervals are 0.05 ms^{-1} for the velocity components, north is up and east is to the right for the wind vectors, and all data are low pass filtered to exclude oscillations at time scales shorter than 36 hours.

Figure 8 Horizontal velocity vector fields: a) depth-averaged, b) near surface, c) mid-water, and d) near bottom, sampled during the peak downwelling

event on day 9. Vectors are shown for every other grid point with the maximum value for each panel given in the panel legend. The near bottom vectors are magnified by a factor of two relative to the other panels.

Figure 9 Horizontal velocity vector fields: a) depth-averaged, b) near surface, c) mid-water, and d) near bottom, sampled during the peak upwelling event on day 12. Vectors are shown for every other grid point with the maximum value for each panel given in the panel legend. The near bottom vectors are magnified by a factor of two relative to the other panels.

Figure 10a Satellite AVHRR temperature image for April 10th, the time of warmest SST associated with the peak downwelling of day 9.

Figure 10b Satellite AVHRR temperature image for April 13th, the time of coldest SST associated with the peak upwelling of day 12.

Figure 11 Time series of the vertically integrated: a) along-shelf and b) across-shelf momentum balance terms and the c) across-shelf transports, along with d) the across-shelf ageostrophic momentum residual, all sampled at the 20 m isobath offshore of Sarasota FL. from the stratified model simulation

Figure 12 The across-shelf momentum balance during the peak downwelling event on day 9 sampled offshore from Sarasota FL. from the stratified model simulation. The panels are: a) Coriolis; b) pressure gradient; c) their sum, or the ageostrophic residual; d) friction (primarily vertical); e) the sum of the Coriolis, pressure gradient, and friction terms; f) advective acceleration; g) the sum of e and f; and h) the local acceleration. Contour intervals are given in each panel and shaded regions are negative.

Figure 13 The across-shelf momentum balance during the peak upwelling event on day 12 sampled offshore from Sarasota FL. from the stratified

model simulation. The panels are: a) Coriolis; b) pressure gradient; c) their sum, or the ageostrophic residual; d) friction (primarily vertical); e) the sum of the Coriolis, pressure gradient, and friction terms; f) advective acceleration; g) the sum of e and f; and h) the local acceleration. Contour intervals are given in each panel and shaded regions are negative.

Figure 14 Time series of the vertically integrated vorticity balance terms sampled at the 20 m isobath offshore of Sarasota FL. from the stratified model simulation.

Figure 15 Horizontal distribution fields for the vertically integrated vorticity balance terms during the peak downwelling event on day 9: a) the material rate of change, plus tilting and stretching of relative vorticity; b) the stretching of planetary vorticity by changes in the free surface, plus the planetary beta terms; c) the bottom pressure torque; and d) the bottom stress torque. Contour intervals and ranges are given with each panel and shaded regions are negative.

Figure 16 Horizontal distribution fields for the vertically integrated vorticity balance terms during the peak upwelling event on day 12: a) the material rate of change, plus tilting and stretching of relative vorticity; b) the stretching of planetary vorticity by changes in the free surface, plus the planetary beta terms; c) the bottom pressure torque; and d) the bottom stress torque. Contour intervals and ranges are given with each panel and shaded regions are negative.

Figure 17 An analysis of the along-shelf component of vorticity during the peak downwelling and upwelling responses on a) day 9 and b) day12, respectively. From left to right in each panel are 1) the tilting of planetary vorticity filaments by the sheared along-shelf jet, 2) the buoyancy torque, 3) the dissipation of relative vorticity by the sheared across-shelf flow, and 4) the local rate of change of relative vorticity, plus the remainder of other omitted terms. The contour interval is 10^{-7} s^{-2}.

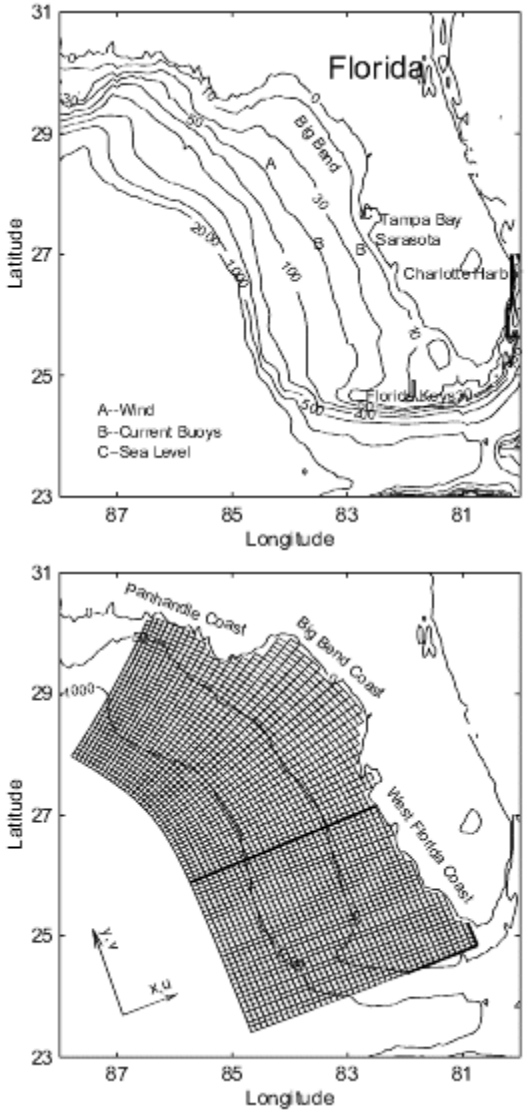
Florida
Big Bend
Tampa Bay
Sarasota
Charlotte Harb
Florida Keys
A--Wind
B--Current Buoys
C--Sea Level
Latitude
Longitude
31
29
27
25
23
87
85
83
81

Panhandle Coast
Big Bend Coast
West Florida Coast
Latitude
Longitude
31
29
27
25
23
87
85
83
81

Figure 1

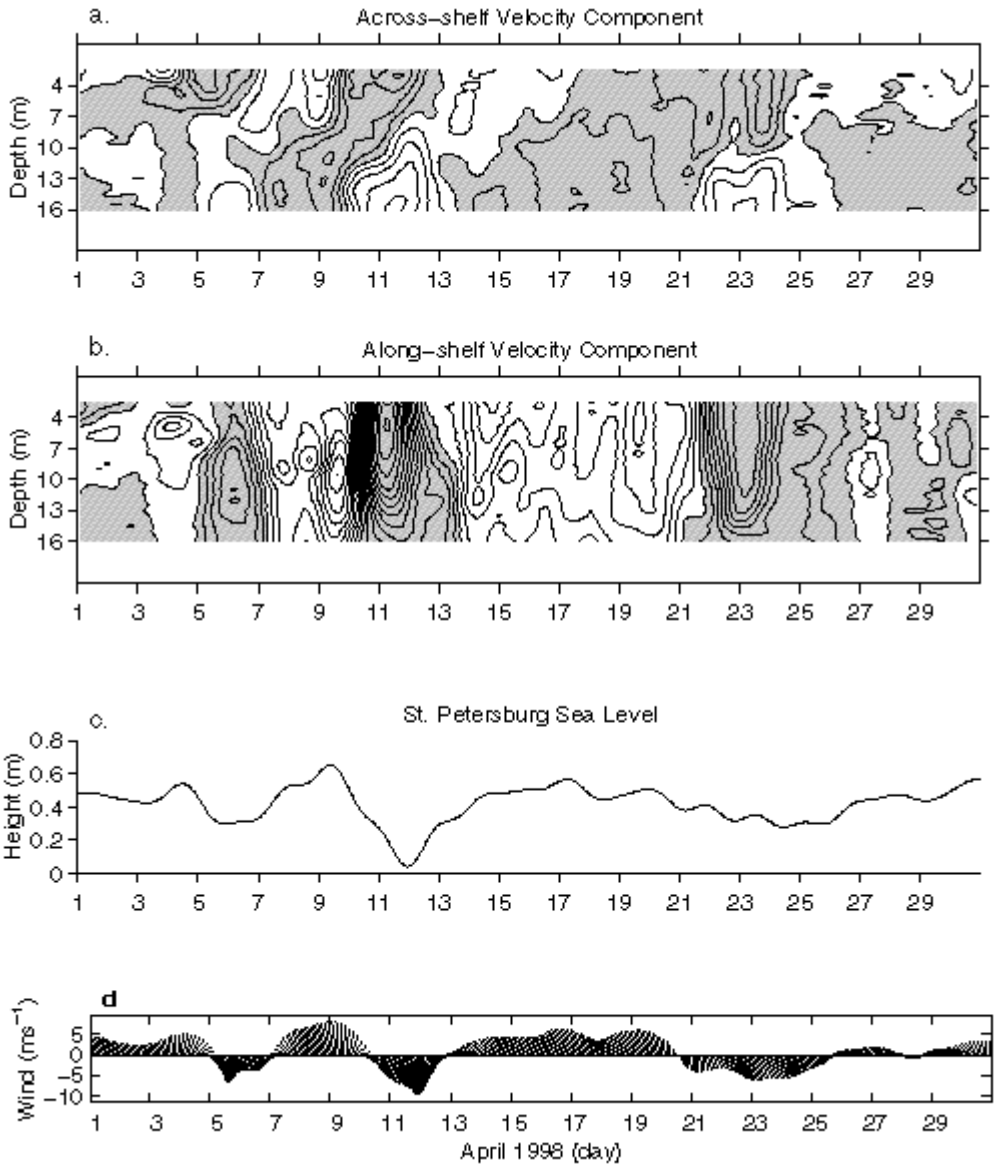
a.
Across–shelf Velocity Component
Depth (m)
4
7
10
13
16
1 3 5 7 9 11 13 15 17 19 21 23 25 27 29
b.
Along–shelf Velocity Component
Depth (m)
4
7
10
13
16
1 3 5 7 9 11 13 15 17 19 21 23 25 27 29
c.
St. Petersburg Sea Level
Height (m)
0.8
0.6
0.4
0.2
0
1 3 5 7 9 11 13 15 17 19 21 23 25 27 29
d
Wind (ms^{-1})
5
0
−5
−10
1 3 5 7 9 11 13 15 17 19 21 23 25 27 29
April 1998 (day)

Figure 2

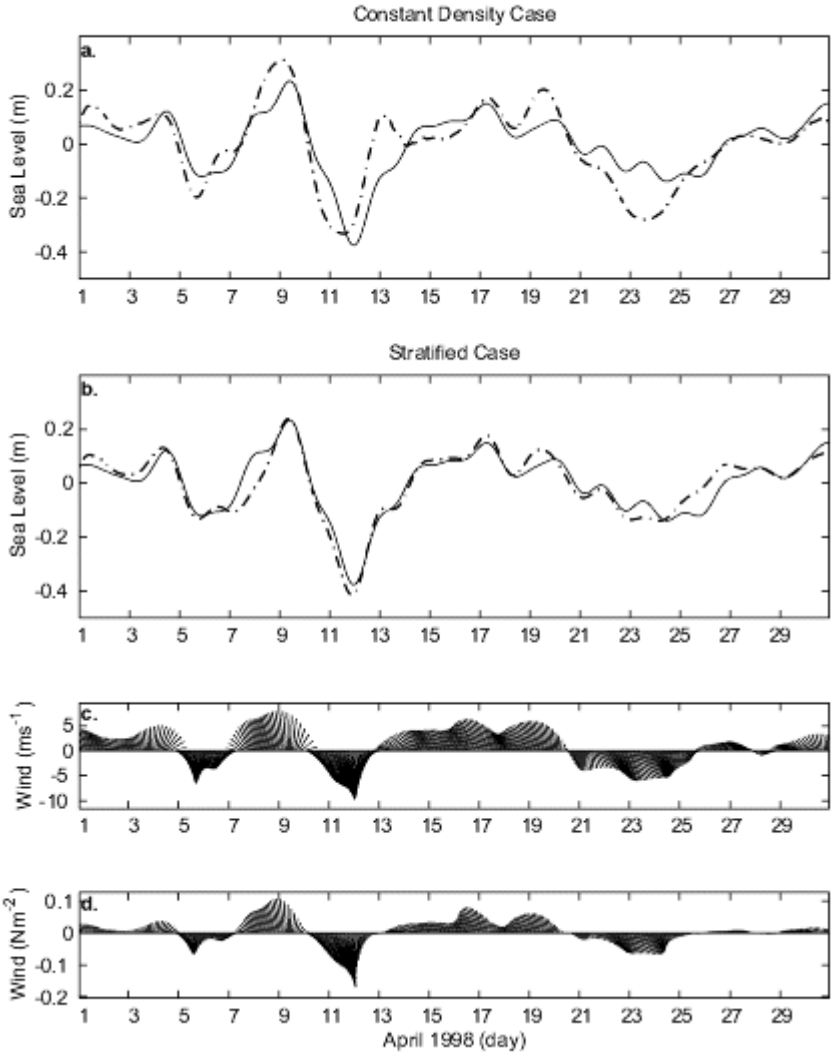
Constant Density Case
a.
Sea Level (m)
0.2
0
-0.2
-0.4
1 3 5 7 9 11 13 15 17 19 21 23 25 27 29
Stratified Case
b.
Sea Level (m)
0.2
0
-0.2
-0.4
1 3 5 7 9 11 13 15 17 19 21 23 25 27 29
c.
Wind (ms-1)
5
0
-5
-10
1 3 5 7 9 11 13 15 17 19 21 23 25 27 29
d.
Wind (Nm-2)
0.1
0
-0.1
-0.2
1 3 5 7 9 11 13 15 17 19 21 23 25 27 29
April 1998 (day)

Figure 3

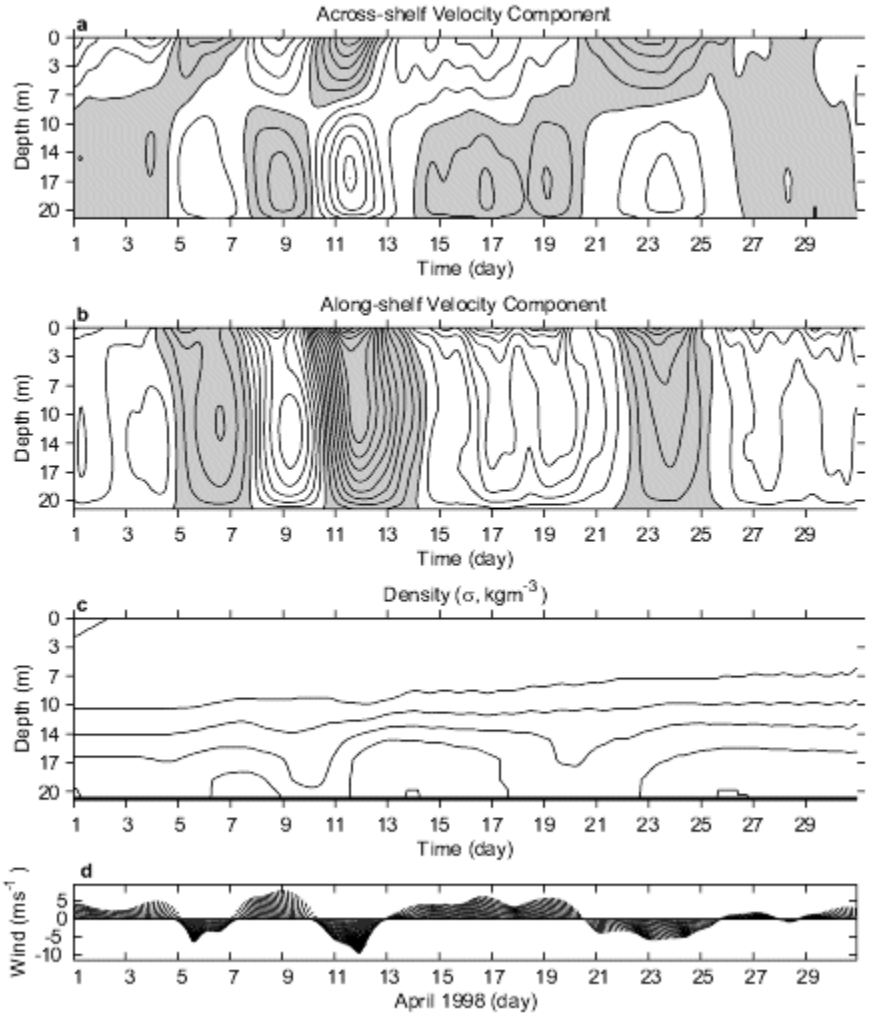
Across-shelf Velocity Component
a
Depth (m)
0
3
7
10
14
17
20
1 3 5 7 9 11 13 15 17 19 21 23 25 27 29
Time (day)
Along-shelf Velocity Component
b
Depth (m)
Time (day)
Density (σ, kgm-3)
c
Depth (m)
Time (day)
d
Wind (ms-1)
5
0
-5
-10
April 1998 (day)

Figure 4

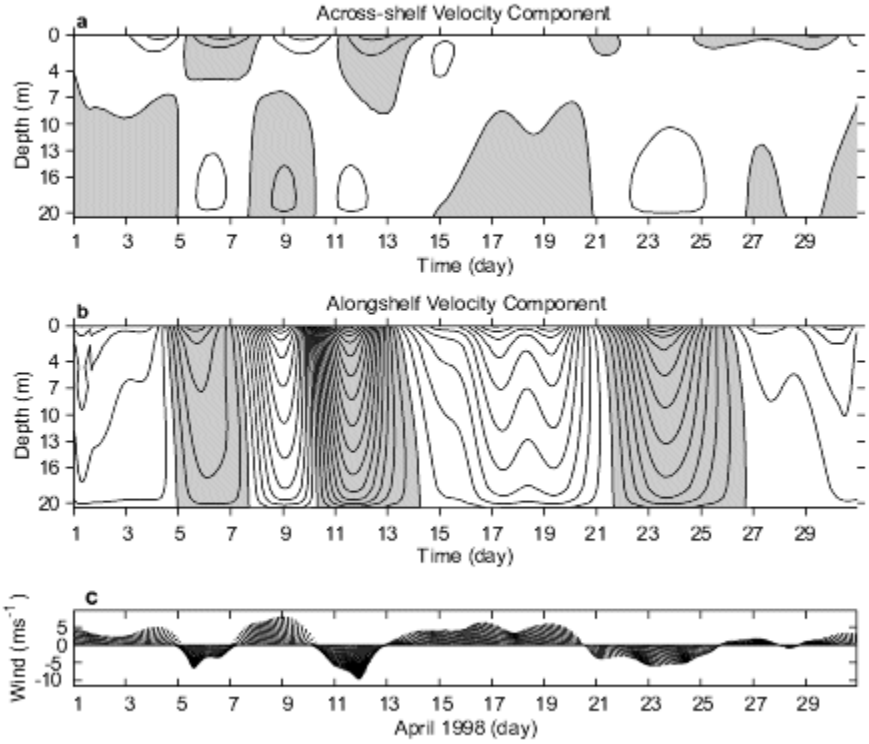
a
Across-shelf Velocity Component
Depth (m)
0
4
7
10
13
16
20
1 3 5 7 9 11 13 15 17 19 21 23 25 27 29
Time (day)
b
Alongshelf Velocity Component
Depth (m)
0
4
7
10
13
16
20
1 3 5 7 9 11 13 15 17 19 21 23 25 27 29
Time (day)
c
Wind (ms-1)
5
0
-5
-10
1 3 5 7 9 11 13 15 17 19 21 23 25 27 29
April 1998 (day)

Figure 5

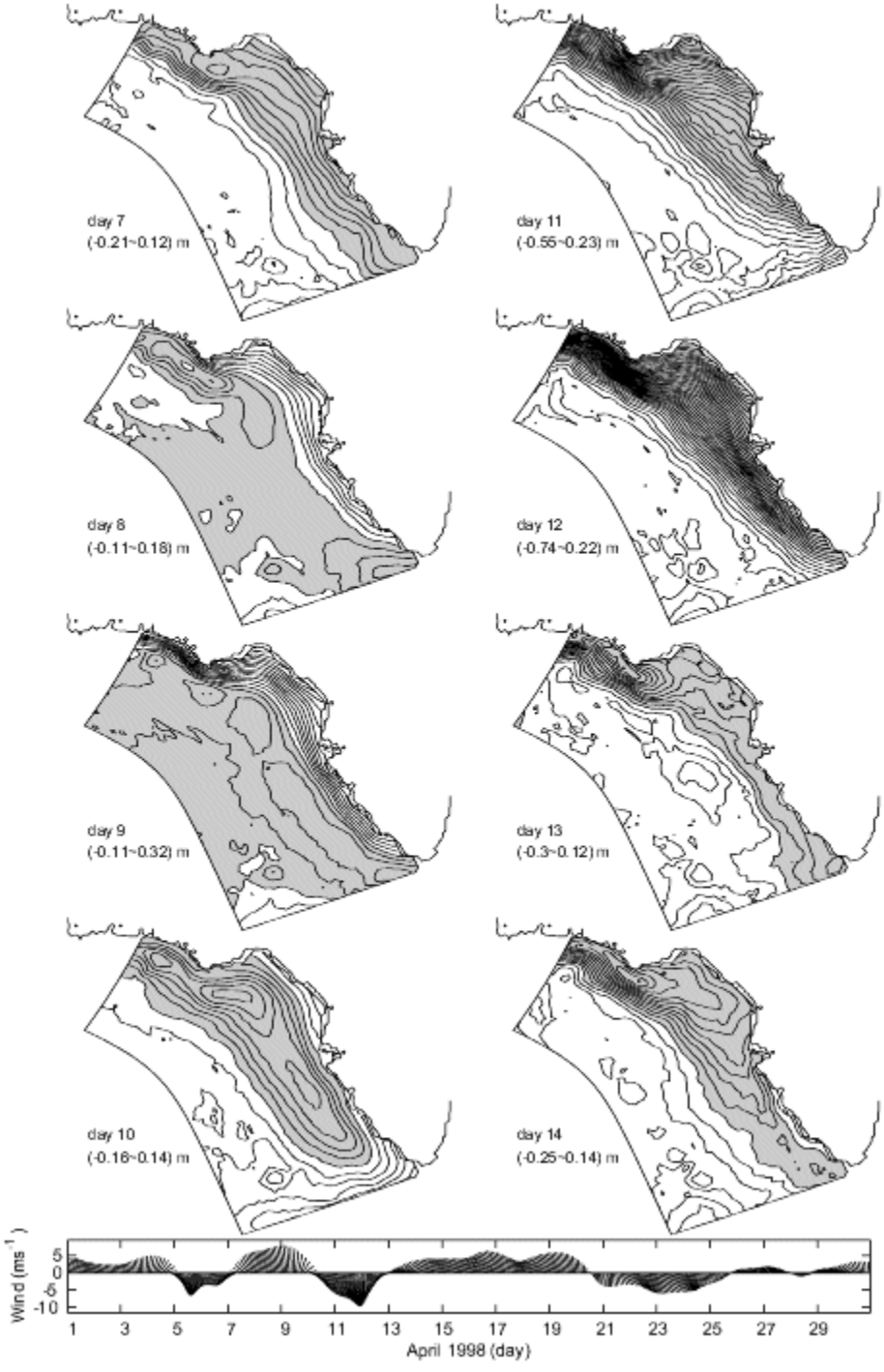
day 7
(-0.21~0.12) m
day 11
(-0.55~0.23) m
day 8
(-0.11~0.18) m
day 12
(-0.74~0.22) m
day 9
(-0.11~0.32) m
day 13
(-0.3~0.12) m
day 10
(-0.16~0.14) m
day 14
(-0.25~0.14) m
Wind (ms-1)
5
0
-5
-10
1
3
5
7
9
11
13
15
17
19
21
23
25
27
29
April 1998 (day)

Figure 6

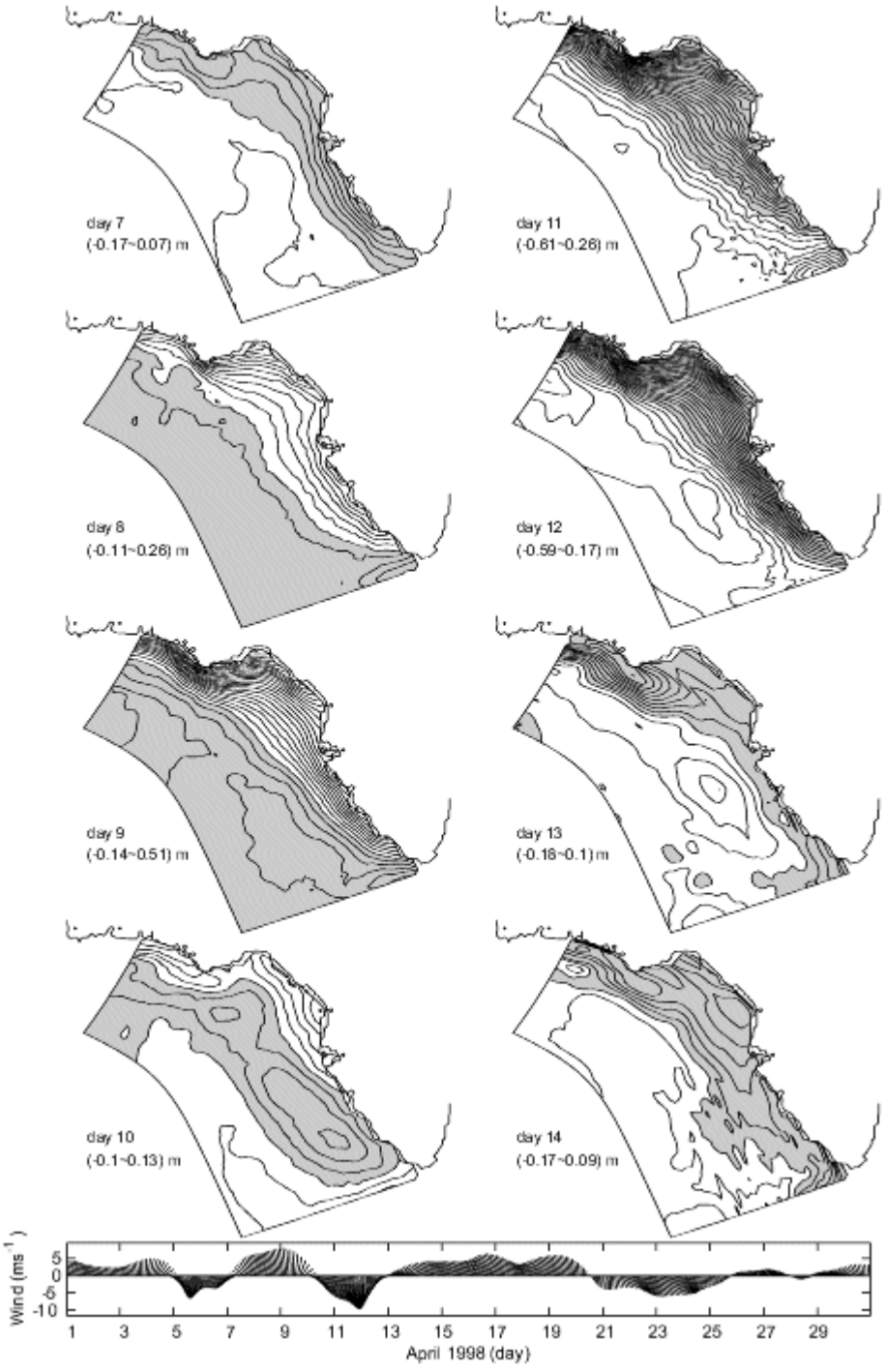
day 7
(-0.17~0.07) m
day 11
(-0.61~0.26) m
day 8
(-0.11~0.26) m
day 12
(-0.59~0.17) m
day 9
(-0.14~0.51) m
day 13
(-0.18~0.1) m
day 10
(-0.1~0.13) m
day 14
(-0.17~0.09) m
Wind (ms-1)
5
0
-5
-10
1
3
5
7
9
11
13
15
17
19
21
23
25
27
29
April 1998 (day)

Figure 7

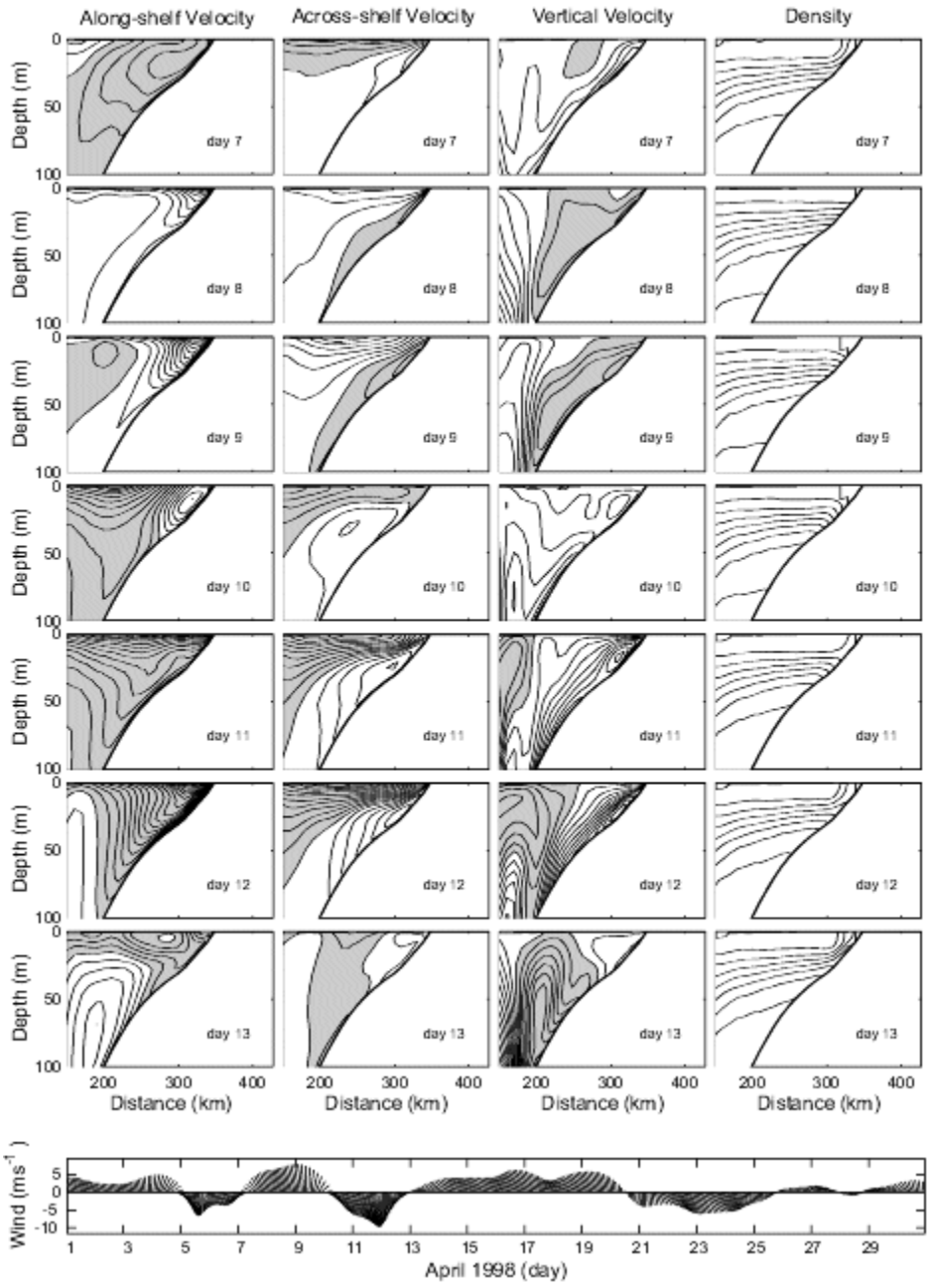
Along-shelf Velocity
Across-shelf Velocity
Vertical Velocity
Density
Depth (m)
0
50
100
day 7
day 8
day 9
day 10
day 11
day 12
day 13
200
300
400
Distance (km)
Wind (ms^{-1})
5
0
-5
-10
1
3
5
7
9
11
13
15
17
19
21
23
25
27
29
April 1998 (day)

Figure 8

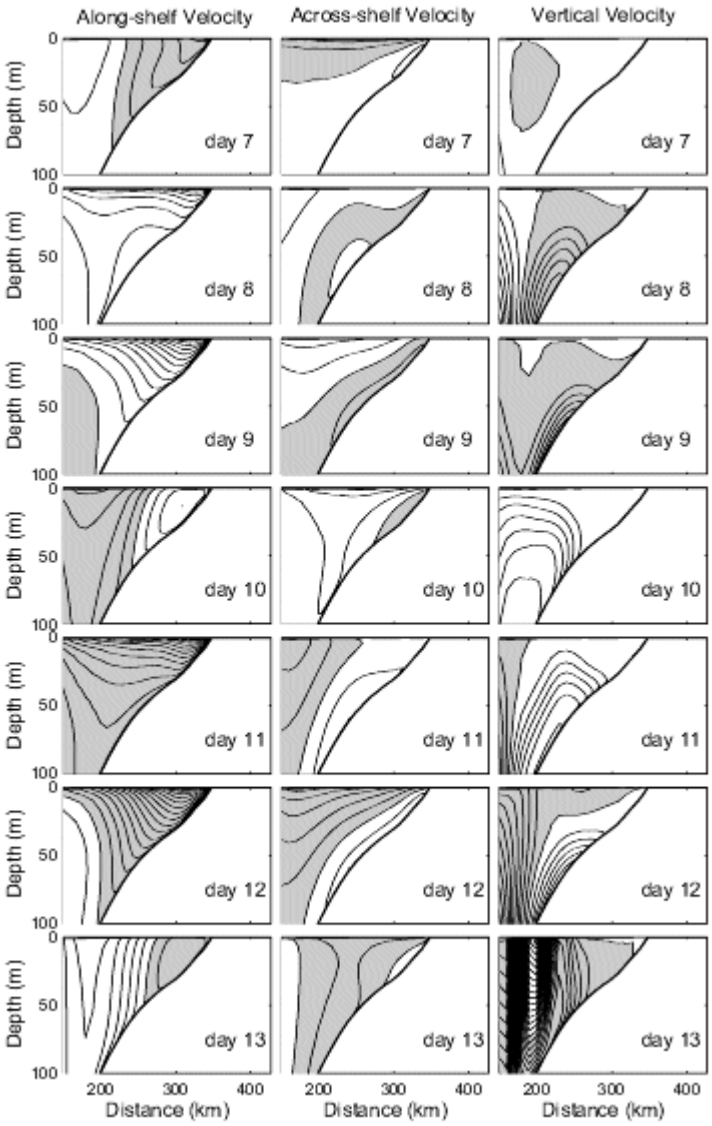
Along-shelf Velocity
Across-shelf Velocity
Vertical Velocity
Depth (m)
0
50
100
day 7
day 8
day 9
day 10
day 11
day 12
day 13
200
300
400
Distance (km)

Figure 9

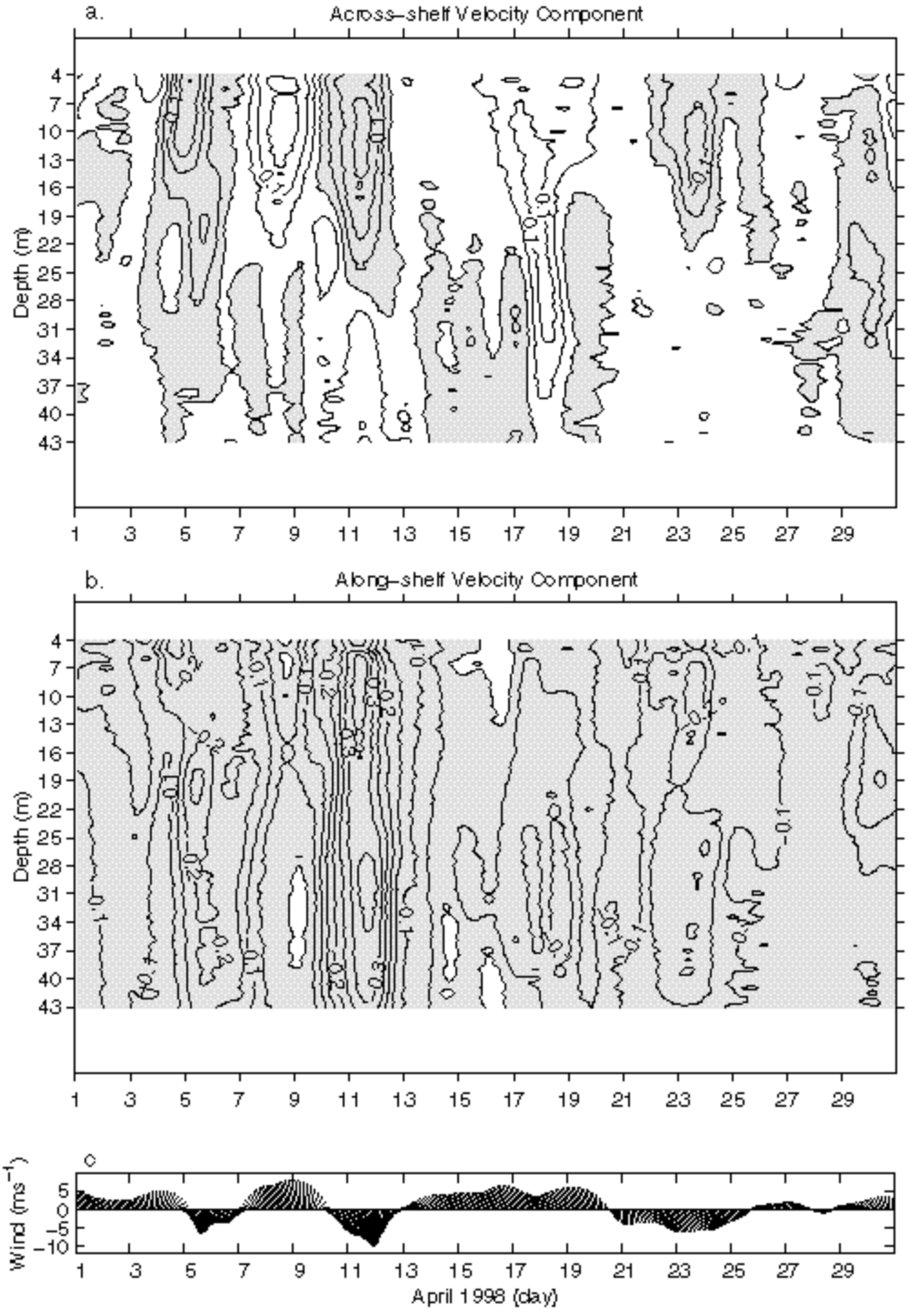
a.
Across–shelf Velocity Component
Depth (m)
b.
Along–shelf Velocity Component
Depth (m)
c
Wind (ms^{-1})
April 1998 (day)

Figure 10

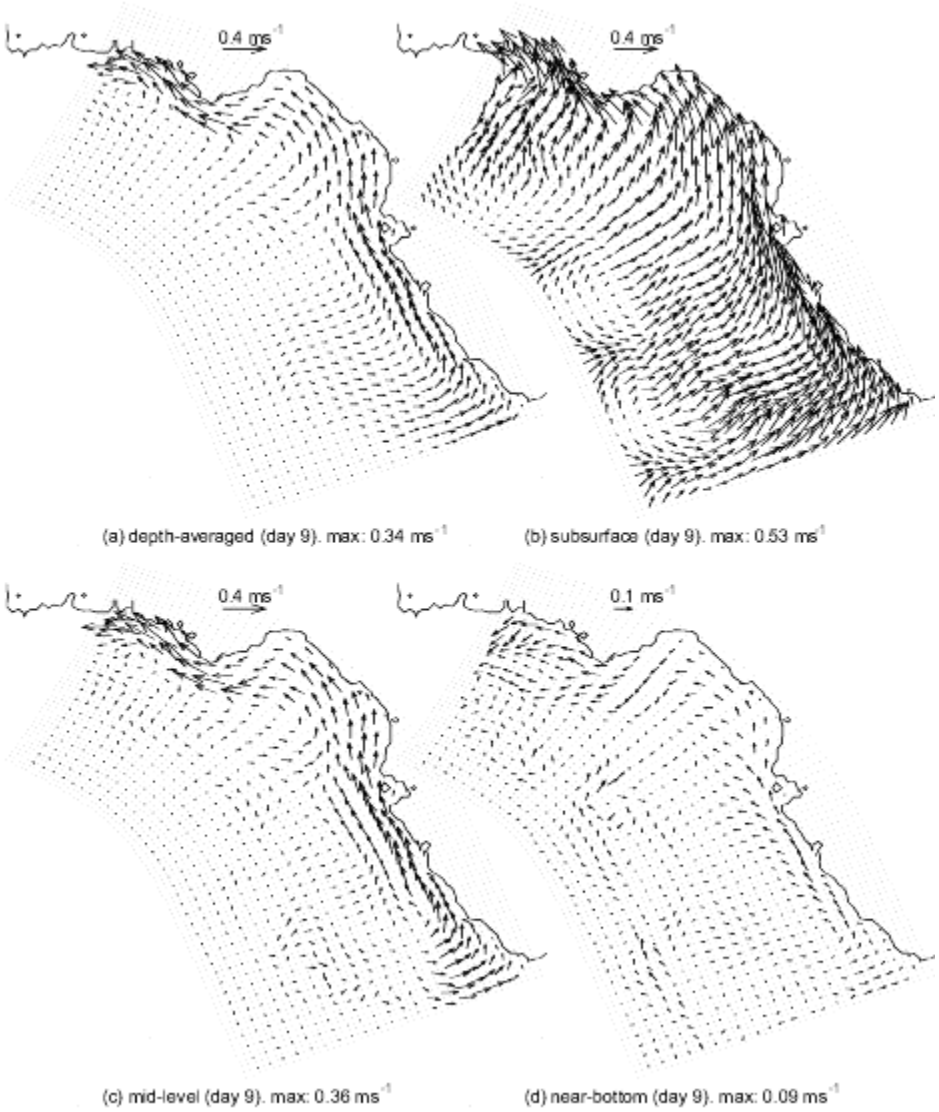
0.4 ms-1
0.4 ms-1
(a) depth-averaged (day 9). max: 0.34 ms-1
(b) subsurface (day 9). max: 0.53 ms-1
0.4 ms-1
0.1 ms-1
(c) mid-level (day 9). max: 0.36 ms-1
(d) near-bottom (day 9). max: 0.09 ms-1

Figure 11

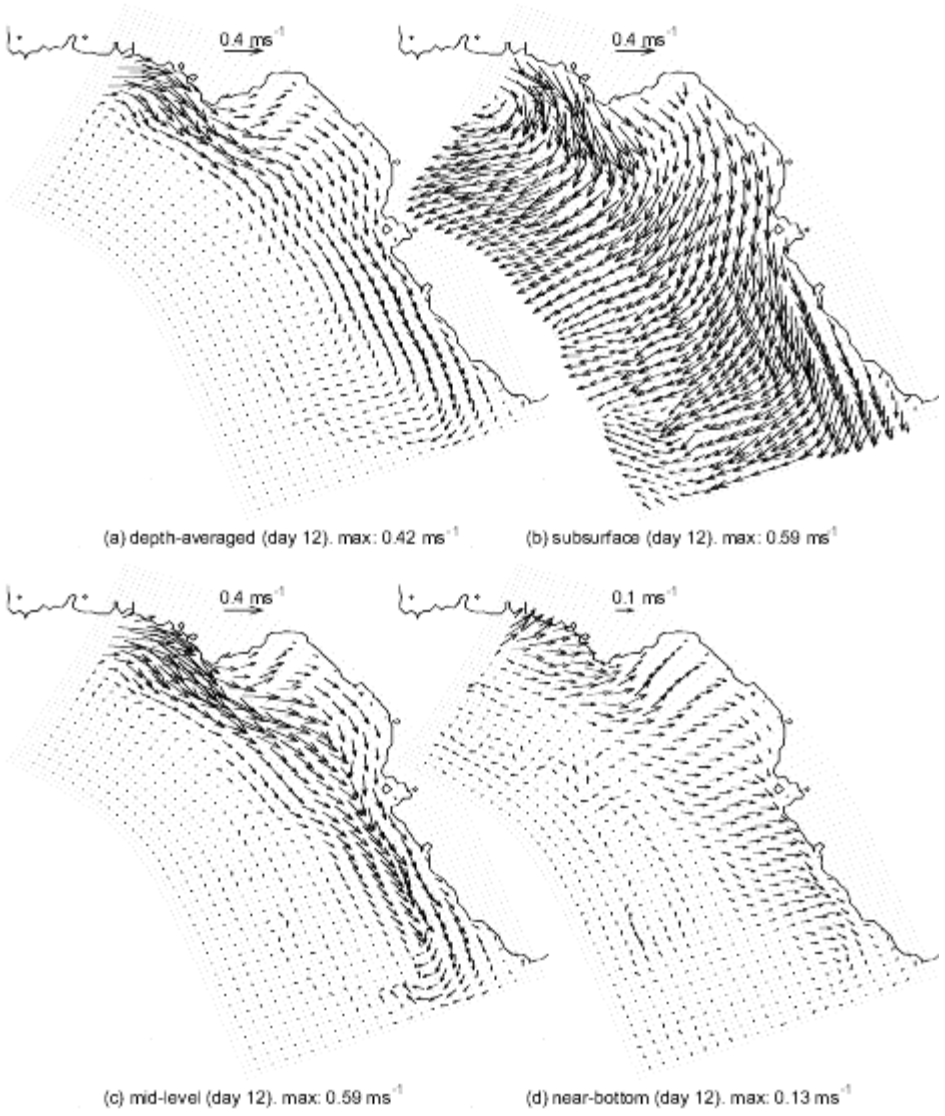
0.4 ms-1
0.4 ms-1
(a) depth-averaged (day 12). max: 0.42 ms-1
(b) subsurface (day 12). max: 0.59 ms-1
0.4 ms-1
0.1 ms-1
(c) mid-level (day 12). max: 0.59 ms-1
(d) near-bottom (day 12). max: 0.13 ms-1

Figure 12

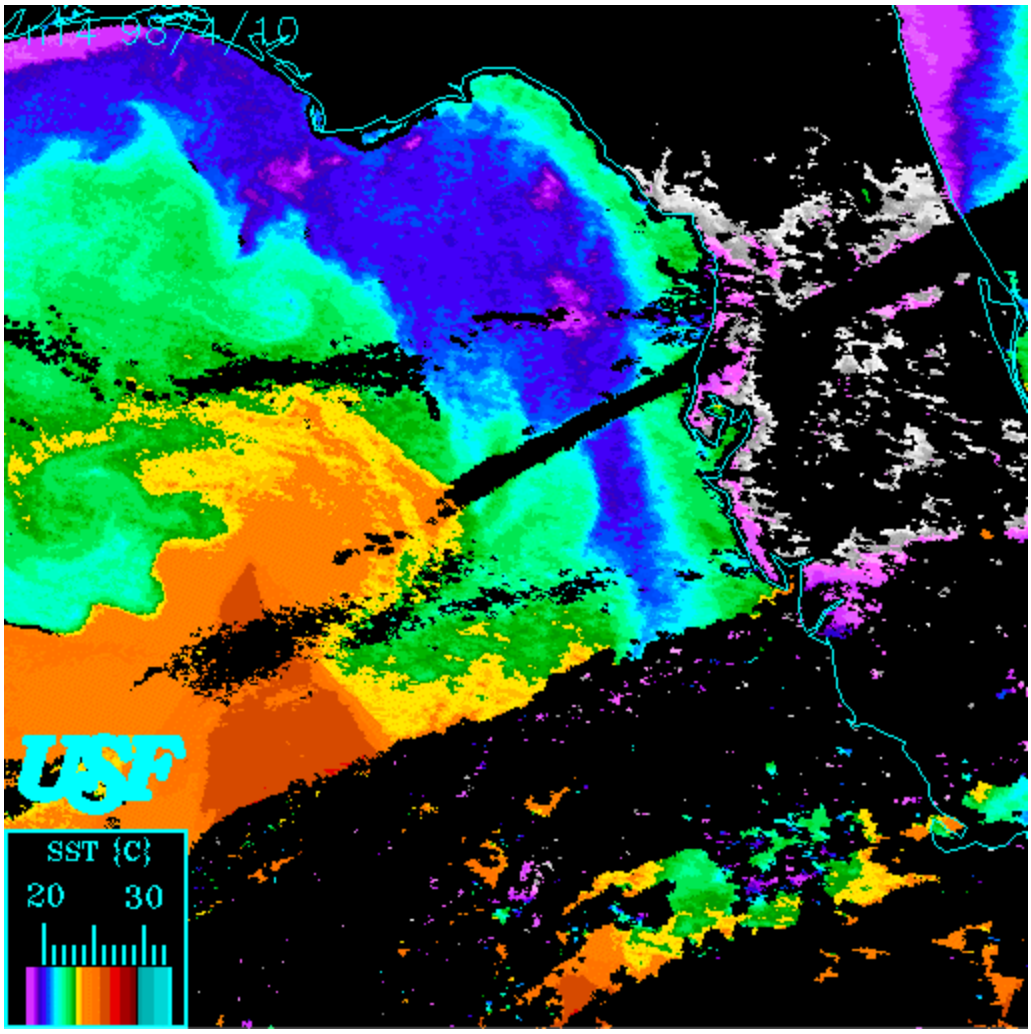

Figure 13

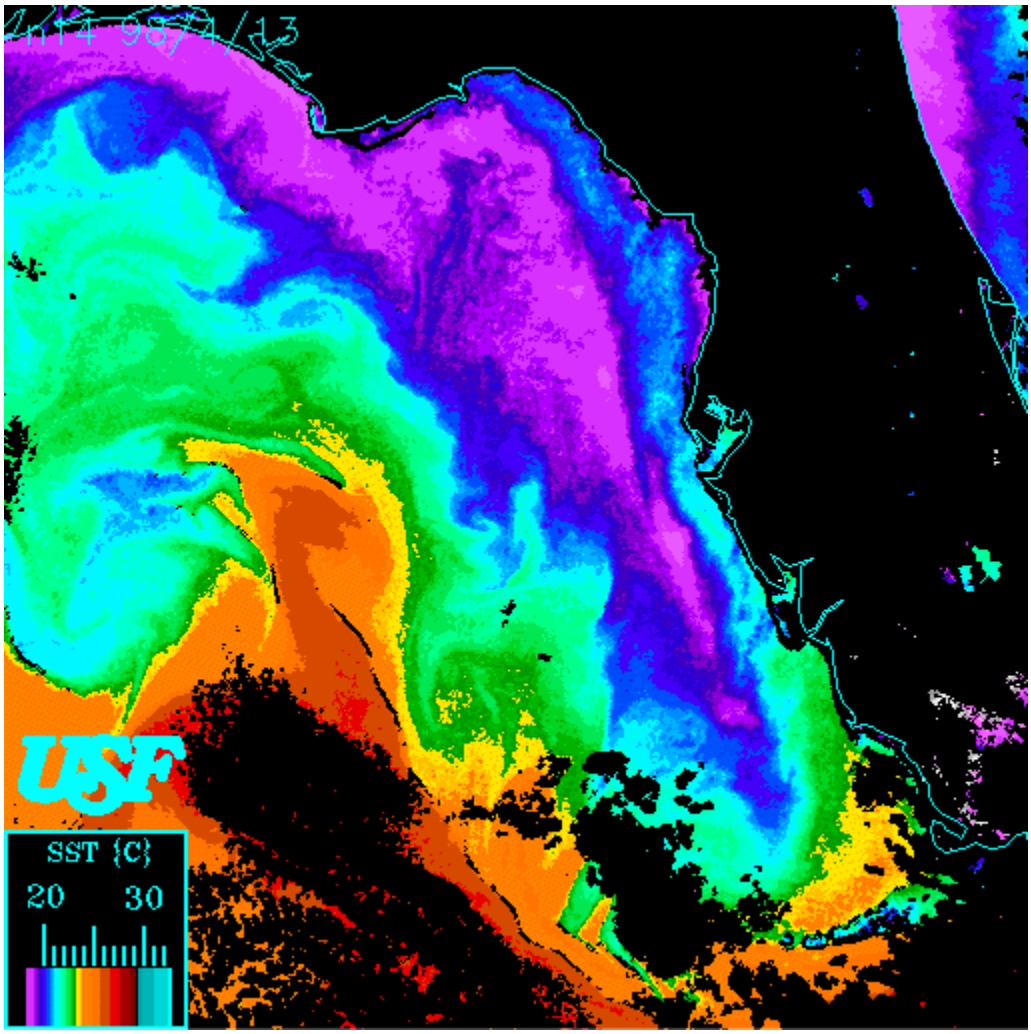

Figure 14

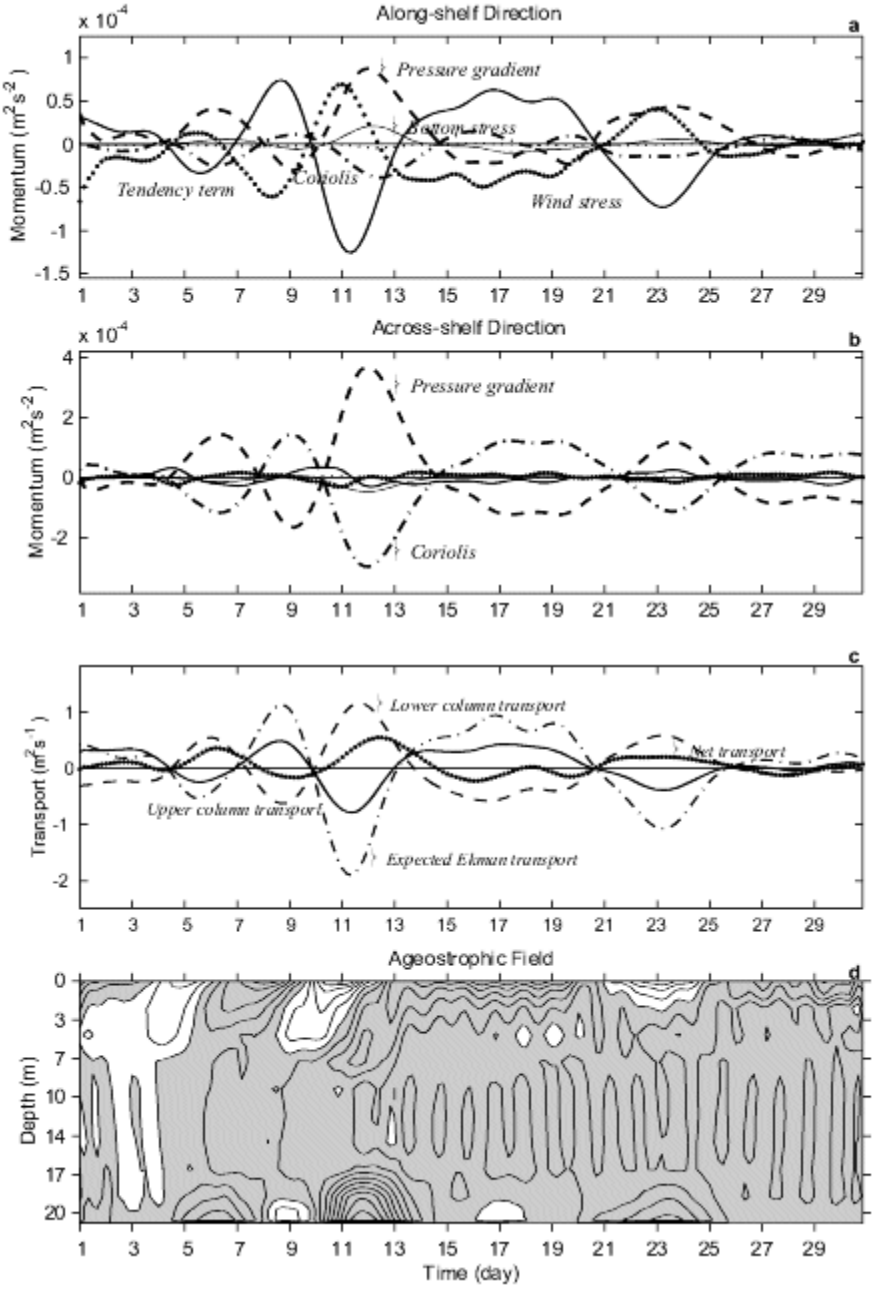
Along-shelf Direction
a
x 10^-4
Momentum (m^2 s^-2)
Pressure gradient
Bottom stress
Tendency term
Coriolis
Wind stress
Across-shelf Direction
b
Pressure gradient
Coriolis
c
Transport (m^2 s^-1)
Lower column transport
Net transport
Upper column transport
Expected Ekman transport
Ageostrophic Field
d
Depth (m)
Time (day)

Figure 15

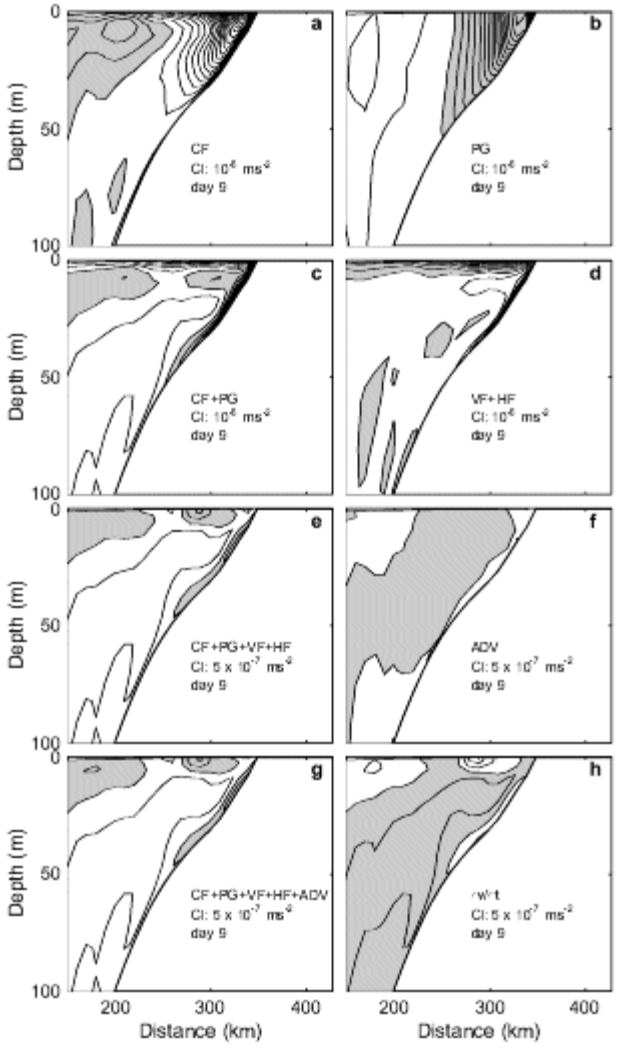
a
CF
CI: 10⁻⁶ ms⁻²
day 9
b
PG
CI: 10⁻⁶ ms⁻²
day 9
c
CF+PG
CI: 10⁻⁶ ms⁻²
day 9
d
VF+HF
CI: 10⁻⁶ ms⁻²
day 9
e
CF+PG+VF+HF
CI: 5 x 10⁻⁷ ms⁻²
day 9
f
ADV
CI: 5 x 10⁻⁷ ms⁻²
day 9
g
CF+PG+VF+HF+ADV
CI: 5 x 10⁻⁷ ms⁻²
day 9
h
-w'·t
CI: 5 x 10⁻⁷ ms⁻²
day 9
Depth (m)
0
50
100
200
300
400
Distance (km)

Figure 16

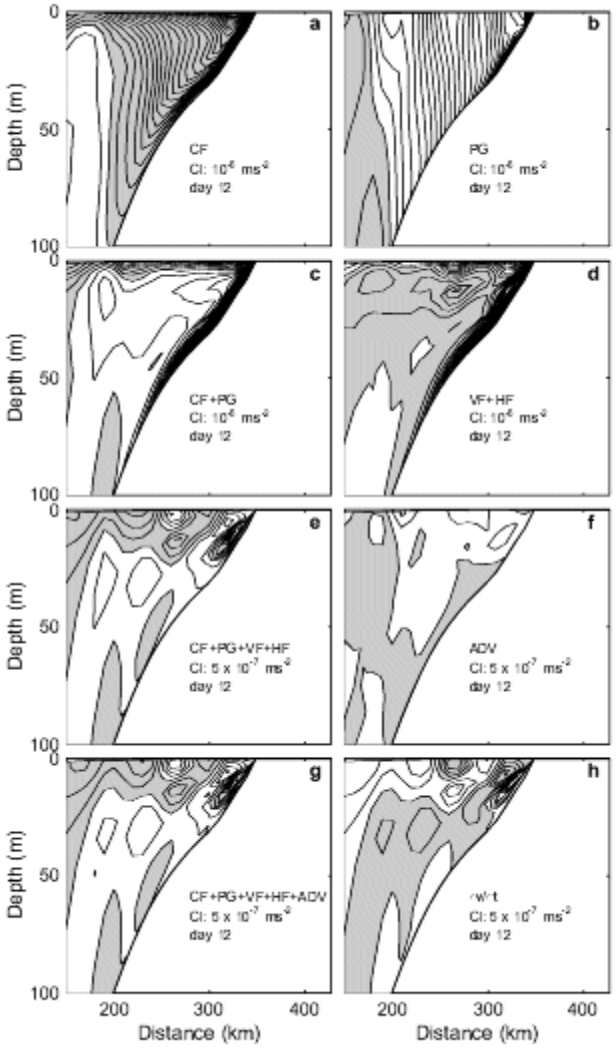
a
CF
CI: 10^-6 ms^-2
day 12
b
PG
CI: 10^-6 ms^-2
day 12
c
CF+PG
CI: 10^-6 ms^-2
day 12
d
VF+HF
CI: 10^-6 ms^-2
day 12
e
CF+PG+VF+HF
CI: 5 x 10^-7 ms^-2
day 12
f
ADV
CI: 5 x 10^-7 ms^-2
day 12
g
CF+PG+VF+HF+ADV
CI: 5 x 10^-7 ms^-2
day 12
h
∂w/∂t
CI: 5 x 10^-7 ms^-2
day 12
Depth (m)
0
50
100
200
300
400
Distance (km)

Figure 17

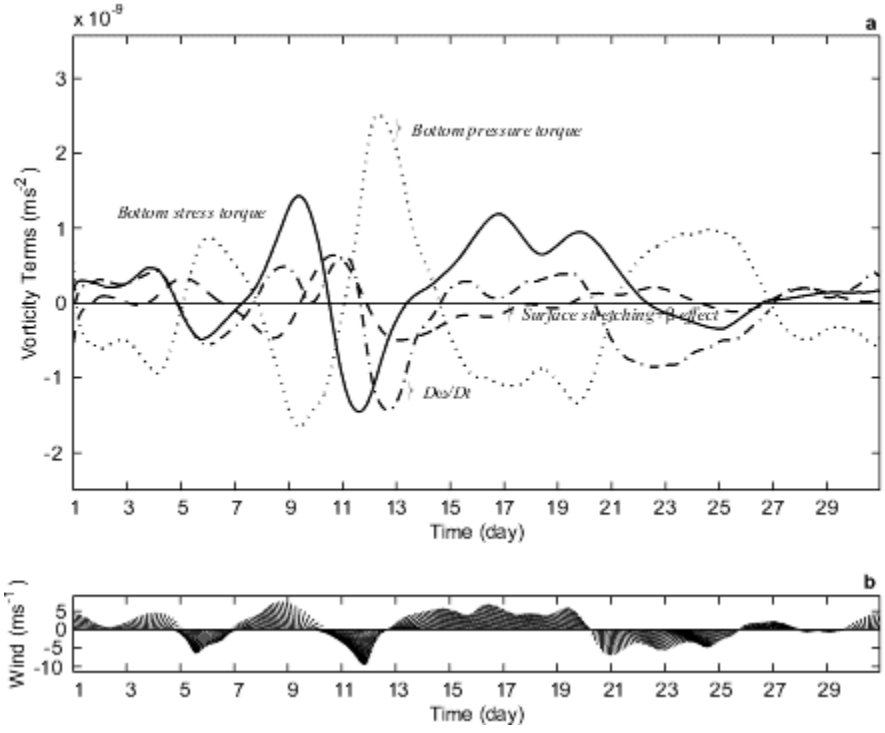
x 10^-9
a
Vorticity Terms (ms^-2)
Bottom pressure torque
Bottom stress torque
Surface stretching+β effect
Ds/Dt
Time (day)
b
Wind (ms^-1)
Time (day)

Figure 18

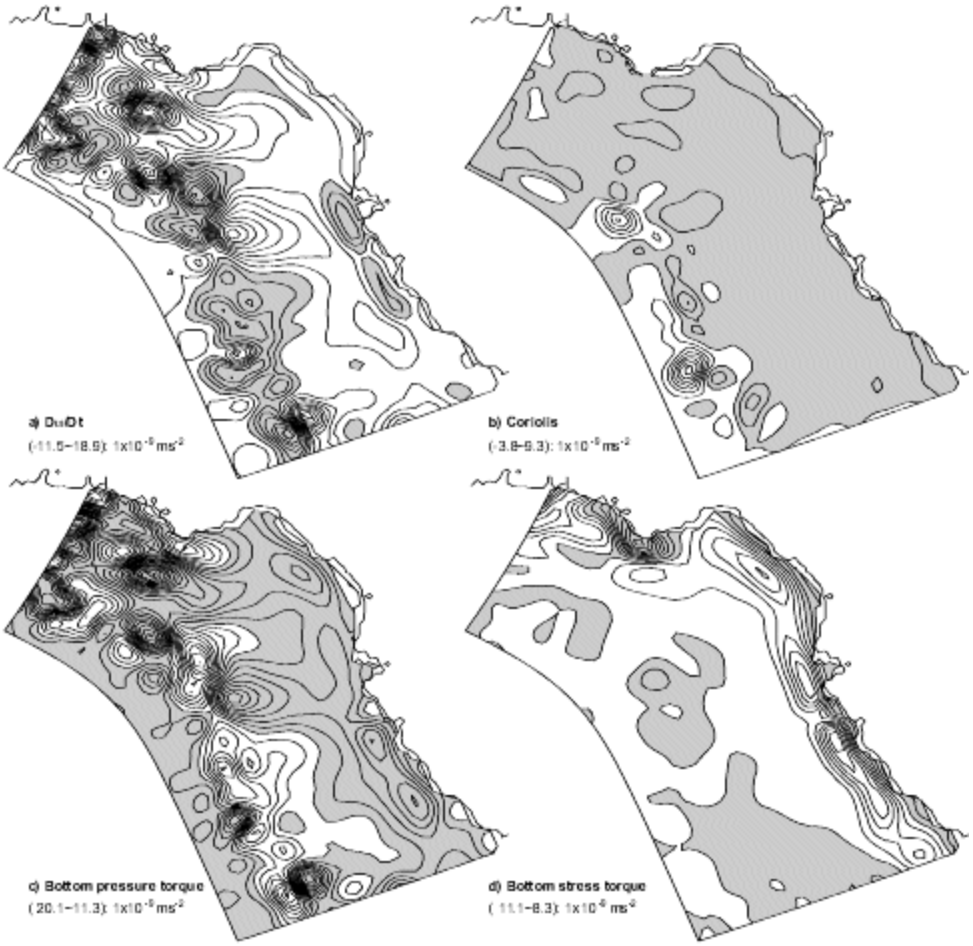
a) Du/Dt
(-11.5–18.9): 1x10⁻⁶ ms⁻²
b) Coriolis
(-3.8–6.3): 1x10⁻⁶ ms⁻²
c) Bottom pressure torque
(-20.1–11.3): 1x10⁻⁶ ms⁻²
d) Bottom stress torque
(-11.1–8.3): 1x10⁻⁶ ms⁻²

Figure 19

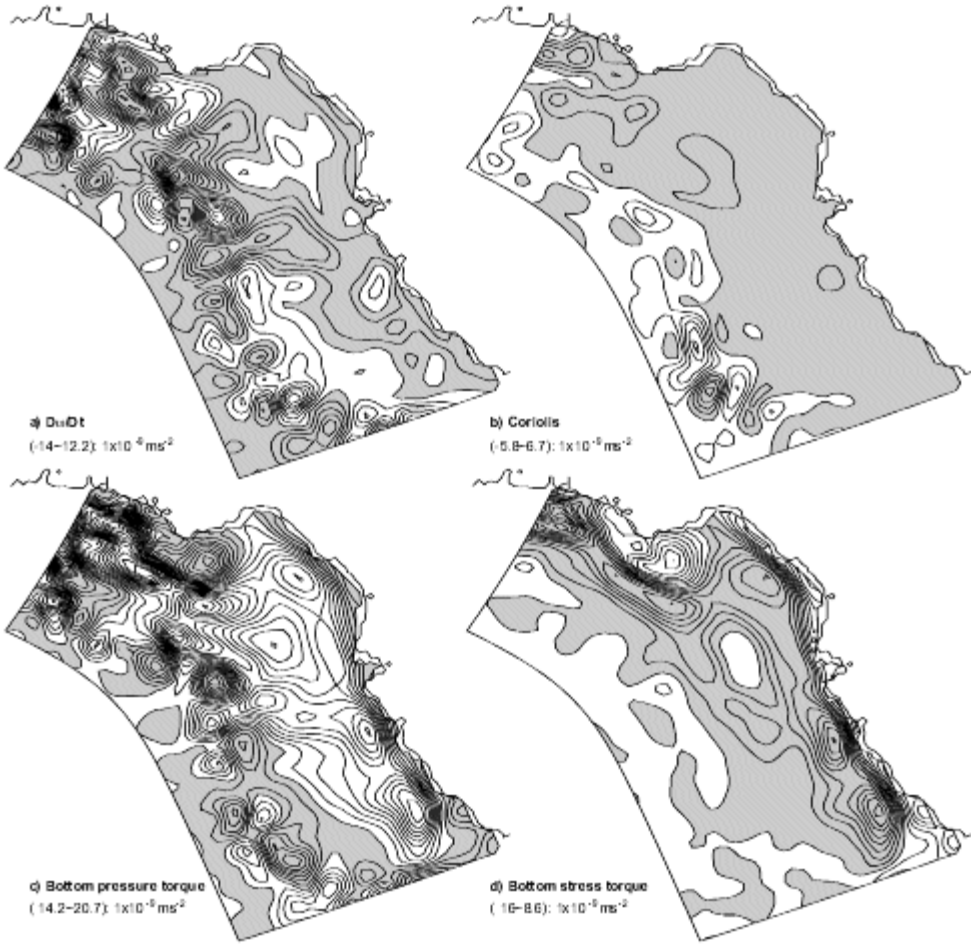
a) Dv/Dt
(-14–12.2): 1x10⁻⁶ ms⁻²
b) Coriolis
(-5.8–6.7): 1x10⁻⁶ ms⁻²
c) Bottom pressure torque
(-14.2–20.7): 1x10⁻⁶ ms⁻²
d) Bottom stress torque
(-16–8.6): 1x10⁻⁶ ms⁻²

Figure 20

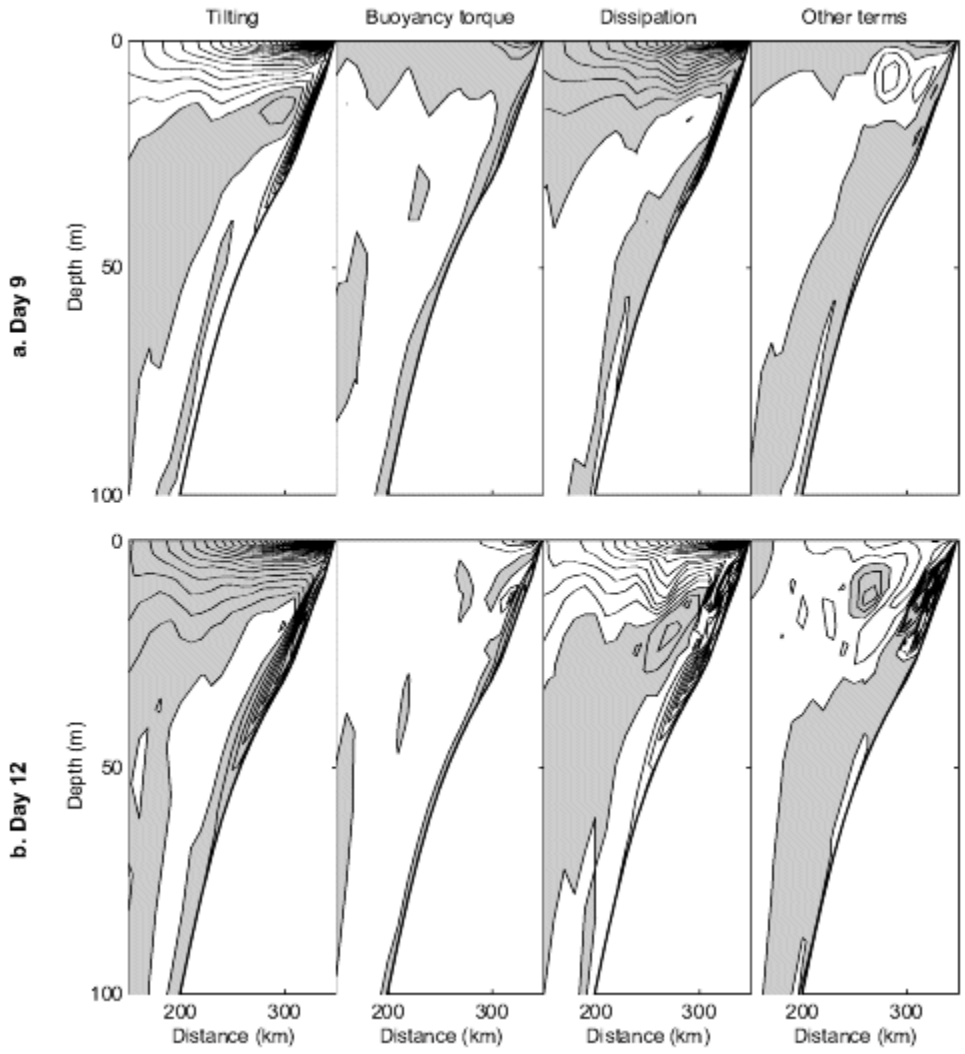
Tilting
Buoyancy torque
Dissipation
Other terms
a. Day 9
b. Day 12
Depth (m)
0
50
100
200
300
Distance (km)

Figure 21

5e. West Florida shelf circulation and temperature budget for the 1999 spring transition

West Florida Shelf Circulation and Temperature Budget for the 1999 Spring Transition

Ruoying He

and

Robert H. Weisberg*

College of Marine Science, University of South Florida
140 7th Ave. South, St. Petersburg, Florida, 33701

Continental Shelf Research, in press, 2001

*Corresponding author. Tel: 1-727-553-1568; Fax: 1-727-553-1189
E-mail address: weisberg@marine.usf.edu

Abstract

Mid-latitude continental shelves undergo a spring transition as the net surface heat flux changes from cooling to warming. Using *in-situ* data and a numerical circulation model we investigate the circulation and temperature budget on the West Florida Continental Shelf (WFS) for the spring transition of 1999. The model is a regional adaptation of the primitive equation, Princeton Ocean Model forced by NCEP reanalysis wind and heat flux fields and by river inflows. Based on agreements between the modeled and observed fields we use the model to draw inferences on how the surface momentum and heat fluxes affect the seasonal and synoptic scale variability. We account for a strong southeastward current at mid-shelf by the baroclinic response to combined wind and buoyancy forcing, and we show how this local forcing leads to annually occurring cold and low salinity tongues. Through term-by-term analyses of the temperature budget we describe the WFS temperature evolution in spring. Heat flux largely controls the seasonal transition, whereas ocean circulation largely controls the synoptic scale variability. These two processes, however, are closely linked. Bottom topography and coastline geometry are important in generating regions of convergence and divergence. Rivers contribute to the local hydrography and are important ecologically. Along with upwelling, river inflows facilitate frontal aggregation of nutrients and the spring formation of a high concentration chlorophyll plume near the shelf break (the so-called 'Green River') coinciding with the cold, low salinity tongues. These features originate by local, shelf-wide forcing; the Loop Current is not an essential ingredient.

1. Introduction

Located at the eastern edge of the Gulf of Mexico, the West Florida Continental Shelf (WFS) is one of the broadest continental shelves in North America. Between its southern and northern ends, bounded by the Florida Keys and the Florida Big Bend, respectively, the WFS isobaths vary smoothly, and they generally parallel the coastline. This geometry changes along the Florida Panhandle in the north where the coastline undergoes a right angle bend, and the shelf width decreases to a minimum at the DeSoto Canyon.

Long-term observations (*Weisberg et al.*, 1996) show that the WFS circulation, forced by tides, winds, buoyancy, and possible interactions with the Gulf of Mexico Loop Current, varies on time scales from semi-diurnal to inter-annual. Monthly mean currents at mid-shelf suggest a seasonal cycle with along-shore flows either to the southeast in spring, or to the northwest in late summer to early autumn. *Weisberg et al.* (1996) hypothesized that these seasonal currents are of a baroclinic nature based on an observed thermal wind shear and the seasonal reversal of the across-shelf density gradient. As a consequence of the spring transition in surface heat flux from cooling to warming, they argued that spatial differences in heating (from the coast to offshore by increasing depth and from the south to north by solar declination) forms a mid-shelf cold tongue and a seasonally maximum across-shelf density gradient that supports a southeastward current. Here we examine this locally forced, seasonal circulation hypothesis by focusing on the spring transition for 1999, a year when the Loop Current, as evidenced in relatively flat isopycnal topography at the shelf break, did not have a strong direct influence the WFS. Our objective is to describe the circulation and temperature budget for spring 1999 with respect to the shelf-wide winds, surface heat fluxes, and river inflows.

An argument used to describe the transition from wintertime horizontal stratification to summertime vertical stratification for mid-latitude shelves is that decreased winds and increased solar heating conspire to form a thermocline. The details of this process are not well understood, however. *Chapman and Gawarkiewicz* (1993) reason that nonlinearity in the equation of state can account for the elimination of horizontal stratification by spatially uniform heating, but *Morey* (1999) point out that this argument is valid only for certain salinity and temperature ranges. Other processes must also be important. *Morey* (1999), using a two-dimensional model with a sloping bottom, argue that the surface heat flux divided by the water depth is the critical factor in the seasonal transition, essentially the differential heating argument advanced earlier. The degree to which their argument is valid in the fully three-dimensional sense and the regional partition between ocean dynamical and local heating affects are also topics of our paper.

The observational record [e.g. *Niiler,* 1976; *Mitchum and Sturges*, 1982; *Cragg et al*, 1983; *Marmorino*, 1983; *Mitchum and Clark*, 1986a] shows that the WFS circulation and sea level variations are highly correlated with the synoptic scale wind stress variations. The passage of cold fronts also affects the local temperature balance (e.g., *Price,* 1976). Along with these local synoptic scale

variations are baroclinic effects that originate with the Loop Current at the shelf break [e.g., *Paluszkiewicz et al*, 1983]. What remains unclear are the relative importance between the momentum and buoyancy that are input either locally, or at the shelf break.

Such questions are of multi-disciplinary interest since, despite its oligotrophic description, the WFS supports highly productive ecosystems. These include episodic toxic dinoflagellate blooms (red tides) near the coast (*Steidinger*, 1981; *Vargo et al*, 1985), a seasonal chlorophyll plume near the shelf break (*Gilbes et al*, 1996), and important commercial and recreational fisheries throughout the WFS. Parallel programs of *in situ* measurements and numerical model experiments are presently in place for an improved understanding of the circulation and how it affects seasonally varying water properties and influences organism growth and distribution.

This paper focuses on local wind and buoyancy forcing during the spring transition of 1999, independent of the Loop Current. We use the primitive equation, Princeton Ocean Model (POM) described by Blumberg and Mellor (1987) forced by National Center for Environmental Predication (NCEP) reanalysis winds and net surface heat flux and by river inflows. The only role of the adjacent Gulf of Mexico is to set the vertical distribution of temperature and salinity for initializing the model density field. Once begun, the integration proceeds solely on the basis of local forcing. By running twin experiments, one with heat flux and the other without, we explore the relative importance of wind and buoyancy in effecting the seasonal and synoptic scale variability.

Section 2 describes the model and forcing fields. Section 3 compares model results with *in-situ* observations. Based upon these comparisons the model is used in section 4 to describe the seasonal mean circulation on the WFS for spring 1999 and the evolution of the corresponding temperature and salinity fields. Section 5 presents a term-by-term analysis of the three-dimensional temperature budget. The results are summarized and discussed in section 6.

2. Model and Forcing fields

2.1. Model

We use the POM for the following reasons. First, it has an embedded turbulence closure submodel (*Mellor and Yamada, 1974, 1982; Galperin et al., 1988*) for parameterizing vertical turbulence mixing. Second, it employs a sigma coordinate in the vertical which, with the turbulence closure sub-model, is well suited to study the nonlinear dynamics over a shallow, gently sloping continental shelf. Third, its orthogonal curvilinear coordinates in the horizontal are convenient for resolving the near-shore regions.

Previous WFS POM applications include *Yang et al.* (1999a,b), *Li and Weisberg* (1999a,b), *Weisberg et al.* (2000), and *Weisberg et al.* (2001). *Yang et al.* (1999a) studied the WFS response to climatological monthly mean wind forcing. Qualitative agreements were found between the model and observations to some extent, but monthly mean wind stress alone could not account for the southeastward current observed at mid-shelf in spring (*Weisberg et al.*, 1996). *Li and Weisberg* (1999a,b) focused on synoptic scale winds, respectively describing the kinematics and dynamics of WFS responses to idealized upwelling favorable wind forcing under constant density. The inner-shelf length scale was found to be a frictional one, consistent with the analytical work of *Mitchum and Clarke* (1986b). The same model was also applied to a specific upwelling case study with both constant density and stratified conditions (*Weisberg et al.* 2000). A comparison of *in-situ* data with model results confirmed a simple Ekman-geostrophic route to spin-up and identified regional upwelling centers promoted by coastline and isobath geometries. The utility of this model in replicating the longer-term synoptic scale variability and the sensitivity of the WFS response to its background density state was then shown by *Weisberg et al.* (2001). An asymmetry in the inner-shelf responses to upwelling and downwelling favorable winds was found that helps to clarify the scale of the inner-shelf response. Consistent with Ekman dynamics, the inner shelf is the region with divergent bottom boundary layer. Since thermal wind effects can either enhance or decrease the bottom boundary layer development, the inner-shelf under stratified conditions can respond asymmetrically to upwelling and downwelling favorable winds.

Many WFS circulation questions remain. For instance, the relative effects of buoyancy and wind forcing have not been considered. While previous drifter and current meter measurements hint at seasonally varying circulation patterns (*Tolbert and Salsman*,1964; *Gaul*, 1967; *Williams et al.*, 1967; *Weisberg et al.*, 1996; *Yang et al.*, 1999b), there are no definitive measures of these. The communication of water between the deep ocean and the shelf and the communication of water between different regions of the shelf remain poorly understood. To address these questions it is necessary to explore a broader region and consider more complete forcing functions than in previous studies.

The model domain (Fig 1) extends from the Florida Keys in the southeast to west of the Mississippi River in the northwest, and it has one open boundary arcing between these two locations for which a radiation boundary condition (*Orlanski, 1976*) is used. The model domain includes the major rivers that impact

the WFS and the Desoto Canyon region where the shelf is narrowest, and its orthogonal curvilinear grid has horizontal resolution that varies from less than 2km near the coast to 6 km near the open boundary. Vertically, the sigma coordinate has 21 layers with higher resolution near the surface and bottom to better resolve the frictional boundary dynamics. In total, the model has 121×81×21 grid points. Horizontal diffusivities are parameterized using the *Smagorinsky* (1963) formulation with a coefficient of 0.2. Bottom stress, τ_b, is calculated by a quadratic law with variable drag coefficient having a minimum value of 0.0025. A mode splitting technique is used for computational efficiency (*Blumberg and Mellor, 1987*). Here we use external and internal time steps of 6 seconds and 360 seconds, rspectively.

The model is initialized at rest with horizontally uniform stratification. Stratification above 200m is based on temperature and salinity observations taken during a March 1999 trans-shelf hydrographic survey [from the Ecology of Harmful Algal Blooms (ECOHAB) Program]. Stratification below 200m is based on climatology. From this initial zero-baroclinicity state, the model spins up rapidly, generating baroclinicity in balance with the wind and buoyancy forcing. An alternative is to begin with a baroclinic field and allow the model currents to come into balance diagnostically with this field before proceeding with the spring simulation. The hydrographic data are not sufficient for this, however, and spurious currents due to incorrect density would corrupt the experiment. Consistent with our objective of determining the WFS responses to local, shelf-wide forcing only, our initial baroclinicity-free state is a sensible choice.

Tidal forcing is excluded in the present application since we are not considering high frequency variability. It is recognized that tidal mixing can affect the synoptic and seasonal scales when the tidal currents are large, but here the tidal currents are only a few cm s^{-1}. Modeled and observed tidal current analyses will be reported on separately.

2.2 Atmospheric forcing

Different from previous WFS model studies that considered wind forcing only, here we include both wind and thermohaline forcing. The wind and heat flux fields are from the NCEP daily reanalysis product for the period February 28, 1999 to June 1, 1999. These values, with a grid resolution of $2.5^o \times 2.5^o$, are interpolated onto the model grid. The NCEP winds agree well with *in-situ* buoy winds for the spring 1999 season. Unlike the winds, however, coarse resolution renders the NCEP heat flux unrealistic because of smaller scale WFS temperature structures. We correct for this using a relaxation method (*e.g., Ezer et al*, 1992; *Chu et al*, 1999). Thus, the surface heat flux forcing is given by

$$K_H \frac{\partial \theta}{\partial z} = \left(\frac{Q_H}{\rho C_P} \right) + C(\theta_{obs} - \theta)$$
$$K_H \frac{\partial S}{\partial z} = 0 \qquad (1)$$

where Q_H is the net heat flux, θ_{obs} is an interpolation of the monthly-mean satellite observed sea surface temperature, and C_p is the specific heat. The

salinity flux in this study is set to be zero. The relaxation coefficient, *C*, or the reciprocal of the restoring time per unit area, is set at 1m/day. Such relaxation prevents deviations from observed monthly-mean SST in an attempt to force realistic baroclinic flow structures. These structures are facilitated by turbulence mixing through the coefficients K_M and K_H computed with the *Mellor and Yamada* (1982) 2.5 level turbulence closure sub-model.

2.3Lateral boundary forcing.

Gulf of Mexico Loop Current forcing is excluded in this study for two reasons. First, previous observations and model studies concluded that persistent forcing of the middle and inner-shelf by the Loop Current is minimal (*Marmorino*, 1982, 1983 a,b). Second, modeling the effects on the WFS of an aperiodically varying Loop Current and its associated eddies (e.g., Sturges and Leben, 2000) remains a great challenge (*Marmorino*, 1982; *Cooper*, 1987), presupposing that the Loop Current itself is being described properly. To better assess the role of the Loop Current as a WFS boundary condition it will be necessary to nest a regional model with a larger Gulf of Mexico/Caribbean/Atlantic Ocean model. This is beyond the scope of the present paper that focuses on local, shelf-wide forcing only. We find, however, that local forcing is capable of driving much of the observed synoptic and seasonal scale variability.

Seven major rivers are introduced into the model domain for land derived buoyancy forcing. These are the Mississippi, Mobile, Apalachicola, Suwannee, Hillsborough, Peace and Shark rivers. We use the technique of *Kourafalou et al* (1996)(also see *Pullen* 2000), whereby interpolated monthly mean mass flux data for these rivers are input to the top sigma level at the grid cells closest to the rivers' locations.

We define the spring season here as March 1 to May 31, and we focus on this period for 1999. As an initial value problem we begin from a state of rest on February 28. With no initial baroclinicity the spin-up phase proceeds rapidly over the course of a few pendulum days, consistent with the barotropic response arguments for a gently sloping shelf of *Clarke and Brink* (1985). Under the conditions of surface cooling that occurs prior to the spring warming transition in mid-March, convective mixing very efficiently adjusts the initial density field on the shallow shelf. In other words, the "memory" of initial density field for this spring transition experiment is short, and sensitivity experiments that we performed using longer spin-up times showed very little difference from the present model results.

3. Model and Data Comparisons

3.1 Sea level

Since the model is forced without tides, all of the model and data comparisons are shown after low-pass filtering to exclude tidal and inertial period oscillations. Sea surface height comparisons are given in Fig. 2 at four different tide-gauge stations from Pensacola in the northwest to Naples in the southeast. Agreement is good at all of these with squared correlation coefficients exceeding 0.80. We conclude that coastal sea level for this three-month period responds primarily to local, shelf-wide forcing.

3.2 Currents

Comparisons are made between the modeled and observed velocity vector time series at the 50m, 30m, 25m, 20m, and 10m isobaths (moorings CM2, EC3, NA2, EC4, EC5, and EC6 in Fig. 1). As examples, we show the modeled and observed vector time series at the 50m, 25m, and 10m locations in Figs. 3-5, respectively. The observations are from acoustic Doppler current profilers (ADCP), and for each location we show comparisons at three different depths: near-surface, mid-water column, and near-bottom. These comparisons are quantified by a complex correlation analysis (*e.g., Kundu* 1976). Defining the modeled and observed velocity vectors in the Argand plane as $w_1 = u_1 + iv_1$ and $w_2 = u_2 + iv_2$, respectively, the complex squared correlation coefficient is

$$\rho(w_1, w_2) = \frac{\overline{[w_1^*(t) w_2(t)]}^2}{\overline{[w_1^*(t) w_1(t)]}\ \overline{[w_2^*(t) w_2(t)]}} \qquad (2)$$

where the overbar denotes a time average. The complex correlation has an amplitude and a phase, the amplitude being the correlation coefficient and the phase being the angle (measured counterclockwise) between the modeled and the observed currents. Like sea level, the modeled and observed currents also compare well as measured by the two sets of numbers provided with each plot. The left-hand sets are the seasonal mean east and north velocity components. The right-hand sets are the squared correlation coefficient, phase angle, and regression coefficient. At all stations and depths the squared correlation coefficients range between 0.62 and 0.82, and the orientations agree to within –10 to +20 degrees. More importantly, as seen directly from the time series, the model gets the sense of the velocity rotation correct in both the surface and bottom Ekman layers. A deficiency in the modeled currents, however, lies in the amplitudes. The regression coefficients show that the model underestimates the observed velocity fluctuations by between 20 to 50 percent.

Notwithstanding the amplitude disparity, the model reproduces the patterns of current variability reasonably well. The systematic underestimate of the currents may be the result of the low resolution NCEP forcing fields, and hence too much smoothing when interpolating these fields onto the model grid. Model performance also degrades between the shallowest and deepest comparison sites, i.e., the 10m isobath currents agree better than the 50m isobath currents. This is expected based on the frictional scale of the inner-shelf

response to wind forcing (*e.g., Weisberg et al*, 2001). The 50m isobath is at the outer half of the inner-shelf so we anticipate a decreased correlation there.

The modeled and observed velocity comparisons are summarized in Fig. 6 where we show the mid-depth seasonal mean vectors and hodograph ellipses at all of the mooring locations. The mean vectors compare reasonably well, and while the ellipse semi-major axes are off by between 20-50%, the orientations and eccentricities tend to agree. On the basis of these agreements we now use the model to discuss the WFS circulation in spring 1999.

4. Mean Circulation

4.1 Flow fields

The seasonal mean circulation, obtained by averaging the model flow fields from March 1 to May 31, is presented in Fig 7. Three-dimensional flow features arise because of the WFS geometry that includes partial blocking by the Florida Keys, the coastline changes of the Big Bend, and the intrusion of Desoto Canyon. These features are depicted in horizontal velocity field maps given for sigma layers 2 (near-surface), 10 (mid-level), 20 (near-bottom), and for the depth-average.

The mid-level and depth-averaged fields are similar (and with the same scale), and they show the general nature of the 1999 spring season currents. A jet exists with axis situated between the mid-shelf and the shelf break. This jet originates along the northern coast east of the Mississippi River, and it flows along the relatively narrow Florida Panhandle shelf as a closely confined coastal feature. The coastal jet bifurcates at Cape San Blas into a mid-shelf part that heads along-isobath toward the southeast and a coastal part that hugs the Big Bend coastline. The mid-shelf part is consistent with the spring season southeastward current described by *Weisberg et al*. (1996). This mid-shelf current again bifurcates upon approaching the Florida Keys with a portion turning toward Florida Bay and another portion turning farther offshore. Why this occurs and how it affects the Florida Bay/Florida Keys region are evident in the near-bottom and near-surface flow fields (note the scale changes). Near the bottom we see a convergence of vectors on Florida Bay and the Florida Keys. In contrast to this, near the surface we see flow paralleling the Florida Keys. The near bottom flow upwells, feeding the near surface flow, and the second bifurcation is due to the recirculation associated with the upwelling. *Li and Weisberg* (1999a) discussed a similar recirculation due to the Florida Keys for the case of upwelling winds under a constant density setting. From the surface current map we can appreciate why surface drifters originating in the north do not penetrate the southeast portion of the WFS; the so-called 'Forbidden Zone' described by *Yang et al.* (1999b). We also note that the currents within the Big Bend and those that flow southward near-shore between Cedar Key and Sarasota are much weaker than the currents at mid-shelf. As will be shown in the next section, this is a consequence of a surface heat flux-induced cyclonic circulation that adds destructively (constructively) to the wind driven flow near-shore (offshore).

Three-dimensionality in the flow field is further evident in the vertical component of velocity shown for near-bottom, middle, and near-surface sigma levels in Fig. 8. Upwelling is prominent north of the Florida Keys with a maximum near the Dry Tortugas, as is often evident in satellite SST imagery (e.g., *Weisberg et al*., 2000). Upwelling is also prominent west of DeSoto Canyon, around Cape San Blas, and along the west Florida coastline. Other regions show downwelling. This vertical circulation is a function of both the bottom boundary layer and the interior. The near bottom *w* can be reconciled based on the near bottom horizontal velocity field (Fig. 7) and the bottom kinematic boundary condition. Mid-water column divergence then accounts for the

transition of *w* from its near-bottom to near-surface values. Upwelling occurs along the entire near-shore domain near the bottom, whereas upwelling is more localized near the surface.

4.2 Temperature and salinity field

The modeled surface temperature and salinity fields sampled at the end of the model run on May 31 are presented in Fig. 9. Since the initial model temperature and salinity fields are horizontally uniform, this figure shows the combined effects of the momentum and buoyancy fluxes in changing the surface temperature and salinity. The two principal features are the mid-shelf cold tongue that extends southeastward from Cape San Blas and the low salinity tongue that also extends southeastward, but displaced seaward of the cold tongue. Both of these features occur annually on the WFS. The cold tongue is imposed to some extent through the surface heat flux relaxation, whereas the low salinity tongue is a fully prognostic result of the model.

The low salinity tongue derives as a river plume, accumulating fresh water primarily from the Mississippi River with additions from the Mobile and Apalachicola Rivers. Modulated interannually, the low salinity tongue extends southward each year, and in some years (1993, for instance – see *Dowgiallo* et al., 1995) it can be traced around the Florida peninsular to the Carolinas. Using Coastal Zone Color Scanner data between 1979 and 1986, *Gilbes et al*. (1995) reported a spring chlorophyll plume at mid-shelf (termed the 'Green River') that also extends southeast from Cape San Blas. Their explanations for the plume included: *i*. nutrient fluxes from the Apalachicola River; *ii*. nutrient fluxes from the Mississippi and Mobile Rivers; *iii*. seasonal changes in steric height between the shelf and deeper Gulf of Mexico; and *iv*. circulation of water from the Loop Current. Our results help to clarify these speculations. Consistent with *Weisberg et al*. (1996) the 'Green River' is associated with both the cold tongue and the low salinity tongue. The low salinity tongue, at least in 1999, appears to originate at the Mississippi River. It is advected eastward, on average, by the spring coastal jet and then southeastward where the jet bifurcates at Cape San Blas. This bifurcation, in part, is related baroclinically to the cold tongue; hence the offset between the low salinity and cold tongues. Since the Loop Current is not included in our model, and since it did not extend to the northeast Gulf of Mexico in spring 1999, we can rule out the Loop Current as a primary conveyance of these salinity and temperature features. What remains unclear is the relative importance of land-derived versus upwelling-derived nutrients in fueling the chlorophyll plume. Aggregation of nutrients and phytoplankton by the frontal regions of the cold tongue/low salinity tongue complex can nevertheless account for the 'Green River'.

To explore the roles of momentum and heat flux in the formation of these surface temperature and salinity features we ran a model twin experiment forced by NCEP winds only. Fig 10 shows the seasonal mean circulation with wind forcing only for comparison with Fig.7 with both wind and heat flux forcing. Differences occur in all fields. The most obvious is the location of the jet, as seen in either the depth-averaged or the middle level fields. With wind forcing

only the jet has a stronger coastal expression over the entire WFS, as contrasted with a stronger mid-shelf jet under wind and heat flux forcing. Baroclinicity explains the difference. With wind and heat flux forcing a dynamical feedback occurs with the cold tongue causing a cyclonic baroclinic circulation that adds constructively (destructively) with the wind forced circulation at mid-shelf (near-shore). A baroclinic circulation also arises without heat flux, but this adds constructively with the wind forced circulation near-shore. This latter effect for wind forcing only is seen in the surface temperature field of Fig. 11. Surface temperature is colder everywhere since the ocean circulation merely rearranges it. By virtue of mean upwelling the near-shore region is colder than the offshore region which causes a southward baroclinic circulation that adds constructively with the southward wind-driven circulation.

Given the importance of surface heat flux on the seasonal circulation it is instructive to see how the baroclinic contribution evolves. This is shown in Fig. 12 for the March, April, and May monthly mean, depth-averaged flows relative to the seasonal mean. March shows an anticyclonic circulation with southeastward flow near-shore. During April, once the effects of positive heat flux set in, we see the formation of the mid-shelf jet and a cessation or reversal of the near-shore flow. This further develops into a strong mid-shelf/shelf-break current in May as the cyclonic baroclinic flow becomes fully developed. This is consistent with the *Weisberg et al* (1996) hypothesis on the origin of the springtime southeastward current.

Temperature cross-sections at various positions along the WFS provide further information on the cold tongue evolution. These are shown for wind and heat flux forcing and for wind forcing only on March 15, April 15 and May 15, in Figs. 13, 14, and 15, respectively, at four transects offshore of DeSoto Canyon, Cape San Blas, the Big Bend, and Sarasota. Since the heat flux is initially out of the ocean the March 15 transects, with or without heat flux, are similar at depth. They differ on the shelf where surface cooling, coupled with efficient convective mixing, produces typical wintertime horizontal stratification. By April 15, with a reversal in the sign of the heat flux, the two cases depart everywhere. The Big Bend transect shows a dome of cold water at mid-shelf in the heat flux case. This originates primarily by the burial (by water being heated from above) of the cold water previously formed in the Big Bend. Water is warmer in the shallows near-shore for the same reason that they were colder in the previous season (a similar heat flux over a shallower layer will result in a larger internal energy change per unit area). There are also secondary contributions from upwelling at the shelf break. Here the shelf break upwelling is from the Big Bend as opposed to the DeSoto Canyon, and this is in part a consequence of bottom topography. The shelf break in the Big Bend occurs about 20m deeper than in the DeSoto Canyon. Hence, less upwelling is required for water to rise onto the shelf in the Big Bend than in the DeSoto Canyon. This finding is clear in continuous animations where we also see that the advective time scale between the DeSoto Canyon and the Big Bend is longer than the synoptic weather time scale. For spring 1999, at least, we do not see a direct connection between the DeSoto Canyon and Big Bend regions as would be evidenced by continuous isotherms.

Note that while 21^{0}C waters occur on the shelf offshore of both the DeSoto Canyon and Big Bend regions these waters are not seen on the shelf at the intervening Cape San Blas cross section. Local upwelling in the Big Bend region (due to a relatively deep shelf break) is therefore important, and it may help to explain the relatively high productivity of the Florida Middle Grounds. A similar subsurface cold-water core is seen farther south off Sarasota and for the same reasons. It is smaller in magnitude because of differential cooling and heating from north to south, i.e., when the heat flux reversed from cooling to warming the temperatures off Sarasota were already warmer than those in the Big Bend. Dynamically, the doming of cold water at mid shelf (and hence the cold tongue) induces the cyclonic baroclinic circulation. This is further facilitated by the no heat flux bottom boundary condition that bends the isotherms perpendicular to the bottom. These combined effects of differential heating (near-shore to offshore by bottom slope and southward to northward by solar declination) and dynamical feedbacks (baroclinic pressure gradients associated with the temperature gradients) conspire to cause the spring season temperature transition from well mixed to stratified with a cold tongue at mid shelf.

The May 15 transects show the continued evolution of these processes. By now the mid-shelf isotherm doming has relaxed due to continued heating and so has the mid-shelf circulation due to decreased winds and baroclinicity. The location of the jet is now farther offshore at the shelf break, and the modeled temperature agrees with observed ECOHAB Program hydrography.

4.3 Lagrangian drifters

Model-simulated Lagrangian drifter tracks provide additional information on the evolution of the cold and low salinity tongues and the regions for possible communication between the deep ocean and the shelf. Dynamically passive particles released in the model on April 1stare tracked through May 31st. These are shown in Figs. 16 and 17 for particles originating either near the surface or the bottom, respectively. Most evident for the particles released near the surface is advection by the mid-shelf jet and the bifurcations at Cape San Blas and north of the Florida Keys. The particle trajectories agree with the Eulerian maps previously shown and with the cold and low salinity tongue features. With the exception of those in the mid-shelf jet the particle displacements are not very large. The near-surface drifters also show a propensity to flow either along-isobath or offshore. The near-bottom released drifters show subtle, but important differences, particularly in the Florida Big Bend/Middle Ground region. There we see onshore flow between the shelf break and the mid-shelf. This is consistent with the changes in hydrography discussed in the previous section, supporting our speculation that the Big Bend may be an important region for deep ocean/shelf interactions.

5. Temperature Budget

5.1 The temperature equation

To analyze the temperature budget, the temperature equation is recast from its modeled flux divergence, *sigma level* form to an advective, *z-level* form. Thus, we diagnose

$$\frac{\partial T}{\partial t} = -u\frac{\partial T}{\partial x} - v\frac{\partial T}{\partial y} - w\frac{\partial T}{\partial Z} + \frac{\partial}{\partial z}\left(K_H \frac{\partial T}{\partial z}\right) + \frac{\partial}{\partial x}\left(A_H \frac{\partial T}{\partial x}\right) + \frac{\partial}{\partial y}\left(A_H \frac{\partial T}{\partial y}\right)$$

(3)

a *b* *c* *d* *vf* hf_x hf_y

which equates the local rate of change of temperature *(a)* to a combination of the flow field advective rate of change *(b+c+d)*, and the rates of change by vertical diffusion *(vf),* and horizontal diffusion *(hf_x+hf_y)*. The temperature balance is explored using: *i*. time series of vertical averages, *ii*. time series of vertical profiles at four different locations, and *iii*. term by term spatial maps of the sea surface temperature rates of change.

The four analysis locations (see Fig 1) are chosen with respect to the cold tongue and the upwelling region north of the Florida Keys. Point A is on the 50m isobath at the seaward side of the Big Bend shelf subsurface cold dome. Point B is on the 40m isobath west of Tampa Bay where the cold tongue begins to taper off. Point C is on the 15m isobath offshore of Sarasota on the inshore side of the cold tongue. Point D is north of the Florida Keys. A term-by-term analysis of (3) quantifies the contributions by each physical process in changing the temperature.

5.2 Depth-averaged balances.

A depth-averaged temperature equation is obtained by vertically integrating equation (3). Since horizontal temperature diffusion is generally at least an order of magnitude less than the other terms, the depth-averaged diffusion term is essentially the depth-averaged vertical diffusion, $Q/(\rho C_P H)$, where *Q* is the net surface heat flux, ρ and C_P are the seawater density and specific heat, and *H* is the water depth. The temperature variations depend on both ocean advection and diffusion. With a two-dimensional model, *Morey* (1999) proposed that temperature, in a depth-averaged sense, could be well represented without advection, i.e.,

$$\frac{dT}{dt} = \frac{\partial T}{\partial t} = \frac{Q(t)}{\rho c_P H}$$

(4)

The validity of this assertion for various locations on the WFS can be evaluated by a fully three-dimensional analysis.

Time series of the depth-averaged ocean advection and diffusion terms and their sum for locations A-D are shown in Figs. 18a-18d, respectively. While not shown in these figures, we note that the sum of these two terms is nearly exactly equal to the negative of the local rate of temperature change, which is essentially a check on our budget analysis. At station A, the depth-averaged rates of change are relatively small, and a clear distinction exists between the

balances occurring on seasonal and synoptic time scales. The seasonal change (as given by the three-month mean values) is primarily by surface heat flux, whereas the synoptic variability (as given by the standard deviations) is primarily by ocean advection. Although a relatively small contribution to the seasonal change, the ocean advection does provide a cooling influence that offsets the surface heating by about 4% at this location. Thus, of the total change in vertically averaged temperature (1.66^0C), the contributions by ocean circulation and surface heat flux are a cooling of -0.07^0C and a warming of 1.73^0C, respectively. In contrast with the seasonal change, for synoptic scale variability we see that the ocean circulation is twice as effective as the surface heat flux in changing the vertically averaged temperature at station A.

Somewhat different results are found at station B. While surface heat flux and ocean circulation again control the seasonal and synoptic scale variability, respectively, the relative magnitudes and the signs change. Of the total change in vertically averaged temperature (3.05^0C), both the ocean circulation and the surface heat flux at the southern terminus of the cold tongue contribute to warming at 0.68^0C and 2.37^0C, respectively. The ocean circulation also plays a proportionately larger role in the synoptic scale variability at station B than at station A.

The relative importance of the ocean circulation versus surface heat flux continues to change approaching shallower water. At the 15m isobath, station C, of the total change in vertically averaged temperature (4.76^0C), the contributions by ocean circulation and surface heat flux are cooling of -1.24^0C and a warming of 6.00^0C, respectively. The shallower the water, the larger the total spring transition change. However, the role of the ocean circulation in this change varies in both magnitude and sign with location. For instance, at station D in the upwelling region north of the Florida Keys, the ocean circulation provides a cooling influence of 2.79^0C that partially offsets the surface heat flux warming influence of 8.11^0C. Without the upwelling influence by ocean circulation the water temperature north of the Florida Keys would be much warmer. Along with these increased effects by the ocean circulation on the seasonal mean temperature change, the magnitude of the controlling ocean circulation effect on the synoptic scale variability also increases with decreasing water depth. The temperature budget on all time scales is a complex one requiring a fully three-dimensional description.

5.3 Vertical profiles of the term by term balances

The temperature budget three-dimensionality is further explored through time series of the depth profiles of the individual terms that comprise the temperature balance at these four stations (Figs.19-22). In each of these figures the left hand panels show the horizontal and vertical components of the ocean advection and their sum, and the right hand panels show the diffusion, the diffusion plus the advection (which is nearly exactly equal to the negative of the local rate of change of temperature), and the temperature. With the exception of the initial portion of the record when the surface heat flux is out of the ocean and convective mixing is evident, the immediate impact of the surface heat flux is

primarily in the near surface region (Fig. 19). Without convective mixing, it is then only through turbulence mixing, brought about by the ocean circulation dynamics, that the surface heat flux effect accumulates downward to make its contribution to the depth-averaged spring transition. From the vertical distributions of the seasonal means shown to the right of each panel we see that turbulence mixing distributes the surface heat flux over about 20m depth. Along with its role in turbulence mixing, the direct role of the ocean dynamics through advection on the synoptic scale variability is seen in both horizontal and vertical directions. Omission of any coordinate direction would compromise the model's ability to describe the temperature evolution. For instance, the strong stratification at the end of May at station A is due largely to the combined effects of horizontal and vertical advection. Similar conclusions follow from station B (Fig. 20). Station C (Fig. 21), in shallow water, shows the additional effect of turbulence mixing in the bottom Ekman layer. Here, temperature is elevated near the bottom by ocean circulation-induced mixing. The role of the ocean circulation in promoting mixing is seen in the covariability between the advection and diffusion terms. These interactions are even more evident at station D (Fig. 22) where warming by near-bottom turbulence mixing is required to partially offset the cooling influences by horizontal advection and upwelling. Another interesting feature of the shallow water regions is the tendency for large changes in stratification by the ocean circulation. Two downwelling events culminating in destratification and warming by advection are seen at station C around April 5th and May 10th. Similarly, but in an opposite sense, stratification caused by horizontal advection is seen at this station at the end of May.

5.4 Term by term contributions to the seasonal change in SST

The contributions to the seasonal mean rate of change of sea surface temperature (SST) by each of the advection and diffusion terms are discussed with respect to Fig. 23. The left panels show the advection terms and their sum, and the right panels show the horizontal and vertical diffusion terms, and the sum of all terms. Of particular interest here is the spatial distribution of the processes controlling SST over the model domain. Horizontal diffusion is minimal everywhere except for north of the Florida Keys where it is still the smallest of the terms. Vertical diffusion controlled by the surface heat flux, warms everywhere with maximum warming tendencies stretching along mid-shelf from the Big Bend to the Florida Keys. This warming is the seasonal signal associated with spring, which displays the spatial inhomogeneities mentioned earlier. The difference between this map and the local rate of change of SST is the ocean circulation. By advecting relatively cool water southward, advection provides a cooling influence over the WFS with largest values north of the Florida Keys. With regard to total advection, Cape San Blas divides the entire domain into two sections. To the west, and extending along the north Florida coastline to the Mississippi River, advection tends to provide a warming influence, whereas to the east, along the west Florida coastline, advection tends to provide a cooling influence. Without advection, the center of the cold tongue on the WFS would be some 3-5^{0}C warmer.

6. Summary

Mid-latitude continental shelves undergo a spring transition as the net surface heat flux changes from cooling to warming. Using *in-situ* data and a numerical circulation model we investigate the circulation and temperature budget on the WFS, including the northeast Gulf of Mexico shelf from the Mississippi River to the Florida Keys, for the spring transition of 1999. The data consist of sea level from coastal stations, velocity profiles from instruments moored across the shelf between the 50m and 10m isobaths, and hydrography from ship surveys. The model is a regional adaptation of the primitive equation, POM forced by NCEP reanalysis wind stress and heat flux fields and by river inflows. Based on agreements between the modeled and observed fields we use the model to draw inferences on how the surface momentum and heat fluxes affect the seasonal and synoptic scale variability.

Spring season features of the WFS include a mid-shelf southeastward current, cold and low salinity tongues, and a high chlorophyll plume. We account for the southeastward current in 1999 by the combined responses to local, shelf-wide wind and buoyancy forcing. Wind stress drives a circulation that tends to be strongest near-shore. Heat flux provides a cyclonic contribution that adds constructively (destructively) at mid-shelf (near-shore), thus forming the observed mid-shelf jet. This heat flux-induced baroclinic circulation is related to the spring season cold tongue. By advecting Mississippi (and other) River water it forms the low salinity tongue that is displaced seaward of the cold tongue. Convergence of nutrients and associated phytoplankton growth then accounts for the high chlorophyll concentrations ('Green River') that are co-located with these surface features. These findings support the hypothesis advanced by *Weisberg et al*. (1996) on the origin of the southeastward current and cold tongue through differential heating from the coast to offshore (by shoaling topography) and from south to north (by solar declination). Since we arrive at these features with a model experiment that explicitly omits the Gulf of Mexico Loop Current we argue that the Loop Current is not an essential element of these spring transition features.

Through term-by-term analyses of the temperature budget we describe the evolution of WFS temperature in spring. Surface heat flux largely controls the seasonal transition, whereas ocean circulation largely controls the synoptic scale variability. These two processes are closely linked, however. Since the ocean circulation controls the turbulence mixing, the effects of the ocean circulation are of increasing importance with decreasing water depth. For instance, warming by turbulence mixing near the bottom only occurs when the bottom Ekman layer is well developed by strong currents. Thus, the water column can warm even under upwelling influence if the mixing is large enough. The water column is also found to either stratify or destratify in response to ocean circulation changes. Examples of these effects are shown. While our temperature analyses support the *Morey* (1999) one dimensional temperature balance argument advanced on the basis of a two dimensional model we demonstrate that the temperature balance is more complicated in time and space and requires fully three-dimensional thermodynamics.

Bottom topography and coastline geometry are important in generating regions of convergence and divergence and hence upwelling centers. In particular, we show that the region north of the Florida Keys has strong upwelling in spring and we speculate on the importance of the Florida Big Bend as a region for communication between the deeper Gulf of Mexico and the WFS. The shelf break there is about 20m deeper than at the DeSoto Canyon thereby requiring less upwelling for deeper waters to broach the shelf. This may be one reason why the Florida Middle Grounds are productive. The northeast Gulf of Mexico shelf from Cape San Blas to the Mississippi River also shows mean upwelling during spring 1999.

Acknowledgements

This work was supported by grants from the Office of Naval Research, grant # N00014-98-1-0158 and the National Oceanic and Atmospheric Administration, grant #NA76RG0463. We also benefited from an evolving program with previously support from the United States Geological Survey and the Minerals Management Service. Ocean Circulation Group staff (Messrs. R. Cole, J. Donovan, C. Merz, and P. Smith) contributed to the field work and analyses, as did students W. Hemme and J. Virmani. We thank F. Muller-Karger for providing assistance with the monthly mean SST fields. NCEP reanalysis data provided by NOAA-CIRES Climate Diagnostics Center, Boulder, CO was obtained from their web site at http://www.cdc.noaa.gov/

References

Blumberg, A. F., and G. L. Mellor, A description of a three-dimensional coastal ocean
circulation model, *Three-Dimensional Coastal Ocean Models*, Vol. 4, N. Heaps
(ed.), 208-233, AGU, Washington, D. C., 1987.

Chew, F., On the offshore circulation and a convergence mechanism in the red tide
region off the west coast of Florida. *EOS Trans*. AGU 36, 963-974, 1955a.

Chu, P. Edmons, N. and Fan, C. Dynamical mechanisms for the south china sea seasonal
circulation and thermohaline varibilities. *J. Phys. Oceanogr*., 29, 2971-2989, 1999

Chapman, D.C and G. Gawarkiewicz, On the establishment of the seasonal pycnocline in the
Middle Atlantic Bight, *J. Phys. Oceanogr*., 23, 2487-2492, 1993

Clarke, A. J., and K. H. Brink, The response of stratified, frictional flow of shelf and slope
waters to fluctuating large-scale, low-frequency wind forcing, *J. Phys. Oceanogr*.,
15, 439-453, 1985.

Cooper, C., A numerical modeling study of low-frequency circulation on the west
Florida shelf, *Coastal Engineering*, 11, 29-56, 1987.

Cragg, J., G. Mitchum, and W. Sturges, Wind-induced sea-surface slopes on the West
Florida shelf, *J. Phys. Oceanogr*., 13, 2201-2212, 1983.

Dowgiallo, M.J., ed., Coastal oceanographic effects of the summer 1993 Mississippi River
flooding, Special NOAA Report, March 1994, 77pp.

Ezer, T., and G. Mellor, A numerical study of the variability and separation of the Gulf
Stream, induced by surface atmopheric focing and lateral boundary flows*. J. Phys. Oceanogr*. 22, 660-682, 1992

Galperin, B., L. H. Kantha, S. Hassid, and A. Rosati, A quasi-equilibrium turbulent
energy model for geophysical flows, *J. Atmos. Sci*., 45, 55-62,1988.

Gaul, R. D., Circulation over the continental margin of the northeast Gulf of Mexico. Ph.D.
Dissertation, Department of Oceanography, Texas A&M University, College Station, 156pp, 1967

Gilbes, F., C. Thomas, J. J. Walsh, and F. E. Muller-Karger, An episodic chlorophyll
plume on the West Florida Shelf, *Continental Shelf Research*, 16, 1201-1224,
1996.

Kourafalou, V. H., L.-Y. Oey, J.D. Wang, and T.L. Lee, The fate of river discharge on the
continental shelf. 1: Modeling the river plume and the inner shelf coastal current. *J.Geophys. Res.,* 101, 3415-3434, 1996

Kundu, P.K. An analysis of inertial oscillations observed near the Oregon coast. *J. Phys*.
Oceanogr. 6, 879-893, 1976

Li, Z., and R. H. Weisberg, West Florida continental shelf response to upwelling
Favorable wind forcing, part II: kinematic description. *J.Geophys. Res.,* 104, 13507-13527, 1999

Li, Z., and R. H. Weisberg, West Florida continental shelf response to upwelling
favorable wind forcing, part II: dynamical analyses, *J. Geophys. Res*., 104, 23427-23442,1999.

Marmorino, G. O, Variability of current, temperature, and bottom pressure across the
West Florida continental shelf, winter, 1981-1982, *J. Geophys. Res*., 88, c7,
4439-4457, 1983a.

Marmorino, G. O, Summertime coastal currents in the Northeastern Gulf of Mexico,
J. Phys. Oceanogr., 13, 65-77, 1983b.

Mellor, G.L. and T. Yamada, A hierarchy of turbulence closure models for planetary boundary
layer, *J. Atmos. Sci.,* 13, 1791-1806, 1974

Mellor, G. L. and T. Yamada, Development of a turbulence closure model for geophysical fluid
problems, *Rev. Geophys.,* 20, 851-875, 1982

Mitchum, T. G., and A. J. Clarke, The frictional nearshore response to forcing by synoptic scale winds, *J. Phys. Oceanogr.*, 16, 934-946, 1986a.

Mitchum, T. G., and A. J. Clarke, Evaluation of frictional, wind forced long wave theory on the West Florida shelf, *J. Phys. Oceanogr.*, 16, 1029-1037, 1986b.

Mitchum, T. G., and W. Sturges, Wind-driven currents on the West Florida shelf, *J. Phys. Oceanogr.*, 12, 1310-1317, 1982.

Morey, S. L., The spring transition of thermal stratification on a mid-latitude continental shelf. Ph. D. dissertation, COAPS, Florida State University Tallahassee, 1999

Niiler, P. P., Observations of low-frequency currents on the West Florida continental shelf, *Memoires Societe Royale des Sciences de Liege*, 6, X, 331-358, 1976.

Orlanski, I., A simple boundary condition for unbounded hyperbolic flows, *J. Comput. Phys.*, 21, 251-269, 1976.

Pullen, J.D., Modeling studies of the coastal circulation off northern California, *Ph.D. Dissertation*, Oregon State University, 2000

Paluszkiewicz, T., L. Atkinson, E.S. Parmentier, and C.R. McClain, Observation of a Loop Current front eddy intrusion onto the West Florida Shelf, *J. Geophys. Res.*, 88, 9636-9651, 1983

Price, J. F., Several aspects of the response of shelf waters to a cold front passage, *Memories Societe Royale des Sciences de Liege*, 6, X, 201-208, 1976

Smagorinsky, J., General circulation experiments with primitive equations I: The basic experiment. Mon. Weather. Rev., 91, 99-164, 1963

Sturges, W., and R. Leben, Frequency of ring separation from the Loop Current in the Gulf of Mexico: A revised estimate. *J. Phys. Oceanogr.*, 30, 1814-1819, 2000

Tolbert, W. H. and G.G. Salsman, Surface circulation of the eastern Gulf of Mexico as
determined by drifter bottle studies, J. Geophys. Res., 69, 223-230, 1964

Vargo, G. A. and E. Shanley, Alkaline phosphates activity in the red-tide dinoflagellate
ptychodiscus brevis, Mar. Ecol., 6, 251-264, 1985

Weisberg, R. H., B. D. Black, H. Yang, Seasonal modulation of the West Florida
continental shelf circulation, *Geophys. Res. Lett*., 23,2247-2250, 1996

Weisberg, R. H., B. D. Black, Z. Li, A upwelling case study on the Florida's west coast.
J. Geophys. Res. 105, 11459-11469, 2000

Weisberg, R. H., Z. Li, F. Muller-Karger, West Florida shelf response to local wind
forcing, April 1998. *J.Geophy. Res.,* in press, 2001

Williams, J., Grey, W.F., Murphy, E.B., J. J. Grane, Memoirs of the Hourglass cruise. Report of
the Marine Research Laboratory, Florida of National Research, St. Petersburg, IV, part III, 134 pp, 1977

Yang, H., R. H. Weisberg, Response of the west-Florida continental shelf to climatological
monthly mean wind forcing, *J. Geophy. Res.,* 104, 5301-5320, 1999

Yang, H, R. H. Weisberg, P. P. Niiler, W. Sturges, W. Johnson, Lagrangian circulation
and forbidden zone on the West Florida Shelf. *Continental shelf Res.* 19. 1221-
1245, 1999

List of Figures

Figure 9 Sea surface temperature and sea surface salinity fields at the end of spring 1999 model simulation (May 31, 1999).

Figure 10 Modeled seasonal mean velocity vectors for the depth averaged and near-surface, mid-water column, and near-bottom sigma levels, k=2, 10, and 20, respectively, from the model twin experiment forced with wind stress only.

Figure 11 Sea surface temperature at the end of spring 1999 simulation (May 31, 1999) for the model twin experiment forced by wind stress only.

Figure 12 Evolution of the monthly mean, depth averaged velocity vectors for March, April, and May relative to the spring 1999 seasonal mean.

Figure 13 Modeled temperature sections sampled on March 15 across transects originating at DeSoto Canyon, Cape San Blas, Florida Big Bend, and Sarasota. The contour interval is 1^0C.

Figure 14 Same as Figure 13 except sampled on April 15.

Figure 15 Same as Figure 13 except sampled on May 15.

Figure 16 Modeled near-surface Lagrangian drifter trajectories for the period April 1, 1999 to May 31, 1999. Drifters were started along nine different transects with initial positions given by solid dots.

Figure 17 Same as Figure 16 except for near-bottom Lagrangian drifter trajectories.

Figure 18a The relative contributions to the depth-averaged temperature balance by ocean circulation and diffusion at station A. Three time series are shown: the advection, the diffusion, and their sum (which equals the local rate of change of depth-averaged temperatuere). Accompanying each time series are their seasonal means and standard deviations in units of ^{0}C day^{-1} as measures of the seasonal and synoptic scale variability.

Figure 18b Same as Figure 18a except for station B.

Figure 18c Same as Figure 18a except for station C.

Figure 18d Same as Figure 18a except for station D.

Figure 19 Time series of the depth profiles of the individual terms that comprise the temperature balance at station A. The left hand panels show the

horizontal and vertical components of the ocean advection and their sum, and the right hand panels show the diffusion, the diffusion plus the advection, and the temperature. To the right of each panel is the seasonal mean profile. The contour interval for each of the budget terms is $0.05^{O}C\ day^{-1}$, and the contour interval for temperature is $0.5^{O}C$. Shading indicates warming and clear indicates cooling.

Figure 20 Same as Figure 19 except for station B.

Figure 21 Same as Figure 19 except for station C.

Figure 22 Same as Figure 19 except for station D.

Figure 23 The contributions made to the seasonal mean rate of change of SST by each of the advection and diffusion terms. The left panels show the advection terms and their sum, and the right panels show the horizontal and vertical diffusion terms, the sum of all terms. The contour interval is $0.02^{0}C\ day^{-1}$. Bold lines indicate warming and thin lines indicate cooling.

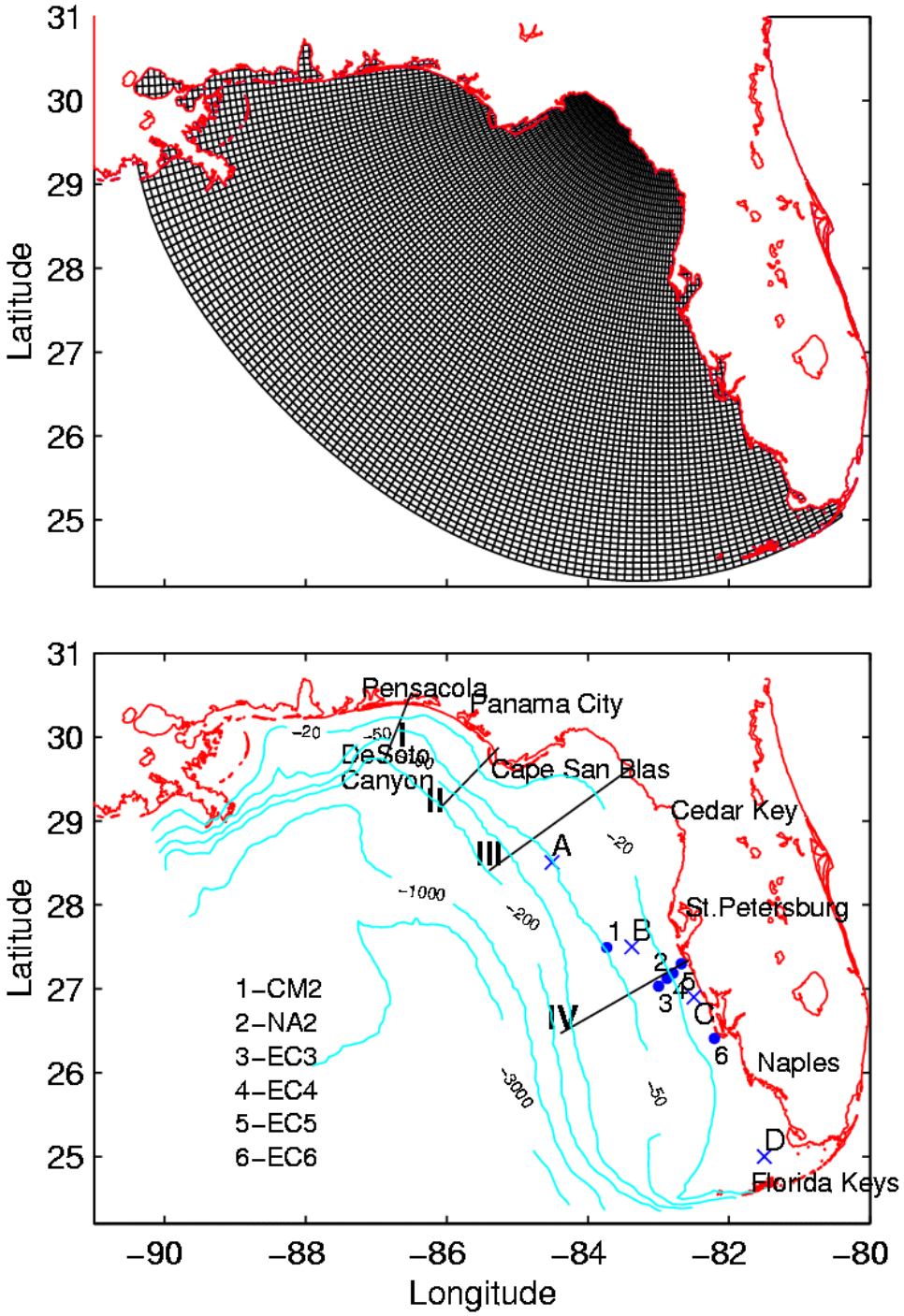
Latitude
Longitude
Pensacola
Panama City
DeSoto
Canyon
Cape San Blas
Cedar Key
St.Petersburg
Naples
Florida Keys
I
II
III
IV
A
B
C
D
1
2
3
4
5
6
1–CM2
2–NA2
3–EC3
4–EC4
5–EC5
6–EC6
-20
-50
-100
-200
-1000
-3000

Figure 1

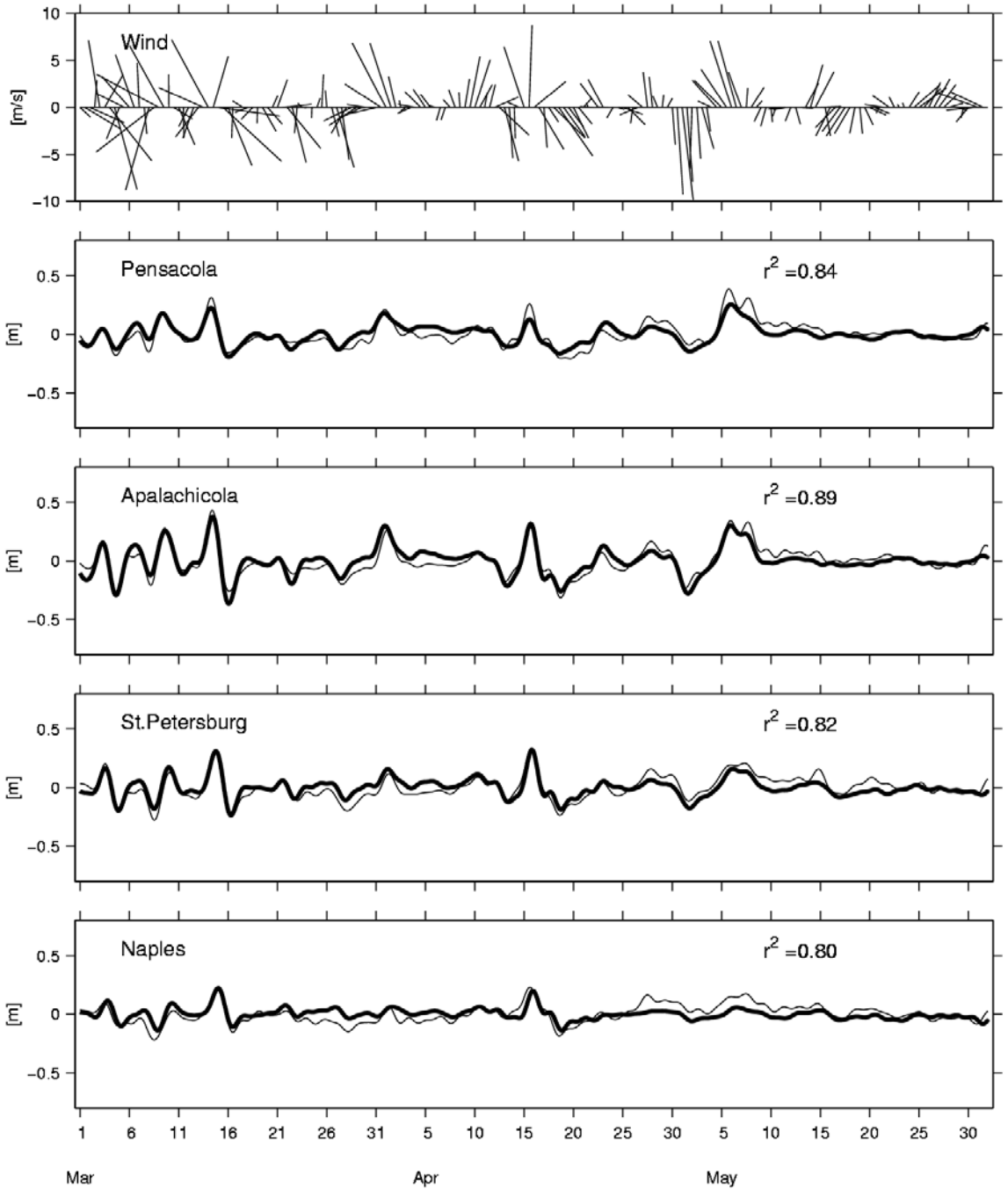
Wind
[m/s]
10
5
0
−5
−10
Pensacola
r2 =0.84
Apalachicola
r2 =0.89
St.Petersburg
r2 =0.82
Naples
r2 =0.80
[m]
0.5
0
−0.5
1 6 11 16 21 26 31 5 10 15 20 25 30 5 10 15 20 25 30
Mar
Apr
May
1999

Figure 2

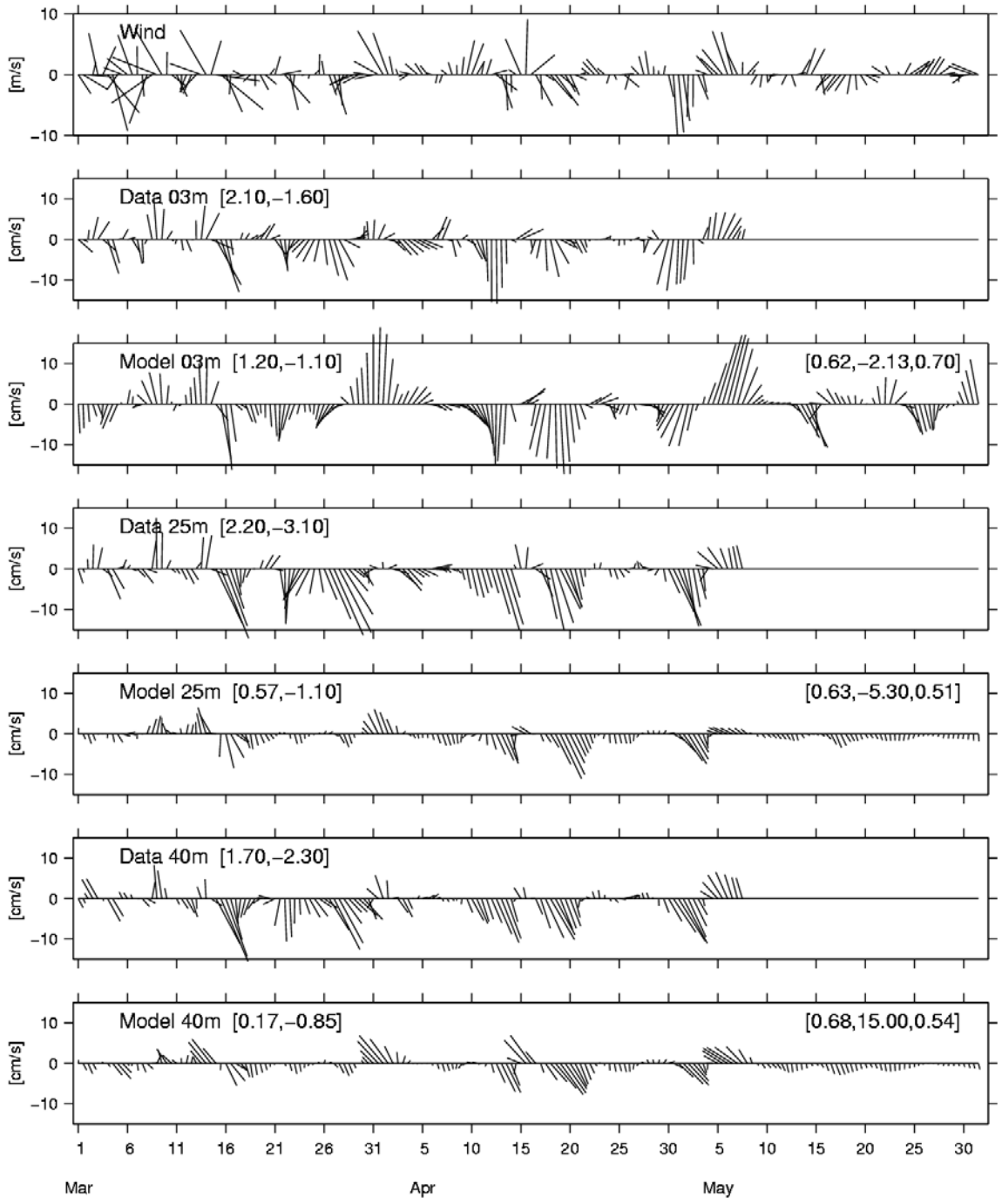
Wind
Data 03m [2.10,–1.60]
Model 03m [1.20,–1.10]
[0.62,–2.13,0.70]
Data 25m [2.20,–3.10]
Model 25m [0.57,–1.10]
[0.63,–5.30,0.51]
Data 40m [1.70,–2.30]
Model 40m [0.17,–0.85]
[0.68,15.00,0.54]
[m/s]
[cm/s]
10
0
–10
1 6 11 16 21 26 31 5 10 15 20 25 30 5 10 15 20 25 30
Mar
Apr
May
1999

Figure 3

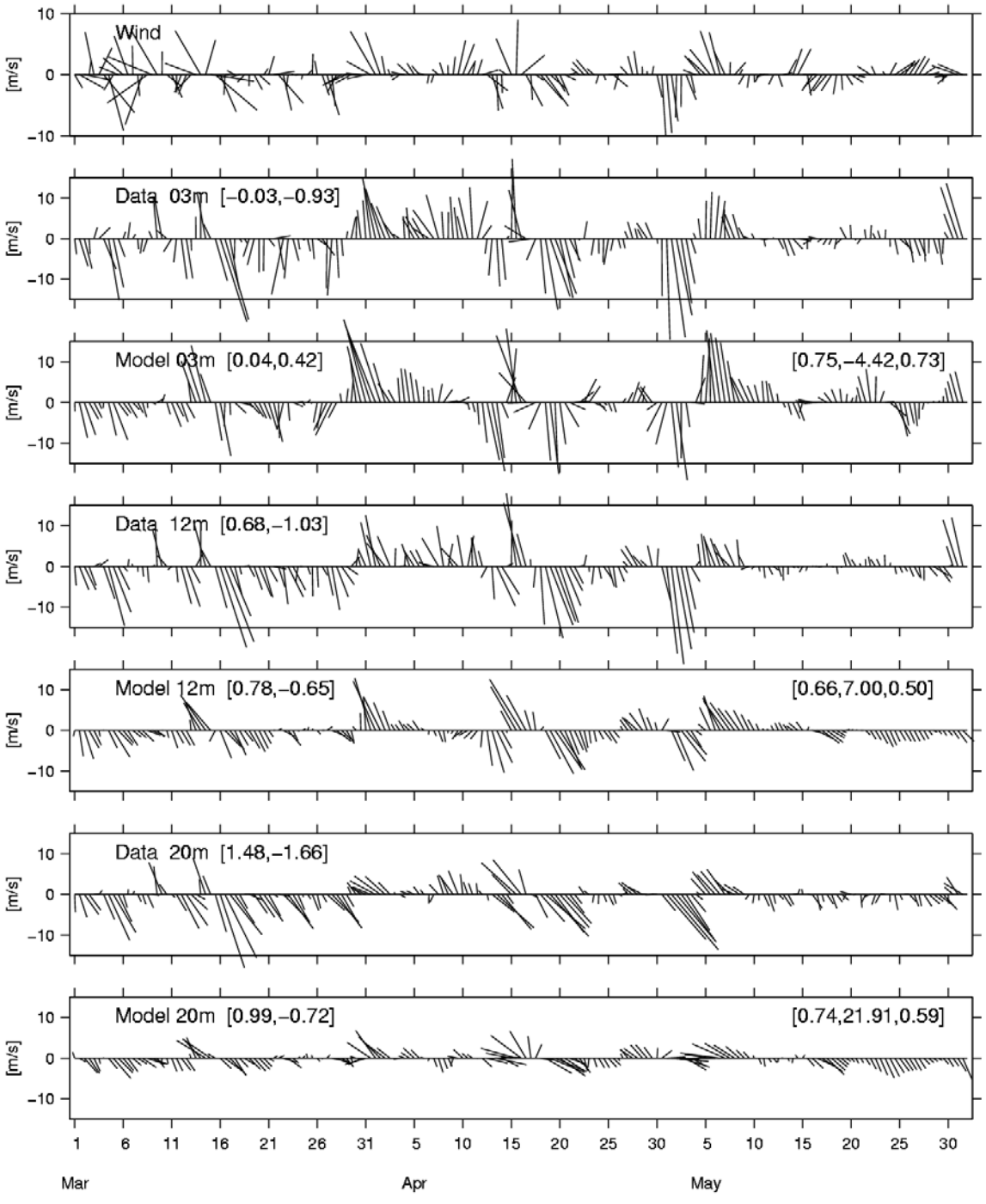
Wind
Data 03m [−0.03,−0.93]
Model 03m [0.04,0.42]
[0.75,−4.42,0.73]
Data 12m [0.68,−1.03]
Model 12m [0.78,−0.65]
[0.66,7.00,0.50]
Data 20m [1.48,−1.66]
Model 20m [0.99,−0.72]
[0.74,21.91,0.59]
[m/s]
10
0
−10
1 6 11 16 21 26 31 5 10 15 20 25 30 5 10 15 20 25 30
Mar
Apr
May
1999

Figure 4

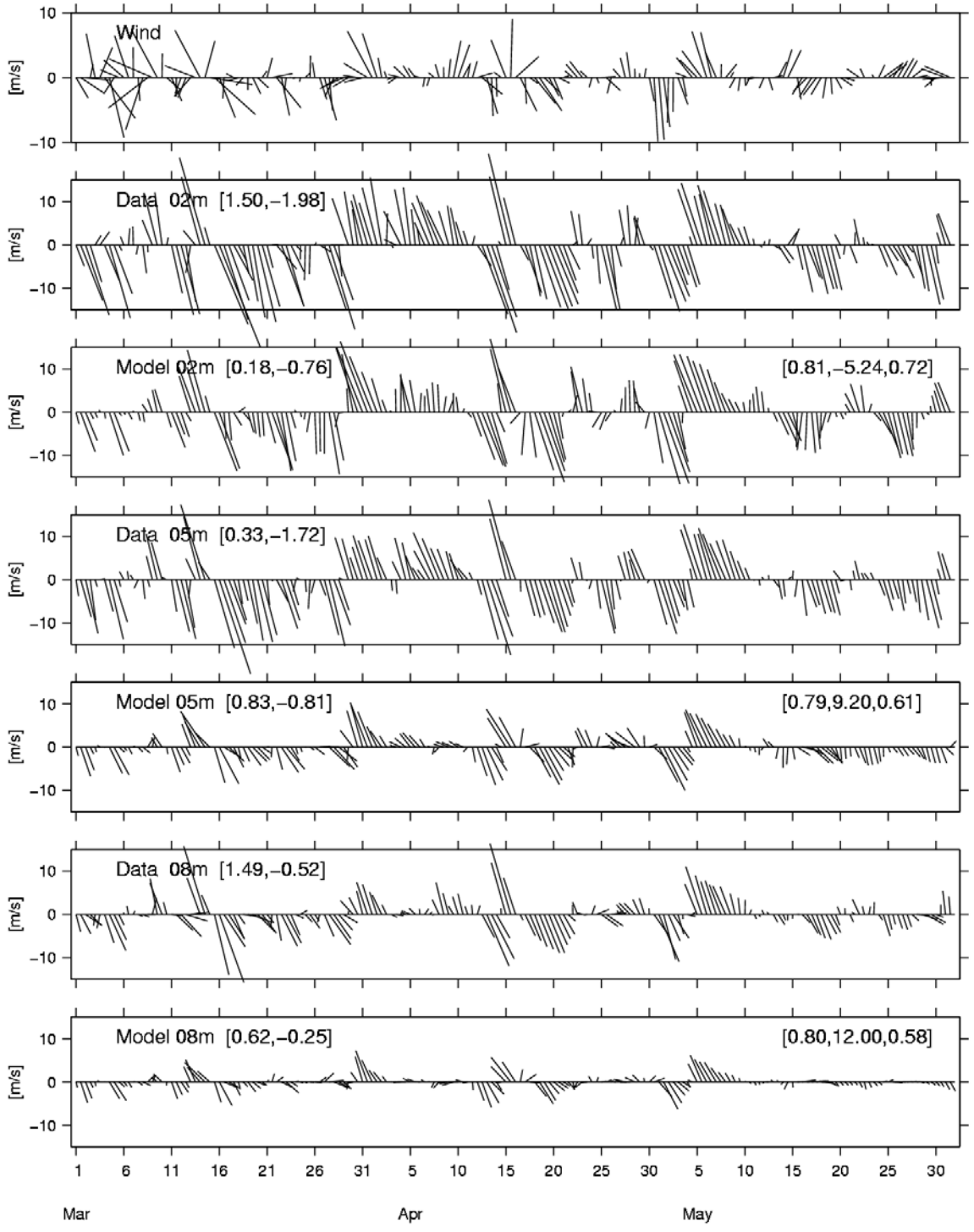
Wind
Data 02m [1.50,–1.98]
Model 02m [0.18,–0.76]
[0.81,–5.24,0.72]
Data 05m [0.33,–1.72]
Model 05m [0.83,–0.81]
[0.79,9.20,0.61]
Data 08m [1.49,–0.52]
Model 08m [0.62,–0.25]
[0.80,12.00,0.58]
[m/s]
10
0
–10
1 6 11 16 21 26 31 5 10 15 20 25 30 5 10 15 20 25 30
Mar
Apr
May
1999

Figure 5

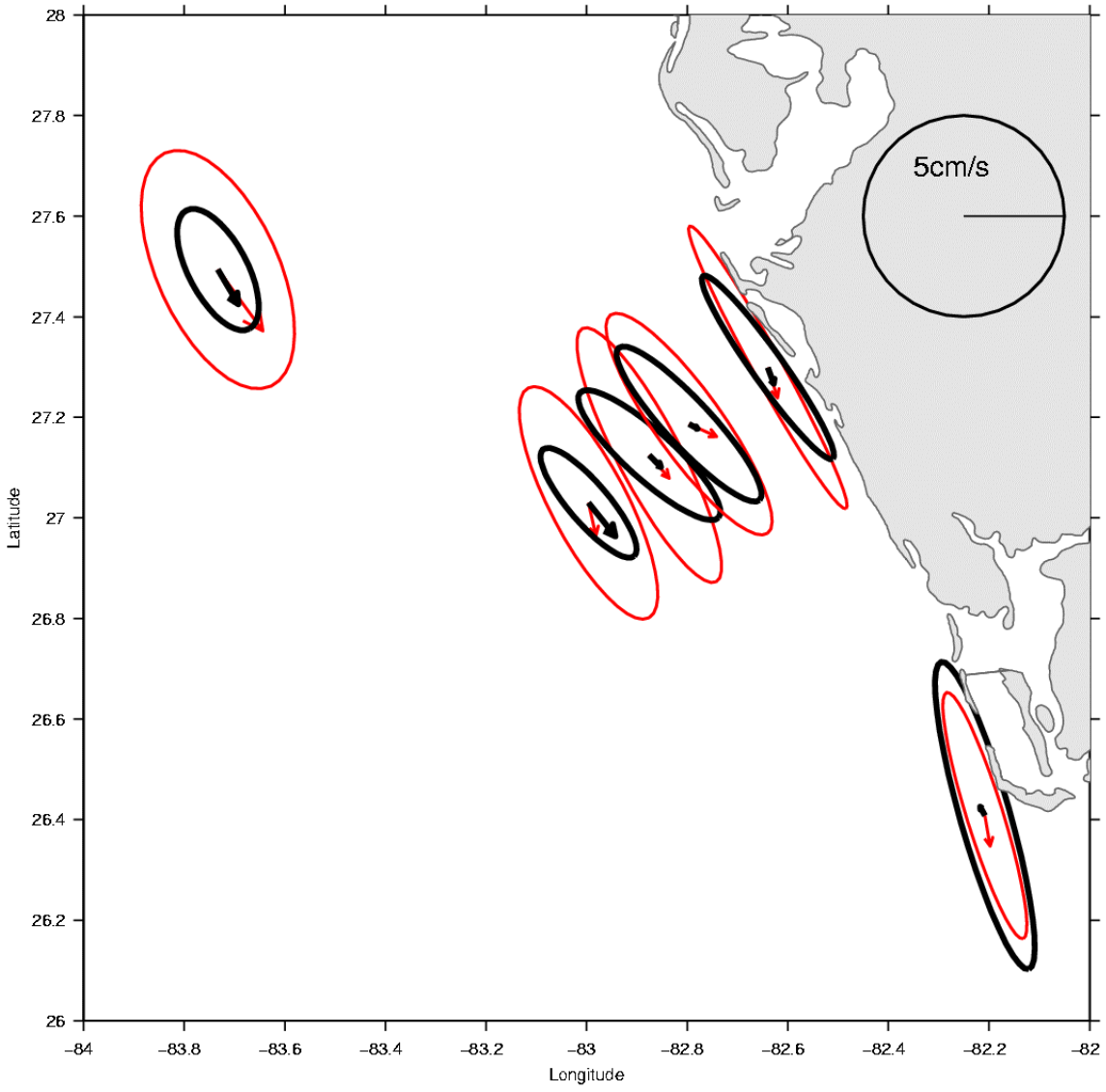
5cm/s
Latitude
Longitude
28
27.8
27.6
27.4
27.2
27
26.8
26.6
26.4
26.2
26
-84
-83.8
-83.6
-83.4
-83.2
-83
-82.8
-82.6
-82.4
-82.2
-82

Figure 6

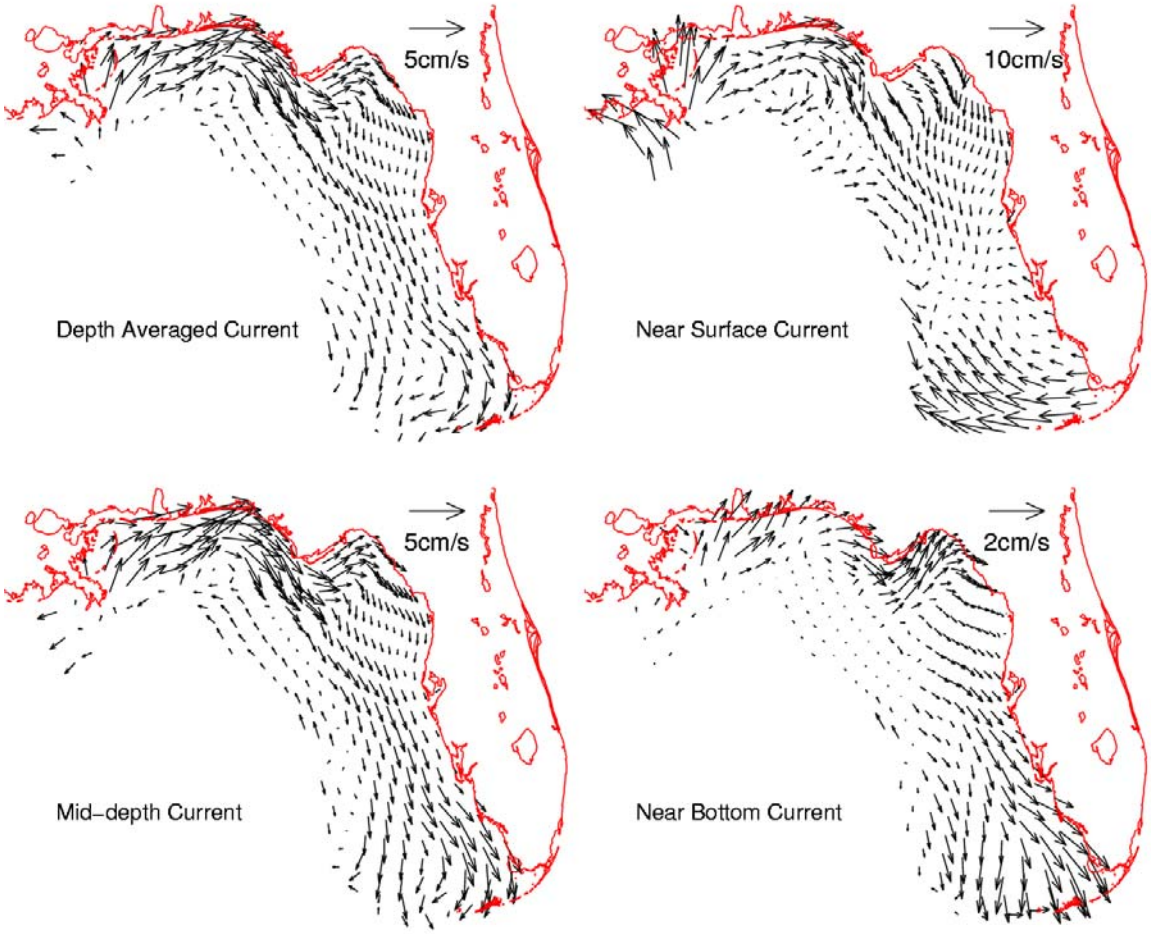
5cm/s
Depth Averaged Current
10cm/s
Near Surface Current
5cm/s
Mid–depth Current
2cm/s
Near Bottom Current

Figure 7

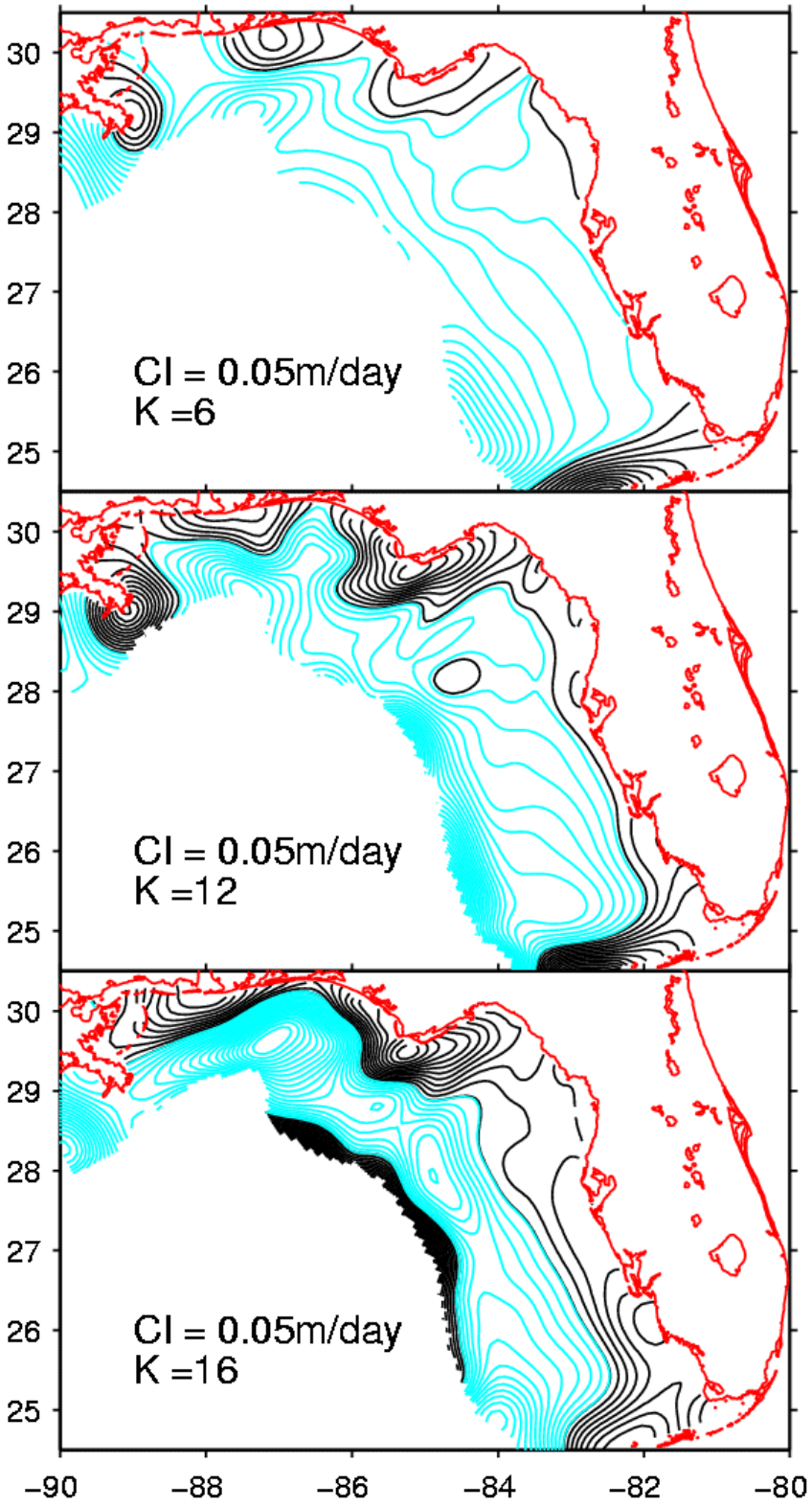
CI = 0.05m/day
K =6
CI = 0.05m/day
K =12
CI = 0.05m/day
K =16
30
29
28
27
26
25
−90
−88
−86
−84
−82
−80

Figure 8

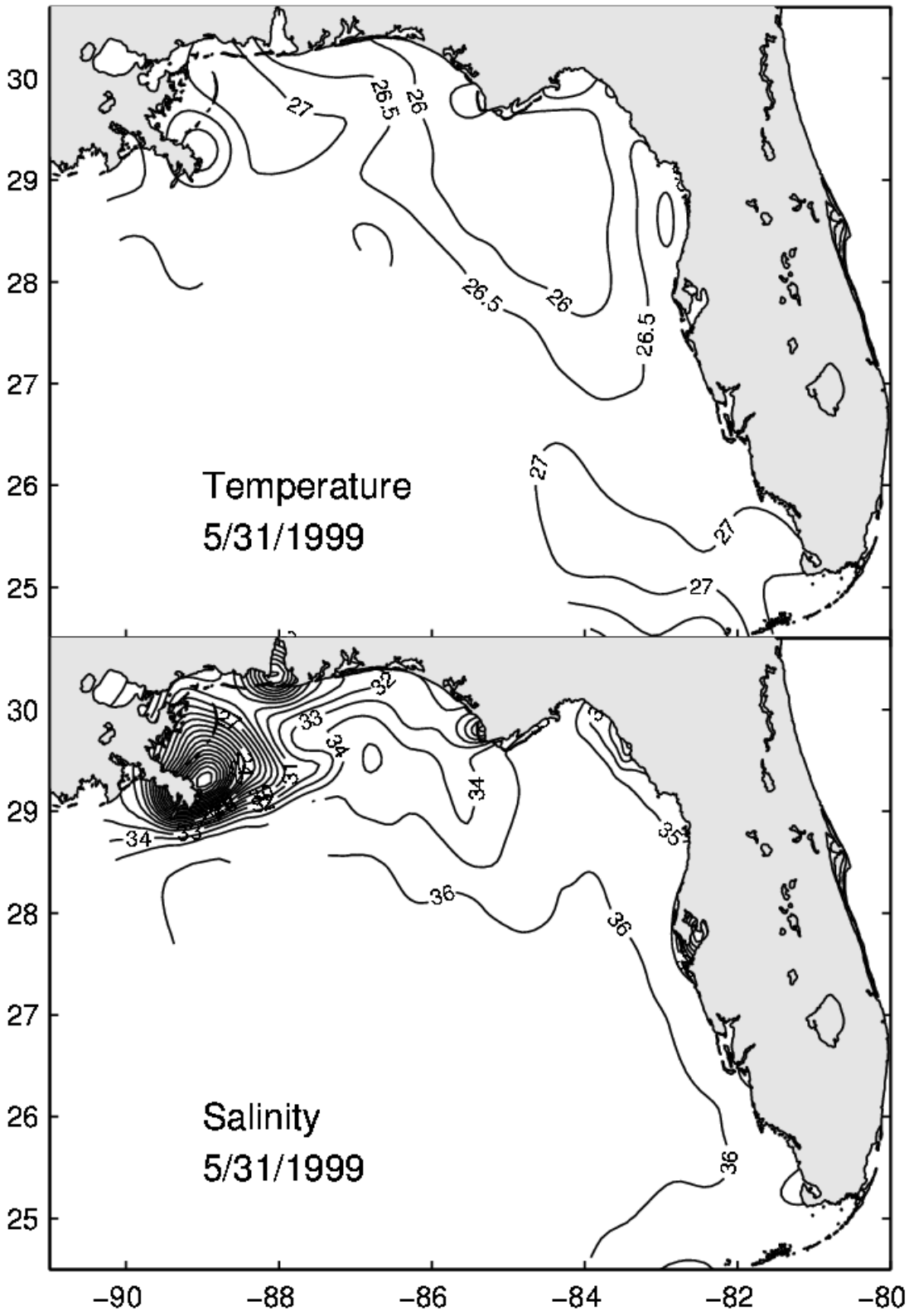
Temperature
5/31/1999
Salinity
5/31/1999
30
29
28
27
26
25
−90
−88
−86
−84
−82
−80

Figure 9

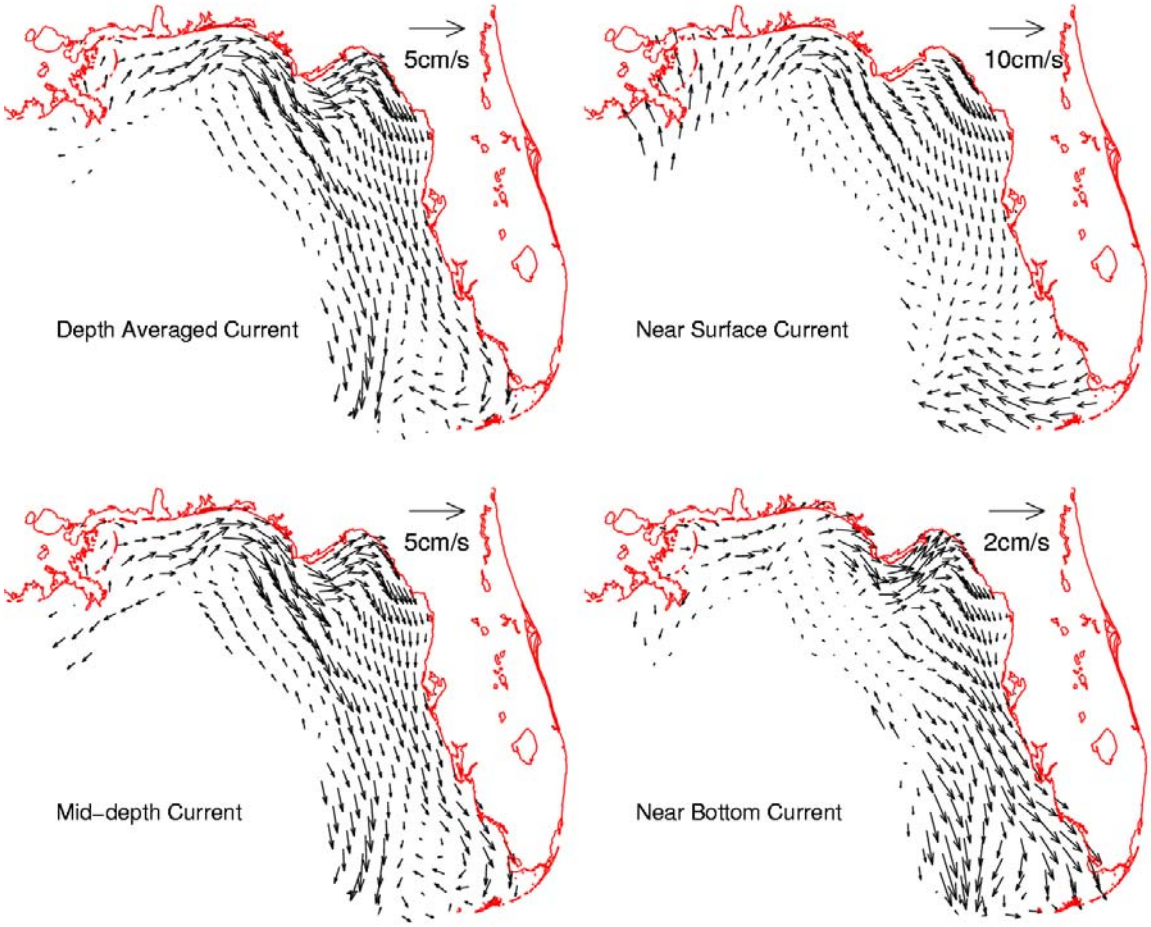
5cm/s
Depth Averaged Current
10cm/s
Near Surface Current
5cm/s
Mid–depth Current
2cm/s
Near Bottom Current

Figure 10

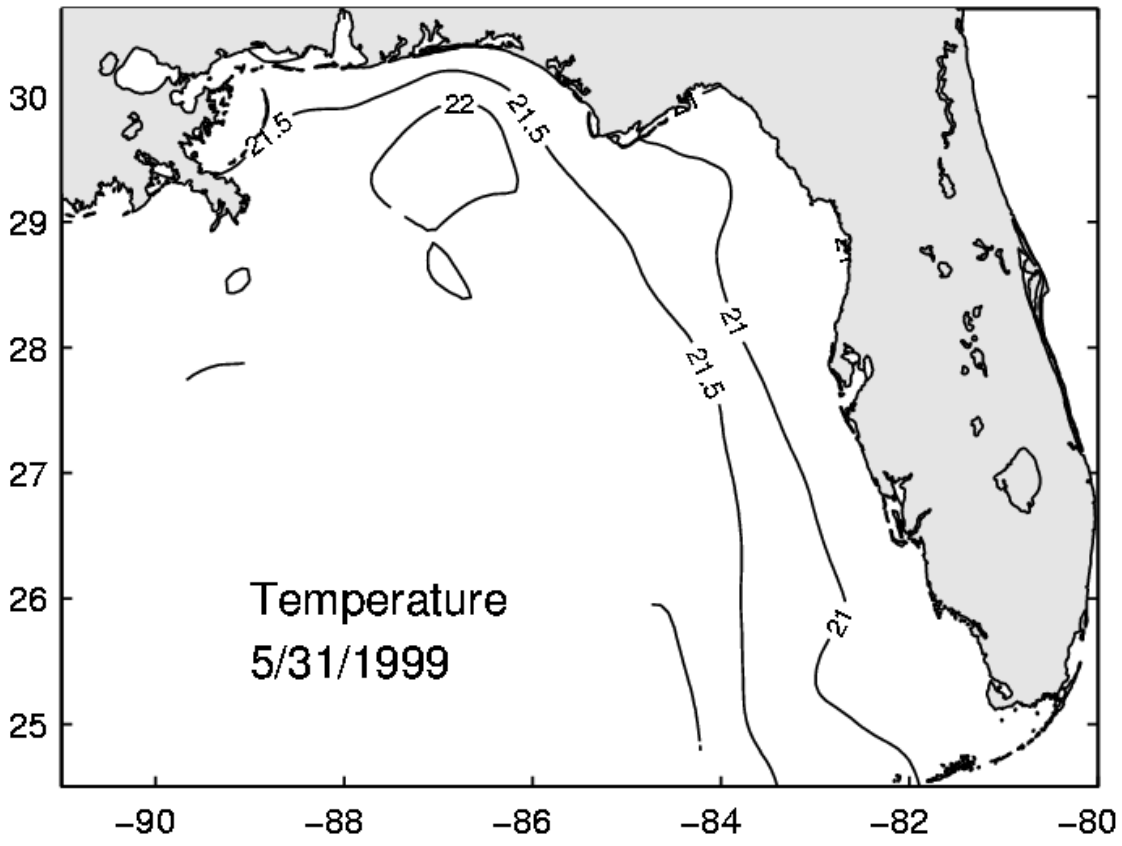

Figure 11

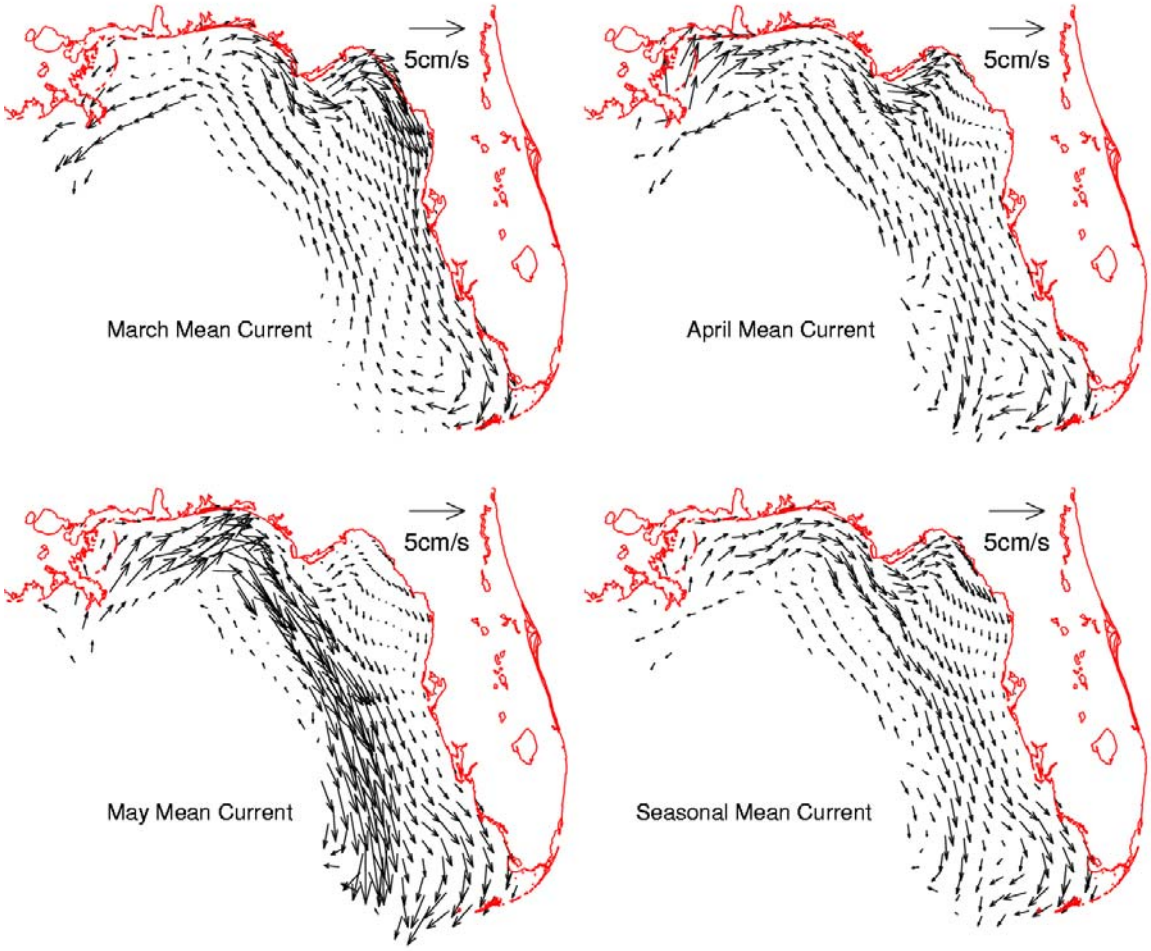
5cm/s
March Mean Current
5cm/s
April Mean Current
5cm/s
May Mean Current
5cm/s
Seasonal Mean Current

Figure 12

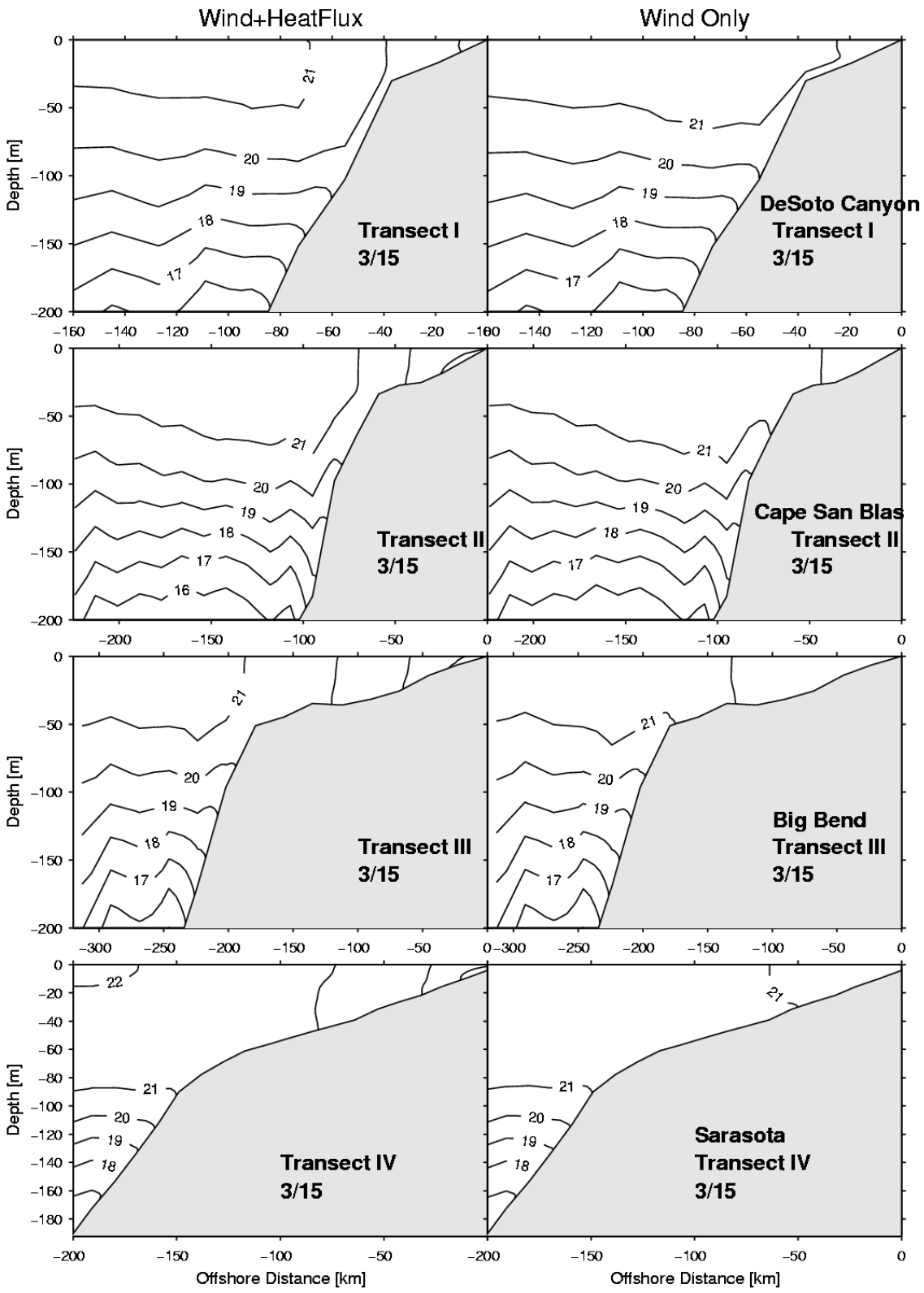
Wind+HeatFlux
Wind Only
Depth [m]
Transect I
3/15
DeSoto Canyon
Transect I
3/15
Transect II
3/15
Cape San Blas
Transect II
3/15
Transect III
3/15
Big Bend
Transect III
3/15
Transect IV
3/15
Sarasota
Transect IV
3/15
Offshore Distance [km]
Offshore Distance [km]

Figure 13

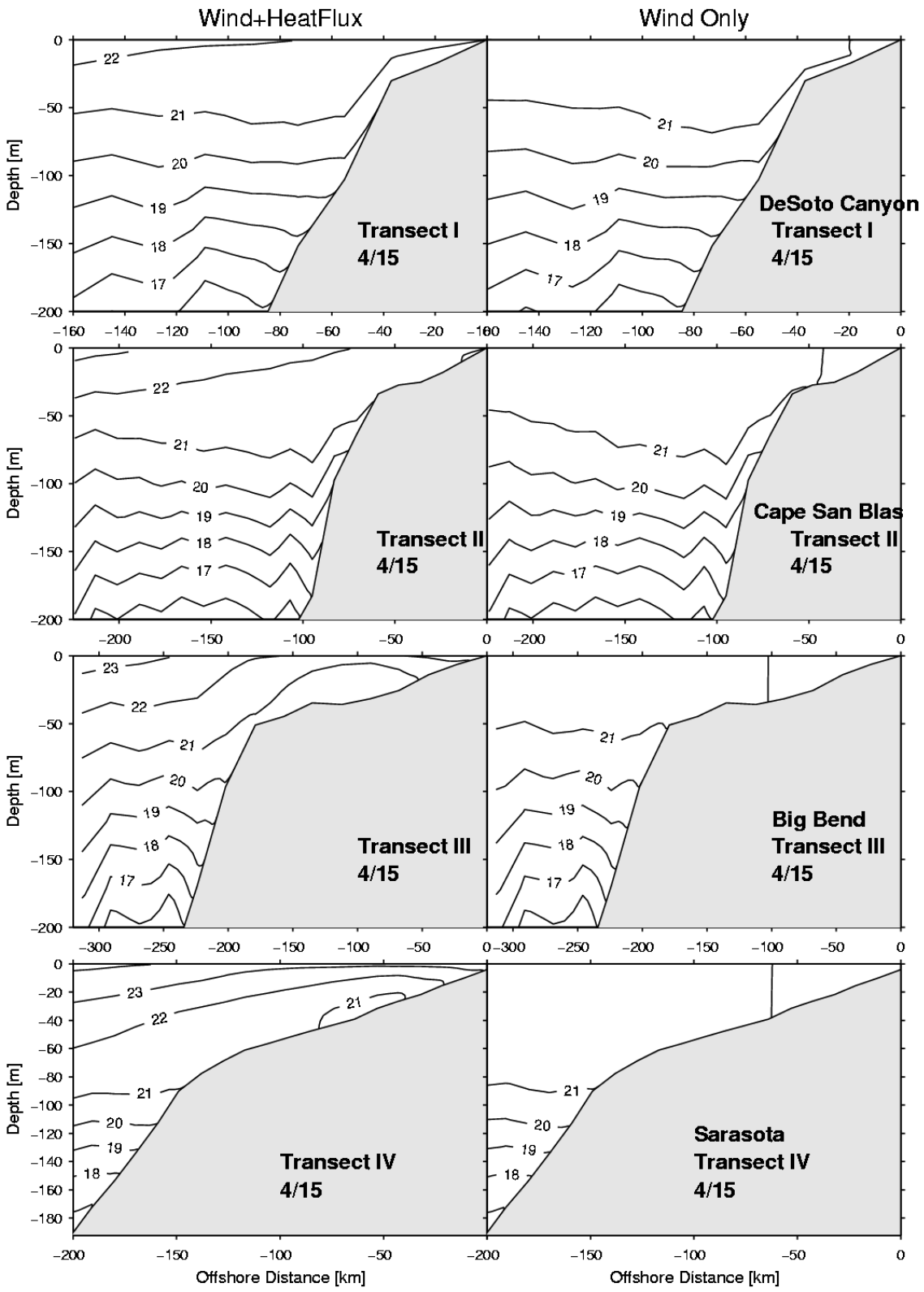
Wind+HeatFlux
Wind Only
Depth [m]
Transect I
4/15
DeSoto Canyon
Transect I
4/15
Transect II
4/15
Cape San Blas
Transect II
4/15
Transect III
4/15
Big Bend
Transect III
4/15
Transect IV
4/15
Sarasota
Transect IV
4/15
Offshore Distance [km]
Offshore Distance [km]

Figure 14

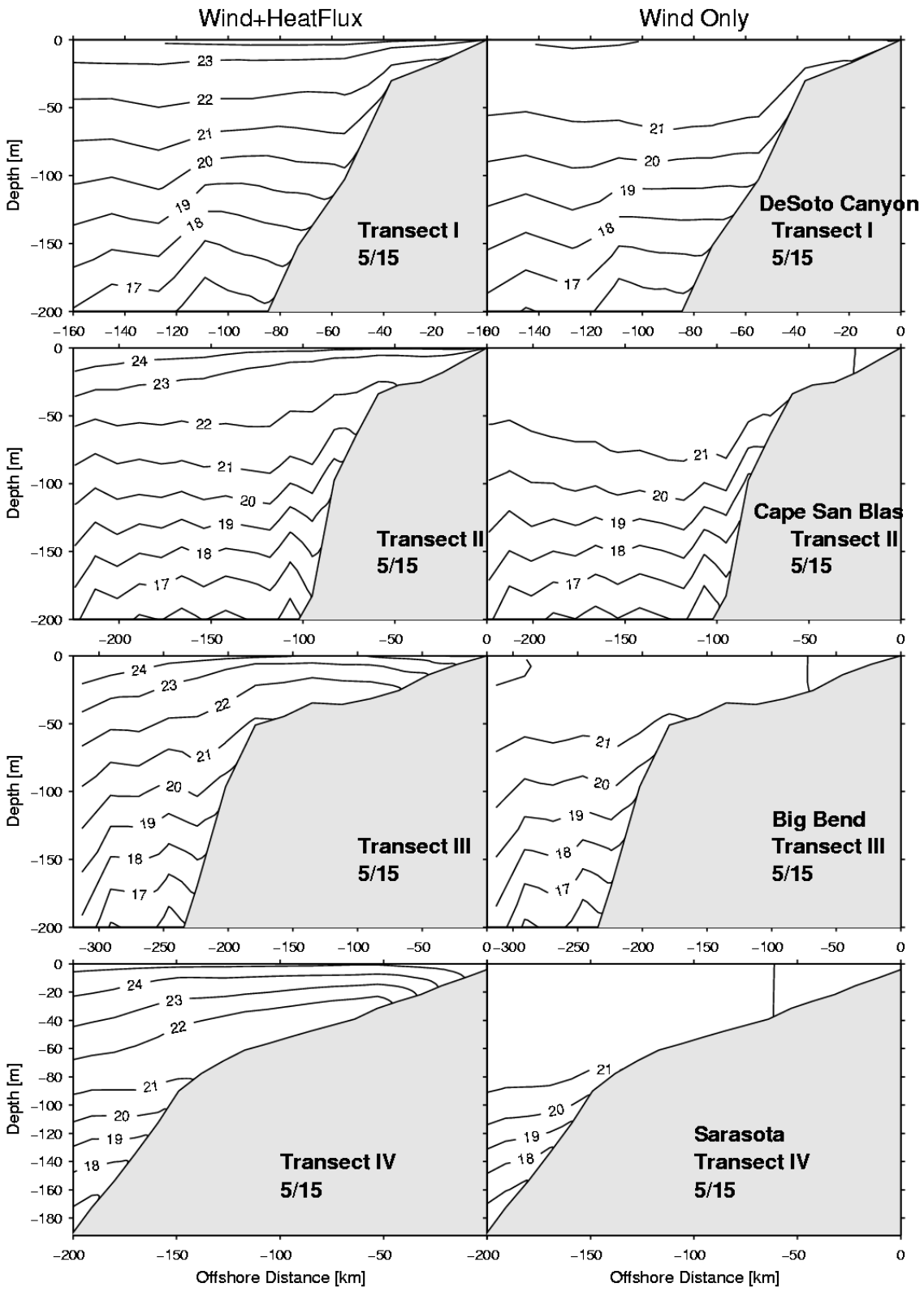
Wind+HeatFlux
Wind Only
Depth [m]
Transect I
5/15
DeSoto Canyon
Transect I
5/15
Transect II
5/15
Cape San Blas
Transect II
5/15
Transect III
5/15
Big Bend
Transect III
5/15
Transect IV
5/15
Sarasota
Transect IV
5/15
Offshore Distance [km]
Offshore Distance [km]

Figure 15

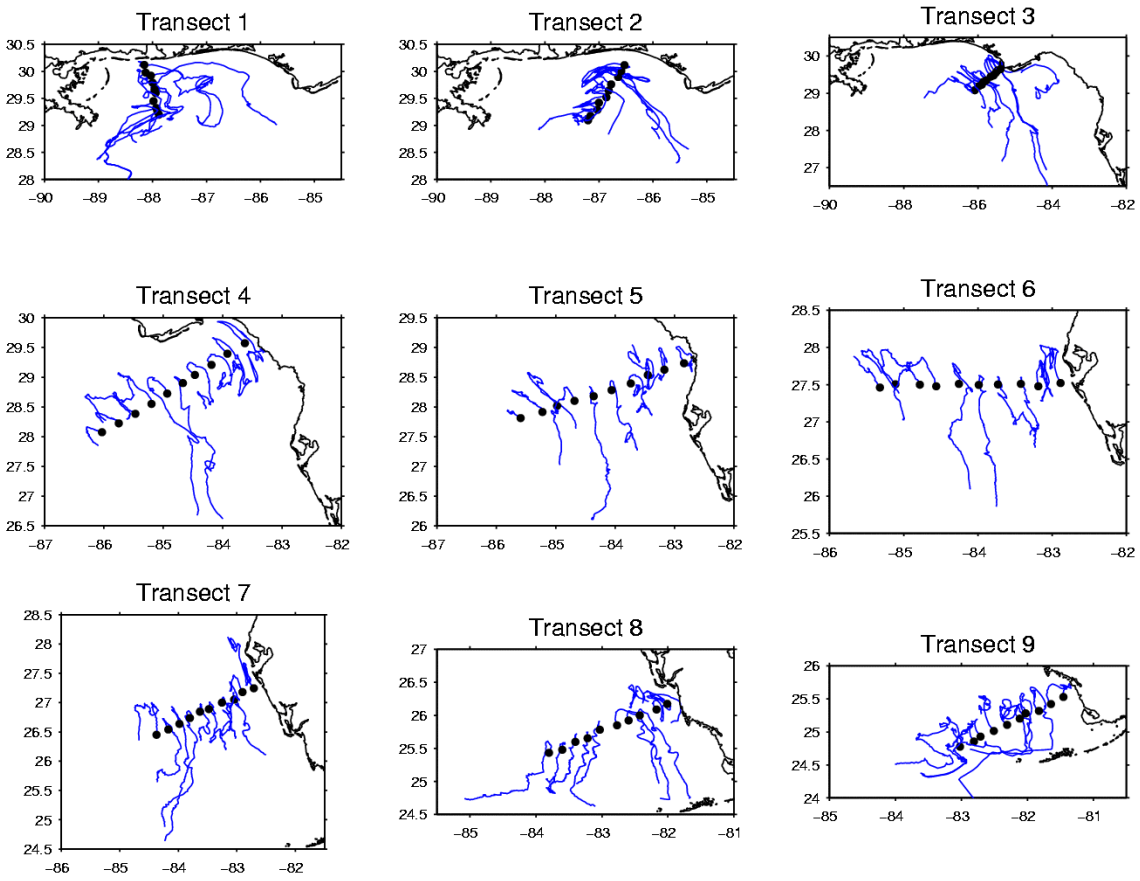
Transect 1
Transect 2
Transect 3
Transect 4
Transect 5
Transect 6
Transect 7
Transect 8
Transect 9

Figure 16

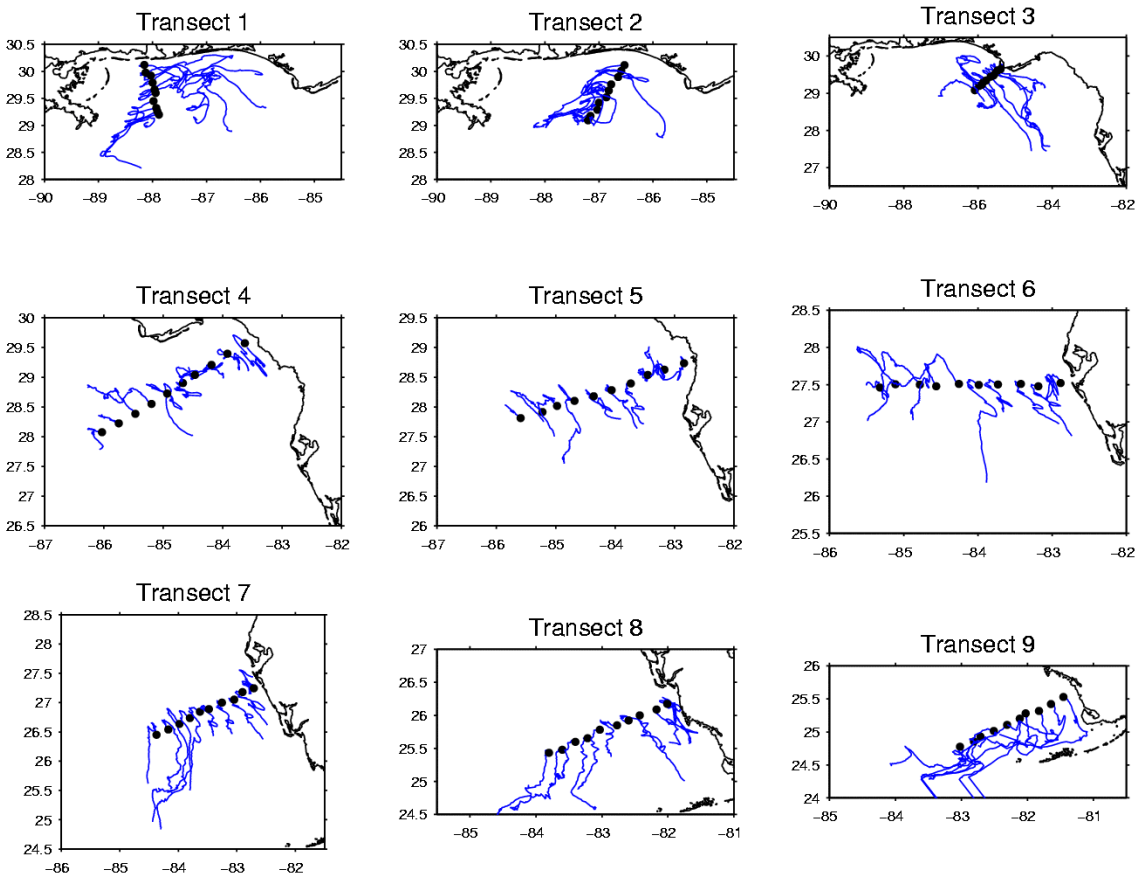
Transect 1
Transect 2
Transect 3
Transect 4
Transect 5
Transect 6
Transect 7
Transect 8
Transect 9

Figure 17

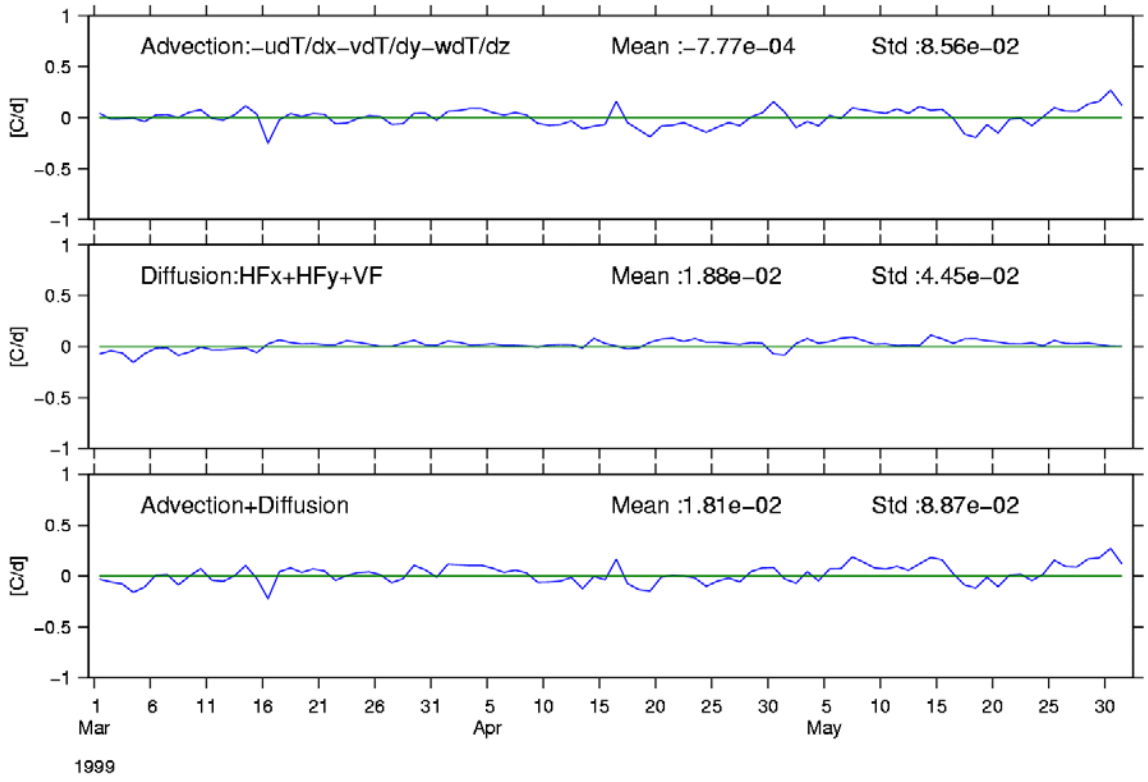

Figure 18a

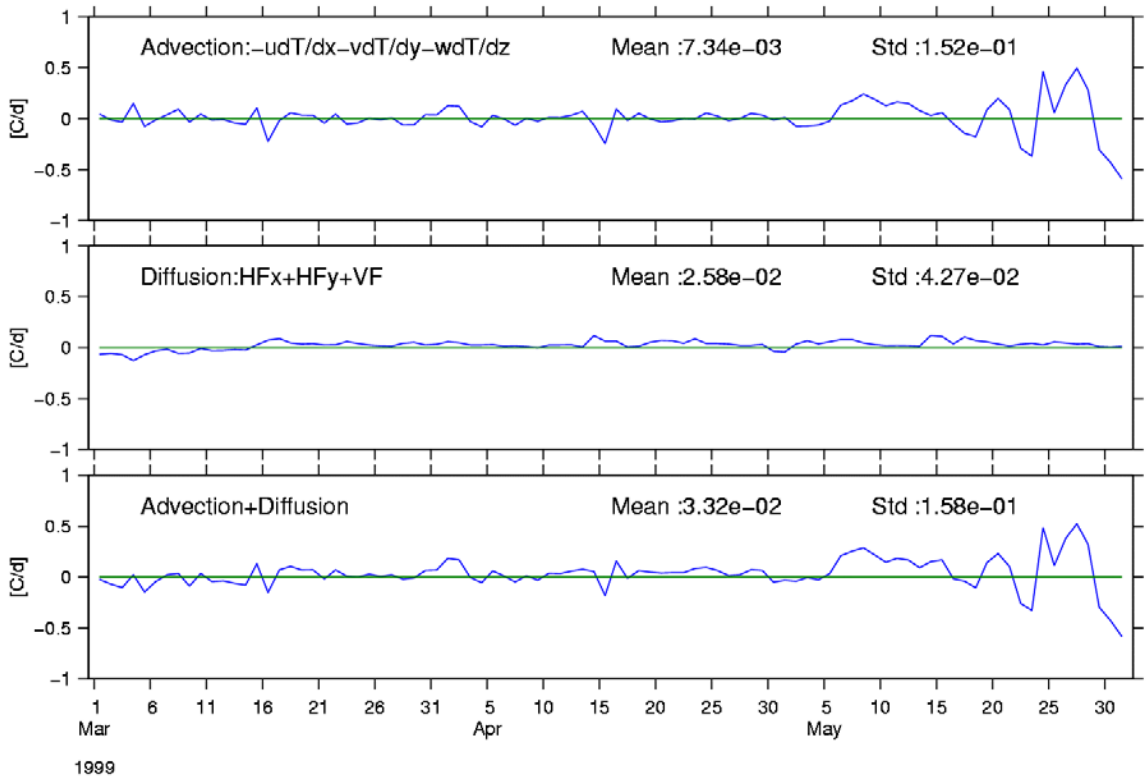

Figure 18b

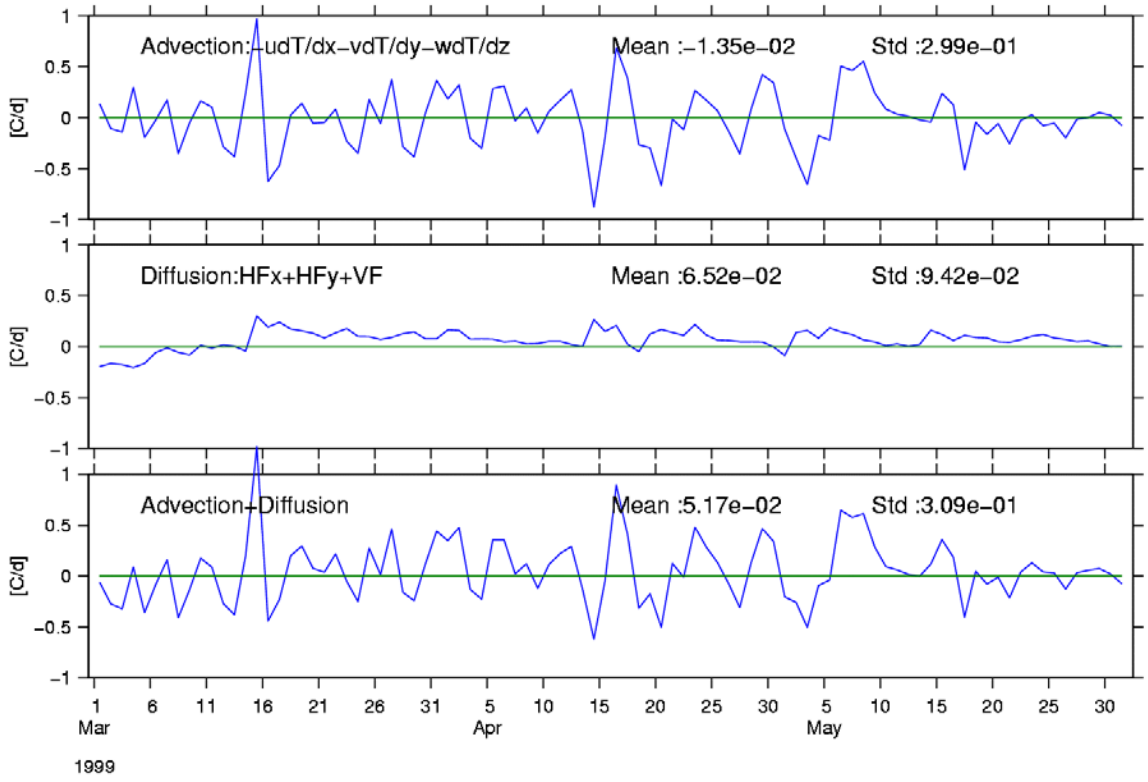

Figure 18c

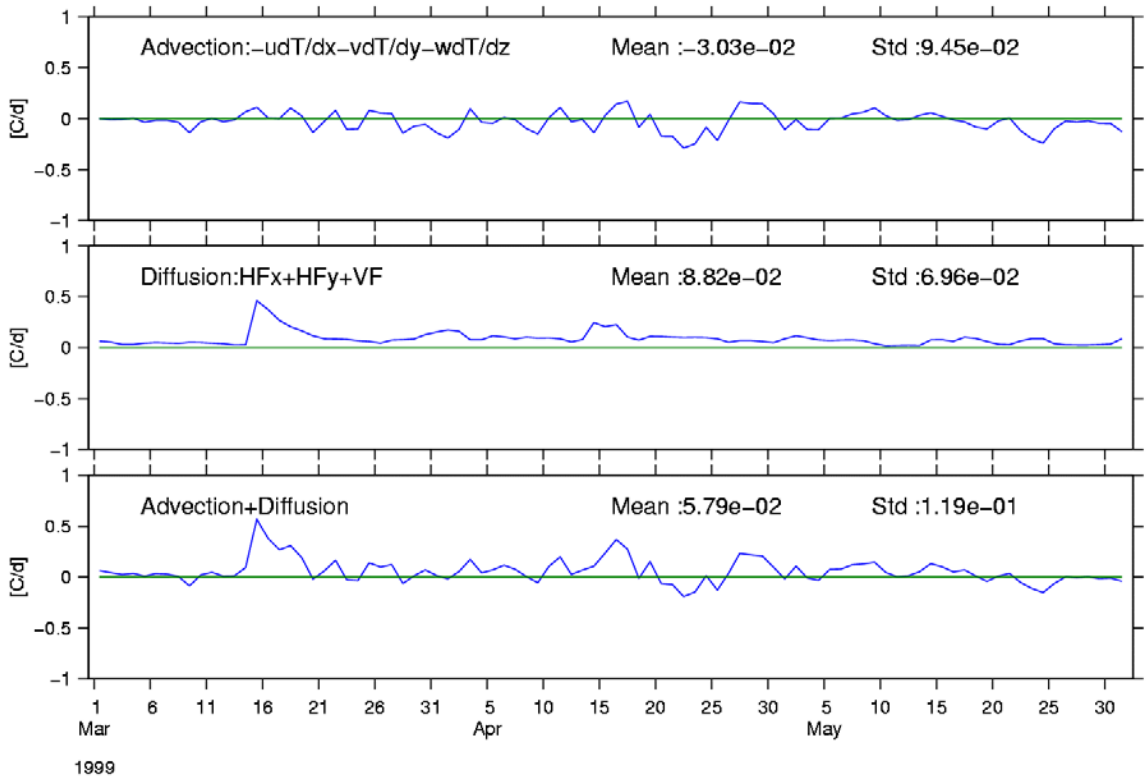

Figure 18d

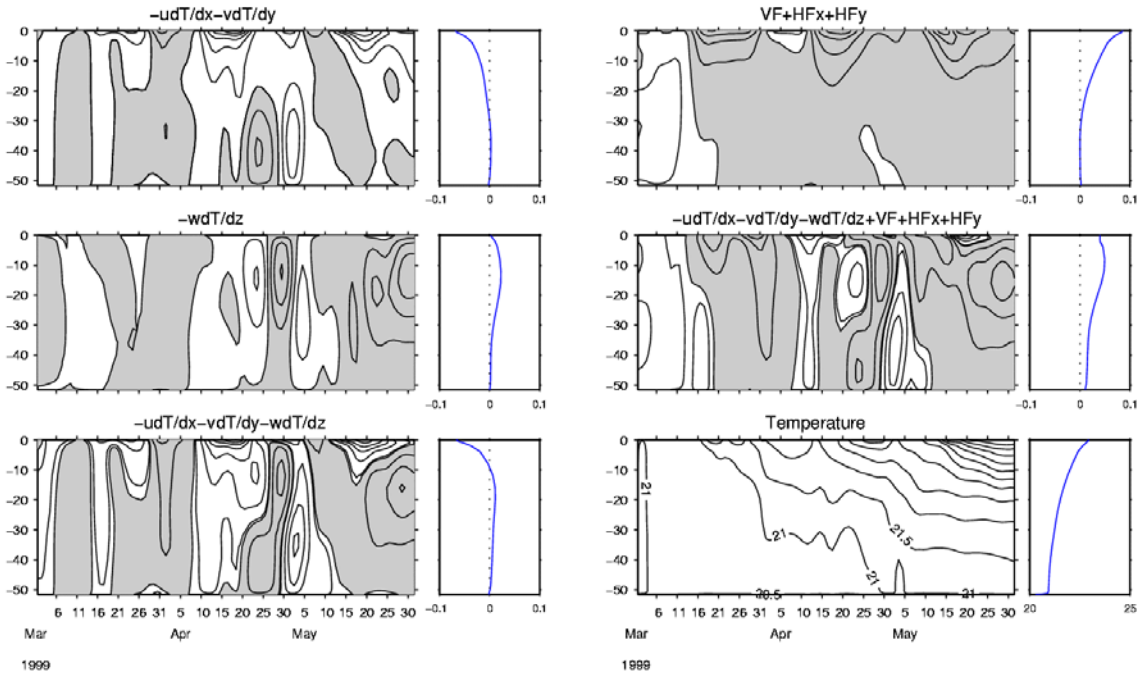

Figure 19

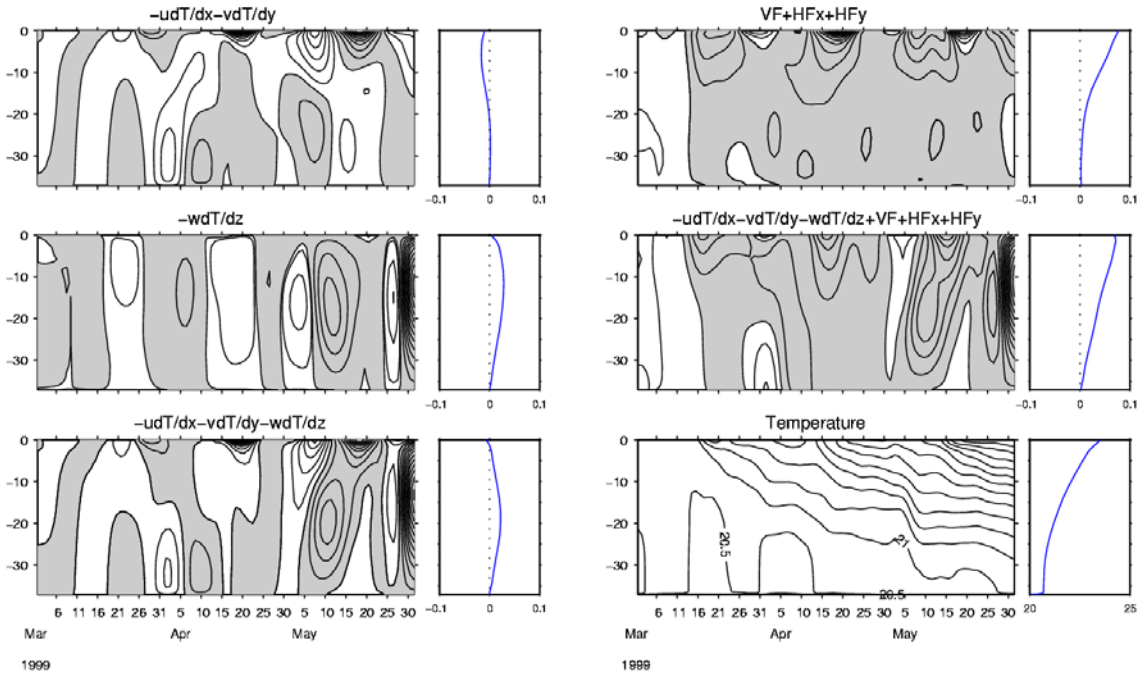

Figure 20

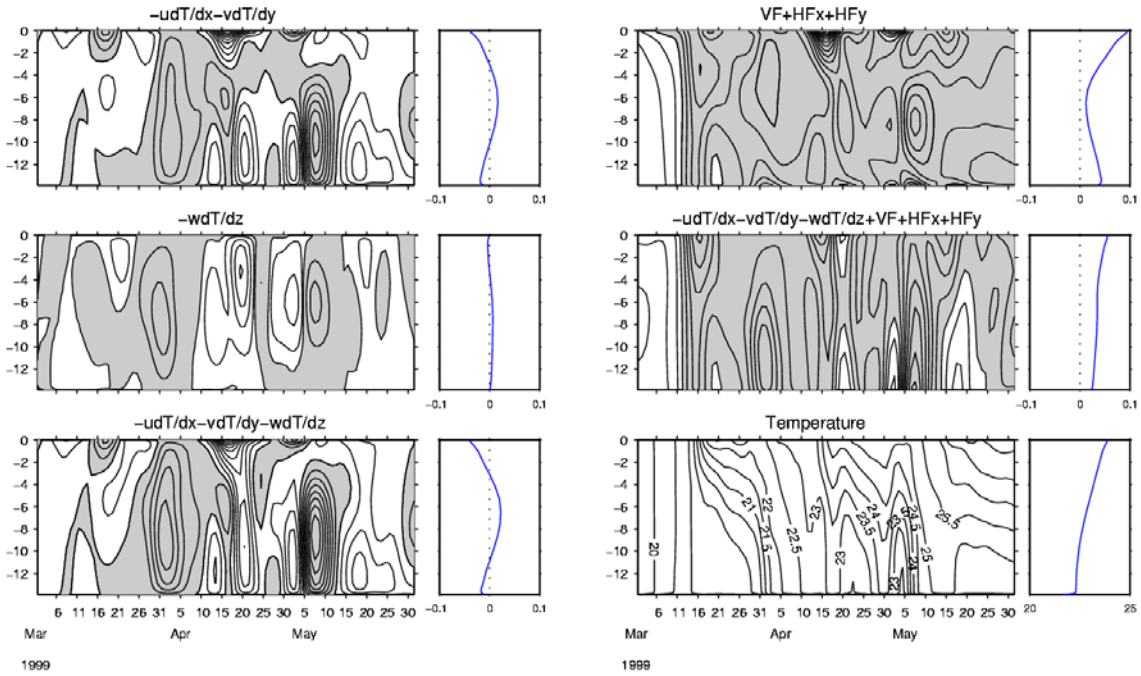

Figure 21

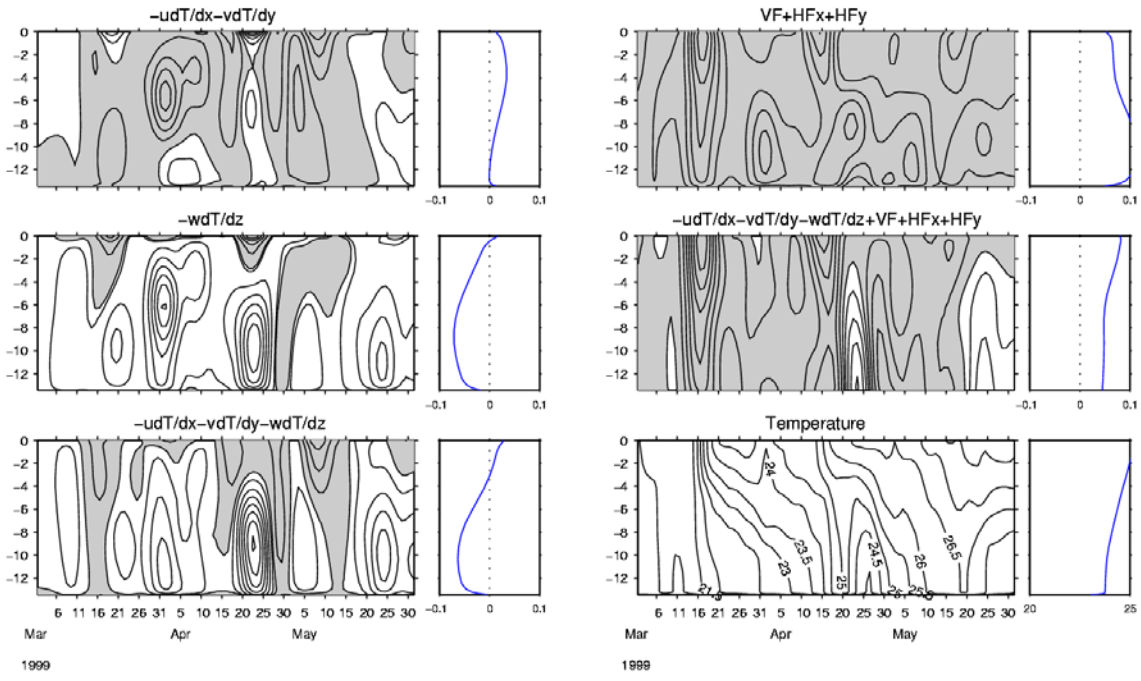

Figure 22

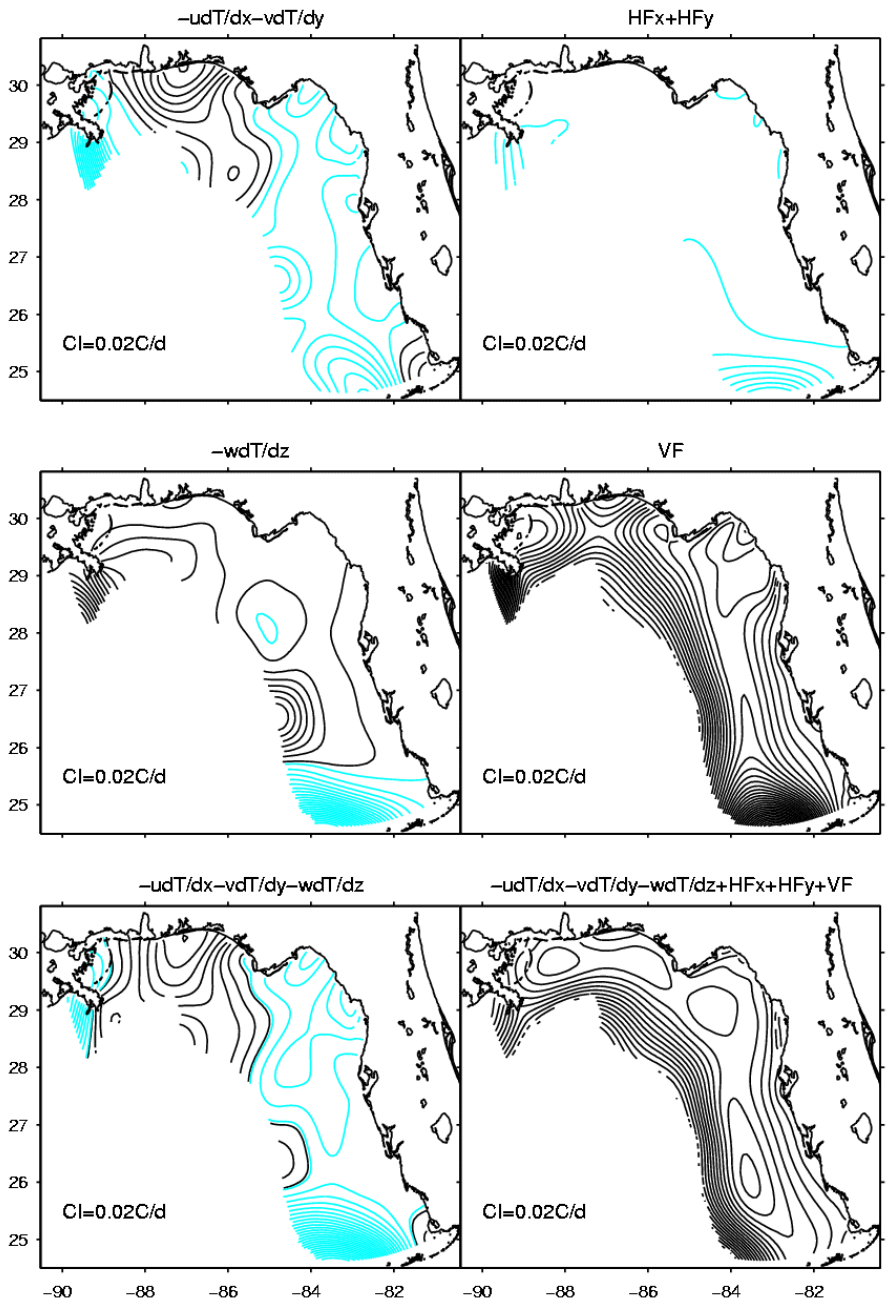
–udT/dx–vdT/dy
HFx+HFy
–wdT/dz
VF
–udT/dx–vdT/dy–wdT/dz
–udT/dx–vdT/dy–wdT/dz+HFx+HFy+VF
CI=0.02C/d
30
29
28
27
26
25
–90
–88
–86
–84
–82

Figure 23